

QATAR UNIVERSITY

COLLEGE OF ARTS AND SCIENCES

DEVELOPMENT OF FUNCTIONALIZED DATE PITS ADSORBENT FOR THE  
REMOVAL OF BORON, LITHIUM, AND MOLYBDENUM FROM GROUNDWATER

IN THE STATE OF QATAR

BY

AYESHA YOUSEF AHMAD

A Dissertation Submitted to

the College of Arts and Sciences

in Partial Fulfillment of the Requirements for the Degree of

Doctorate of Philosophy in PhD in Biological and Environmental Sciences

June 2021

© 2021 Ayesha Yousef Ahmad. All Rights Reserved.

## COMMITTEE PAGE

The members of the Committee approve the Dissertation of  
Ayesha Yousef Ahmad defended on 15/04/2021.

---

Prof. Mohammad Ahmad Al-Ghouti  
Thesis/Dissertation Supervisor

---

Prof. Majeda Khraisheh  
Committee Member

---

Prof. Nabil Zouari  
Committee Member

---

Dr. Perumal Balakrishnan  
Committee Member

Approved:

---

Ibrahim AlKaabi, Dean, College of Arts and Sciences

## ABSTRACT

AHMAD, AYESHA, Y. Doctorate: April: 2021:

PhD in Biological and Environmental Sciences

Title: Development of a Functionalize Date Pits Adsorbent for the Removal of Boron, Lithium, and Molybdenum from Groundwater in the State of Qatar

Supervisor of Dissertation: Mohammad, Ahmad, Al-Ghouthi.

Groundwater (GW) quality deterioration is one of the main water security issues in Qatar. Although the GW in the State of Qatar is not used as drinking water for the public, it is widely used for agricultural, domestic, and recreational projects. In this study, 41 GW samples were used to investigate the GW quality in Qatar. The integrated physiochemical analysis along with hydro-chemical faces analysis, geochemical modeling, statistical and geostatistical analysis was conducted. The results showed that the GW samples mainly have the following cations  $\text{Na}^+ > \text{Ca}^{2+} > \text{Mg}^{2+} > \text{K}^+$  abundantly, while  $\text{Cl}^- > \text{SO}_4^{2-} > \text{HCO}_3^- > \text{NO}_3^-$  were the main anions. The analysis of spatial variability using multiple spatial interpolated methods (ArcGIS Software) revealed high levels of total dissolved solids (TDS), sodium absorption ratio (SAR), and some cations and anions in the coastal and south Qatar. While the spatial variability for nitrate and boron suggested the influence of human activities. Boron (B) and molybdenum (Mo) levels in some samples exceeded the World Health Organization (WHO), GCC Standardization Organization (GSO), Qatar drinking water guidelines, and the US Environmental Protection Agency (EPA) (US-EPA) lifetime health advisory. Lithium (Li) levels in 39 samples exceeded the GSO. As a

result, the removal of B, Li, and Mo from GW using activated carbon (AC), bentonite, roasted date pits (RDPs), and (MDPs) as adsorbents were investigated. Date pits are agricultural waste that is used as inexpensive, eco-friendly, and efficient adsorbent due to the presence of functional groups. The percent removal capacity of B, Li, and Mo are studied under various experimental conditions including pH, initial concentration, and temperature. Surface characterization, morphology, and functional groups on the external surface of the adsorbents are investigated using Fourier transform infrared spectroscopy (FTIR), Brunauer Emmett Teller (BET), and scanning electron microscopy (SEM). FTIR showed that the availability of different oxygenated functional groups. SEM and BET indicated the surface area and porosity of the adsorbents. The result obtained successfully demonstrated the potential of using MDPs as an inexpensive, eco-friendly, and efficient adsorbent for B, Li, and Mo removal from GW.

Four adsorption models, namely Langmuir, Dubinin-Radushkevich, Freundlich, and Temkin are applied to investigate the adsorption process. For instance, it is found that the Langmuir model describes well the adsorption of Mo by AC at 25 °C, the adsorption of Mo by Bentonite at 35 °C, the adsorption of Li by Bentonite at 45 °C, the adsorption of Mo by RDPs at 35 °C, the adsorption of Mo by RDPs at 45 °C, and the adsorption of boron by bentonite at 45 °C.

The Freundlich isotherm model describes well the adsorption of Mo by AC at 25 °C, the adsorption of Li by AC at 35 °C, the adsorption of Mo by bentonite at 35 °C, the adsorption of Mo by bentonite at 45 °C, the adsorption of Mo by RDPs at 35 °C, the adsorption of Mo by RDPs at 45 °C, the adsorption of Li by MDPs at 35 °C, and the adsorption of boron by MDPs at 35 °C.

The negative values of Gibbs energy ( $\Delta G^\circ$ ) indicate a spontaneous and favorable adsorption process that is more favorable and spontaneous of the adsorption at high temperatures. The positive entropy values ( $\Delta S^\circ$ ) that controlled the adsorption process suggest the possibility of some structural changes or readjustments in the adsorbate–adsorbent complex.

MDPs showed the highest adsorption of Mo in all real GW samples. The adsorption of Mo increased with the increase in Mo concentrations, and the maximum Mo removal at 25 °C is 80%. All adsorbents, namely MDPs, RDPs, AC, and bentonite showed the same maximum percent of Li removal that reached 19% in GW sample 3. The maximum percent of boron removal at 35 °C is 40% using MDPs followed by RDPs, AC, and bentonite with 38%, 37%, and 36%, respectively.

## DEDICATION

*This dissertation and the work to which it refers are the results of my own efforts. Any ideas, data, images, or text resulting from the work of others (whether published or unpublished) are fully identified as such within the work and attributed to their originator in the text, bibliography, or in footnotes.*

## ACKNOWLEDGMENTS

I would like to thank Allah who granted me the health and strength that allowed me to overcome life's difficulties, fulfill my responsibilities as a mother of four children and accomplish this academic achievement. I would also like to thank my sons; Ibrahim, Yousef, and my daughters; Salha and Deema for dealing with a student mother who is more stressed and busier than usual.

I would like to express my gratitude to my supervisor Prof. Mohammad Ahmad Al-Ghouti from Qatar University for supervising the work, providing me the valuable information and generous support during this project. His incredible attention, advice, and guidance are highly appreciated. Special thanks to my committee members for their supervision help, and support.

Appreciations must go to the Environmental Science Center and Central Laboratories Unit at Qatar University for their help during the samples' analysis and measurement.

## TABLE OF CONTENTS

DEDICATION.....	vi
ACKNOWLEDGMENTS .....	vii
LIST OF TABLES .....	xiii
LIST OF FIGURES.....	xv
CHAPTER 1: INTRODUCTION.....	1
Groundwater Hydrogeology for the State of Qatar .....	1
Approaches to Achieve Sustainable Use and Management of Groundwater Resources in Qatar.....	3
Research Focus.....	10
<i>Research Rationale</i> .....	10
<i>Research Questions</i> .....	12
<i>Research Objectives and Hypotheses</i> .....	13
CHAPTER 2: RESEARCH REVIEW.....	17
Groundwater Interactions .....	17
Sustainable Groundwater Management .....	21
Water Resources Evaluation.....	22
Management of the Groundwater Quantity .....	25
Management of the Groundwater Quality .....	31
Groundwater Treatment .....	39



<i>Activated Carbon Adsorbent</i> .....	43
<i>Bentonite Clay Adsorbent</i> .....	46
<i>Date Palm Pits Adsorbent</i> .....	48
<i>Modified Date Palm Pits Adsorbent</i> .....	51
Groundwater Modelling and Mapping Using GIS .....	52
Drivers, Pressures, State, Impact, Response (DPSIR) Framework for Groundwater Resources Management .....	62
CHAPTER 3: RESEARCH METHODOLOGY .....	65
Sampling.....	65
<i>Selection of Sample Points</i> .....	65
<i>Sampling Documents</i> .....	66
<i>Sampling Steps</i> .....	66
Sample Analysis .....	67
<i>Field Analyses</i> .....	67
<i>Physiochemical Characteristics Analysis</i> .....	67
<i>Chemical Elements Analysis</i> .....	68
<i>Hydrogeochemical Water Quality Analysis</i> .....	69
<i>Statistical Analysis</i> .....	69
<i>Geo-statistical Analysis</i> .....	70
Adsorption Isotherm Experiment .....	71

<i>Adsorbent Preparation and Characterization</i> .....	72
<i>Optimization and Design of Adsorption Process</i> .....	73
<i>Modeling Adsorption Process</i> .....	75
<i>Adsorption Thermodynamic</i> .....	78
Statistical Analysis .....	79
CHAPTER 4: RESULTS AND DISCUSSION .....	81
Physical and Chemical Properties of the Collected GW Samples .....	81
<i>Major Anions Analysis</i> .....	83
<i>Major Cations Analysis</i> .....	86
<i>Trace Elements &amp; Heavy Metals Analysis</i> .....	88
Hydrogeochemical facies & General Water Quality Diagrams .....	88
Irrigation Water Quality & Irrigation Hazard Diagrams .....	92
Hydrogeochemical Saturation Index (PHREEQC Analysis) .....	95
Statistical Analysis .....	99
Comparisons with Standard and Guidelines .....	106
Comparing Interpolation Methods .....	109
Spatial Variability Analysis .....	113
Physical and Chemical Characteristics of Adsorbates .....	118
<i>Lithium</i> .....	119
<i>Boron</i> .....	120

<i>Molybdenum</i> .....	121
Physical and chemical characterization of the Adsorbents .....	122
<i>Brunauer Emmett Teller (BET) Analysis</i> .....	124
<i>The Fourier Transform Infrared Spectroscopy (FTIR) Analysis</i> .....	125
<i>The Scanning Electron Microscopy (SEM) Analysis</i> .....	131
Study the effect of pH on the Adsorption process .....	137
Study the Effect of Initial Adsorbate Concentration on Adsorption Process.....	143
Study the Effect of Temperature on Adsorption Process .....	147
Adsorption Models .....	153
<i>Monolayer Adsorption and the Langmuir Isotherm</i> .....	154
<i>Temkin Isotherm</i> .....	155
<i>Freundlich Isotherm</i> .....	156
<i>Dubinín–Radushkevich (D-R) Isotherm</i> .....	157
Thermodynamic Study .....	163
Mixture Solutions Adsorption Experiments .....	168
Real GW Adsorption Experiments .....	172
Statistical Analysis for Adsorption Experiments.....	177
Comparative Adsorption Study.....	179
CHAPTER 5: CONCLUSION.....	186
REFERENCES .....	191

APPENDIX .....	226
Appendix A: Groundwater Physical and Chemical Analysis. ....	226
Appendix B: Geostatistical Analysis.....	230
Appendix C: Statistical Analysis .....	256
Appendix D: Stiff Plots .....	268
Appendix E: Physical and Chemical Characteristic of Adsorbate .....	271
Appendix F: Adsorption Models.....	275
Appendix G: Statistical Analysis for Adsorption Experiments .....	299

## LIST OF TABLES

Table 1. <i>Some Nonconventional Adsorbents for The Removal of Pollutants from Water</i> .....	43
Table 2. <i>Interpolation methods Comparison (Li and Heap, 2014)</i> . ....	58
Table 3. <i>Saturation Indices Statistics Summary</i> .....	97
Table 4. <i>Average Well Depth by Hydrological Basins</i> .....	101
Table 5. <i>RMSE values obtained by the IDW interpolation method for different parameters</i> .....	110
Table 6. <i>RMSE values obtained by RBFs interpolation method for different parameters</i> .....	111
Table 7. <i>RMSE values and prediction indices obtained by the SK interpolation method for different parameters</i> .....	112
Table 8. <i>Crystal Radius, Hydrolysis Constant and Electronegativity for Adsorbate Ions</i> .....	119
Table 9. <i>Brunauer Emmett Teller (BET) Surface Area Parameters for Different Adsorbents</i> .....	125
Table 10. <i>Functional Groups on Activated Carbon (Socrates, 2015; Ewen and Geoffrey, 2019)</i> .....	130
Table 11. <i>Functional Groups on Bentonite (Socrates, 2015; Ewen and Geoffrey, 2019)</i> .....	130
Table 12. <i>Functional Groups on RDPs (Socrates, 2015; Ewen and Geoffrey, 2019)</i> . .....	131
Table 13. <i>Functional Groups on MDPs (Socrates, 2015; Ewen and Geoffrey, 2019)</i> .	

.....	131
Table 14. <i>The Effect of Temperature on Lithium Adsorption</i> .....	149
Table 15. <i>The Effect of Temperature on Molybdenum Adsorption</i> .....	149
Table 16. <i>The Effect of Temperature on Boron Adsorption</i> .....	149
Table 17. <i>Langmuir, Dubini-Radushkevich, Freundlich Parameters for the Adsorption Process by Activated Carbon.</i> .....	157
Table 18. <i>Langmuir, Dubini-Radushkevich, Freundlich Parameters for the Adsorption Process by Bentonite.</i> .....	159
Table 19. <i>Langmuir, Dubini-Radushkevich, Freundlich Parameters for the Adsorption Process by RDPs.</i> .....	160
Table 20. <i>Langmuir, Dubini-Radushkevich, Freundlich Parameters for the Adsorption Process by MDPs.</i> .....	161
Table 21. <i>Thermodynamic Parameters of Lithium Adsorption</i> .....	164
Table 22. <i>Thermodynamic Parameters of Molybdenum Adsorption</i> .....	164
Table 23. <i>Thermodynamic Parameters of Boron Adsorption</i> .....	165
Table 24. <i>The effect of the concentration of a mixture solution of lithium, molybdenum and boron on the adsorption process</i> .....	169
Table 25. <i>The Concentration of lithium, molybdenum and boron on the three studied GW samples.</i> .....	174
Table 26. <i>Comparative Study for Lithium Adsorption at 25 °C</i> .....	180
Table 27. <i>Comparative Study for Molybdenum Adsorption at 25 °C</i> .....	180
Table 28. <i>Comparative Study for Boron Adsorption at 25 °C</i> .....	180

## LIST OF FIGURES

<i>Figure 1. A. Qatar location map (Baalousha, 2016), B. Qatar geological map (Shomar et al., 2014), and C. Qatar land use map (Shomar et al., 2014).</i>	4
<i>Figure 2. Maps generated for A. boron, B. lithium and C. molybdenum concentrations in the Qatar's groundwater using the interpolation technique.</i>	15
<i>Figure 3. Scheme of the research questions.</i>	16
<i>Figure 4. Groundwater interactions with contaminants pathways.</i>	17
<i>Figure 5. Groundwater management interacting domains.</i>	21
<i>Figure 6. A. Comparison of average annual rainfall volume (billion m<sup>3</sup>) in GCC countries, B. Annual Groundwater withdrawal (billion m<sup>3</sup>) in GCC countries, and C. Total annual water resources and use (Million m<sup>3</sup>) in GCC countries (FAO, 2016).</i>	26
<i>Figure 7. A. The percentage of water resources in Qatar in 2016; B. The percentage of the utilization and discharge of treated sewage effluent (TSE) in Qatar in 2017; C. The percentage of the abstraction from GW basins; D. The percentage of the use of GW wells; E. Classification of GW r wells by salinity in 2014 in the south of Qatar (Al-Mashabiya) using FAO salinity classification; and F. Classification of GW wells by salinity in 2014 in the north of Qatar using FAO salinity classification (MDPS, 2017).</i>	27
<i>Figure 8. Comparison of the average TDS (mg/L) levels in groundwater in GCC Countries.</i>	28
<i>Figure 9. Percentages of irrigation techniques used in Qatar for the year 2001 (FAO, 2008).</i>	29
<i>Figure 10. Boron and lithium concentrations in groundwater of some GCC countries.</i>	

.....	36
<i>Figure 11. Groundwater categories A. Piper diagram B. Durov Diagram (El-Alfy et al., 2017).</i>	38
<i>Figure 12. Activated carbon structure showing different functional groups on the surface (Mochida et al., 2006).</i>	45
<i>Figure 13. Crystal structure of the individual montmorillonite particle (Apted &amp; Ahn 2017).</i>	47
<i>Figure 14. The mechanism of chloride and iodide ions adsorption on Ag–bentonite (Buzetky et al.,2020).</i>	48
<i>Figure 15. Binding mechanism of the date pits, cellulose and lignin, respectively with metal ion M<sup>2+</sup> (Al-Ghouti et al. 2010).</i>	50
<i>Figure 16. Interpolated map using kriging methods for electrical conductivity (EC) and total dissolved solids (TDS) of Wadi Usfan, western Saudi Arabia (Marko et al., 2013).</i>	55
<i>Figure 17. Vulnerability map of Qatar using EPIK and DRSATIC models (Baalousha, 2016).</i>	56
<i>Figure 18. DPSIR framework for groundwater resources in Qatar.</i>	64
<i>Figure 19. Groundwater sampled wells.</i>	65
<i>Figure 20. Adsorption process steps.</i>	72
<i>Figure 21. Distribution of A. major anions and B. major cations in the GW of the study area.</i>	84
<i>Figure 22. Piper Plot a. classification of Water Quality Types, b. Piper Plot for All GW Samples b. Piper Plot for South Basin Samples and c. Piper Plot for North Basin Samples.</i>	91



<i>Figure 23. Hydro-geochemical plots for GW Samples a. Schoeller Plot, b. Durov Plot, c. Ternary Plot and d. Ludwig Langelier plot. ....</i>	<i>92</i>
<i>Figure 24. Wilcox plot for groundwater samples. ....</i>	<i>95</i>
<i>Figure 25. A. Saturation Indices (SI) for All Sample Locations, B. SI for North Basin, C. SI for South Basin. ....</i>	<i>98</i>
<i>Figure 26. Hydrological Basin for the State of Qatar. ....</i>	<i>101</i>
<i>Figure 27. A. Principal Component Analysis Plot, B. Eigenvalues Loading plot. ....</i>	<i>105</i>
<i>Figure 28. Scheme of Date pits modification Methodology. ....</i>	<i>124</i>
<i>Figure 29. FTIR for activated carbon. ....</i>	<i>127</i>
<i>Figure 30. FTIR for bentonite. ....</i>	<i>128</i>
<i>Figure 31. FTIR for RDPs. ....</i>	<i>128</i>
<i>Figure 32. FTIR for MDPs. ....</i>	<i>129</i>
<i>Figure 33. Comparison FTIR between MDPs and RDPs. ....</i>	<i>129</i>
<i>Figure 34. Morphology characteristic of AC, RDPs and MDPs adsorbents. ....</i>	<i>133</i>
<i>Figure 35. Morphology characteristic of AC, RDPs and MDPs before and after the adsorption of Li. ....</i>	<i>134</i>
<i>Figure 36. Morphology characteristic of AC, RDPs and MDPs before and after the adsorption of the mixture of Li, Mo and B. ....</i>	<i>135</i>
<i>Figure 37. Morphology characteristic of AC, RDPs and MDPs before and after the adsorption of Mo. ....</i>	<i>136</i>
<i>Figure 38. Morphology characteristic of AC, RDPs and MDPs before and after the adsorption of B. ....</i>	<i>137</i>
<i>Figure 39. Study the effect of pH on lithium adsorption using activated carbon, bentonite, RDPs, and MDPs. ....</i>	<i>139</i>

<i>Figure 40. Study the effect of pH on molybdenum adsorption using activated carbon, bentonite, RDPs and MDPs. ....</i>	142
<i>Figure 41. Study the effect of pH on Boron adsorption using activated carbon, bentonite, RDPs and MDPs. ....</i>	143
<i>Figure 42. Study the effect of concentration on lithium adsorption. ....</i>	144
<i>Figure 43. Study the effect of concentration on molybdenum adsorption. ....</i>	145
<i>Figure 44. Study the effect of concentration on boron adsorption. ....</i>	147
<i>Figure 45. Study the effect of temperature on lithium adsorption using activated carbon, bentonite, RDPs and MDPs. ....</i>	150
<i>Figure 46. Study the effect of temperature on molybdenum adsorption using activated carbon, bentonite, RDPs and MDPs. ....</i>	151
<i>Figure 47. Study the effect of temperature on Boron adsorption using activated carbon, bentonite, RDPs and MDPs. ....</i>	152
<i>Figure 48. Van 't Hoff plot for adsorption process using bentonite. ....</i>	166
<i>Figure 49. Van 't Hoff plot for adsorption process using activated carbon. ....</i>	167
<i>Figure 50. Van 't Hoff plot for adsorption process using RDPs. ....</i>	167
<i>Figure 51. Van 't Hoff plot for adsorption process using MDPs. ....</i>	168
<i>Figure 52. The effect of the concentration of a mixture solution in boron adsorption. ....</i>	171
<i>Figure 53. The effect of the concentration of a mixture solution in lithium adsorption. ....</i>	171
<i>Figure 54. The effect of the concentration of a mixture solution in molybdenum adsorption. ....</i>	172
<i>Figure 55. The Study of boron adsorption from GW Samples at 25 °C. ....</i>	174

<i>Figure 56. The Study of Lithium adsorption from Real GW Samples at 25 °C.....</i>	<i>175</i>
<i>Figure 57. The Study of Molybdenum adsorption from GW Samples at 25 °C.....</i>	<i>175</i>
<i>Figure 58. The Study of boron adsorption from GW samples at 35 °C.....</i>	<i>176</i>
<i>Figure 59. The Study of lithium adsorption from GW samples at 35 °C.....</i>	<i>176</i>
<i>Figure 60. The Study of molybdenum adsorption from GW samples at 35 °C. ....</i>	<i>177</i>
<i>Figure 61. Schematic diagram of adsorption onto cellulose structure.....</i>	<i>184</i>
<i>Figure 62. Schematic diagram of adsorption onto Phenylpropanoid units found in lignin.....</i>	<i>185</i>

## CHAPTER 1: INTRODUCTION

Qatar is a semi-arid country located between latitudes north  $24.27^{\circ}$ - $26.10^{\circ}$  and longitudes east  $50.45^{\circ}$ - $51.40^{\circ}$  along the eastern region of the Arabian Peninsula (MDPS, 2018). The total surface area of Qatar is  $11,586 \text{ km}^2$ ; it is about 180 km in length and about 90 km in width (Baalousha, 2016). Qatar has flat rocky surfaces; nevertheless, it consists of some hills of 100 m above sea level (MDPS, 2017). The northern region of Qatar is relatively low elevations and increases slowly to the west and southwest; it is about 103 m above sea level in the southwest to about 6 m below sea level in Dukhan Sabkha (Sadiq & Nasir, 2002). Qatar is mostly located over a uniform limestone bed, and the oldest exposed rocks are the Lower Eocene Rus Formation that contains mostly of dolomite and limestone with few outcrops of Miocene (covering about 8%) of the surface area (MDPS, 2017). Karst is extensive in Qatar, it involves depressions, sinkholes, caves, and solution hollows. It is associated with the calcareous, dolomitic, and gypsiferous, anhydrite horizons of the Eocene Rus and Dammam Formations. It happened because of preferential dissolution related to the variation in composition between dolomitic, calcitic, and gypsum rocks (Sadiq & Nasir, 2002).

### Groundwater Hydrogeology for the State of Qatar

Qatar is located on the Arabian Peninsula, in the eastern region as shown in Figure 1A. The northern region of Qatar is relatively few elevations that are higher in the west and southwest, it is about 6 m below the sea level in Dukhan Sabkha to about 103 m above the sea level in the southwest. Qatar is mostly located over a uniform limestone bed. The oldest exposed rocks are the Lower Eocene Rus Formation, which

mostly contains dolomite and limestone with some dispersed rocks of Miocene (covering about 8%) of the surface area (MDPS, 2017). Karst is extensive in Qatar, it involves depressions, sinkholes, caves, and solution hollows. It is associated with the calcareous, dolomitic, and gypsiferous, anhydrite horizons of the Eocene Rus and Dammam formations. It happened because of preferential dissolution related to the variation in composition between dolomite, calcite, and gypsum rocks (Sadiq & Nasir, 2002).

Potable water has been found in Eocene age rocks in Qatar while the brackish GW has been found in upper Cretaceous age rocks (Shamrukh, 2012). In Qatar, the descriptions of the Middle Eocene age are Dammam formation, Rus formation, while Umm er-Radhuma is the Early Eocene/Paleocene age as shown in Figure 1B (Shomar et al., 2014; Al-Naimi & Mgbeojedo, 2018). The Dammam formation appears over most of the Qatar peninsula, the depth of the formation is about 50 m. The upper part has limestone, called the Abarug Member, underlain by chalky limestone, called the Umm Bab member and the lower part has a massive clayey fossiliferous limestone, known as the Dukhan member, underlain by the Midra Shale member of low carbonate (Al-Saad, 2005). The upper part is significantly fractured and has solution cavities (Alsharhan et al., 2001). The Rus formation conformably lies under the Dammam formation. The depth of Rus formation varies from 28-44 m in the north and central of Qatar, and about 110 m in the south-west of Qatar (Al-Yousef, 2003). It contains an abundance of limestone, dolomite, anhydrite, and some marl (UNDP, 2013). Umm er-Radhuma formation conformably lies under the Rus. It comprises a dense sequence of about 300-500 m of brownish or grayish limestone that is dolomitic and well porous in the upper part, which is characterized by the presence of well-fractured karstic dolomite (Jafari & Bernardeau, 2019). Most wells in the center and

south of Qatar reportedly tap the Rus formation aquifer, above the confining gypsum that covers up the Umm er-Radhuma formation aquifer. In north Qatar, most wells reportedly tap both the Rus and the upper of Umm er-Radhuma formation aquifer. While in the Abo Samra (southwest) GW wells reportedly tap the Alat aquifer of the Dammam formation, and some tap deep older Aruma aquifer of Aruma formation, which comes from Saudi Arabia (Al-Yousef, 2003). The aquifer of Dammam formation is unconfined in many areas due to erosion of the confining layers and/or the formation of karst structures (Alsharhan et al., 2001). The land use map in Figure 1C shows that most of the agriculture activities are in the north of Qatar due to the larger size (19% of Qatar surface area) and fewer salinity levels (500-3000 mg Cl/L) of the northern aquifer than in southern aquifer (> 5000 mg Cl/L) (Shomar et al., 2014).

#### Approaches to Achieve Sustainable Use and Management of Groundwater Resources in Qatar

In arid regions, water resources management is a very complicated practice due to the limited water availability and accessibility, in addition to climate change (Rajmohan et al., 2019). GW is highly affected by both natural and anthropogenic activities, which might make it unsuitable for domestic and irrigated agriculture (Mallick et al., 2018). For example, sea-level rise, saline water intrusion, high evaporation rates, and mineral weathering may increase the salinity and metals concentrations in the GW due to the dissolution of minerals under specific pH and redox levels (El-Alfy et al., 2017; Al-Shidi, 2014). The deterioration of GW quantity and quality is caused by the high demand for freshwater (Etteieb et al., 2015). Rapid urbanization, high agricultural development, and extensive GW pumping may affect GW quantity and quality (Al-Shidi, 2014). In addition, spills, sewage, and fertilizer leaching might

influence the GW quality (Mallick et al., 2018).

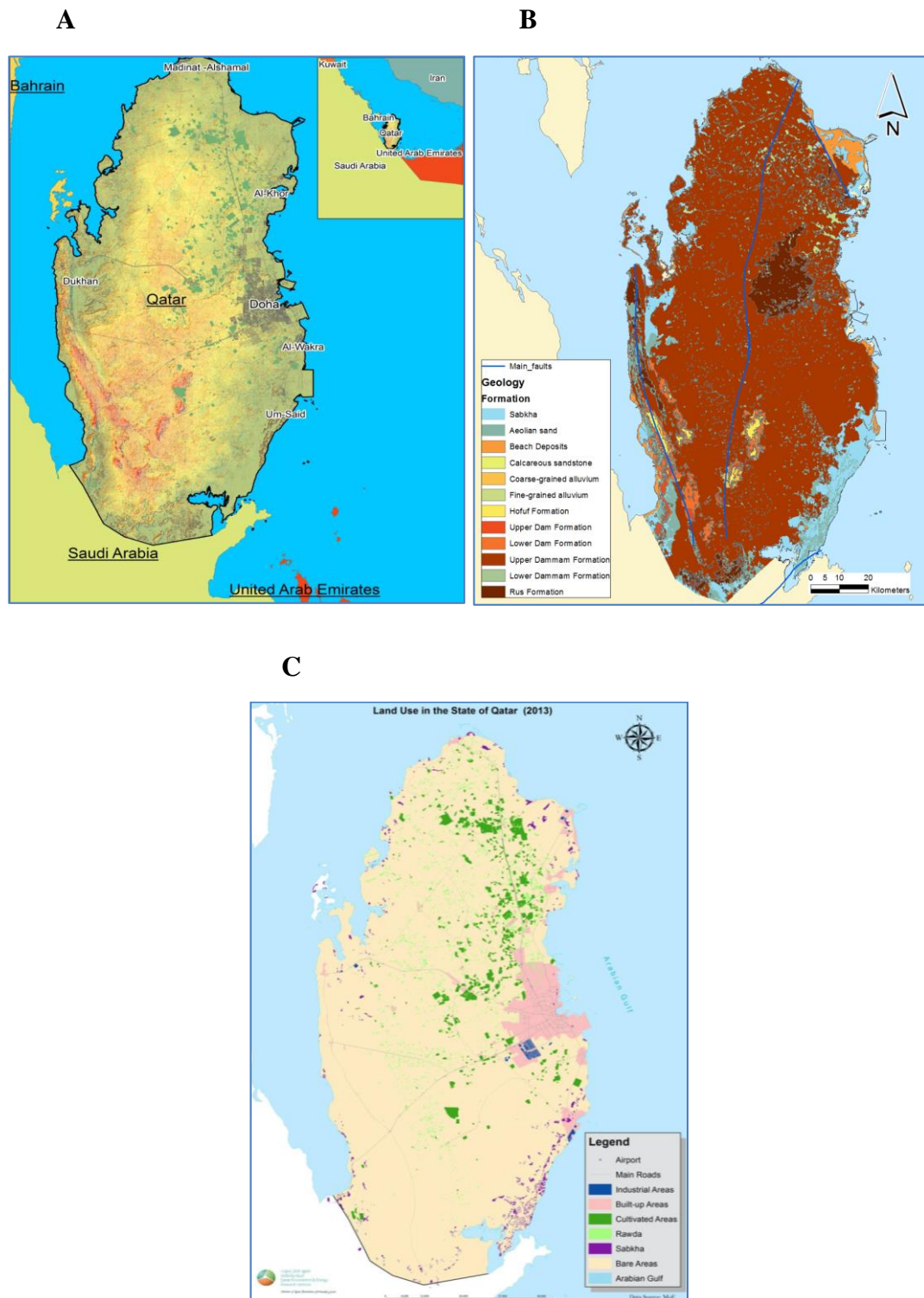


Figure 1. A. Qatar location map (Baalousha, 2016), B. Qatar geological map (Shomar et al., 2014), and C. Qatar land use map (Shomar et al., 2014).

The State of Qatar is located in the Arabian Gulf, which is considered as one of the semi-arid regions, with no surface water and restricted water resources from little rainfall; therefore, freshwater natural resources in Qatar are limited to GW (MDPS, 2017). Qatar has 80 mm average precipitation annually (MDPS, 2017). Desalination of seawater represents 59% of the total water production in Qatar, followed by a GW abstraction of about 30%, then treated wastewater that is used for agriculture and green spaces irrigation of about 11% (Baalousha,2016). All the fresh GW in Qatar comes from local rainfall, except for the confined slightly brackish water in Abu Samara, which receives inflow GW from west Saudi Arabia (UNDP, 2013). The annual recharge mainly comes from the infiltration of runoff, which is generally collected in surface depressions. The recharge of the GW by rainfall is estimated to be 25 million m<sup>3</sup> per year, which is similar to previous studies that estimated 7 to 10% of the annual rainfall (the average annual rainfall volume about 0.052 billion m<sup>3</sup>) in the north of Qatar, and 3.5-5% in the south of Qatar (Baalousha et al., 2018). However, the current GW abstraction reached 252.1 million m<sup>3</sup> per year, the annual water deficit due to the GW abstraction ranged from 100 million per year to 158 million m<sup>3</sup> per year during the period 2008 – 2014 (MDPS, 2017; SWS, 2009). The GW abstraction is mostly for agricultural uses accounting for 92% of the total abstracted GW of about 230 million m<sup>3</sup> per year. In 2014, no GW wells were characterized as non-saline or slightly saline, while 60% of GW wells were moderately saline and 40% highly saline (MDPS, 2017). Current GW abstraction greatly exceeds the rate of rainfall-induced recharge and this continues to result in the GW levels declining (MDPS, 2017). About 70% of the abstraction was from the north basin, such that the wells drill the Rus formation, which is of a depth 60-70 m. The overall number of wells with various uses was greater than 8509 where 74% of the overall wells are



farm wells of about 6299 wells (SWS, 2009). The GW basins in Qatar were classified into north, south, Abou-Samra, and Doha GW basins (SWS, 2009). The vast majority of wells are in the north, and south GW basins, the north, and south GW basins make up about 70 % and 28 % of total wells in Qatar, respectively (SWS, 2009). The over-extraction of Qatar's GW aquifers can reduce the aquifer levels, causing seawater intrusion; thus, the GW is highly vulnerable to salinization (Kuiper et al., 2015).

Climate change such as the decrease in precipitation and increase in evapotranspiration has a destructive result on the GW level due to the decrease in the GW recharge (Hoyos et al., 2016). For example, high evaporation of shallow GW may cause the dissolution of mostly halite and gypsum (Shomar, 2015). Among other climate processes, sand/dust storms and soil erosion may cause significant changes in the topsoil geochemistry (Shomar, 2015). Salinization of GW is a significant environmental issue. GW salinization mainly occurs as a result of high GW extraction which introduces the saline water from the deep underlying basement rock, from deep-buried valleys, or from adjacent surface water bodies, which also could be aggravated by drought and sea-level rise (Suursoo et al., 2017). The GW salinization might increase the total dissolved solids and enhance water-rock interaction (Vinson et al., 2013). A strong relationship between elevated levels of naturally occurring element levels such as the trace elements and minerals present in soils and rocks with salinity, as the hydrogeochemical condition has an important function in the distribution of these natural elements in the GW (Walsh et al., 2014). Soil with high salinity and metal mobility are significantly correlated, and this could increase the metal levels in GW (Shomar, 2015). The water resources are globally threatened by different contaminants (Manickum et al., 2014). For example, fertilizers, pesticides, and sewage can be an anthropogenic source of toxic elements in GW

(Seyedmohammadi et al., 2016). The produced water or coproduced water from oil and gas industries is very salty and contains a mixture of organic and inorganic residues; and generally, this produced water is disposed of with or without treatment to the sea or into the deep aquifer (Shomar, 2015). According to Shomar (2015) and Smedley & Kinniburgh (2017), the physicochemical characterization of the produced water and aquifer determine the different severe reactions and environmental consequences that might happen.

A study, investigating the physicochemical characteristics of carboniferous aquifers demonstrated that hydrogeochemical changes are induced not only natural but also anthropogenic processes (Galitskaya et al., 2013). The prime reason for hydrogeochemical changes is the disturbing of the hydrodynamic regime, such as the exploitation of the GW (Galitskaya et al., 2013). The local hydrogeological formations must be considered when allowing the maximum production rates as well as for developing a water quality-monitoring plan (Suursoo et al., 2017). The GW quality is also affected by rock interaction within the aquifer and the soil above the aquifer. Shallow coastal aquifers are more vulnerable to be contamination from surface soil due to the relatively short distance needed to reach the water table (Shomar, 2015; Kuiper et al., 2015). Carbonate aquifers in Qatar are within the karst formation and depressions; generally, karst aquifers are susceptible to pollution (Sadiq & Nasir, 2002). Anthropogenic contamination from agricultural effluents, and wastewater, above very fractured strata, could infiltrate contaminant very fast into the aquifer and extend over a large area (Baalousha, 2016). This is crucial, especially with the high economic growth, and the population of Qatar increases from 600,000 in 2000 to 2,685,000 in 2018 (MDPS, 2016). In Qatar, shallow GW with high hydraulic conductivity in the coastal and northern aquifers are of a high vulnerability

because of the depression areas, consequently, the southwest aquifers showed low vulnerability because of thick formations and vadose zone with a clay layer (midra shale), that block infiltration of water (Baalousha, 2016). In summary, the quality of GW can be affected by natural and anthropogenic variables such as climate change, drought, overexploitation, and socioeconomic development. Thus, assessing the GW resource in arid countries such as Qatar is of high importance due to its critical economic and social values as there are no other renewable water resources (Abdel-Satar et al., 2017).

Sustainable management of water resources relies on an integrated assessment of the hydrogeochemical systems (Khan et al., 2019). Various combined hydro-chemical processes determine the quality of GW along with its flow paths such as biological processes, weathering, ion exchange, and dissolution. The dissolution generally happens in the recharge zones and ion exchange happens along the flow path. On the other hand, ion exchange, evaporation, and precipitation take place mainly in the discharge zones (Mallick et al., 2018). Thus, the formation of the hydro-chemical facies/water types is a result of the geochemistry of the GW, which is further controlled by the geological structure and mineralogy of the aquifer (Ravikumar & Somashekar, 2015).

Different methodologies have been used to study the hydrogeochemical process and to investigate the quality of the GW such as multivariate statistical analysis, geochemical modeling, and using stable isotopes (Mallick et al., 2018). The current study evaluates the quality of the GW and related hydrogeochemical processes using up-to-date hydro-chemical graphical methods, geostatistical, and statistical analysis. Further, the study demonstrated the effects of agricultural practices in view of the natural influences (geological, hydrogeological, and climatic) and the anthropogenic

influences (agricultural) to support farmers, decision-makers, stakeholders to achieve sustainable GW management.

The cost-benefit analyses to help decision-making are derived by the analysis of ecological characteristics such as water quality, engineering such as water treatment technologies, societal demands such as food supply, and people perception of water quality. Thus, to achieve sustainable use and management of GW in Qatar, supply and demand management practices should be adopted. The major GW consumption is agriculture activities. Therefore, the management plan should focus on these activities. For demand management, educating the agricultural sector of the consequences of GW mining, encouraging the use of alternative sources of water, and the use of efficient irrigation techniques to lower GW extraction is of importance. For example, farmers should be encouraged to use desalinated seawater and treated sewage effluent (TSE) for irrigation rather than abstract GW. In addition, farmers are encouraged to adopt developed irrigation and agronomic practices such as using water-efficient irrigation methods (sprinkler and drip irrigation systems) and replacing water-intensive crops with water-efficient crops. In addition to developing cost reliable and efficient treatment techniques for low GW quality. The supply management should include developed monitoring systems, managed storage, recovery projects, and artificial recharge-by-recharge wells and lagoons using treated wastewater and desalinated seawater. In Qatar, the small number of GW users make some significant institutional approaches to sustain the quantity and quality of GW. Recently the GW characterization and measurement using advanced technology in data analysis, remote sensing and modeling generate significant data and knowledge to decision-makers with lower uncertainty. Remote sensing such as monitoring GW storage with reasonable accuracy using satellite gravimetry technology known as

Gravity Recovery and Climate Experiment (GRACE). Lower uncertainty of estimation of the quantity and locations of depletion GW resources result in sustainable and responsible management. To protect the GW quality, the monitoring strategy should include vulnerability maps using geostatistical analysis and interpolation models. In addition, the classification of aquifer systems should be developed.

#### Research Focus

The overarching research objective is to understand the distributions of some chemical element contamination in GW for the state of Qatar and develop functionalized date pits adsorbent for the removal of boron, lithium, and molybdenum from the groundwater.

#### *Research Rationale*

Qatar has recently undertaken the challenge to become the most self-reliant and sustainable country in the Middle Eastern region. Since then, the agriculture and farming industry has been blooming to increase food production in the country. Today, in Qatar, GW is the major renewable water resource comprising around 47.5 million m<sup>3</sup>/year. Qatar has been historically relying on GW (92% of the total abstraction) and treated wastewater (TWW) (nearly 35% of the total production in 2015) for agricultural activities (MDPS, 2017). GW abstraction is 30 times higher than average recharge rates; this has led to a dramatic drop in the GW table and an increase in salinity (MDPS, 2018). Previous research has shown that the total dissolved solids (TDS) in Qatar's GW vary from 1000 mg/L - 7500 mg/L which can cause reverse osmosis (RO) membrane scaling and therefore, requires expensive pre-treatment methods (Elsaid, 2017). The preliminary results have also shown that the

quality of the GW is declined, and several contaminants including toxic metals and metalloids are exceeding permissible limits. Boron (B), lithium (Li), and molybdenum (Mo) were found to be 1.28 mg/L, 0.08 mg/L, and 0.02 mg/L, respectively. These elements are of great concern as they can potentially induce toxicity to agricultural products. In addition to metals and metalloids, numerous studies have shown the presence of pathogenic microorganisms and other emerging toxic organic chemicals in TWW posing a significant risk to public and environmental health upon reuse (Al-Maadheed et al., 2019; Shomar and Hawari, 2017).

Since TWW and GW resources are predicted to be the most accessible and available in Qatar, it is essential to develop novel treatment approaches that are low-cost and environmentally friendly to improve the quality of these water sources in Qatar. This will help to enhance water security at the national level and resolve the problems of safe TWW reuse to yield GW with superior quality and quantity. The latter being the prime objective of the Qatar National Development Strategy (2018-2022). This is also in line with our previous studies (Ashfaq et al., 2018) in which Driver-Pressure-Status-Impact-Response (DPSIR) framework was used to analyze water resources in Qatar.

Qatar depends 100% on seawater desalination to meet the different needs of water. However, GW is the national strategic reservoir at all levels. High priority is given to GW management and protection. Generally, GW contamination by toxic elements may result from the natural and anthropogenic sources, such as the weathering of the earth's surface, wastewater used for irrigation land, in addition to effluent from city sewage and industrial wastewater (Assubaie, 2015; Karnib et al., 2014; Nriagu et al., 2007). From our preliminary study of the physicochemical characterization of the GW in the State of Qatar, the mean concentration of B, Li, and Mo (1.28, 0.079, and 0.02

mg/L, respectively) were higher than WHO limits of drinking purposes in some locations (11 out 35 samples). Using inverse distance weighted (IDW) parameters of power 3 and maximum neighbors 15 and type of 8 circular sectors generated the lowest root mean square prediction error (RMSE), consequently the best spatial variation output map as shown in Figure 2. About 11379.11 km<sup>2</sup> of the total area (97.76%) was high in boron levels, which exceeded 0.5 mg/L. High boron concentrations are in the coastal area of Qatar. Consequently, 2.21% (about 258.93 km<sup>2</sup>) of the total area is within this value mainly in the central area of Qatar. Whereas 34.08% (about 3966.88 km<sup>2</sup>) is higher than the USEPA irrigation water guideline of 1.5 mg/L (Singh and Verma, 2019). Also, about 9710.49 km<sup>2</sup> of the total area (83.42%) presented high Li concentrations, which exceeded the WHO drinking water guideline of 0.05 mg/L. High Li concentrations are found in the coastal area of Qatar. Consequently, 16.56% (about 1927.56 km<sup>2</sup>) of the total area is within the WHO drinking water guideline, mainly in the central area of Qatar. Similarly, it was also found that only 0.019% of the total area presented high Mo concentrations, which exceeded the WHO drinking water guideline of 0.07 mg/L. High Mo concentrations are in the central of Qatar. A total of 99.97% (about 11635.82 km<sup>2</sup>) of the area is within the WHO drinking water guideline. Whereas 74.36% (about 8655.09 km<sup>2</sup>) is within the USEPA irrigation water guideline of 0.01 mg/L. From previous studies, 205 samples of Qatar's GW, an elevated Mo (mean = 26.9 µg/L; max = 103 µg/L) were observed (Kuiper et al., 2015).

### *Research Questions*

The scheme of the research questions is shown in Figure 3. The research question is:

1. What are the concentrations of chemical elements in GW and topsoil samples?

2. What is the correlation between the chemical element levels in GW and physicochemical characteristics such as temperature, pH, cations and anions, electrical conductivity, TDS and TOC of the GW, and with the topsoil samples?
3. Will geostatistical interpolation using inverse distance weighted (IDW) be a significant method for mapping chemical element distribution?
4. What is the removal efficiency of lithium, molybdenum, and boron by activated carbon, bentonite clay, date pits, and modified date pits?
5. What is the effect of operating parameters, such as solution pH, temperature, initial adsorbate concentration, on the adsorption process?
6. Will modified date pits be a good adsorbent for the removal of lithium, molybdenum, and boron mixture in comparison with activated carbon, bentonite clay, and non-modified date pits?

#### *Research Objectives and Hypotheses*

**Objective 1:** Study the correlation between the physicochemical characteristics of the GW and soil samples collected from different areas in Qatar.

*Hypothesis 1.1:* pH, major cations and anions, electrical conductivity, total dissolved solids (TDS), total organic carbon (TOC), and temperature will change the behavior and transport of some chemical elements through some mechanisms such as sorption and precipitation. In addition, leaching and dissolution of some chemical elements from surface soil, which could increase their levels in GW.

*Hypothesis 1.2:* Locations with high salinity GW and intensive anthropogenic activities from industrial and agricultural sectors in some areas such as possible deposition and leaching processes from oil and gas production may change the occurrence and mobility of some chemical elements and could increase their



concentrations.

**Objective 2:** Investigate the spatial distribution of elements of concern in GW.

*Hypothesis 2.1:* Generating spatial interpolation maps (continuous surfaces) of GW quality data across Qatar using geo-statistical linear interpolation method such as inverse distance weighted (IDW) is easier than radial basis functions (RBFs), and simple Kriging (SK) due to its simplicity and easy mathematical formulations.

**Objective 3:** Develop adsorbents using the date pits and compare their physicochemical characteristic with those of commercially available adsorbents.

*Hypothesis 3.1:* The surface area for the adsorbents such as activated carbon, bentonite clay, date pits, and modified date pits will be high due to the high porosity structure.

*Hypothesis 3.2:* Modified date pits will be characterized by functional groups of carboxylates (-COO-) because mercapto-acetic acid (C<sub>2</sub>H<sub>2</sub>O<sub>2</sub>S) will convert hydroxyl groups to mercapto groups, which have a high affinity for metal ions.

**Objective 4:** Evaluate the adsorption capacity of activated carbon, bentonite clay, date pits, and modified date pits in removing Li, Mo, and B from GW.

*Hypothesis 4.1:* The removal efficiency of bentonite clay, date pits, and modified date pits will be high due to the large surface area and internal porosity.

*Hypothesis 4.2:* The removal efficiency of modified date pits will be significant due to high functionalize adsorption sites.

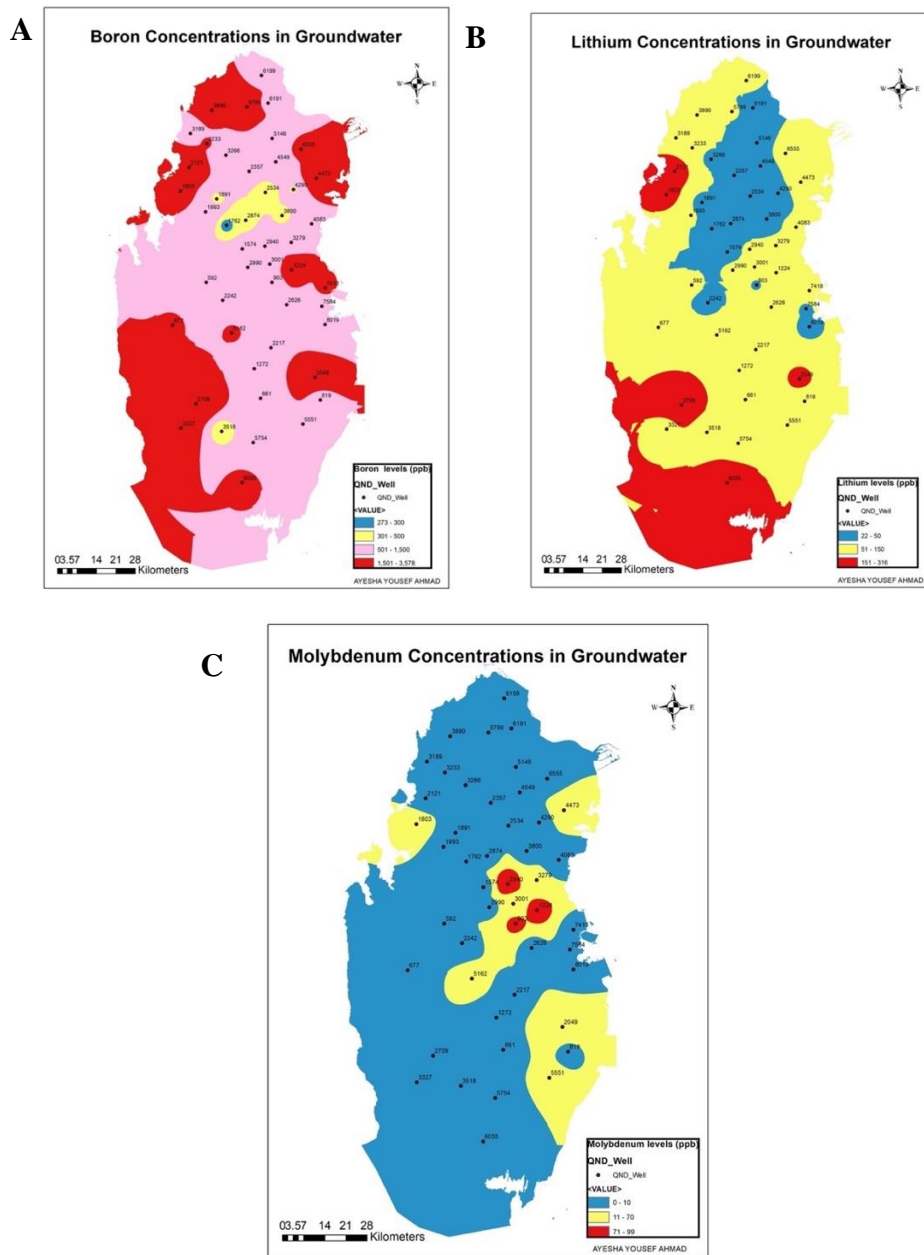
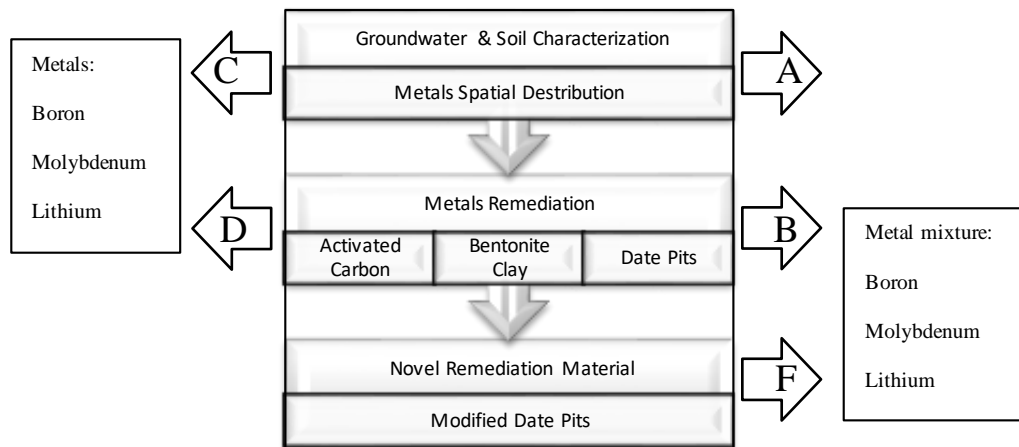


Figure 2. Maps generated for A. boron, B. lithium and C. molybdenum concentrations in the Qatar's groundwater using the interpolation technique.



**KNOWN SCIENTIFIC QUESTIONS:**

**C)** High **Molybdenum** (mean 26.9 µg/L; max 103 µg/L) was observed in Qatar’s groundwater (Kuiper et al., 2015). **Boron** concentration of (mean 2.06 mg/L; max 5.63 mg/L) and **lithium** concentration of (mean 0.11 mg/L; max 0.7 mg/L) was observed in Qatar’s groundwater. Total dissolved solids **TDS** was also high (mean 5447 mg/L; max 51550 mg/L) (SWS, 2009).

**D)** **Activated carbon** removed more than 90% of **Molybdenum** from liquor sample (Pagnanelli et al., 2011). 60% **boron** removal by activated carbon can be obtained from an initial boron level of 5 mg/L at pH 8–9 (Bonilla-Petriciolet et al., 2017). However, Bodzek (2015) stated that high doses of activated carbon required to remove 90% of boron from water. Seron (1996) showed the effect of applying treatments to the activated carbon such as ammonia or electrochemical treatment enhanced **lithium** adsorption.

**Bentonite** efficiently removed 81.3% of **Molybdenum** from water (Mojiri et al., 2017). Adsorption capacity for **boron** using bentonite was 0.9 mg/g while it was 0.09 mg/g by using activated carbon (Vhahangwele, 2015). 3800 ± 380 ppm of **lithium** was significantly adsorbed by bentonite (Hoyer, 2015).

**Date pit** ash has high **boron** removal efficiency (Al-Ithari et al., 2011; Al.Haddabi et al., 2015).

**UNKNOWN SCIENTIFIC QUESTIONS:**

**QUESTIONS:**

**A)** What is the correlation between the metal levels and physicochemical characteristics of the groundwater and topsoil samples?

(Objective 1)

**B)** Will geo-statistical interpolation using inverse distance weighted (IDW) be a significant method for mapping metals distribution? (Objective 2)

**E)** What is the removal efficiency of lithium, molybdenum and boron mixture by activated carbon, bentonite clay, date pits and modified date pits?

(Objective 3&4)

**F)** Will modified date pits be a good adsorbent for the removal of lithium, molybdenum and boron mixture in comparison with activated carbon, bentonite clay and non-modified date pits?

(Objective 4)

Figure 3. Scheme of the research questions.

## CHAPTER 2: RESEARCH REVIEW

### Groundwater Interactions

Interactions between GW and surface water bodies (known as hyporheic) and with the surface terrestrial environment are the main GW contaminants pathways (Smith, 2005). Figure 4 shows the potential contaminating sources from agriculture such as fertilizer, urban such as wastewater, and industry such as spills and leaks as well as the GW interaction with surface water bodies such as rivers and lakes. GW interactions may affect the transport of contamination within the ecosystem (IAEA, 1999). These interactions can be effective in removing and diluting the contaminant from reaching GW (IAEA, 1999).

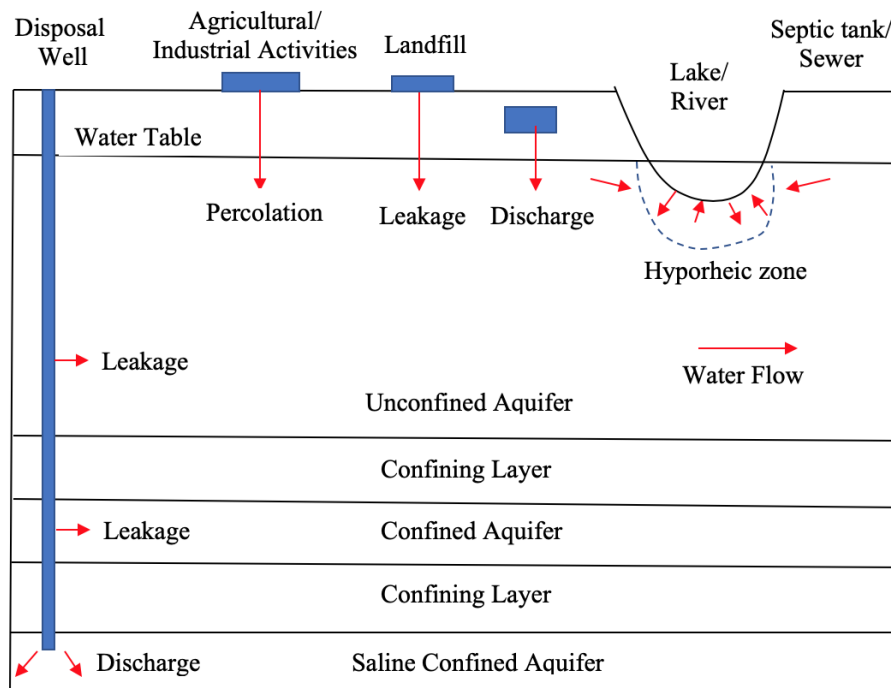


Figure 4. Groundwater interactions with contaminants pathways.

Furthermore, GW flux supplies organic matter and oxygen to stygofauna which live in the GW ecosystem (Humphreys, 2008). Numerous stygobitic species are a relict

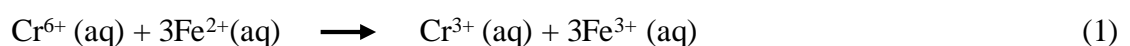
group of faunas that have diminished from surface systems (The relict group was once a diverse and widespread group then a significant change happened in their habitat and a subset of the group is survived in confined hospitable habitat) (Danielopol & Griebler, 2008). They are engineers of ecosystems that keep a good quality of GW for example the burrows the tubificid worms which adjust water flows and re-spread the sediments particle are significantly important to maintain the biogeochemical functions (Porter, 2007). Another GW interaction is the rock-water interactions within the aquifer. Re-distribution of elements may occur between the rock and aqueous system due to different mechanisms such as dissolution, precipitation, sorption, and desorption (Kumar et al., 2016). Rock-water interactions highly influence the quality of the GW through dissolution and cation exchange, which are the major mechanisms (Yehia et al., 2017).

The level of chemicals in a certain GW relies on the occurrence of the elements in the aquifer matrix and the mobility and the removal mechanisms from the GW by adsorption and precipitation (Porcelli, 2008). Therefore, the element levels in GW are controlled by the aquifer characteristic and the physicochemical characteristic of elements. The geological, hydrogeological, hydrological, physical, chemical, and biological characteristics of the aquifers control element levels and GW quality (Porcelli, 2008; Jakeman et al., 2016). The intrinsic properties of geologic and hydrogeological formations are aquifer lithology and the aquifer properties, which include permeability, effective porosity, and hydraulic conductivity gradient such as flow directions (Jakeman et al., 2016; Danielopol & Griebler, 2008). Here, flow directions and velocities are to provide information on rates of water recharge to the subsurface, locations, and rates of GW discharge to the surface and in any other features that represent boundaries for the GW flow system (Jakeman et al., 2016). The

aquifer's hydrological properties include precipitation and its rainfall water chemistry and spatiotemporal evapotranspiration, while the aquifer's biological properties such as meio- and micro-organisms and vegetation (Humphreys, 2008; Danielopol & Griebler, 2008; Porcelli, 2008). Rock-water interaction depends on mineralogical composition, the geochemical/hydro-chemical and physical conditions within the aquifer matrix such as the weathering of the rock, water flow, redox conditions, and soil ions retention time (Yehia et al., 2017). The physical characteristics of the aquifer that control mineral levels in GW are dense of the aquifer and the temperature of the water (Baeza et al., 2008). The geochemical processes that influence elements' behavior include dissolution, precipitation and/or co-precipitation, sorption (e.g. ion exchange, chemisorption), and biologically mediated reactions (Carvalho et al., 2017). Mainly high levels of calcium and carbonate ions indicate rock-water interaction, whereas high levels of Na and Cl ions indicate evaporation/crystallization actions. The ion ratio plot helps to identify different processes like ion exchange, mineral dissolution, and precipitation (Kanagaraj & Elango, 2016).

The transfer mechanisms of elements in GW are controlled by their physicochemical characteristics such as solubility and aqueous speciation, precipitation, adsorption and desorption capacities, volatility (Carvalho et al., 2017), and sensitivity to redox conditions which have a significant effect on the mobility of metals (Poinsot & Geckeis, 2012). For example, Maxwell et al. (2015), stated that metals, like cadmium (Cd) and zinc (Zn) complexes with organic matter in the soil are not stable; while copper (Cu), lead (Pb), or mercury (Hg) complexes are stable; nevertheless, some studies reported that dissolved organic matter may decrease Cd adsorption by the formation of some complexes. Cd and Zn are highly attached to clay minerals, carbonates, or hydrous oxides. Cadmium also can be precipitated such as cadmium

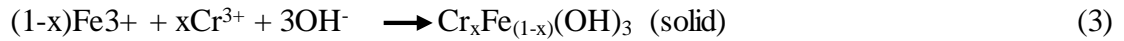
carbonate, hydroxide, and phosphate. The oxidation states of the toxic ions such as  $\text{Cd}^{2+}$ ,  $\text{Pb}^{2+}$ ,  $\text{Hg}^{2+}$ , and  $\text{Ag}^+$  are the most stable (Hashim et al., 2011; Wongsasuluk et al., 2013). The mobility of metals speciation, which may cause leaching to the aquifer, depends on various reactions in the soil environment such as acid/base, precipitation/dissolution, oxidation/reduction, sorption, or ion exchange processes (Fujinaga, 2016). Knowing that element speciation is the distribution of its chemical forms or species among different phases, thus, heavy metals forms can be divided into solid species that tend to be less mobile in comparison with colloidal or dissolved forms, and the labile complexes that in equilibrium with their environment whereas the inert complexes are not (Tamunobereton, 2011). In the GW management process, knowledge about metals speciation is important to understand their mobility. For instance, the mobility of the metals that are bound to solid can be enhanced by lowering the pH, changing the redox, increasing the inorganic salts, which compete for heterogeneous reactions and dissolved complexation, and increasing natural or synthetic complexing agents (Bourg, 1995). For example, Santos, (2002) study the spill on GW samples that reduce water pH, increase EC and S, Ca, Mg and K and heavy metals (Zn, Cd, Pb, and Cu) levels. Therefore, the authors change the pH of the polluted GW to the previous values before the spill to change metal speciation of Pb and Cu to less available forms as they precipitate while Zn and Cd remain available in mobile forms. Another example is stated by Hashim et al. (2011) to reduce Cr (VI) from chromium industry effluents using ferrous sulfate as reaction equation 1:



Then the rapid precipitation could happen when the pH was near neutral as reaction equation 2:



In addition, if excess Fe was available, then the reaction will be as equation 3:



### Sustainable Groundwater Management

Sustainable use and management of GW are very important processes for environmental, economic, and social development as shown in Figure 5. For example, due to the great spread technologies of extraction and distribution GW besides the low prices of these technologies, the quantity, and quality of GW are changed; so new irrigation technologies should be adopted such as root-zone irrigation, greenhouse technologies, or by saving the water consumptions through the reuse of wastewater in homes (Brown, 2018).

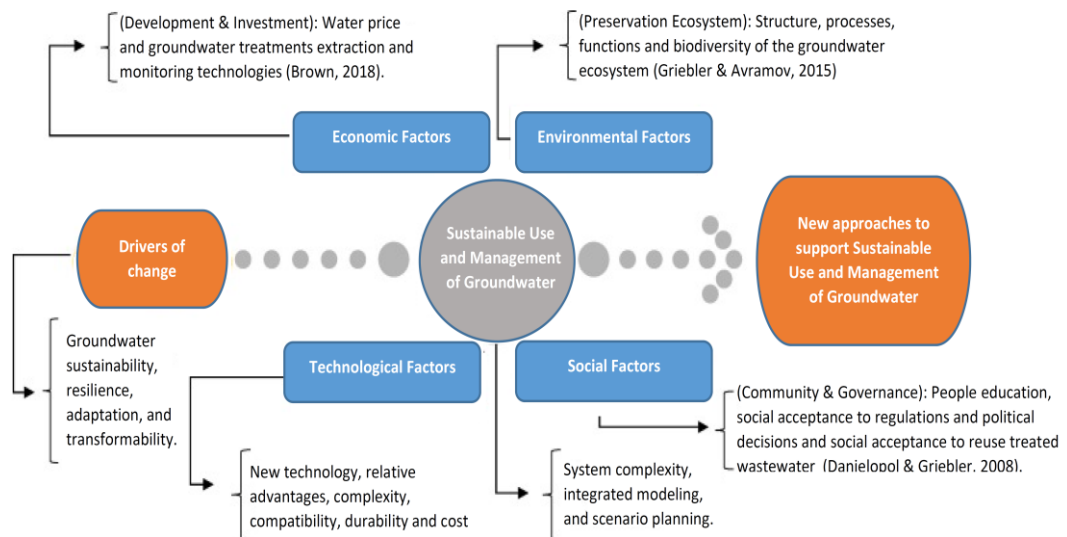


Figure 5. Groundwater management interacting domains.

However, GW deterioration was unnoticed for long periods, due to the invisibility of the GW resources, limited data, insufficient knowledge, inadequate detection and monitoring systems, and absence of integrated institutional (social, economic, and



ecological) frameworks (Jakeman et al., 2016). There is growing concern regarding the protection GW dependent ecosystems (GDE) to support sustainable water management that includes the protection of humans, flora, and fauna. Nevertheless, to protect GDEs, a comprehensive dataset is required for each location (Hoyos et al., 2016). The conservation of the quality and quantity of Qatar's GW resources contributes to supporting the implementation of the national development strategy (NDS) goals 2018-2022 that "ensure availability and sustainable management of water and sanitation for all" (MDPS, 2017).

### Water Resources Evaluation

The state of Qatar is a semi-arid country with no surface water and restricted water resources from little rainfall from May to November (MDPS, 2017). The mean annual rainfall is 80 mm per year (WMO, 2013), while the rate of evapotranspiration is about 2000 mm/y (Darwish et al., 2014). According to FAO (2016), the average annual rainfall volume for the Gulf Cooperation Council (GCC) countries is about 273.9 billion m<sup>3</sup>. Figure 6A shows the comparison of average annual rainfall volume in the GCC. It shows that the average annual rainfall volume for Qatar and Bahrain are very little of about 0.88 and 0.052 billion m<sup>3</sup>, respectively. Whereas the highest percentage of about 90% is from Saudi Arabia. Oman makes about 7% of the total annual rainfall for the GCC countries followed by UAE and Kuwait of about 2% and 1%, respectively.

Due to the low elevation in the surface of most of the GCC countries and the high evaporation rate, it is difficult to directly harvest the surface water runoff. Therefore, GW recharge is very limited. Figure 6B compares the total actual renewable water resources (billion m<sup>3</sup>) and the annual GW withdrawal (billion m<sup>3</sup>) between the GCC

countries according to FAO, (2016). As shown in Figure 6B, the GW withdrawal is very high in all GCC countries and it exceeds the total actual renewable water resources except in Oman. However, Oman GW withdrawal as a percentage of total actual renewable water resources is high 87%. The highest GW withdrawal as a percentage of total actual renewable water resources is from the UAE of about 2031%, followed by Kuwait withdrawal of about 2465%, then Saudi Arabia, Qatar, and Bahrain of about 943, 455 and 219.8 %, respectively.

The total annual water resources and use (million m<sup>3</sup>) in all GCC countries for the year 2005 as FAO (2016) are shown in Figure 6C. The highest percentages of the total water resources in the GCC are the surface and GW, and the highest percentages of water use are for irrigation and livestock. This paper emphasizes the importance of water in the GCC countries. The lack of freshwater resources is the main obstacle against sustainable GW management. Due to its larger population along with the adaptation of huge agricultural programs, Saudi Arabia alone consumes about 82% of the total water resources, whereas Bahrain, Qatar, and Kuwait, respectively, consume less water (Al-Rashed & Sherif, 2000).

Furthermore, Figure 7A shows the percentage of water resources in the state of Qatar for the year 2016. The GW is the single natural resource of fresh water in Qatar. As shown in Figure 7A, the main source of total water production is the seawater desalination of about 61%, followed by the GW abstraction of about 25%. The treated wastewater for agriculture and green spaces irrigation of about 13%, in addition to 1% water produced by the industrial sector for their own uses such as desalinated water (MDPS, 2017). Moreover, all wastewater treatment plants in Qatar have at least a secondary treatment level. The largest operational plant, treating 245,500 m<sup>3</sup> of wastewater on a daily basis, provides tertiary treatment for nitrogen and phosphorus

removal by biological treatment using an anaerobic-anoxic-aerobic method. Figure 7B presents the percentage of the utilization and discharge of treated sewage effluent (TSE) in the state of Qatar for the year 2017.

Furthermore, Figure 7C presents the percentage of the abstraction from GW basins in the year 2009 (SWS, 2009). The GW safe yield is defined as “the amount of water which can be withdrawn from a GW basin annually without producing an undesirable result such as decreasing GW recharge and depletion of aquifers” (Zhou, 2009). In the State of Qatar, the GW safe yield is estimated at about 55.8 million m<sup>3</sup> per year, whereas the current GW abstraction reached 250.8 million m<sup>3</sup> per year (MDPS, 2017). The annual water deficit is mainly due to the GW abstraction, which ranged from 97 million m<sup>3</sup> per year to 158 million m<sup>3</sup> per year during the period 2008 – 2016 (MDPS, 2017). GW abstraction is mostly for agricultural uses (about 296 million m<sup>3</sup> per year in recent years; 92% of total abstracted GW). Current GW abstraction greatly exceeds the rate of rainfall-induced recharge and this continues to result in declining GW levels and degradation of GW quality.

Figure 7D presents the percentage of the use of GW wells. The overall number of wells with various uses is greater than 8509 where 74 % of the overall wells are farm well (about 6299 wells), 15% are municipal wells, 3 % domestic wells, and 8% are industrial wells (SWS, 2009). The over-extraction of Qatar's GW aquifers can reduce the aquifer levels; causing seawater intrusion; thus, the GW is highly vulnerable to salinization (Kuiper et al., 2015). The freshwater lens in the northcentral part of Qatar has decreased in the area such that in 1971 it underlay around 15% of the country, and it is decreased in 2009 to around 2% of the country; the freshwater lens is around 11% of its size in 1971(SWS, 2009). In the year 2014, the GW levels in central and north were insignificantly above sea level. However, the GW level in Al-Mashabiya south

of Qatar was significantly below sea level (MDPS, 2017). According to FAO (1992) and based on the salinity classification, there is no well in Qatar characterized as non-saline in September 2014, whereas in April 1998, the percentage of the non-saline wells was 8%. The percentage of the little saline wells decreased from 19% to 11%, whereas the percentage of the high or very highly saline wells enhanced from 17% to 20%. In 2012, 69% of the wells were classified as moderately saline, making their waters harmful to sensitive crops, causing high soil salinity, and increasing the risk of higher sodicity (the amount of sodium held in a soil) (MDPS, 2017). Figures 7E and 7F represent the classification of the GW wells by salinity in 2014 in south and north of Qatar (Al-Mashabiya) using FAO salinity classification (non-saline water: < 0.7 dS/m, slightly saline water: 0.7-2 dS/m, moderately saline water 2-10 dS/m, highly saline: 10-25 dS/m, very highly saline 25-45 and brine >45 dS/m (1 dS/m = 1 mmho/cm) (MDPS, 2017).

According to the studies shown in Figure 8, all GCC countries except Oman showed moderately saline GW as the mean TDS in GW is higher than 1500 mg/L, while Oman showed slightly saline water according to salinity classification FAO (1992).

#### Management of the Groundwater Quantity

GW is a highly important natural resource that makes about 30% of the global freshwater and about 99% of the global liquid freshwater (Parkinson, 2010). The worldwide decline of the water table and GW storage during the last six months of the twentieth century was correlated with the significant GW extractions and climate changes such as global warming (Jakeman et al., 2016).

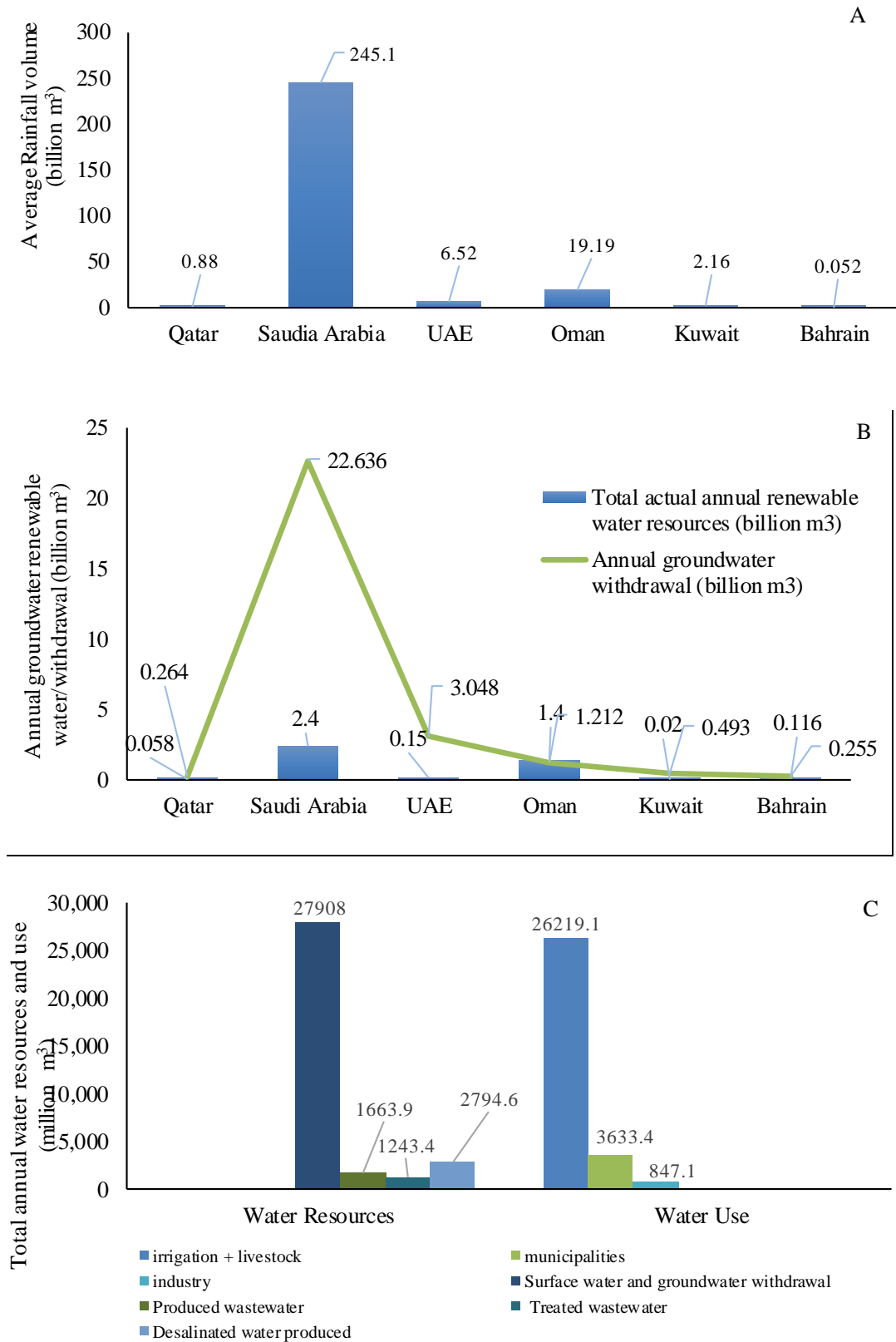


Figure 6. A. Comparison of average annual rainfall volume (billion m<sup>3</sup>) in GCC countries, B. Annual Groundwater withdrawal (billion m<sup>3</sup>) in GCC countries, and C. Total annual water resources and use (Million m<sup>3</sup>) in GCC countries (FAO, 2016).

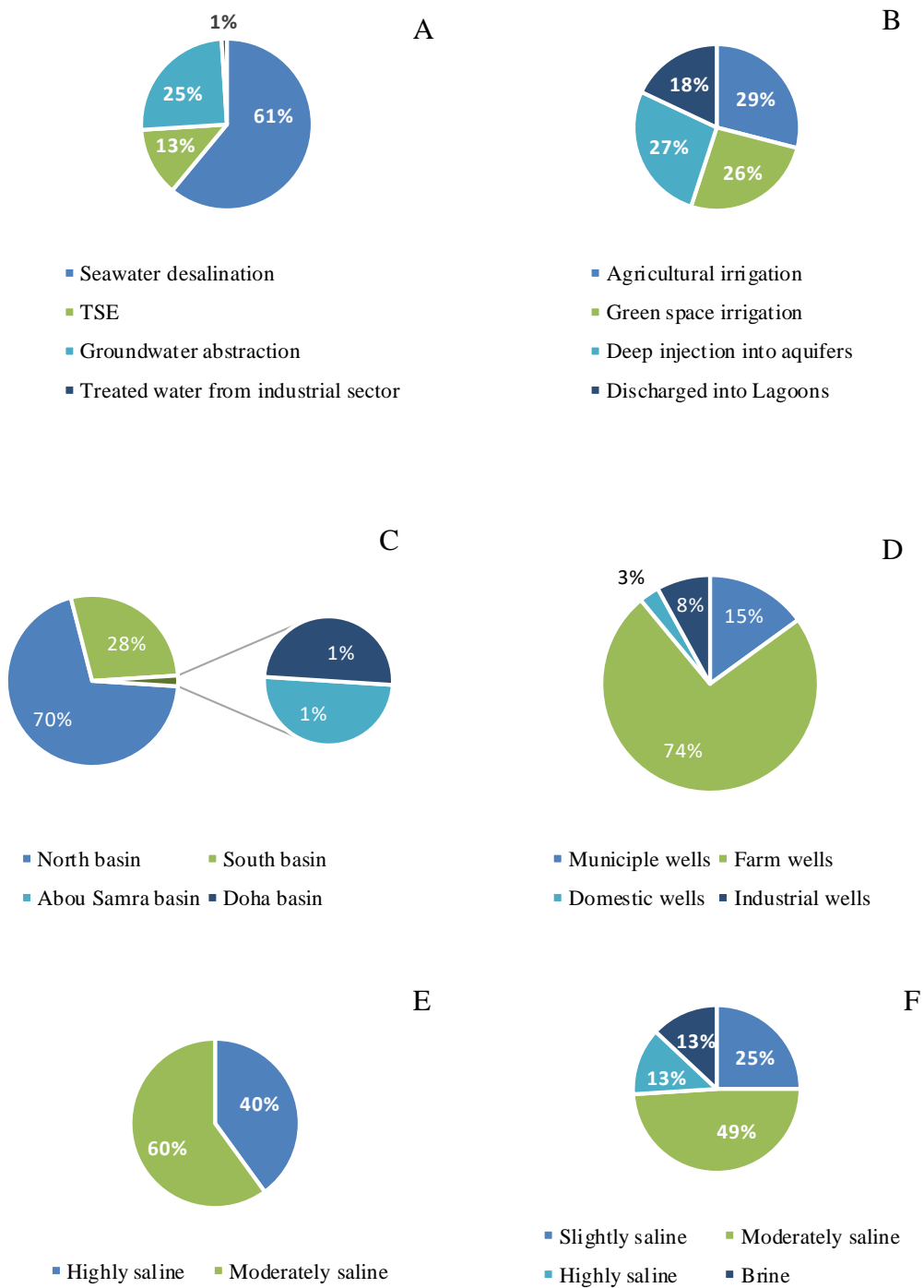


Figure 7. A. The percentage of water resources in Qatar in 2016; B. The percentage of the utilization and discharge of treated sewage effluent (TSE) in Qatar in 2017; C. The percentage of the abstraction from GW basins; D. The percentage of the use of GW wells; E. Classification of GW wells by salinity in 2014 in the south of Qatar (Al-Mashabiya) using FAO salinity classification; and F. Classification of GW wells by salinity in 2014 in the north of Qatar using FAO salinity classification (MDPS, 2017).

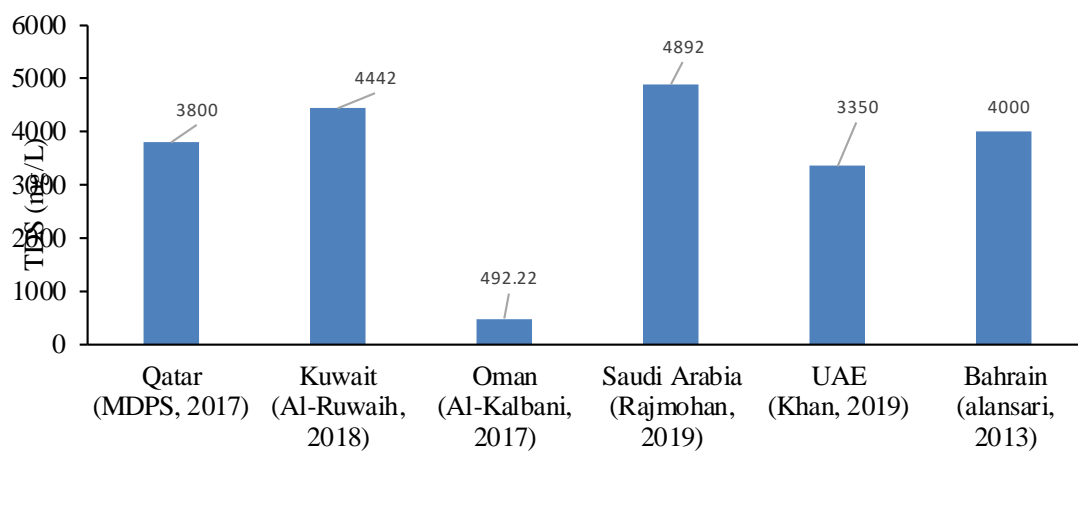


Figure 8. Comparison of the average TDS (mg/L) levels in groundwater in GCC Countries.

GW supplies significant percentages of freshwater to about 2 billion people, such it makes about 40% of the world's irrigation water and about 50% of the world's municipal water (Jakeman et al., 2016). Food demand required GW as a source for irrigated food production. Climate changes will enhance global water demand for food production by 70–90 %. According to that, the abstraction from non-renewable GW, which makes 18% of world gross irrigation water demand will significantly be increased (Jakeman et al., 2016).

In Qatar, the GW safe yield is about 55.8 million m<sup>3</sup> per year. However, the GW abstraction is about 250.8 million m<sup>3</sup> per year, which depletes aquifers, decreases GW levels, and rising salinity levels (Ashghal & Schlumberger, 2013). This is crucial especially with the high economic growth and the population of Qatar increase from 600,000 in 2000 to 2,685,000 in 2018 (MDPS, 2017). In 2011, irrigated agriculture used about 36.2% of total water resources in Qatar, where about 43% of the water used for agriculture is used to irrigate fodder crops and about 70% is used for flood

irrigation (Ismail, 2015). According to FAO, (2008), the most commonly used irrigation technique in Qatar for the year 2000/2001 is surface irrigation.

According to FAO (2008), surface irrigation such as by basins and furrows, which is irrigated about 9707.2 ha. While sprinkler irrigation is irrigated about 1813 ha, the dripper is irrigated about 868.6 ha and the bubbler is irrigated about 546 ha as shown in Figure 9.

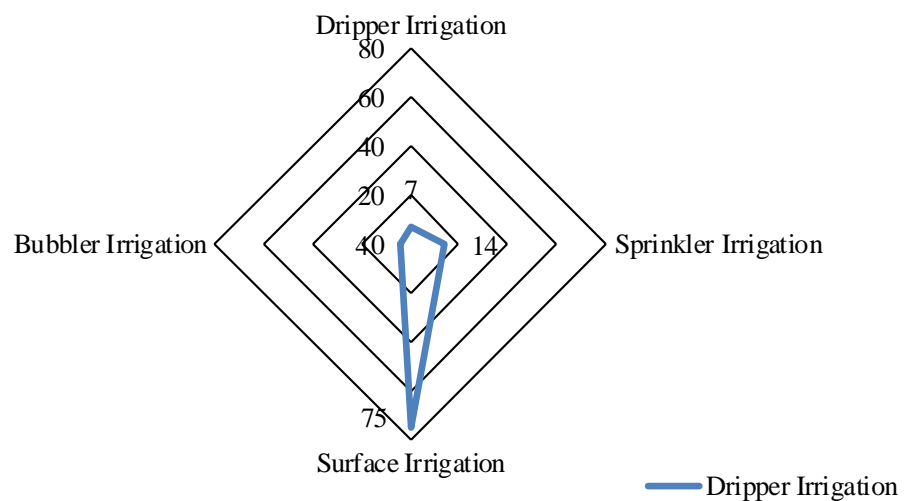


Figure 9. Percentages of irrigation techniques used in Qatar for the year 2001 (FAO, 2008).

Inadequate irrigation management and poor efficiency of irrigation system are directly related to GW management. Thus, Qatar’s government has supported agriculture and irrigation projects, research and studies which comprise crop water requirements of the main crops in Qatar, irrigation with saline water and its economics, enhancement the use of TSE for forage production mainly Rhode’s grass to feed livestock, modern greenhouses, and irrigation systems to increase the efficiency of the GW use (Hukoomi, 2019). In Qatar, it is estimated that a three-time



enhancement in domestic livestock herd size would be achieved by more than two times the share of TSE to agriculture/fodder production by 2020 (Brown, 2018).

Artificial recharge of GW aquifers by treated sewage effluent (TSE) injection, recharge wells and recharge from irrigation is about 54.6% of the annual additions to the GW reserve, whereas 43.4% of GW recharge is from rainfall and about 2% from its inflow from Saudi Arabia (SWS, 2009). Artificial Recharge is used to manage GW quality and quantity by using infiltration ponds or ditches, or injection wells that are used to increase infiltration, treat water through soil layers, and store GW in aquifers. It should be considered that treated water with quality as drinking water guidelines could be used to direct or indirect recharge, while water with degraded quality could be used for infiltration recharge that enhances additional natural treatment. However, artificial recharge management should search for simple and cheap pre-or post-water treatment technologies. The economic cost plays an important role in artificial recharge management. For example, infiltration ponds may reduce the costs of recharge water treatment. The planning and production development and water resources department in Kahramaa (Qatar general electricity and Water Corporation) established restrictions on future GW extraction by decreasing or restricting the use of wells (Kahramaa, 2016). Future projects for GW management are stated on the Kahramaa website such as monitoring GW abstraction from farms using advanced well water monitoring systems such as online from remote (Kahramaa, 2018a). In addition to the establishment of about 60 recharge and monitoring wells to enhance direct recharge and productivity of the aquifer system from rain (Kahramaa, 2018b). Kahramaa also conducting experiments to re-inject the aquifer artificially with desalinated water to meet water security (Kahramaa, 2016).

## Management of the Groundwater Quality

GW has higher concentration levels of natural elements than surface water because it passes through rocks and soil formations, dissolving different compounds and minerals (Caridi et al., 2017). Since mid of the 20th century, an extraordinary change in the world's ecosystems has been noticed due to the natural and anthropogenic activities, which rapidly altered the GW ecosystem structures and functions; the anthropogenic degradation of GW ecosystems is firmly correlated to the growing demands for natural resources (Danielopol & Griebler, 2008). For example, intensive use of water to sustain agriculture, industrial growth, economic development, and human increase. As a result, the environmental problems related to the GW extraction and use are increased (Hoyos et al., 2016) such as the GW depletion, soil collapse, seawater intrusion, loss of biodiversity, and decrease of GW quality because of the increase in different contaminant such as nutrients, salts, chemicals, and pathogens (Jakeman et al., 2016; Griebler & Avramov, 2015).

Climate change such as the decreasing precipitation and increasing evapotranspiration have a destructive result in GW concentrations due to the decrease in GW recharge (Hoyos et al., 2016). In Qatar, significant climate warming is detected at an increasing rate during a 30-year from 1983 to 2012 (Cheng, 2015). For example, high evapotranspiration of the shallow GW may cause the dissolution of mostly halite and gypsum (Shomar, 2015). Among other climate processes, sand/dust storms and soil erosion may cause significant changes in the topsoil geochemistry (Shomar, 2015). GW salinity is a significant environmental issue; salinization mainly happens as a result of intensive g GW use; leading to saline water introduce from deep underlying basement rock, from deep-buried valleys or from adjacent surface water bodies, which also could be aggravated by drought and sea-level rise (Suursoo et al., 2017).

Salinization may increase the total dissolved solids and enhance water-rock interaction (Vinson et al., 2013). A strong relationship is existing between elevated levels of naturally occurring element levels with salinity, as the hydro-geochemical condition has an important function in the distribution of these natural elements in GW (Walsh et al., 2014). A significant correlation between the high salinity of soil and metal concentration in the GW is present (Shomar, 2015). For example, the study of Acosta et al., (2011) shows that the soil salinity enhances heavy metal mobilization as shown by Pb, Cd Cu, and Zn release from the soil by competition with calcium for sorption sites, complexation with chlorides, complexation with sulfates, and competition with Mg and/or Ca.

Moreover, there are anthropogenic sources of GW contamination with metals, including leachate from landfill sewage, waste disposal, agrochemicals, and industrial waste, or industrial spills and leaks (Rehman et al., 2017). The water resources are globally threatened by different contaminants from residential, municipal, commercial, industrial, and agricultural activities (Manickum et al., 2014). The spillage and leakage of an industrial chemical such as methyl tertiary-butyl ether (MTBE) by accident is considered as a serious GW contamination (Jakeman et al., 2016). Besides, fertilizers, pesticides, sewage, and industrial wastes can be an anthropogenic source of toxic elements in GW (Seyedmohammadi et al., 2016). The produced water or coproduced water from oil and gas industries is very salty and contains a mixture of organic and inorganic residues; generally, in the past this produced water is disposed of with or without treatment to the sea or into the deep aquifer (Shomar, 2015). Different severe reactions and environmental consequences occur according to the physicochemical characterization of the produced water and aquifer (Shomar, 2015; Smedley & Kinniburgh, 2017). Another new anthropogenic

source of GW contamination is known as the emerging organic contamination (EOCs) such as synthetic micro-organic compounds used in healthcare, food preservation, and pharmaceutical products (Jakeman et al., 2016).

The chemical, physical, and biological characteristics of the aquifers function together and alter GW quality (Jakeman et al., 2016). Physical processes such as dispersion/dilution and filtration, chemical processes such as complexation, acid-base reactions, oxidation-reduction, precipitation-solution, and adsorption-desorption, and biochemical processes such as microbial respiration and cell synthesis influence water quality in aquifers (Bartram & Balance, 1996). As an example, McCarthy (2001) stated that with increasing the temperature and precipitation with climate change, the weathering of base cation might increase and change alkalinity of infiltration water; increase the temperature might also enhance the growth of microorganism, which plays a role in oxidation/reduction of elements and alter the quality of GW. The study of physicochemical characteristics of the carboniferous aquifers demonstrated that hydro-geochemical changes are induced from not only natural but also anthropogenic processes (Galitskaya et al., 2013). The prime reason for hydro-geochemical changes is the disturbing of hydrodynamic regimes such as climate change (sea level rise and spatial /temporal alteration in precipitation and evapotranspiration) and overexploitation of the GW (Jakeman et al., 2016). Thus, local hydrogeological formations must be considered when allowing the maximum production rates as well as for developing a water quality-monitoring plan (Suursoo et al., 2017). In addition, the GW quality is affected by rock interaction within the aquifer and soil above the aquifer. Shallow coastal aquifers are more vulnerable to be contamination from surface soil due to the high population densities and relatively short distance needed to reach the water table (Shomar, 2015; Kuiper et al., 2015). The Saq and Wajid

aquifers in Saudi Arabia have low salinity of TDS lower than 1500 mg/L. However, the carbonate aquifer has a salinity that reaches 15,000 mg/L in the east of Saudi Arabia and toward the Arabian Gulf (Al-Rashed& Sherif, 2000; Rajmohan et al., 2019). Carbonate aquifers such that in Qatar are within the karst formation and depressions; generally, the karst aquifers are susceptible to pollution (Sadiq & Nasir, 2002). Anthropogenic contamination from the agricultural effluents and wastewater, above many fractured strata, could infiltrate contaminant very fast into the aquifer and extend over a large area (Baalousha, 2016). In Qatar, shallow GW with high hydraulic conductivity in the coastal and the north aquifers are of a high vulnerability because of the presence of depression areas. Consequently, the southwest formation is thick formations with a thick vadose zone with a clay layer (midra shale) that block infiltrations of water and lower the vulnerability of the southwest aquifers (Baalousha, 2016).

In summary, due to the complicated GW systems such as recharge, discharge, and land use, natural and anthropogenic variables such as climate change, drought, overexploitation, and socio-economic development could change water quality (Jakeman et al., 2016). There is a worldwide growing concern regarding the quality of the GW because of the significances of the water to support people's life. The expanding use of GW resources for agriculture and irrigation purposes requests a careful hydro-geochemical evaluation of the GW. High-quality water resources are significant factors to sustain social and economic development (Manickum et al., 2014). In arid countries such as Qatar, GW is the most valuable natural resource; hence, assessment of the presence of chemicals in GW, as well as other water quality parameters, is vital for sustainable use. The levels of potentially toxic metals are significant factors affecting GW quality (Yehia et al., 2017). An investigation of the

potentially harmful elements in GW sources is of importance to protect public health. In Qatar, there is a significant freshwater shortage because of the low annual rainfall, in addition to the large amount of GW extraction that resulting in severe GW deterioration. Some deterioration of GW quality has already been observed in the coastal areas in the north and east sides of Qatar due to the current high extractions. The expanded use of the GW resources for agriculture and irrigation purposes requires a careful hydro-geochemical evaluation of the GW in the state of Qatar to develop effective recommendations by the concerned authorities.

GW in the GCC countries is of a limited quantity and mostly poor quality due to the high agricultural and some oil-related activities to increase the recovery and the production of oil (Al-Rashed & Akber, 2015). In 2009, the department of agriculture and water resources (DAWR) in the State of Qatar has conducted a national GW survey to understand and manage the GW resources through collecting information on GW occurrence, GW quality, recharge rates, and GW use (SWS, 2009). The water quality monitoring results showed that sulfate and B were higher than the drinking water standard of 250 and 0.5 mg/L, respectively, or irrigation guidelines of 400 and 1.5 mg/L, respectively. Moreover, fluoride was also found to be above the drinking water guideline of 1.5 mg/L (SWS, 2009). A potential source of Mo in Qatar's GW (mean = 26.9 µg/L; max = 103 µg/L) could be from the oil and gas processing sector as mainly the local natural gas is a sulfur-containing, and Mo is used as a catalyst in the desulfurization process (Kuiper et al., 2015). Qatar plans to produce water for agriculture using energy-efficient desalination plants such as using solar energy (Ismail, 2015). Similar high concentration of Mo of a mean of about 98 µg/L that explained by authors as oil shale rock in the study area that contains high Mo and agricultural activity such as fertilizers (Al-Kuisi et al., 2015).

Figure 10 shows the mean detected values for B and Li in Qatar, KSA, and Oman. The maximum detected value for boron in KSA GW was 3.56 mg/L. This is explained by infiltrating wastewater, that boron is used in soaps and detergents manufacturing.

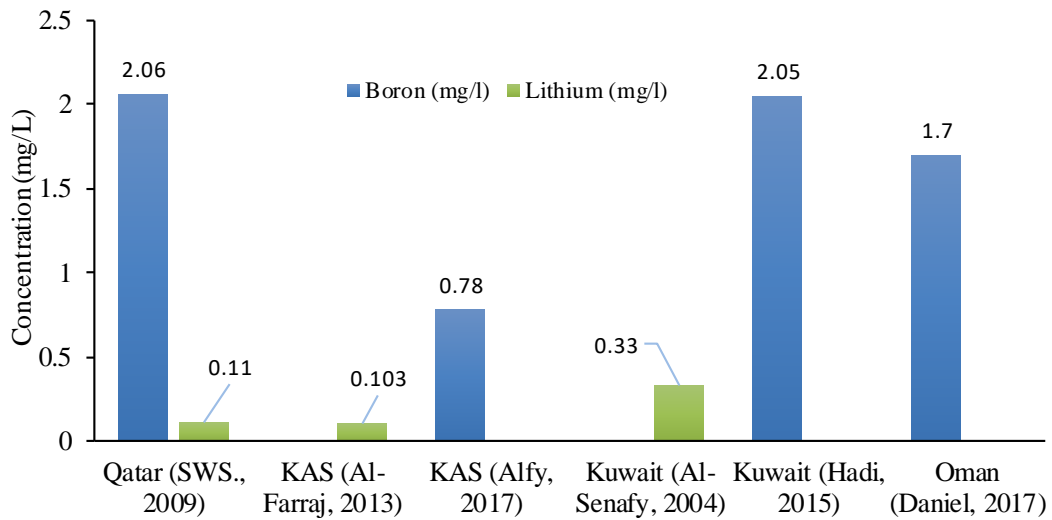


Figure 10. Boron and lithium concentrations in groundwater of some GCC countries.

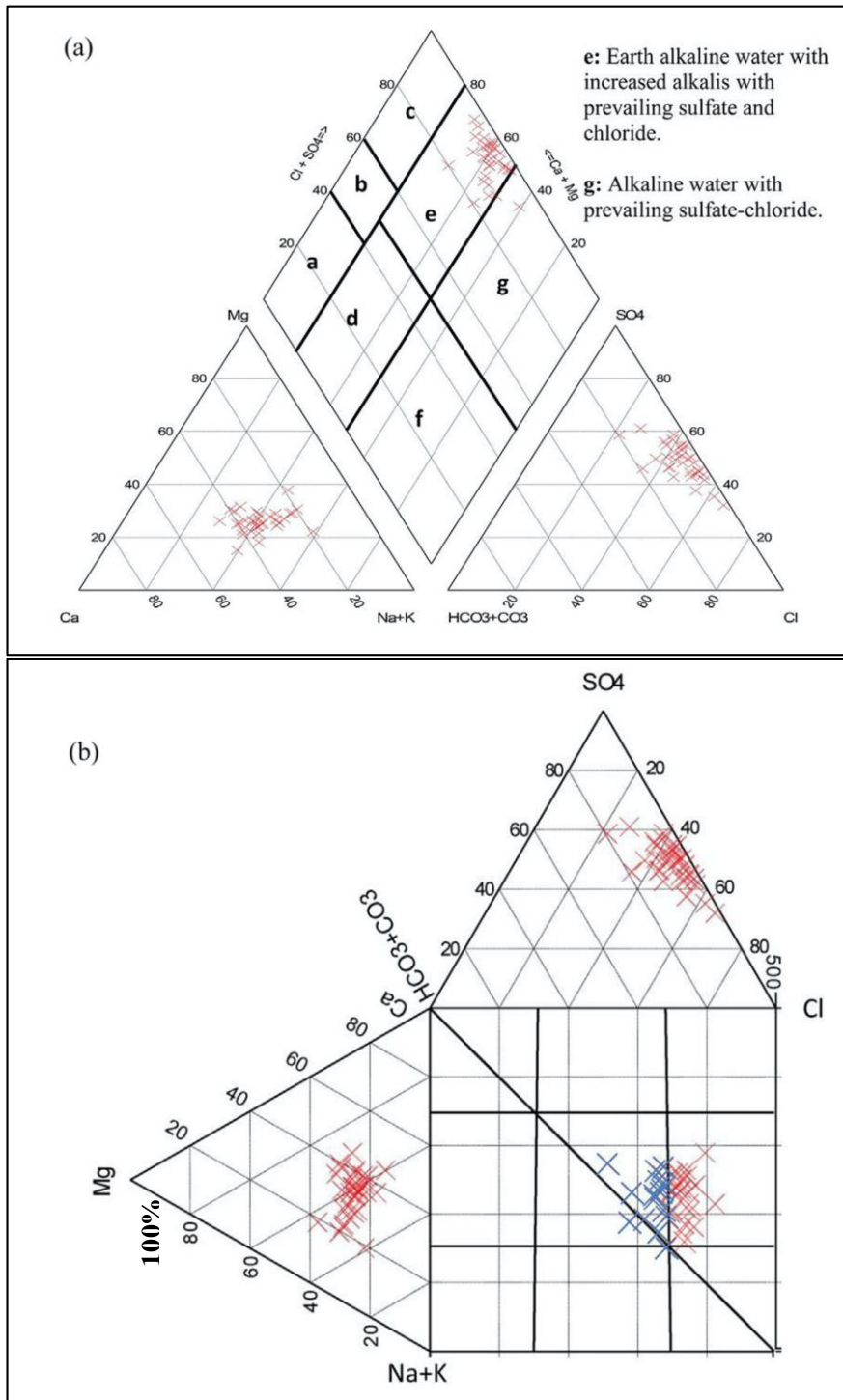
Also, the release of boron from rock water interaction that boron enhancement is occurred by ion exchange of saline GW that decreases Ca and increases Na as shown by Piper and Durov diagrams in Figure 11 (El-Alfy et al., 2017). El-Alfy et al., (2017) indicated from the Piper diagram two types of GW, which are high alkalis with sulfate and chloride as dominant and alkaline water with prevailing sulfate-chloride ions. While Durov diagrams illustrated that about 40% of water is rainfall water ( $\text{Ca}(\text{HCO}_3)_2$ ), and  $\text{MgSO}_4$  and  $\text{CaSO}_4$  which were dissolute of sulfate and carbonate mineral, and then mixed with the irrigation return flow and 60% of water is  $\text{MgCl}_2$  and  $\text{NaCl}$  type, which are derived from the dissolution of Na-Mg-rich host carbonate rocks. These results are supported by the calculated mean values of the mineral phase saturation indices that show under-saturation conditions and consequently increase

GW salinity with the GW path flow from southwest to the southeast (El-Alfy et al., 2017). The study of Daniel et al. (2017) showed that the average boron in Rus formation aquifers is 1.7 mg/L, and in Dammam formation aquifers are 1.04 mg/L due to boron desorption from mineral surfaces (Daniel et al., 2017). In Kuwait, Mo was detected below 0.05 mg/L; however, strontium concentration is up to 36 mg/L, Li levels of up to 2 mg/L, and boron was above the irrigation standard (Al-Senafy, 2004).

The study of GW in Al-Ahssa, Saudi Arabia, showed that the GW was not contaminated by some chemical elements from anthropogenic sources, and it was less than the maximum FAO's guidelines except for Cu, Cd, Fe, and Pb which were very high (Abdel-Satar et al., 2017). Furthermore, the high concentration of Cadmium is detected in UAE was about 0.429 mg/L, which is higher than the WHO permissible limit (Khan et al., 2019). Results of GW of North West Bank in Palestine indicated a possible human risk from some chemical elements.

The study showed that Cr, Mn, Ni, Cu, Mo, and Al were observed in all samples with Co and Thallium (Tl), which are significant toxic metals (Malassa et al., 2014). In another study of GW from Al Minya, Egypt showed that the levels of Cr and Pd are higher than the maximum permissible limits suggested by environmental organizations in different countries; the authors recommended that the GW must not be used for drinking purposes unless it is treated before (Bassioni et al., 2015). Various international concentrations of some chemicals present in GW are illustrated in Appendix A.





About 40% of groundwater samples (blue) show no dominant anion or cation. The remaining 60% of water samples (red) represent the MgCl<sub>2</sub> and NaCl type.

Figure 11. Groundwater categories A. Piper diagram B. Durov Diagram (El-Alfy et al., 2017).

## Groundwater Treatment

GW remediation applies various techniques such as chemical remediation, which is widely used for controlling large plumes contamination. Xie et al. (2018), classified the methods for chemical remediation as chemical precipitation, coagulation, ion exchange, chemical oxidation, chemical reduction, solidification, and stabilization. Chemical remediation requires high operational and maintenance costs and complicated steps; moreover, it generates toxic sludge (Ahmad et al., 2011). Chemical precipitation is relatively expensive according to chemical agent costs and needs safety controls (Zhang et al., 2018). Ion-exchange resins have high regenerated efficiency compared with adsorbents (Hashim et al., 2011). Ozone is broadly used in chemical oxidation due to its strong oxidation characteristic. Nevertheless, the low efficiency of chemical oxidation by ozone in GW remediation is due to the low solubility and fast decay rate of ozone in liquid solutions (Temesgen et al., 2017). Physicochemical remediation methods of GW such as membrane and filtration technologies are of different kinds, like an electro-dialytic membrane, liquid membrane, polymer membrane, ultrafiltration membrane, nanofiber membrane, and reverse osmosis (Yanga et al., 2017). Reverse osmosis generates a lot of wasteful water (Xie et al., 2018). Filtration and membranes are of high capital and energy costs; and there are membrane clogging and sludge discharge complications (Ayanda et al., 2017). Another treatment of GW is biological remediation, which is broadly studied and developed due to various factors such as its cost-effectiveness with fewer by-product pollutants and long-term sustainability (Lofrano et al., 2013). However, biological remediation does not have the ability to remove pollutants from deep aquifers and it considers long-term remediation methods, besides the biosafety issues

that need to be developed (Ayanda, 2017). Various living organisms such as plants, fungi, bacteria, yeast, and algae capture pollutants inside their bodies or enhances the removal of pollutants such as biosurfactants. There are many benefits of biosorption remediation such as it is high economic efficiency, it generates low chemical or biological sludge, it has high removal capacity, there is an opportunity for the recovery of metals, and bio-sorbents regeneration is possible (Ye et al., 2012). Conventional adsorbents, such as ACs are expensive, cause environmental problems, such as the non-biodegradable nature of silica gel, and their regeneration cost is also high. Whereas the non-conventional adsorbents such as natural material sorbents are of extensive source, environment friendly, and low cost. The non-conventional adsorbent could be natural minerals like clay, cellulosic materials such as agricultural wastes, sludge, and fly ash from industrial by-products (Guan et al., 2016). The attractive forces between adsorbed pollutants (adsorbates) and the adsorbent surface are weak Van der Waals forces, hydrogen bonding, and dipole-dipole interaction, which provides significant desorption (Al-Ghouti et al., 2010).

Upon investigating potential treatment options, the operation and maintenance costs in addition to removal efficiency should be considered to keep the system running (Esmeray & Aydin, 2008; Shafiq et al., 2019). The adsorption methods are of high efficiency for the removal of different pollutants, practical, easy, simple, low cost, low chemical and biological sludge and there is a possibility for regeneration of adsorbent and metal recovery (Dodbiba et al., 2015; Ahmad et al., 2011; Huang et al., 2016). Adsorption is like an ion-exchange technique but in ion exchange, the elements are exchanged with ion (counter-ion) on the active sites (Wang & Dong, 2009). Sorption is also assessed as an eco-friendly treatment method (Yang et al., 2009). Adsorption technique is of metals removal selectivity and high efficiency

(Karnib et al., 2014; Amin et al., 2016). Various sorbents are used in adsorption processes for water treatment such as the adsorption of metal ions onto adsorbent surfaces (Shafiq et al., 2019). AC adsorption is a common efficient treatment method (Li et al., 2009). However, the activation process is of high cost (Abdel-Salam et al., 2011). The adsorption of metals using a coal-fired power plant ash as AC was described to be effective (Abdel-Salam et al., 2011).

Various conventional techniques such as advanced oxidation, membrane filtration processes, reverse osmosis, chemical precipitation, ion exchange, and sorption are used for eliminating metals from water. However, these methodologies have their advantages and boundaries in the application. For example, precipitation elements that are soluble in an oxidizing environment and insoluble in the reduced environment (Hashim et al., 2011). In precipitation, the metallic elements become insoluble hydroxides at high pH; for further lowering the solubility of elements, sulfide or carbonate ions are added to water (Taylor, 2015). However, chemical precipitation is inadequate when the metal concentration is low; moreover, it involves a great number of chemicals and generating huge amounts of sludge that will necessitate further treatment (Hashim et al., 2011; Taylor, 2015). The efficiency of the other methodologies in metal removal such as ion exchange and membrane technologies would be high with low chemical consumption and high metal selectivity; however, the operation costs are expensive (Ahmad et al., 2011). Comparatively, the metal adsorption on an adsorbent has the benefit over liquid-liquid extraction, which requires mixing and settling. Sorption techniques (adsorption and ion exchange) become one of the mainly applied techniques for removing metals from GW (Huang et al., 2016).

The adsorption method adsorbed elements on the active sites on a porous particle and

within the surfaces of the pores of the particles. The element is moved from the liquid phase to the surface of a solid and bounds by physical and/ or chemical reactions (Barakat, 2011). Adsorption is like an ion-exchange technique but in ion exchange, the elements are exchanged with ion (counter-ion) on the active sites (Wang et al., 2009). Adsorption and ion exchange methods have some limitations such as the great capital and operational costs, low adsorption capacity, or weak chemical affinity especially at very low metal ion concentration (1 mg/L - 100 mg/L), resulting in secondary pollution or needing rigorous conditions such as anaerobic and carbonate-free (Hilal et al., 2012). However, sorption is assessed as one of the best techniques because of the low cost and the simplicity of design and operation, particularly with moderate and low contaminant levels (Huang et al., 2016). Sorption is also assessed as an eco-friendly treatment method (Yang et al., 2009). Adsorption technique is economically achievable, metal selectivity, simple design, easy operation, and efficient for removing chemical elements (Karnib et al., 2014; Amin et al., 2016). Conventional adsorbents such as ACs are expensive, cause environmental problems such as the non-biodegradable nature of silica gel, and their regeneration cost is also high (Crini et al., 2018). Whereas the non-conventional adsorbents such as natural materials, agricultural wastes, and industrial by-products are of extensive source, environment friendly, and low cost (Guan et al., 2016). Various non-conventional sorbents are used in adsorption processes for water treatment as shown in Table 1.

Table 1. *Some Nonconventional Adsorbents for The Removal of Pollutants from Water*

Adsorbents	Removal of	Reference
Eggshells	Boron	(Al-Ghouti & Khan, 2018)
Date pits	Bromide	(Al-Ghouti et al., 2017)
Coconut husk	Methylene Blue Dye	(Man et al., 2015)
bagasse	Methyl Orange Dye	(Mohamed et al., 2017)
Banana peel	Copper and Lead	(Vilardi & Verdone, 2018)
Wheat straw	Reactive Blue Dye	(Mousa & Taha, 2015)
Bentonite clay	Lead	(Al-Jilil, 2015)
Dolomite	Arsenic	(Shah et al., 2019)
Glasses	Heavy Metals (Cd, Cu, Fe, Pb, and Zn)	(Rashed & Abd-El daiem, 2018)
Tires waste	Boron	(Babiker et al., 2019)
Newspaper waste	Copper	(Mardiah et al., 2018)
Cotton waste	Methylene Blue	(Tenev et al., 2019)
Olive mill waste	Crystal Violet and Methylene Blue	(Sulyman et al., 2018)
PET bottles waste	Copper	(Hassan et al. 2017)

#### *Activated Carbon Adsorbent*

The adsorption of AC is considered one of the best efficient water treatment methods (Li et al., 2009). AC is an efficient adsorbent used in environmental applications, environment protection, and water treatment due to its high surface areas, porosity structure, and surface functional groups (Karnib, 2014). Theoretically, AC could be formed from carbonaceous material of high carbon levels (Al-Ghouti et al., 2017). There are mainly two methods for preparing AC: physical activation and chemical activation. The physical activation is carried out by primary carbonization of the raw material then by controlled gasification at higher temperatures in a stream of an oxidizing gas (Ahmad et al., 2011). While the chemical activation generates the porosity by the impregnation of precursor and the heat treatment (Al-Ghouti et al.,

2017). However, the activation is a high-cost process and commercial AC mainly uses a nonrenewable source such as coal (Ahmad et al., 2011). Low-cost AC produced from peanut husk and rice husk have been significantly used for the treatment of aqueous solutions from metals; moreover, the adsorption characteristics of metals using AC from bottom ash and fly ash from a coal-fired power plant were reported to be effective (Abdel-Salam et al., 2011). However, low adsorption selectivity for boron removal is caused by AC due to low surface-active sites for boron, thus several impregnated AC is utilized to adsorb boron from aqueous solutions (Guan, 2016). The physicochemical natures of boric acid and borate showed that hydrogen bonding and hydrophobic interactions are the possible adsorption mechanisms (Liu, 2009). The maximum boron removal capacity using AC was 3.5 mg/g at pH 5.5 (Köse et al., 2011). 60% boron removal can be obtained from an initial boron level of 5 mg/L at pH 8–9 (Bonilla-Petriciolet et al., 2017). However, Bodzek (2015) stated that high doses of AC required to remove 90% of boron from water. For Mo removal, AC removed more than 90% of Mo from the liquor sample (Pagnanelli et al., 2011). Moreover, for Li adsorption Seron (1996) showed the effect of applying treatments to the AC such as ammonia or electrochemical treatment enhanced Li adsorption. Physically AC could not reduce Li-ion levels from solution due to the electrostatic repulsion between Li cations and positive surface charge of the AC; Li-ions levels were reduced from 10 to 2 ppm using the electrochemical treatment for one day and it reached the full adsorption of 1 mg of Li per gram of physically AC. While chemically AC reached the equilibrium of 0.45 mg Li per gram of chemically AC treated with ammonia.

In summary, Babel (2003) stated the advantages and disadvantages of AC such that AC adsorption has many advantages such as high efficiency in removing different

chemicals from water at low levels, the applicability of thermal regeneration and maintenance, flexibility, and simplicity of the system design such as start-up and shut down as required. The surface functional groups as shown in Figure 12, the large surface area, and selected pore size and distribution are significant characteristics of AC (Mochida et al., 2006). However, AC adsorption has some limitation such as limited to some chemicals at low concentrations, highly soluble organics or those with low molecular weights, dust, and suspended solids lead to clog and block the system, high operating costs due to carbon costs system requirements, and unmanaged waste disposal of contaminated carbon cause some problem if it is not regenerated.

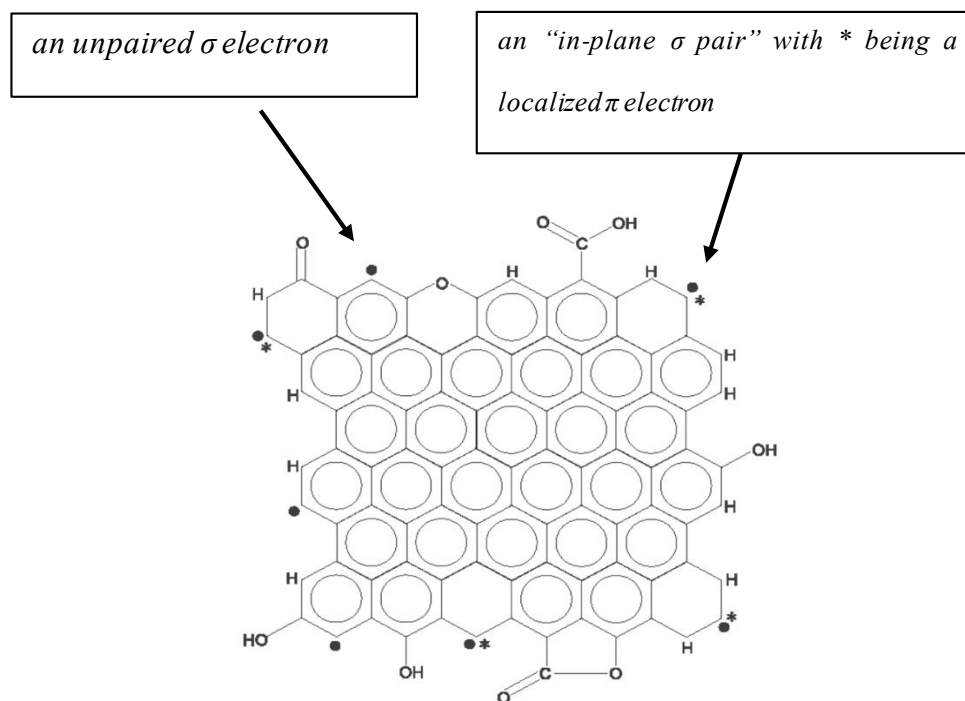


Figure 12. Activated carbon structure showing different functional groups on the surface (Mochida et al., 2006).



### *Bentonite Clay Adsorbent*

Bentonite clay has concerned with significant attention in the removal of metal ion pollutants from water due to its great properties such as the significant adsorption capacity, chemical, and mechanical stability, large specific surface area, complex porosity, lamellar structure, high cation exchange capacity, and low-cost (Zhao, 2008; Pan et al., 2011; Huang et al., 2016). However, the presence of different pollutants in water may result in interference and competition on adsorption sites (Bonilla-Petriciolet et al., 2017). The study by Akpomie & Dawodu (2015) showed the potential bentonite as a low-cost and eco-friendly adsorbent for the removal of nickel and manganese ions from the solution. Another study by Wongsasuluk, et al. (2013) illustrated that the adsorption of the metal ion in the modified bentonite is greater than that in the original clay and the order of adsorption capacity is NaOH bentonite and AC > HCl bentonite and H<sub>2</sub>SO<sub>4</sub> bentonite > bentonite for lead and copper adsorption whereas for the adsorption of cadmium, the order was HCl bentonite > NaOH bentonite > H<sub>2</sub>SO<sub>4</sub> bentonite > bentonite; they explained the results according to high active sites and surface heterogeneity of modified bentonite. In saline conditions, the swelling capacity, cation exchange capacity of bentonite is decreased lead to magnesium precipitation in montmorillonite interlayer spaces, and the distribution coefficients of cations decrease (Suzuki et al., 2008). Adsorption of boron onto bentonite clays was increased by modifying the clay surface with nonyl-ammonium chloride, which changes it from hydrophilic to hydrophobic (Karahan et al., 2006). Mojiri et al. (2017) stated that the ion-exchange and/or adsorbent properties of bentonite clay have been studied due to its structure as bentonite efficiently removed 81.3% of Mo (VI) from water. The adsorption capacity for boron using bentonite was 0.9 mg/g while it was 0.09 mg/g by using AC (Vhahangwele, 2015). A 3800 ± 380

ppm of Li was significantly adsorbed by bentonite (Hoyer, 2015).

Bentonite clay is a geological name for soil materials with a large level of swelling minerals, as commonly is montmorillonite. Regular minerals found in bentonites are quartz, feldspars, gypsum, calcite, pyrite, and various iron oxides/hydroxides. Besides, bentonite has high concentrations of amorphous and organic compounds. Sulfate minerals, like gypsum and anhydrite, have a relatively significant solubility, which reduces when the temperature is raised. Montmorillonites belong to the smectite group of clay minerals. This so-called 2:1 clay layer consists of double tetrahedral silicon oxide sheets sandwiching an octahedral aluminum oxide sheet as shown in Figure 13.

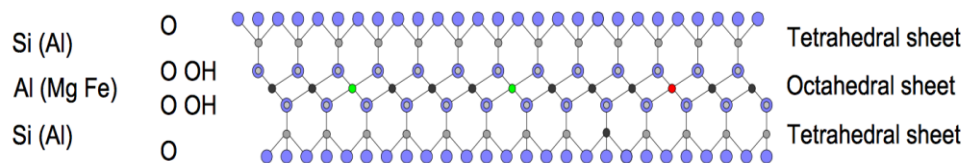


Figure 13. Crystal structure of the individual montmorillonite particle (Apted & Ahn 2017).

The smectite clay layers are negatively charged in the crystal structure because of the broken bonds for isomorphous substitutions of Mg for Al in the octahedral sheet or Al for Si in the tetrahedral sheets. This permanent negative charge is exchanged by cations and caused cation exchange capacity (Pan et al., 2011). The forces such as electrostatic interaction and van der Waals forces attach the ions (Kul & Koyuncu, 2010). In solution, Cations compete for interaction on the surface functional sites of bentonite. The higher the valence ion is, the easier and stronger the adsorption of clay minerals will be thus, the sorption ability is of order  $\text{Na}^+ < \text{K}^+ < \text{Ca}^{2+}$  on bentonite

(Yang et al., 2009). The study by Buzetzky et al. (2020) showed that the adsorption of chloride and iodide ions on Ag–bentonite occurred in the bulk aqueous phase and the interlayer space of montmorillonite. The mechanism of chloride and iodide ions adsorption on Ag–bentonite is shown in figure 14.

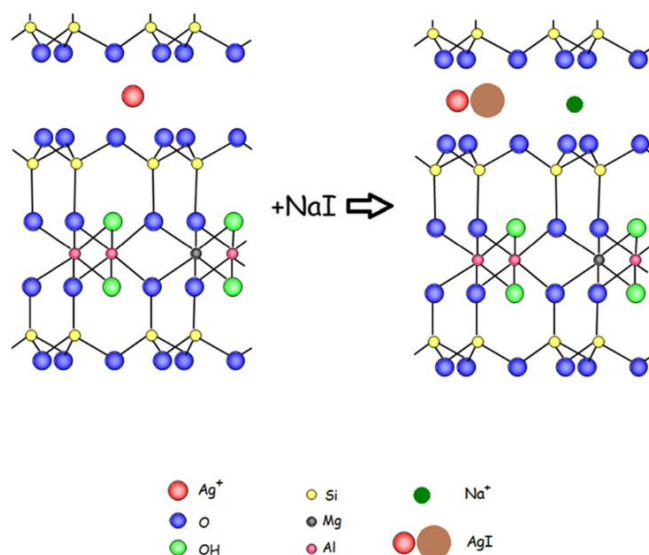


Figure 14. The mechanism of chloride and iodide ions adsorption on Ag–bentonite (Buzetzky et al.,2020).

#### *Date Palm Pits Adsorbent*

It is believed that date palm (*Phoenix dactylifera* L.), one of the most ancient plants, corresponding to the family (Arecaceae) with about 200 genera and 500 species (Al-Mahmoud, 2011; Maryam, 2016). It is grown worldwide in the Middle East, East, North and South Africa, and some areas of Europe and the USA. Date palm is distributed within oasis ecosystems and therefore developing sustainable cultivation in saline and aridity soils (Jaradat, 2013). The world’s annual production of date fruits is about 6.8 million tons (Jain, 2014). The rich date fruit is of significant nutrition factor for people, and social, economic, and ecological values. Socio-economic values

come from various products, which are made from the date palm trees such as utilizing products from its fiber. Furthermore, it is used to produce bio-fuel due to elevated percentage of carbohydrates, (44-88%) total sugars in fruit, thus consider as an important origin for renewable energy that reduces the use of fossil energy (Al-Ameri, 2016). Due to its canopy that facilitates the growth of other plants around the oases, which gives ecological habitat and shelter for many living organisms, which gives it ecological value (Dhawan, 2013; Maryam, 2016).

Date palm pits are about 10% of the fruit weight. Although date pits are seen as a waste by-product, they are used for purposes such as a dietary-fiber and food for cattle and poultry, extraction oil from the pits, making a caffeine-free drink from roasting date pits, and in water purification process (Hossain, 2014). Date palm waste is of great potential for adsorption metals because it is lignocellulosic fibers, which consists of cellulose, hemicellulose (44.4 wt.% carbon, 49.4 wt.% oxygen, and 6.2 wt.% hydrogens), and lignin (62 wt.% carbon and 32 wt.% oxygen) with a high number of carbon atoms of low polarity and great adsorption (Ahmad et al., 2011; Shafiq et al., 2019). Functional groups of lignin are alcohols, ketones, aldehydes, phenolic, carboxylic, and ether groups which bind with some metals to form coordination complexes agricultural by donating a pair of electrons (Bonilla-Petriciolet et al., 2017). A small adsorbent dosage of date pits can remove metals and it required a short contact time for equilibrium (Shafiq et al., 2019). The sorption of cadmium ions onto a mixture of olive stones and dates pit is spontaneous, and the equilibrium process was obtained in 20 min and presents an endothermic nature (Babakhouya, 2010). The date pit ash has high boron removal efficiency (71%) (Al-Ithari et al., 2011); while Al.Haddabi et al. (2015) stated the maximum removal efficiency of boron by date pit ash was 47% at neutral pH. The possible effectiveness

of date pits as a low-cost adsorbent for various metals and organic compounds was proven earlier (El-Hendawy, 2009). Al-Ghouti et al. (2017) showed that the adsorption efficiency of the raw date pits towards cadmium and copper ions obtained from Langmuir and Freundlich models is found to be 35.9 and 39.5 mg/g respectively where Freundlich isotherm indicated a heterogeneous surface binding; also, it is shown that the highest adsorptions of copper by small size date pits particles. The date pits comprise three main groups, specifically cellulose, hemicellulose, and lignin which characterize by oxygen functional groups such as hydroxyl, ether, and carbonyl (Ahmad et al., 2011). Figure 15 shows the hydrogen bonding and electrostatic attraction which were noticed as adsorption mechanisms for copper and cadmium ions; the binding of two cellulose/lignin units and by two hydroxyl groups in the cellulose/lignin unit were also noticed (Al-Ghouti et al., 2010).

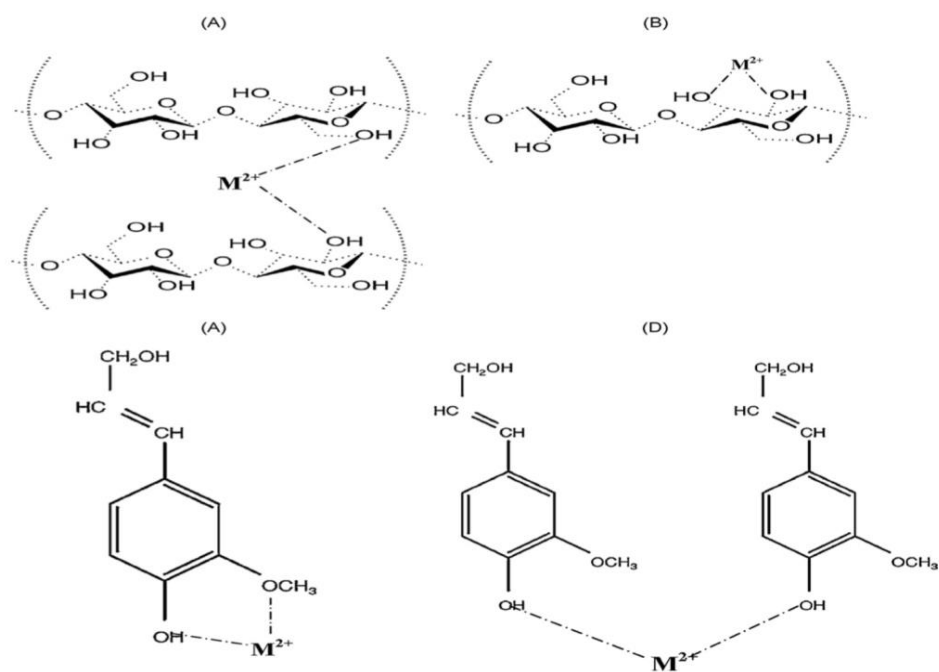


Figure 15. Binding mechanism of the date pits, cellulose and lignin, respectively with metal ion  $M^{2+}$  (Al-Ghouti et al. 2010).

Another study by Banat (2002) showed that the removal efficiency of copper and zinc using raw date pits were 0.15 mmol/g and 0.09 mmol/g, respectively; the adsorption study indicated a multilayer adsorption surface of raw date pits. Further study showed that the maximum removal capacities were 7.40 and 33.44 mg copper ion per gram of raw date pits and an AC prepared from it respectively and 6.02 and 17.24 mg cadmium ion per gram of raw date pits and activated carbon prepared from it respectively and the results were best fitted by Freundlich model (Hilal et al., 2012). Organics' natural material sorbents were better than minerals sorbents for the boron adsorption (Liu et al., 2009).

#### *Modified Date Palm Pits Adsorbent*

To enhance the number of active binding sites, natural sorbents require additional modifications. The functional group attached to the adsorbents as different groups helps in the removal of different metals from water such silica group that has a high affinity to cadmium, zinc, and copper; the hydroxyl group has a high affinity to chromium and the nitro group has a high affinity to lead (Xu & McKay, 2017). Date pits modifications could be achieved through physical pretreatment such as drying, grinding, and heating, it is easy, simple, and low cost; while chemical modification could be achieved by pretreatment washing with acids such as mercaptoacetic acid, alkalies such as (NaOH, KOH) and Fe salt or Fe oxide mineral coating (Shafiq et al., 2019). The organic components in the cortex, like cellulose, can be ionized with an alkaline treatment, thus the active sites can be enhanced by negative charges that can adsorb metal cations (Al-Qahtani, 2016). Modified date palm trunk with the acid treatment of such a biopolymer creates a suitable environment for its ring-opening, then the acid-treated with NaOH and carbon disulfide (CS<sub>2</sub>) to synthesis utilize

xanthate date palm trunk (XDPT) adsorbent. The xanthate group showed efficient removal of Pb (II) ions from water by the formation of stable complexes with lead ions (Yadav et al., 2013). Pretreated banana by alkalization with NaOH, the maximum adsorption capacity was  $\text{Cr}^{3+} < \text{Cd}^{2+} < \text{Zn}^{2+}$ , whereas it was  $\text{Cd}^{2+} < \text{Cr}^{3+} < \text{Zn}^{2+}$  for kiwi and tangerine; the results showed that the natural sorbent was effective for remediating heavy metals from water (Al-Qahtani et al., 2016). NaOH-modified date pits characterized by functional groups of carboxylates ( $-\text{COO}^-$ ) which were efficient for removing dyes; where the carboxylic ( $-\text{COOH}$ ) groups characterized the non-modified date pits (El-Messaoudi, 2015). Modified date palm waste by NaOH with mercaptoacetic acid ( $\text{C}_2\text{H}_2\text{O}_2\text{S}$ ) to change the abundant hydroxyl groups to mercapto groups, which showed significant removal of  $\text{Cu}^{2+}$  from water (Shafiq et al., 2019; Amin, 2016).

#### Groundwater Modelling and Mapping Using GIS

It should be noted that in GW management, the objective is to not only monitor and assess GW but more to make use of the information to construct a good decision. For example, if GW monitoring and assessment showed some locations of GW contamination then the question is whether to use remediation and what type of remediation to use (Sethi & Molfetta, 2019). Making decisions will almost always have some extent of risks such as the risk of a wrong decision or the risk of selection an unappropriated treatment technique (Vargas, 2004). Geographic information system (GIS) is a significant tool for analyzing and visualizing spatially continuous data, resulting on reduce the risk of making the wrong decision and supports management and planning processes. Water resources study is considered the second scientific field that highly applies geo-statistics (Li & Heap, 2011). In GW studies,

GIS is used to investigate sample locations, manage the inventory data, study the correlation between GW quality and different natural or anthropogenic disturbances, investigate the vulnerability to contamination, estimate GW flow, and integrate GW quality assessments (Balakrishnan, 2011). ArcGIS software has geostatistical analysis, which significantly combined geostatistics and GIS analysis. The geostatistical analysis includes spatial interpolation to estimate or predict attribute data anywhere from a limited number of observations. Besides, geostatistical analysis develops spatial interpolation techniques to model the spatial correlation of the variables such as GW quality parameters and to investigate the variability in space and time (Seyedmohammadi et al., 2016). To produce high precision maps for GW quality variables, data needs to be collected from all coordinates within the study area. Such sample collection for the whole area is not viable due to time, money, and labor-consuming (Li & Heap, 2011). GW samples are considered data points in GIS with some spatial data, which depend on polygons; these sampled points will be used to predict values of non-sampled points within the same field area, therefore values to whole polygons will be assigned and continuous data (surface data) will be produced. Surface data represented by a grid that divides the whole site into small cells where each cell is assigned a value. High precision of surface data representation depends on the size of the cells, such that small cell sizes will produce higher detailed maps than large cell sizes. Geostatistical Analysis incorporates different interpolation methods, each has special advantages and gives different output. However, in some instances, methods give the same output surface; in other instances, the output can be a little different.

Spatial interpolation is defined as a process of prediction or estimation values for unsampled locations from the measured points taken at known locations



(Paramasivam, 2019). Interpolation methods are grouped into deterministic (non-geostatistical interpolation) and geostatistical interpolation. Deterministic interpolation methods produce surfaces from measured values depend on either the degree of similarities such as on inverse distance weighted (IDW) method or the extent of smoothing such as radial basis functions (RBFS) method (Njeban, 2018). They do not provide a measure of uncertainty (error) of the predictions. Deterministic interpolation methods can be grouped to global interpolation such as global polynomial, which calculates predict values from the entire dataset; and local interpolation such as IDW and RBFS which predicts values from the measured points within neighborhoods (Paramasivam, 2019). Geostatistical interpolation contains several methods, which are all in the kriging family such as ordinary, simple, universal, probability, indicator, and disjunctive kriging in addition to cokriging (Magesh and Elango, 2019). Geostatistical interpolation methods exploit the statistical characteristics of the measured points to create surfaces. They include spatial autocorrelation (the statistical relationships between the measured values) (Keranen & Kolvoord, 2017). Geostatistical methods create prediction, error associated with the predictions, probability, and quantile output surfaces. An interpolation method that estimates a value that is exactly as the measured point at a sampled location is known as an exact interpolator such as IDW and RBFS. While the interpolation method that estimates a different value from the measured point is known as an inexact interpolator such as kriging. The study of Bajjali, (2005) compares IDW and kriging methods to model the effect of four artificial recharge dams on the quality of GW in Oman. The authors showed that the kriging and IDW produced realistic smooth interpolated surface maps that both interpolated maps show decreasing in the salinity. In addition, in KSA the study of Marko et al. (2013), showed that the kriging method

produced good mapping for water quality parameters using the best semi-variogram model based on RMSE varies for each water quality parameter; an example is shown in Figure 16 for electrical conductivity (EC) and TDS interpolated map of western Saudi Arabia.

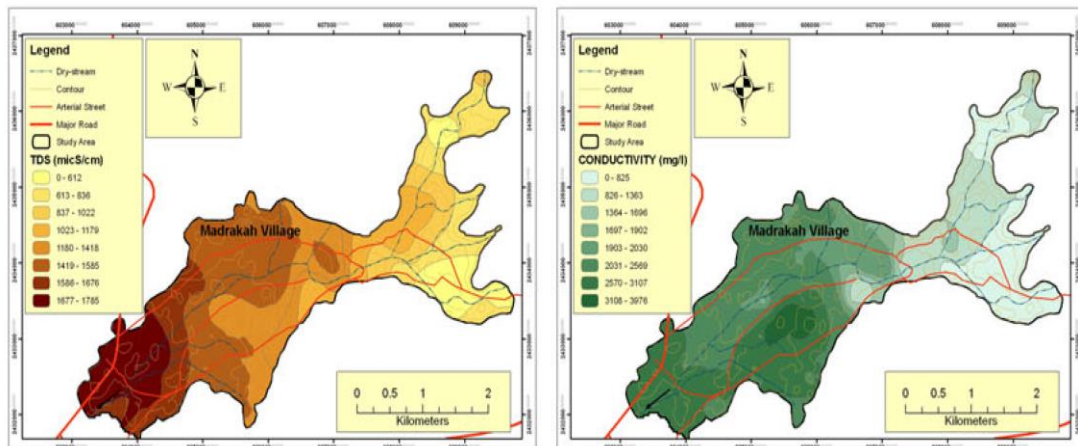


Figure 16. Interpolated map using kriging methods for electrical conductivity (EC) and total dissolved solids (TDS) of Wadi Usfan, western Saudi Arabia (Marko et al., 2013).

GW vulnerability and risk mapping models have three types of techniques of vulnerability assessment maps: statistical techniques, process-based simulation techniques, and overlay and index-based techniques (Kumar et al. 2015). Index-based techniques overcome the limitations of the statistical techniques and process-based simulation techniques; thus, it is widely preferred due to their sensitivity and simplicity. Index-based techniques have three types, namely parametric, non-parametric and hybrid models (Thapa et al., 2018). Different models are suitable for different geophysical environmental conditions (Kumar et al. 2015). The vulnerability maps produced by all the vulnerability assessment models give an insight into the GW contamination and its spatial distribution. Baalousha (2016), showed that vulnerability

mapping using parametric index-based techniques is a significant tool for GW management and protection aquifers as it can also be used for GW monitoring. As shown in figure 17, the most widely used DRASTIC model and Epik model, which are used for GW vulnerability mapping of karst aquifers in particular.

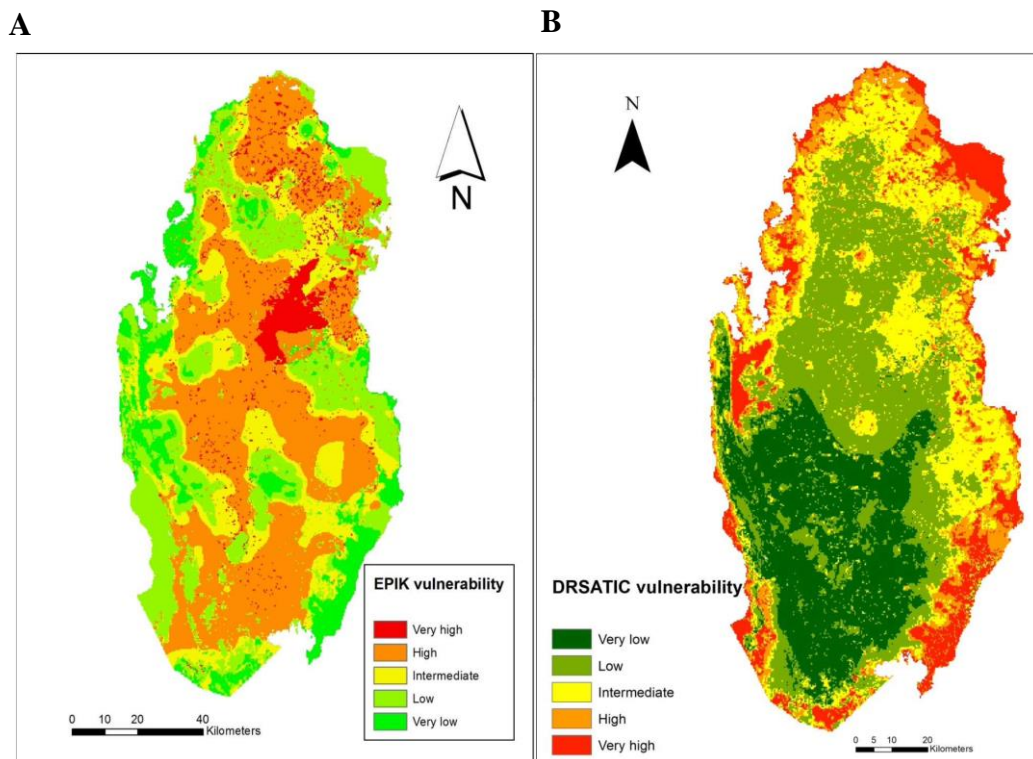


Figure 17. Vulnerability map of Qatar using EPIK and DRSATIC models (Baalousha, 2016).

In recent years, geo-statistics is broadly used in various disciplines such as geological, hydrological, and environmental studies (Nas, 2009). Geo-statistical and spatial interpolation methods are used in monitoring and assessing GW quality and quantity (Chung et al., 2019). The study by Balakrishnan, (2011) has assessed and mapped GW quality in India using GIS spatial interpolation techniques such as IDW and Kriging. Another example is the study by Baalousha, (2016) which demonstrated the GW vulnerability maps in Qatar. Geo-statistical and GIS analyses are incorporated in ArcGIS software (Elumalai et al., 2017). The spatial interpolation is used to estimate

or predict values for unsampled points from finite sampled observations at known locations that will save sampling time, money, and labor (Chung et al., 2019). Spatial interpolation analysis reveals the spatial variation in space and time of the attribute data (Seyedmohammadi et al., 2016). The sampled points are used to estimate points of non-sampled points, then the values for the whole area (polygon) are produced and continuous data (surface data) is generated (Saleh & Balakrishnan, 2019). ArcGIS has various interpolation techniques, each having unique advantages and produces different interpolated outputs; nevertheless, the techniques may produce the same interpolated output in specific cases (Elumalai et al., 2017). Spatial interpolation techniques are classified into deterministic or non-geostatistical interpolation and geostatistical interpolation. IDW and RBFS are deterministic interpolation methods, which use simple mathematical models to determine an unknown point from the surrounding known points. While geostatistical interpolation such as kriging uses more complex geostatistical models that include the statistical correlations between the sampled points also known as spatial autocorrelation (Xiao et al., 2016). The comparisons between the spatial interpolation methods according to several criteria have been conducted by Li & Heap (2011), as shown in Table 2.

Variations in natural resources like GW and associated environmental issues have been studied spatially and temporally applying deterministic and geostatistical techniques of interpolation in ArcGIS (Gunaalan et al., 2018). Simple kriging (SK) is a geostatistical technique whereas IDW and RBFs methods are deterministic interpolation techniques (Gidey et al., 2018). The ArcGIS Geostatistical Analyst extension has been employed for a detailed analysis of alterations in different spatial variables and found to bridge geo-statistics and GIS analysis with tangible results (Uyan and Cay, 2013).

Table 2. *Interpolation methods Comparison (Li and Heap, 2014).*

	IDW	RBFS	Kriging
Class of interpolation	Local deterministic interpolation	Local deterministic interpolation	Geostatistical interpolation
Predicted values	One prediction per location	One prediction per location	Prediction and measurement of the prediction uncertainty
Modeling spatial autocorrelation	Implicit: the model builds on the assumption of spatial autocorrelation in the data.	No	Yes
Output type	Prediction	Prediction	prediction, probability, and prediction error
Level of assumption / Complexity of the model	Few	Intermediate: Normal distributed data	Many: data transformation (data originates from a stationary stochastic system), trend removal and de-clustering
Input data values	Exact: the output surface contains exact values of the input data.	Exact: the output surface contains exact values of the input data.	Inexact: produces values, which correspond to the input data value. If the measurement error is zero, then kriging is an exact interpolator
Output surface	Not smooth	Smooth	Intermediate
Uncertainty of the prediction values	No	No	Yes

The boundaries need to be demarcated precisely for an accurate interpolation (Gunaalan et al., 2018), effective prediction of unknown factors of locations using available values and sample sizes (Stahl et al., 2006), acceptable spatial sample locations (Güler, 2014), normality of the existing sets of data (Wu et al., 2016), attained spatial resolution (Hengl, 2007), and the method of interpolation (Xie et al., 2011). The ambiguity in the analysis will be amplified if the spatial variation in water quality measurements is not represented properly by the well locations or sampling sites (Wagner et al., 2012). Xie et al. (2011) found that the size of the polluted area affected the efficacy of the interpolation methods used to describe the presence of heavy metals in soil spatially. Seyedmohammadi et al. (2016) found ordinary kriging (OK) to be better than five other spatial interpolation methods for estimating the spatial dissemination of electrical conductivity (EC) in GW. Comparing different spatial interpolation methods employed to predict EC, TDS, and pH, Empirical Bayesian kriging was found to be superior to other methods (Gunarathna et al., 2016a,b).

To estimate a point for an unsampled location, IDW employs the sampled points at the neighborhood of the predicted location and that the sampled point nearest to the predicted locations has more effect on the estimated point. IDW is an interpolation method in which each point value has a weight that diminishes as a function of distance (Magesh & Flango, 2019). IDW is an estimation method in which each point value has a weight that reduces with distance, which is calculated using equation 4.

$$Z_p = \frac{\sum_{i=1}^n \left( \frac{Z_i}{d_i^p} \right)}{\sum_{i=1}^n \left( \frac{1}{d_i^p} \right)} \quad (4)$$

Where  $Z_i$  is the value of the known point (numeric attributed),  $d_i$  is the distance to a known point,  $Z_p$  is the unknown point (numeric attributed to being interpolated),  $n$  is

the number of observations, and  $p$  is a user-selected exponent (powers of the distance) (Paramasivam & Venkatramanan, 2019).

The optimization of the IDW model could be achieved by selecting the lowest root mean square (RMS) by changing the power value. Thus, IDW will never generate a value that is higher than the maximum value (Bashir & Fouli, 2015). The disadvantages of IDW are that it is sensitive to outliers, clustering, and sampling configuration (Li & Heap, 2011).

In comparison between RBF with IDW, the RBFs may estimate points outside the measured points range (Balakrishnan, 2011). However, they are both an exact interpolator. The advantage of RBFs is that it creates a smooth output surface for gradually changing surfaces such as elevation. Whereas the disadvantage of RBFs is that it is unfit with the significant changes in the sampled points within short distances, and with the sample data that contains uncertainty, measurement of error, or outliers (Chung et al., 2019).

Similar to IDW interpolation, kriging gives weights from the distance around measured points to estimate unmeasured locations. However, kriging weights are determined by the distance and the spatial orientation of the known points or semi-variograms (Li & Heap, 2011). The most common semi-variogram model is spherical which is used in this study. The simple idea of spherical semi-variogram models is that unsampled points can be predicted by the weighted sum of the sampled points within a certain radius (Chung et al., 2019). Because the variogram alters with distance, the weights rely on the distribution of the sampled points' distribution. An empirical variogram can be quantified from sampled points by the following equation 5 (Chung et al., 2019):

$$\gamma(h) = \frac{1}{2n} \sum_{i=1}^n (Z(x_i) - Z(x_i + h))^2 \quad (5)$$

Where  $\gamma(h)$  is the predicted semi-variance at a separation distance or lag  $h$ ,  $h$  is the distance among sampled values,  $n$  is the number of pairs of samples separated by  $h$  and  $Z$  is the measured points.

Thus, kriging models depend on semi-variogram models of spatial autocorrelation to quantify weights, which decreases the variance in the estimated value, in terms of distance and direction to predict points and uncertainty associated with the predictions (Balakrishnan, 2011). The performance of kriging models is better than non-geostatistical models in that kriging estimates uncertainty associated with the predictions (Li & Heap, 2011). The geostatistical interpolation is believed to be an unbiased optimized estimation model for depicting regionalized variables (Xiao et al., 2016). However, kriging is an inexact model such that the output surface does not contain the exact values of the input data, and the interpolated values may exceed the minimum and maximum measured point (Li & Heap, 2011). Kriging is a smoothing process because the variance of the kriged values is lower than that of the original data (Myers, 1991), however, it has some smoothing deficiency (Xiao et al., 2016). Besides, kriging needs more computing and modeling time (Balakrishnan, 2011).

Generally, different interpolation techniques will produce unlike outputs with the same input data, thus, no interpreter is more accurate than others under all circumstances (Arslan & Turan, 2015). The accuracy should be judged by the sample quantity and the understanding of the study area with the spatial arrangement of the sample locations. Cross-validation is a tool to evaluate how well the model estimates points at locations with no data, and it helps to decide the best model that performs better than another model on a particular data set (Davis, 1987). It does not imply that the model, in general, will always perform better (Syed et al., 2003). In addition, it helps to optimize and search several possibilities of models' parameters such as



power, neighborhood, and the order of detrending to better utilize the data (Liu et al., 2012).

According to Falivene et al., (2010), cross-validation omits one measured sample point and uses the rest of the data to estimate a value at that location, the point is then returned into the dataset, and a different point is omitted, all data points are estimated by the same steps. To assess the model pairs of the original data value and predicted values, they are compared by subtracting them, then squared and added, the resulting sum is known as a "least squares" fit. Thus, cross-validation produces three values, for each location, the original data point, the predicted point, and the minimized estimation variance. (Xia et al., 2016). A variety of cross-validation statistics are used to examine how close the predicted values are to the known values, to explore how well the variogram "fits" the data, and to assess the performance of the interpolation methods for this particular analysis (Syed et al., 2003). For IDW and RBFs methods, results are usually stated as the mean error (ME) and root mean squared error (RMSE).

Their root means square standardized error must be near to one if the standard errors are valid. If the root-mean-square standardized error is higher than one, it indicates underestimating, while if it is lower than one, it indicates overestimating (Singh & Verma, 2019).

#### Drivers, Pressures, State, Impact, Response (DPSIR) Framework for Groundwater Resources Management

DPSIR framework was established by the Organization of Economic Cooperation and Development, which was evolved from the Pressure, State, and Response (PSR) model (OECD, 1993). The addition of Driver and Impact terms into PSR models aids the policymakers to understand cause and effect relationships (Sun et al., 2016).

Previously, the information from the DPSIR model was used to analyze water resources of Qatar (Ashfaq et al., 2018), to develop Integrated Water Resources Management (IWRM) systems (Kagalou et al., 2012), Integrated Coastal Zones Management (ICZM) (Pacheco et al., 2006) and to strategically assess the GW resources consumption (Hazarika and Nitivattananon, 2016). It is an adaptive management tool used for analyzing environmental issues such as water resources and then developing cause-effect relationships between human activities and their environmental impacts. Thus, it facilitates the resource managers, hydrologists, and policymakers managing water resources of the region more effectively and sustainably.

The model of DPSIR was used to analyze the GW resources of Qatar as shown in figure 18. DPSIR is useful in describing the relationships between the sources and the consequences of environmental problems. Generally, the “Drivers” term includes all the driving forces acting on regional water resource systems. It is basically comprised of human needs such as water and food. Since 92% of the total consumption of GW is done for agricultural activities, therefore, it can be classified as the main driver for the unsustainable consumption of GW resources of Qatar. The increase in agricultural demands due to population and economic growth has further exacerbated the situation. In addition, climate change such as increasing temperature and decrease rainfall led to reducing the GW recharge.

The “Pressure” term of DPSIR represents the human activities undertaken to fulfill needs and demands. The increase in water abstraction, greater than the recharge rates of GW is leading to unsustainable consumption of water resources and seawater intrusion. These human activities will apply pressures on the environment and available resources, which will lead to changes in the “state” of the environment.

Hence, a decrease in water resources as a result of unsustainable consumption, deterioration in water quantity and quality can be included under the “state” term of DPSIR. These changes in the state of the environmental compartment have resulted in impacts, which can include an increase in the GW and soil salinity that deteriorates crops and plants' health and productivity. Due to this, the farming industry will be affected, and food supply demands would be unfulfilled. Therefore, it is important to devise certain response measures that can help in safeguarding the limited water resources of Qatar. Measures responses are to develop and evaluate water treatment techniques that can help in efficient treatment of GW, to adopt efficient water irrigation practices to conserve limited water resources, to reuse treated wastewater as an alternative water source for irrigation to reduce the pressure on GW resources, to increase the GW storage reservoirs by recharge with treated wastewater or desalinated water, and finally, to develop of certain water-use tariff structures and awareness campaigns for farmers are also advised to ensure efficient utilization of water resources in Qatar.

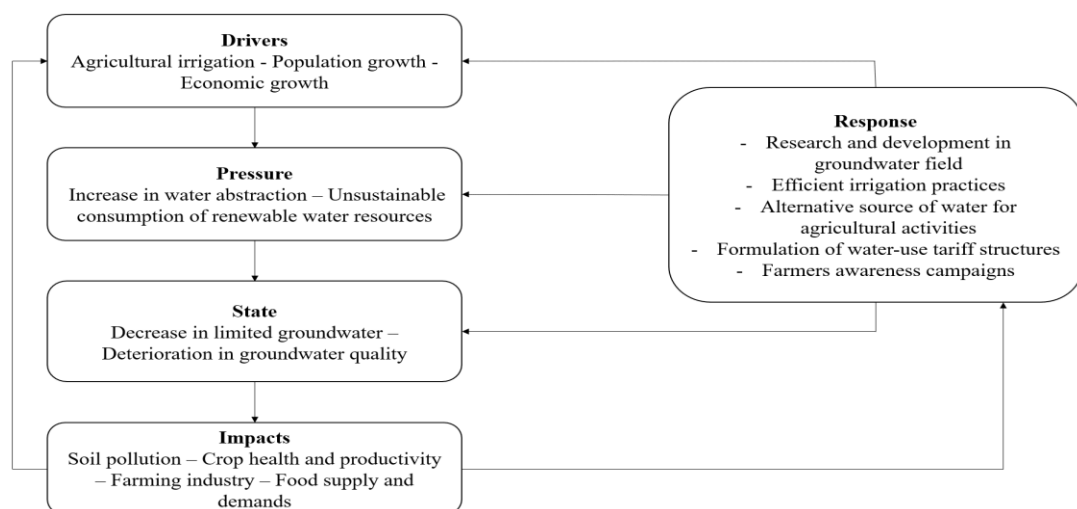


Figure 18. DPSIR framework for groundwater resources in Qatar.

## CHAPTER 3: RESEARCH METHODOLOGY

### Sampling

#### *Selection of Sample Points*

Sampling wells are selected to give good spatial coverage for the studied area. In addition, the sampling wells cover the four GW basins (North, South, Abou-Samra, and Doha) to provide aerial coverage over the entire country aquifers. Sample locations are of existing operation pumping wells on agriculture farms where water discharge could be accessed. Sampling procedures are implemented to ensure that samples are representative of GW conditions, and not stagnant water within the wells. GW samples are collected from 41 locations throughout Qatar as shown in figure 19, direct after the rainy winter season in May 2019 to compare variation with preliminary collected samples in May 2018. In addition, the GW data could be used for summer season comparison for future studies.

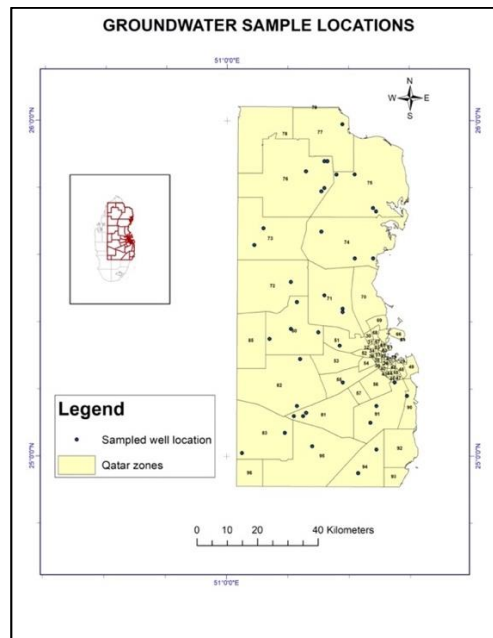


*Figure 19. Groundwater sampled wells.*

### *Sampling Documents*

Sampling documents include geographical coordinates using handheld GPS. Additional information including survey data, location name, site description, photo, town, date of well completion, well/property or farm owner, and use of water. In addition to data sheets of the physiochemical characteristics (pH, electrical conductivity, and temperature) measurements.

### *Sampling Steps*

The sampling technique was quota sampling because the wells were selected after divided wells into north and south quotas, then the wells were selected based on the ability to access private farms and the availability of existing operation pumping wells where water discharge could be accessed. Quota sampling is a non-probability sample such in the current study the samples were selected based on the probability proportionate to the higher north wells/farms distributions than the south wells/farms, also it can be biased; however it inexpensive, easy to perform, and save time (Field et al., 2006). To give good spatial coverage over the entire studied area (farm wells), the sampling wells covered the north and south GW basins. However, the number of north wells is more than the number of the south wells because the north wells are less saline than south wells due to the karst formations in the north that allow rainwater penetration to the aquifer (Sadiq and Nasir, 2002). The sampling procedures were carried out based on ISO 5667-11:2009 to guarantee that the samples are representative of the GW conditions underneath the investigation location and not stagnant water within the wells, thus the water is pumped for an adequate time (at least 30 min). The samples were collected directly from the faucet at the wellhead such that the sample comes freshly from deep in the well.

The sample bottles were pre-cleaned nitric acid, and each sample was acidified by 1 mL nitric acid (50%) pH < 2 for the cation, trace elements, and toxic metals analysis, while for the anion analysis they were not acidified. The sample bottles were rinsed 3-4 times with water from the well and then duplicated polyethylene bottles of one-liter size were filled completely to prevent degassing. Triplicated topsoil samples of 1 kg size are taken into polyethylene bags from three different locations around the well about 1-10 meters. The samples were shoveled by a corer drill of 30 cm × 30 cm with an approximate depth of 10 cm. Any observation, which may affect the results of the analysis, for instance, the production of bubbles, smell, color, and sediment were highlighted and recorded. Any possible sources of contamination in the vicinity of the well site, for instance, oil spills, fertilizers, pesticides, or landfills were also recorded in the field datasheets. The sample bottles were kept securely in a cooler box containing ice until delivered to the laboratory and kept at 4 °C.

## Sample Analysis

### *Field Analyses*

Various parameters were measured immediately on sites, such as temperature, pH, total dissolved solids (TDS), and electrical conductivity (EC) by a portable pH, salinity, and temperature multimeter (Handheld YSI Model 63). The multimeter was calibrated before each field measurement using standard solutions, pH buffer (citric acid and disodium hydrogen phosphate, also known as a citrate-phosphate buffer), and the EC buffer KCl (potassium chloride), and the multimeter electrode was rinsed with distilled water before measurements.

### *Physiochemical Characteristics Analysis*

The pH value was measured again along with the EC in the lab using the multimeter (Handheld YSI Model 63). Electrical conductivity ( $\mu\text{S}/\text{cm}$ ) at 25 °C was used to

determine the TDS value in (mg/L) because total dissolved solids (TDS) are the sum of all dissolved inorganic salts in the water such as carbonate, bicarbonate, chloride, fluoride, sulfate, phosphate, nitrate, calcium, magnesium, sodium, and potassium (Adimalla & Venkatayogi, 2018). The relationships of TDS and specific electrical conductivity (SEC) of the GW were calculated based on equations 6 and 7:

$$\text{TDS} = \text{SEC} \times 0.65 \text{ (for SEC} < 5000 \text{ } \mu\text{S/cm)} \quad (6)$$

$$\text{TDS} = \text{SEC} \times 0.70 \text{ (for SEC} > 5000 \text{ } \mu\text{S/cm)} \quad (7)$$

The factors of 0.70 for greater than 5000  $\mu\text{S/cm}$  and 0.65 for less than 5000  $\mu\text{S/cm}$  were determined from the historical data and verified during the Schlumberger Water Services study in Qatar with a correlation coefficient of 0.99 (SWS, 2009). The total water hardness was calculated using equation 8 as determined by (Al-Shidi, 2014).

$$\begin{aligned} \text{Total Water hardness (mg/L of CaCO}_3\text{)} = \\ \text{Ca (mg/L)} \times 2.497 + \text{Mg (mg/L)} \times 4.118 \end{aligned} \quad (8)$$

The main cations and anions, namely chloride, sulfate, calcium, magnesium, sodium, potassium, fluoride, and nitrate were analyzed using an ion chromatography device (850 Professional IC Detector). The trace element and toxic metals analysis were analyzed using inductively coupled plasma mass spectrometry (ICP-MS) Perkin Elmer, model NexIon 300 D. The soil samples were prepared by acid digestion with  $\text{HNO}_3$  and HF in a hot block apparatus. The prepared samples were analyzed for inorganic chemicals using ICP-MS.

#### *Chemical Elements Analysis*

The samples are analyzed for chemical elements and major cations and anions (bicarbonate, carbonate, chloride, sulfate, calcium, magnesium, sodium, potassium, fluorine, barium, strontium, iron, manganese, silicon, beryllium, aluminum,

ammonium, nitrite, nitrate and phosphate), using by inductively coupled plasma mass spectrometry (ICP-MS) is conducted the central laboratory of Qatar University. Blanks, reference standards, and duplicate and triplicate samples are also analyzed to check the precision and accuracy of analytical procedures.

### *Hydrogeochemical Water Quality Analysis*

Aqua-Chem software is widely used to analyze, plot, and report aqueous geochemistry and water quality of the GW supply wells. Major ions relative levels of the studied GW samples were plotted using AquaChem version 4.0.264 from Waterloo Hydrogeologic, 2003. General water quality diagrams were generated such as Piper, Schoeller, Ternary, Ludwig Langelier, Giggenbach Triangle, Durov, stiff plots, and Wilcox Plot for irrigation hazard Stiff plots. The saturation index (SI) and aqueous mineral phases were calculated using the inverse geochemical modeling along with the thermodynamic program PHREEQC. The changes in saturation state were used to identify the geochemical reactions governing the GW chemistry such that the negative values of SI; suggesting that the GW was undersaturated, while the positive values indicate oversaturation of the GW with respective minerals. Saturation index (SI) is defined by Mallick et al., (2018) as illustrated in equation 9.

$$SI = \log (IAP/K_{sp}) \quad (9)$$

Where IAP is the ion activity production and  $K_{sp}$  is the equilibrium solubility product.

### *Statistical Analysis*

The statistical package for the social sciences (SPSS) was employed to statistically analyze the data. Descriptive statistics were computed such as the minimum,



maximum, mean, median, and standard deviation values. Regression analysis (r) and Pearson's correlation coefficients were also calculated between the quality parameters of the GW samples. The correlation coefficients between the quality parameters pairs of the GW and the soil samples were also computed. The GW quality parameters were examined for significant differences between different locations by the t-test One-way analysis of variance (ANOVA) test. PCA is computed to recognize the pattern of the analyzed variables. Unscrambler X (v10.5, Camo Analytics—USA) following singular value decomposition (SVD) algorithm and XLST A T 2016 (MS Excel 2016, Microsoft—USA) was used for the PCA and clustering of variables. PCA is a significant method to recognize patterns and analyze the variance of a big set of inter-correlated variables and extract the Eigenvalues and Eigenvectors (loadings) for PCs from their associated variance (Ravikumar & Somashekar, 2015). PCA represents the dimensional of the large dataset, increases interpretability, and decreases the loss of information (Jolliffe & Cadima, 2016).

### *Geo-statistical Analysis*

The spatial analysis tool of ArcGIS 10.3.3 software was used to analyze the spatial variation of the GW quality parameters. The GW quality data was used to interpolate the point data at unmeasured locations and generate the surface map using three different interpolation methods, inverse distance weighted interpolation (IDW), radial basis functions (RBFs), and simple Kriging (SK). Cross-validation was applied to assess the best-fit interpolation method. The IDW method was modeled using best-fitted power, while Kriging was used the best-fitted semi-variograms. Cross-validations were computed with trend data to select the lowest root mean square error in the IDW, while Kriging selected the lowest error by comparing the sampled and the

predicted values by employing the empirical semi-variogram models. The comparison between interpolation methods was made based on the cross-validation results, Evaluation of different interpolation methods is established from the RMSE, which are obtained from the integrated interpolation model and cross-validation results. The optimization process is conducted by finding the kernel parameter values for the RBFS model, the power and neighborhood values for the IDW model, and for the SK parameters that give the model with the lowest RMSE. RMSE is used as a cross-validation indicator to assess how well the model fits for the representation of input data. The lowest RMSE results are obtained with the largest number of neighbors.

#### Adsorption Isotherm Experiment

The equilibrium isotherms models provide parameters that describe the interaction between the adsorbent–adsorbate. In the current study, the solid-liquid adsorption is described, where the solid phase is called adsorbent and the liquid phase (GW) contains the adsorbates. The adsorbent is a porous medium that should be of high micropore volume size to increase the adsorption capacity due to the ability of adsorbate to enter the micropore. The adsorption model should have mathematical complexity and accuracy. Different adsorption models are investigated to identify the best-fitted model because no general model fits all adsorbate(s)/adsorbent processes. Adsorption models give a reliable estimation of the adsorption efficiency without using a wide range of experimental data (Al-Ghouti & Da'ana, 2020).

In the current study, the adsorption experiments of B, Li, and Mo are conducted using three types of solutions the first solution contains only a single adsorbate, the second solution is a mixture of the three adsorbates, and the third solution is a real GW. Standard procedures were used to prepare B, Li, and Mo stock solution using boric

acid powder, Li chloride, and sodium molybdate respectively. Five mixture solutions are prepared, where four mixtures have the same concentration of Li, Mo, and B (5 ppm, 10 ppm, 20 ppm, and 30 ppm), while the last mixture solution was prepared using different concentrations (5 ppm for Mo, 10 ppm for Li and 20 ppm for boron). The GW in the current study has a higher boron concentration than Li and Mo. The adsorption experiment is conducted at pH 7 to compare the result with real water pH (mean value of 7.3). The adsorption process involves different stages starting from synthesis adsorbents then different stages of optimization and design of adsorption process as shown in figure 20.

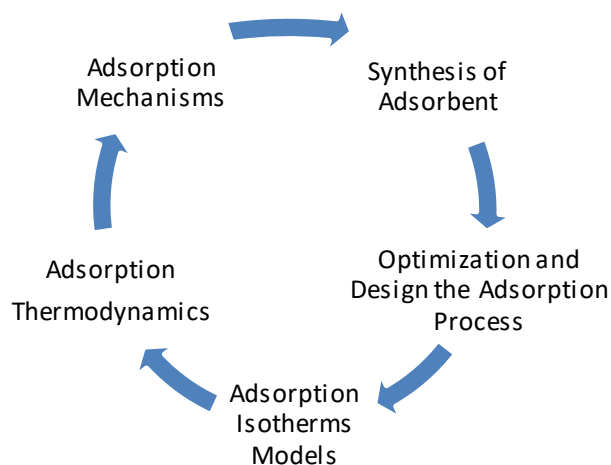


*Figure 20. Adsorption process steps.*

### *Adsorbent Preparation and Characterization*

Commercial bentonite and AC are bought from the local market. The RDPs adsorbent is prepared from Qatari date from the local market. Date pits are rinsed with distilled water and dried for 2 hours in an oven at 65 °C. Then it was roasted at 130 °C for about 3 hours. After that, it ground, then rinsed continuously by deionized water. After that, the samples are dried overnight at 100 °C. The dried date grains are ground

to obtain the desired size of about 0.25 mm-0.125 mm. Next, the samples are sieved; then the samples are preserved in sterilized containers.

The modification steps are adopted from the Yadav et al. (2013) study. Firstly, the date pits powder (about 50 g) is washed with  $H_2SO_4$  (about 100 mL) for half an hour and kept overnight to open the biopolymer ring. Then it is washed with distilled water, centrifuged, and dried. NaOH solution (about 200 mL) is added to date pits with continuous mixing for 60 min. Then mercaptoacetic acid (MAA) ( $C_2H_2O_2S$ ) also known as Thioglycolic acid (TGA) is added with continuous mixing for 3 hours to convert hydroxyl groups to mercapto groups also known as a thiol group or a sulfhydryl group(-SH), which have a high affinity for metal ions and then allowed to stand for overnight. Then the product is filtered, washed, centrifuged, and dried at  $100^\circ C$  overnight.

The surface morphology of the prepared RDPs and the MDPs are analyzed by scanning electron microscope (SEM) and the chemical characterization of the functional group of the sample's surface was performed by FTIR (FT-IR/FT-NIR Spectrometer- Spectrum 400). BET (model Aim Sizer-AM301) was used for the analysis of the surface area and pore size distribution of the adsorbents.

#### *Optimization and Design of Adsorption Process*

Adsorbent process efficiency in treating GW is a function of different parameters such as pH, temperature, initial concentration, pollutant characteristics like adsorbent size, distribution, and the presence of other adsorbates, adsorbent mass, and operation time. The adsorbent and adsorbate characteristics determine the adsorption mechanism like ion exchange, electrostatic interactions, surface precipitation, and chemical reactions. The operating conditions of adsorption processes can be

optimized to maximize the adsorbent efficiency to remove pollutants and to reduce the operational costs.

The first experiment set is prepared to study the effect of pH on adsorbate adsorption. The experiment set contains 45 flasks. Five duplicated flasks are filled with 50 mL Li solution of 100 mg/L concentration (adsorbate) and 50 mg AC (adsorbent). Each flask has a different pH level, namely 2,4,6,8 and 10. HCl and NaOH were used to adjust the pH of the solutions as required. The second group is prepared as the previous set, but the adsorbent is changed by 50 mg bentonite, while the third and fourth are filled with 50 mg RDPs and MDPs respectively. Four blank flasks (the pH was not changed pH= 5) for the four adsorbents are also included in each set. Besides, one flask of standard Li solution without adsorbent was included. The flasks were kept with continuous shaking for 48 hours at 160 rpm and 25 °C. The pH is adjusted using drops from HCl (0.05 M) and NaOH (0.05 M) solutions. After that, the samples were filtered in 15 mL labeled tubes (the bentonite samples were centrifuged due to nanoparticle size). Then, the samples are 100-time diluted in 10-mL tubes (100  $\mu$ L from the sample with 9.9 deionized distilled water (DDW)) to prepare them for ICP-MS analysis.

The second experiment set was prepared to study the effect of initial concentration on the adsorption process. The experiment set contains 22 flasks; 11 duplicated flasks were filled with Li solution of different concentrations (adsorbate) as 5, 10, 15, 20, 30, 40, 50, 60, 80, and 100 mg/L. Then 50 mg of adsorbent is added. The pH was adjusted at the optimum pH. Blank and control flasks are included. The flasks were kept with continuous shaking for 48 hours at 160 rpm and 25 °C. The pH was adjusted using drops from HCl and NaOH solutions. After that, the samples were filtered in 15 mL labeled tubes.

The same experiment set is done for different adsorbents, namely bentonite, RDPs, and MDPs. While the third experiment set is prepared to study the effect of temperature on adsorption performance. The experiment set is prepared as the second experiment set except that the temperature is set at 35 °C. The experiment set is repeated at 45 °C.

### *Modeling Adsorption Process*

Modeling adsorption isotherm involves data from batch adsorption experiments such as a series of equilibrium concentration with its respect to the resulted adsorption efficiency. The controlled variables are temperature, adsorbent mass, agitation, solution volume, and pH. The adsorption capacities ( $q_e$ ) and percentage of removal (%) are calculated by equations 10 and 11 respectively (Al-Ghouti & Da'ana 2020).

$$q_e = \frac{(C_i - C_e) \times V}{m} \quad (10)$$

$$\text{Percentage Removal (\%)} = \frac{C_i - C_e}{C_i} \times 100 \quad (11)$$

Where  $C_i$  and  $C_e$  are the initial and equilibrium concentration (mg/L) respectively,  $m$  is the mass of the adsorbent (g) and  $V$  is the volume of the solution (L).

In the current study, four adsorption models namely Langmuir, Dubinin-Radushkevich, Freundlich, and Temkin are used to describe the adsorption process.

### *Monolayer Adsorption and the Langmuir Isotherm*

Langmuir isotherm model is based on four assumptions: monolayer adsorption coverage, each adsorption site can adsorb only one adsorbate molecule, all adsorption sites are characterized by equivalent energy due to the uniform surface, and the ability of a molecule to adsorb in a given site is independent of the occupation of neighboring. Langmuir isotherm can be modeled using the following equation 12, and

the corresponding  $q_e$  is given by equation 13 (Al-Ghouti & Da'ana 2020).

$$\frac{C_e}{q_e} = \frac{1}{Qb} + \frac{C_e}{Q} \quad (12)$$

$$q_e = \frac{QbC_e}{1+bC_e} \quad (13)$$

Where  $C_e$  is the adsorbate concentration at equilibrium (mg/L),  $Q$  is the maximum adsorption efficiency in equilibrium constant (mg/g),  $b$  is the Langmuir adsorption constant (L/mg),  $q_e$  is the amount of metal adsorbed per gram of adsorbent (mg/g).

Langmuir adsorption constant is related to the increasing in the affinity of the adsorbate by the adsorbent, since it is the inverse of the equilibrium concentration in the liquid phase, the increase in Langmuir adsorption constant implies the increase of the initial slope of the adsorption isotherm. Langmuir adsorption constant is found from the slope of the line that is performed from plotting  $1/q_e$  in y-axis versus  $1/C_e$  in the x-axis, whereas  $Q$  is obtained from the intercept (Al-Ghouti & Da'ana 2020).

#### *Freundlich Isotherm*

Freundlich isotherm model is based on the assumptions that the adsorption occurs on a heterogeneous surface such that the adsorbed concentration increases infinitely with an increase in concentration. The isotherm is modeled by equation 14, and the corresponding  $q_e$  is given by equation 15.

$$\log q_e = \log K_F + (1/n) \log C_e \quad (14)$$

$$q_e = K_F C_e^{1/n} \quad (15)$$

Where  $K_F$  is Freundlich isotherm constant ((mg/g)(L/mg)<sup>1/n</sup>),  $n$  is the adsorption Intensity,  $C_e$  is the equilibrium concentration of adsorbate (mg/L),  $q_e$  is the amount of metal adsorbed per gram of adsorbate at equilibrium (mg/g) (Al-Ghouti & Da'ana 2020).

When  $\log q_e$  is plotted versus  $\log C_e$ , it yields a straight line with a slope equal to  $1/n$

and an intercept equal to  $\log K_F$ . The value of  $n$  gives the type of the isotherm and both  $K_F$  and  $n$  parameters are dependent on temperature.  $1/n$  is the intensity of the adsorption or surface heterogeneity that give the energy relative distribution such that when  $1/n$  is greater than zero ( $0 < 1/n < 1$ ) the adsorption is favorable, when  $1/n$  is greater than 1, the adsorption process is unfavorable, and it is irreversible when  $1/n = 1$ . The irreversibility of the isotherm can be attributed to the concentration that must extremely reduce to a low level before the desorption of adsorbate from the surface (Al-Ghouti & Da'ana 2020).

#### *Dubinin–Radushkevich (D-R) Isotherm*

Dubinin–Radushkevich (D-R) isotherm model is based on the assumption that adsorbent size is comparable to the micropore size, so it expresses the mechanism of adsorption with the distribution of Gaussian energy onto the heterogeneous surfaces. Thus, this model distinguishes between the chemical and physical metal ions adsorption. The adsorption equilibrium can be given by equation 16 independently of temperature using the adsorption potential ( $\varepsilon$ ), and the corresponding  $q_e$  is given by equation 17 (Al-Ghouti & Da'ana 2020).

$$\ln q_e = \ln q_s - K\varepsilon^2 \quad (16)$$

$$q_e = q_s e^{-K\varepsilon^2} \quad (17)$$

Where  $q_e$  is the amount of adsorbate in the adsorbent at equilibrium (mg/g),  $q_s$  is the theoretical isotherm saturation capacity (mg/g),  $K$  is the adsorption energy constant,  $\varepsilon$  is Dubinin-Radushkevich isotherm constant (Al-Ghouti & Da'ana 2020).

Dubinin-Radushkevich isotherm constant ( $\varepsilon$ ), can be calculated by equation 18.

$$\varepsilon = RT \ln [1 + 1/C_e] \quad (18)$$

Where  $R$  is the gas constant (8.314 J/mol K),  $T$  is the absolute temperature and  $C_e$  is the adsorbate equilibrium concentration (mg/L).



The adsorption energy constant is found from the slope of the line that is performed from plotting  $q_e$  in y-axis versus  $\ln C_e$  in the x-axis, whereas Temkin adsorption constant is obtained from the slope, and  $\ln q_e$  is the intercept of the line.

#### *Temkin Isotherm*

Temkin isotherm equation is based on the assumption that the heat of adsorption affects adsorbent–adsorbate interactions, which linearly decreases the concentration of the adsorbate in the layer with coverage. The binding energies are also uniformly distributed on the surface. The Temkin model is given by equation 19 (Al-Ghouti & Da'ana 2020).

$$q_e = \left(\frac{RT}{b_T}\right) \ln A_T + \left(\frac{RT}{b_T}\right) \ln C_e \quad (19)$$

Where  $q_e$  is the amount of adsorbate in the adsorbent at equilibrium (mg/g),  $C_e$  is the equilibrium concentration of the adsorbate (mg/L),  $A_T$  is Temkin isotherm equilibrium binding constant (L/g),  $\left(\frac{RT}{b_T}\right)$  is the constant related to the heat of adsorption (J/mol),  $R$  is the gas constant (8.314 J/mol K),  $T$  is absolute temperature, and  $b_T$  Temkin isotherm constant. The value of  $\left(\frac{RT}{b_T}\right)$  is found from the slope of the line that is performed from plotting  $q_e$  in y-axis versus  $\ln C_e$  in the x-axis, whereas Temkin isotherm equilibrium binding constant is obtained from the slope (Al-Ghouti & Da'ana 2020).

#### *Adsorption Thermodynamic*

The estimation of the thermodynamic parameters such as Gibbs free energy change ( $\Delta G^\circ$ ), standard enthalpy change ( $\Delta H^\circ$ ), and standard entropy change ( $\Delta S^\circ$ ) is essential for the study of the adsorption process because they help to interpret when the adsorption is favorable, spontaneous, endothermic, or exothermic (Al-Ghouti &

Da'ana 2020). The negative values for the Gibbs free energy change,  $\Delta G^\circ$  indicates that the adsorption is likely thermodynamically spontaneous. However, the decrease in  $\Delta G^\circ$  value with the increase in temperature indicates that the adsorption is not favorable at high temperatures. While it is an endothermic reaction if  $\Delta H^\circ$  is a positive value and exothermic if  $\Delta H^\circ$  is a negative value. The affinity of the adsorbent towards the adsorbate is given by the positive  $\Delta S^\circ$  value, implying the increase of randomness and possible structural changes such as complex formation. Thus, important information could be obtained regarding the disorder of the adsorption and the interaction type either it is physisorption or chemisorption, or it is either enthalpy or entropy. The adsorption thermodynamic parameters could be given from equations 20, 21, and 22, then the values of  $\Delta H^\circ$  and  $\Delta S^\circ$  could be found by the plot of  $\ln(K_e)$  versus  $(1/T)$ , The graph is known as the Van't Hoff plot (Al-Ghouti & Da'ana 2020).

$$\Delta G^\circ = -RT \ln K_a \quad (20)$$

$$\Delta G^\circ = \Delta H^\circ - T\Delta S^\circ \quad (21)$$

$$\ln K_a = -\frac{\Delta H^\circ}{RT} + \frac{\Delta S^\circ}{R} \quad (22)$$

Where R is the gas constant (8.314J/mol K), T is the temperature in Kelvin (K), and  $K_a$  is the equilibrium thermodynamic constant that could be calculated from equation 23.

$$K_a = \frac{q_e}{C_e} \quad (23)$$

Thus, it is reasonable to use Langmuir isotherm constant to estimate  $K_a$ . However,  $K_a$  is a unitless value (Bonilla-Petriciolet et al., 2017).

### Statistical Analysis

Analysis of variance is used to statistically test the results of the adsorption experiment because the experimental designs are completely randomized designs

(CRD). ANOVA for two factors using Microsoft Excel 2016 is applied to test the relationship between the initial concentration of B, Li, and Mo and the temperature. While ANOVA for a single factor is applied to study the effect of pH on the adsorption capacity of B Li and Mo because the experiment was a single factor experiment in which the temperature and concentration were constant throughout the experiment. In addition, the Chi-squared test ( $\chi^2$ ) and the coefficients of determination ( $R^2$ ) are used to investigate the best-fit adsorption isotherm model.

## CHAPTER 4: RESULTS AND DISCUSSION

### Physical and Chemical Properties of the Collected GW Samples

The physicochemical characterizations of the collected GW samples are summarized in Appendix A. The temperatures are ranged from 17.3 °C to 31.7 °C with an average of 27.7 °C. The variations of sample temperature might be attributed to the GW recharge with rainfall, that shallow GW has a relatively lower temperature than deep GW. The measurement of the GW pH gives significant information about geochemical equilibrium (Mallick et al., 2018). The interpolated maps shown in Appendix B show that the pH value variation among the study area. The pH values range from 6.8 to 7.9 with an average of 7.3. This reading meets the World Health Organization (WHO) standard, which is (6.5-8.5) (WHO, 2011). An exception from two slightly acidic wells (pH = 6.9 and 6.8), which may be attributed to the use of the fertilizer in the farms near the wells. The result of pH shows the alkalinity of the aquifers due to the interaction between soil and water such as the dissolution of limestone and the equilibrium with calcite dissociation and the production of bicarbonate and hydroxyl ions as the chemical reaction equation 24:



Under normal conditions, the alkaline GW does not show significant concentrations of heavy metals (Shomar, 2015).

The total hardness varied from 275 to 5393 mg CaCO<sub>3</sub>/L with an average of 2120 mg CaCO<sub>3</sub>/L. The total hardness interpolated map shows the total hardness variations in the study area. Alsuhami et al., (2019) stated the degrees of hardness as soft (0 to 75 mg CaCO<sub>3</sub>/L), moderate (75 to 150 mg CaCO<sub>3</sub>/L), hard (150 to 300 mg CaCO<sub>3</sub>/L), very hard (> 300 mg CaCO<sub>3</sub>/L). According to this classification, the total hardness of

the GW is classified as very hard except for one sample, which was hard. The results showed the limitation to use the GW in industrial and irrigation pipes because water should have a total hardness of less than 85 mg CaCO<sub>3</sub>/L and magnesium hardness of less than 40 mg CaCO<sub>3</sub>/L to minimize scaling at elevated temperatures (Al-Shidi, 2014). Srinivasamoorthy et al., (2014) indicated that the presence of calcium carbonate (CaCO<sub>3</sub>) in GW leads to temporary hardness in which heat can be used to reduce it. However, Ca<sup>2+</sup> and Mg<sup>2+</sup> ions cause permanent hardness where ion-exchange processes can be utilized to reduce the ions. An interpolated map shows the TDS variations in the study area. In the current study, the range of the electrical conductivity (EC) was (0.92 - 22.33 μS/cm), and the average of EC was 7.29 μS/cm. The range of TDS was (598 -15633 mg/L) and the average TDS was 5038 mg/L. Ghalib (2017) stated that the classification of EC as low saline (EC = 1500 μS/cm), medium saline (EC between 1500 and 3000 μS/cm), and high saline (EC >3000 μS/cm). According to this classification, there were no samples were having EC less than 500 μS/cm that can be considered similar to freshwater. Only two samples were low salinity of less than 1500 μS/cm. Only one sample was moderately saline of the EC, which was between 1500 and 3000 μS/cm. 38 samples were highly saline of the EC, which were greater than 1500 μS/cm, and do not meet the limits of drinking water (WHO, 2017). While 38 were highly saline with EC greater than 3000 μS/cm, which is unsuitable for water irrigation (Misstear et al., 2017).

The weather, the host rock, and the residence time of the GW in the aquifer are the main factors that change EC values (Alsuhaime et al., 2019). Thus, in this study, the high EC (high salinity) in the GW is due to the aridity of Qatar with low precipitation and high evaporation. Furthermore, agricultural activities such as using fertilizers and keep irrigation using high saline GW may lead to concentrating salts in the soil due to

high evaporation, which may leach of salts and nutrients to the aquifer. Heavy extraction of the GW leads to the migration of the brackish water from the deep aquifer or adjacent seawater.

High TDS levels were detected along with the coastal areas as shown in the interpolation map, which is attributed to the seawater intrusion that will lead to increase TDS, whereas high values in southern areas might be attributed to lower rainfall and deep water (brackish) mixing. However, GW consists of several chemicals that are found at various levels. Generally, 95% of the ions found in the GW are  $\text{Na}^+$ ,  $\text{K}^+$ ,  $\text{Ca}^{2+}$ ,  $\text{Mg}^{2+}$ ,  $\text{Cl}^-$ ,  $\text{SO}_4^{2-}$ ,  $\text{HCO}_3^-$ , and  $\text{NO}_3^-$  (Sundaram et al., 2009). The main source of ions in GW is the lithology of rocks in contrast with anthropogenic sources (Abdel-Satar et al., 2017).

#### *Major Anions Analysis*

As shown in Figure 21A, major anions in the study area were found to be in the following order  $\text{Cl}^- > \text{SO}_4^{2-} > \text{HCO}_3^- > \text{NO}_3^-$ .  $\text{Cl}^-$  was found as the most dominant anion among other tested anions with values between 203.6 mg/L to 30806 mg/L with a mean value of 6289 mg/L, followed by  $\text{SO}_4^{2-}$  ranging from 53.4 to 11596 mg/L with a mean value of 4977 mg/L.  $\text{HCO}_3^-$  values were between 282.3 mg/L and 975.6 mg/L with a mean value of 509.1 mg/L.  $\text{NO}_3^-$  values were in the range of 5.2 and 113.3 mg/L with 37.2 mg/L as a mean value.

Chlorides were common constituents in natural water. Natural sources of  $\text{Cl}^-$  in the GW include road salt, industrial facilities' effluents, sewage water pollutants, and municipal landfills' leachate (Srinivasamoorthy et al., 2014), rainwater, rock-water interactions, saline seeps, while anthropogenic sources are fertilizers such as gypsum fertilizers (Vengosh et al., 2002). In the study area, the  $\text{Cl}^-$  sources are sewage water

pollution, treated wastewater, rock water interaction, and seawater intrusion. Laxative effects and salty tastes in drinking water can be caused by the elevated concentrations of  $\text{Cl}^-$  (Adimalla & Venkatayogi, 2018).  $\text{Cl}^-$  and  $\text{Na}^+$  levels are correlated to the TDS and major ions in the samples.

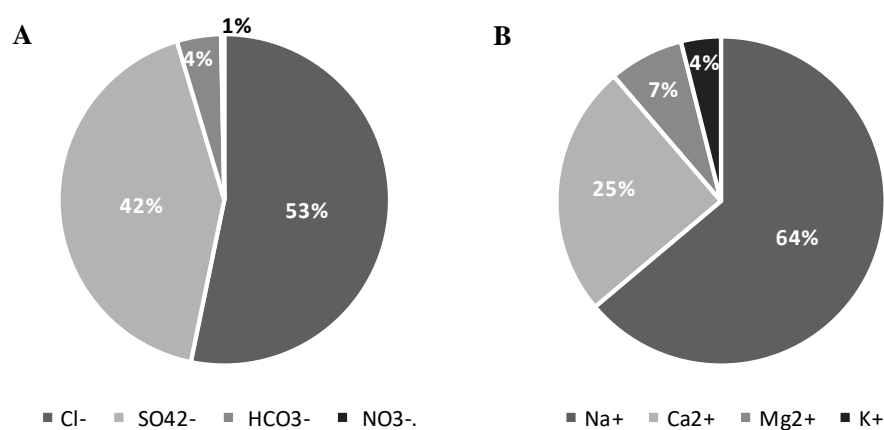


Figure 21. Distribution of **A.** major anions and **B.** major cations in the GW of the study area.

When the sulfide minerals interact with water, they release  $\text{SO}_4^{2-}$  from the oxidation process. The igneous and sedimentary rocks such as gypsum ( $\text{CaSO}_4 \cdot 2\text{H}_2\text{O}$ ) and anhydrite ( $\text{CaSO}_4$ ) are a source of metallic sulfate (Czerewko et al., 2003). The map of sulfate ion ( $\text{SO}_4^{2-}$ ) distribution shows that the highest values are in the southern regions that might be related to sulfate ion dissolution along the flow path, and fertilizers and agriculture wastes leachate from the intensive agriculture activities in the study area. Furthermore, it can be attributed to gypsum and anhydrite dissolution within the limestone sequence. Anthropogenic sources such as industrial activities are attributed to high sulfate in the GW (El-Maghraby et al., 2013). Thus, high  $\text{SO}_4^{2-}$  in some samples are due to natural sources such as gypsum rock dissolution and

anthropogenic sources such as fertilizers from agriculture activities. Water with high  $\text{Cl}^-$  and  $\text{SO}_4^{2-}$  can cause hypertension, osteoporosis, stroke, laxative effect, diarrhea, asthma, dehydration, and gastrointestinal irritation and affect human health (McCarthy 2004; WHO 2004; US EPA 1999).  $\text{SO}_4^{2-}$  induces metals corrosion in the distribution system with low alkalinity water (Ghalib, 2017).

The concentration of bicarbonate and carbonate in the GW may be attributed to the carbonate weathering such as weathering of silicates. When feldspar minerals react with carbonic acid in the water, it causes carbonic acid dissolution (Kumar et al., 2009). High  $\text{HCO}_3^-$  levels in the GW indicate the dominance of mineral dissolution (Ghalib, 2017). According to (SWS, 2009), wells are categorized according to the hydrological basins in which they are found. The hydrological basins are based on the surface water run-off in Qatar and the average well depth by hydrological basin was measured as shown in the statistical analysis section. In this study, the levels of sulfate and chloride show an indirect relationship with the depth of the GW table, while the level of  $\text{HCO}_3^-$  shows a direct relationship with the depth of GW table that  $\text{HCO}_3^-$  might indicate the formation of clay or limestone/dolomite presence in the area. All the parameters, except  $\text{HCO}_3^-$ , increase from inland to coast. It is also noticed that high EC is related to low bicarbonate levels.

Nitrate ( $\text{NO}_3^-$ ) is found naturally in soil by biological oxidation of nitrogenous substances and it is an important plant nutrient. The presence of  $\text{NO}_3^-$  in the GW is from the use of fertilizers, sewage leaching, and agricultural/municipal waste (Mallick et al., 2018). Agriculture activities and organic nitrogen fertilizer from animal manures, human wastes, and sewage sludge, and inorganic nitrogen fertilizers contain  $\text{NO}_3^-$  and/or  $\text{NH}_4^+$  (Rajmohan et al., 2019). In the current study, the high levels of  $\text{NO}_3^-$  could be attributed to the use of fertilizers.  $\text{NO}_3^-$  source in the GW is related to



the infiltrated water quality, type of the soil, and leaching process. Drinking water with a high  $\text{NO}_3^-$  level causes infants to have methemoglobinemia. Furthermore, it causes cyanosis, oral, colon, gastrointestinal, and lymphoma cancers, (Adimalla & Venkatayogi, 2018; Al-Kalbani et al., 2015).  $\text{NO}_3^-$  in the GW had an average concentration of 36.32 mg/L. The central and northern regions of the study area had the highest  $\text{NO}_3^-$  values. High  $\text{NO}_3^-$  in the current study might be ascribed to agriculture activities such as manure use, especially at the shallow GW locations (Shomar, 2015).

The fluoride in the GW ranged from 1.5 mg/L to 8.7 mg/L, and the average value was 3.8 mg/L. Fluoride concentrations in all samples were higher than the drinking permissible limits ( $>1.5$  mg/L). The sources of fluoride in the GW are the erosion of natural deposits such as granite, granite gneisses, and pegmatite (Adimalla & Venkatayogi, 2018; Alshaimi et al., 2019). Fluorosis that fluoride related to the teeth and bones health can be caused by high fluoride levels in drinking water (Rajmohan et al., 2019).

#### *Major Cations Analysis*

As illustrated in Figure 21B, the major cations had the following order  $\text{Na}^+ > \text{Ca}^{2+} > \text{Mg}^{2+} > \text{K}^+$ . The results showed that  $\text{Na}^+$  was mostly dominant among other cations with values varying from 64.2 mg/L to 5547 mg/L with a mean of 1466 mg/L, followed by  $\text{Ca}^{2+}$  ranging from 69.9 mg/L to 1497 mg/L with a mean value of 570.1 mg/L.  $\text{Mg}^{2+}$  values were in the range of 24.4 mg/L to 420.1 mg/L with a mean of 169.1 mg/L, while  $\text{K}^+$  values ranged from 16.3 mg/L to 320.6 mg/L with a mean of 90.1 mg/L.

Sodium has high water solubility. High levels of  $\text{Na}^+$  in the GW occur naturally in some regions from weathering rock-forming minerals such as halite, plagioclase feldspar mineral, and argillaceous sediments. However, high sodium in the GW above natural levels may be related to anthropogenic sources like sewage effluent and leaching from landfills, industrial, road salt, and animal waste sites, or saltwater intrusion (Ghalib, 2017). Various serious health issues can be induced by  $\text{Na}^+$  levels above 200 mg/L, including nervous and kidney disorders, congenital diseases, and hypertension, in addition to circulatory and cardiac problems in the human body (WHO, 2017). In the current study, only two samples were  $\text{Na}^+$  less than 200 mg/L, which may be related to the GW recharge events, leading to the dilution by infiltrated water. Thirty-nine samples were unsuitable for drinking due to the significant  $\text{Na}^+$  level ( $\text{Na}^+ > 200$  mg/L).

Forty samples were above the drinking water guidelines of  $\text{Ca}^{2+}$  of 75 mg/L (highest desirable limit (HDL) and thirty-eight samples were higher than 200 mg/L, which is the maximum allowable limit (MAL) recommended by (WHO, 2017).  $\text{Mg}^{2+}$  levels were unsuitable for drinking. High calcium levels in drinking water cause health issues such as kidney or bladder stones (WHO, 2017). The source of calcium in the GW is the dissolution of carbonates from sedimentary rocks and evaporitic minerals such as limestone or dolomite, calcite, dolomite, aragonite, and the most abundant among others in the study area, gypsum and anhydrite. Furthermore, weathering processes of silicate minerals can lead to the formation of calcium (Alsuhaime et al., 2019). Also, increased concentrations of  $\text{Mg}^{2+}$  may be related to the weathering by hydrolysis of magnesium-rich minerals like  $\text{CaCO}_3$ , and  $\text{CaMg}(\text{CO}_3)_2$ , in addition to the anthropogenic sources such as the intensive agricultural activities in the study area (Alsuhaime et al., 2019).

$K^+$  is commonly found in various rocks, thus, the high  $K^+$  level in the GW is due to the relative solubility of  $K^+$  bearing rocks. Thus, feldspar weathering of igneous rocks and weathering of silicate and clay minerals in sedimentary rocks cause the natural presence of  $K^+$  in GW. Chemicals from industries as well as fertilizers are significant sources for the occurrence of  $K^+$  in GW (Mallick et al., 2018). Generally,  $K^+$  and  $Na^+$  ions in the GW are associated with each other; however, the level of  $K^+$  is lower than  $Na^+$  (Alsuhaime et al., 2019). The high  $K^+$  level in the current study may be due to anthropogenic sources and seawater intrusion.

#### *Trace Elements & Heavy Metals Analysis*

Trace elements commonly form insoluble compounds that promote metal precipitation in an alkaline GW (Abdel-Gawad et al., 2008). Twenty-two trace elements have been analyzed in this study. These were As, B, Li, Se, U, Al, Be, Cd, Cr, Ba, Cu, Pb, Mn, Mo, Ni, P, Sr, V, Zn, Fe, Co, and Ag. The mean values of these elements were less than WHO permissible drinking water guidelines. Appendix C presents the summary of the statistical analysis of the main trace elements in the soil samples. These values are below the regulatory limits of trace elements in soils recommended by (USDA, 2000).

#### *Hydrogeochemical facies & General Water Quality Diagrams*

Hydrochemical properties of the GW are attributed to the GW resident time, lithology, geology, and water regional flow pattern (Alsuhaime et al., 2019). The hydrochemical facies is utilized to analyze the chemical composition of GW and illustrate the origin and chemical water types (Othman, 2005). General water quality diagrams are a convenient method to describe the water types according to the ionic

composition (Adimalla & Venkatayogi, 2018). According to the ratio of anion and cation in the GW, it is usually classified into three main groups, namely bicarbonate, sulfate, and chloride types (Alsuhaime et al., 2019). AquaChem software is widely used to analyze, plot, and report aqueous geochemistry and water quality of the GW supply wells. The general distribution of the anions and cations in the GW is illustrated by a Piper diagram. Figure 22A shows the water quality classifications within a Piper plot. Figures 22B, 22C, and 22D show a Piper plot for all GW samples, south basin samples, and north basin samples, respectively. Figures 23A, 23B, 23C, and 23D show the hydrogeochemical plots Schoeller, Durov, Ternary, and Ludwig Langelier plots respectively. These diagrams provide a “fingerprint” by plotting the common cations and anions. These diagrams allow an “at a glance” characterization of general water quality.

Piper plot shows that in the anion triangle, the GW samples range as chloride to sulfate type and only two samples are bicarbonate type. While in the cation triangle, the GW samples range as sodium and potassium type. As shown in the diamond-shaped part the analyzed GW samples are mostly found in  $\text{SO}_4\text{-Cl}$  and  $\text{Ca-Mg}$  (permanent hardness) part of calcium chloride type (non-carbonate hardness above 50%), and in the field of  $\text{SO}_4\text{-Cl}$  and  $\text{Na-K}$  (saline) of sodium chloride type (non-carbonate alkali above 50%) of water. Only two samples in the field of  $\text{HCO}_3\text{-CO}_3$  and  $\text{Ca-Mg}$  (temporary hardness), magnesium bicarbonate  $\text{Mg}(\text{HCO}_3)_2$  type (carbonate hardness above 50%), indicating the dissolution of rock-forming minerals like the dissolution of sulfate from gypsum and anhydrite and Na-rich carbonate rocks dissolution and halite. These results are consistent with the computed mean values of the mineral phase SI that shows under-saturation of halite, gypsum, and anhydrite and over-saturation of calcite and dolomite. These water types indicate the

presence of ion exchange and reverse ion exchange reaction, deep brackish and seawater intrusion, and wastewater. The GW types are more variable in the north GW basin than in south basins. Two wells in the north GW basin showed magnesium-bicarbonate-type water, indicating high recharge by freshwater, whereas most GW samples are dominated by the combination of sodium-chloride-type and calcium-sulfate-type. The calcium-bicarbonate-type waters were associated with the carbonate depositional facies of the Rus formation in the north of Qatar.

Similar trends were shown by the Ternary, Ludwig Langelier, Schoeller, and Durov diagrams. A high level of  $\text{Cl}^-$ ,  $\text{Na}^+$ , and  $\text{SO}_4^{2-}$  and lower level of  $\text{HCO}_3^-$ , and  $\text{Mg}^{2+}$  ions in the GW samples was observed. The result is consistent with (Ghalib, 2017). Generally,  $\text{Cl}^-$  and  $\text{SO}_4^{2-}$  (strong acids) are dominant over  $\text{CO}_3^{2-}$  and  $\text{HCO}_3^-$  (weak acids), and  $\text{Na}^+$  and  $\text{K}^+$  were above  $\text{Ca}^{2+}$  and  $\text{Mg}^{2+}$  (alkaline earth elements) significantly. Thus, most GW samples were dominated by the combination of sodium-chloride-type and calcium-sulfate-type. The bicarbonate anion depleted relative to other anions except in some north GW basin samples with low salinity. Durov diagram results suggested the geochemical evolution where the rainfall recharges GW with Ca-HCO<sub>3</sub> water type then water flow goes through water-rock interactions and dissolution of minerals such as karst formation in Qatar with dolomite, limestone, and gypsum. This resulted in the formation of Ca-SO<sub>4</sub> and Na-SO<sub>4</sub> water types by ion exchange. Then the flow water mixes with the pre-existing GW, which is mainly of high salinity in Qatar, and finally reverse ion exchange led to the formation of the Na-Cl and Ca-Cl type.

The stiff diagram Appendix D shows a vertical axis of sodium-chloride, calcium-bicarbonate, magnesium-sulfate, and iron-carbonate. The resulted polygonal-shaped illustrate the solute distribution in GW samples. Stiff diagrams results are consistent

with piper plots showing four GW types. The stiff diagram shows that the main water type is sodium chloride, which suggests the intrusion of the brackish water from the deep aquifer or adjacent seawater.

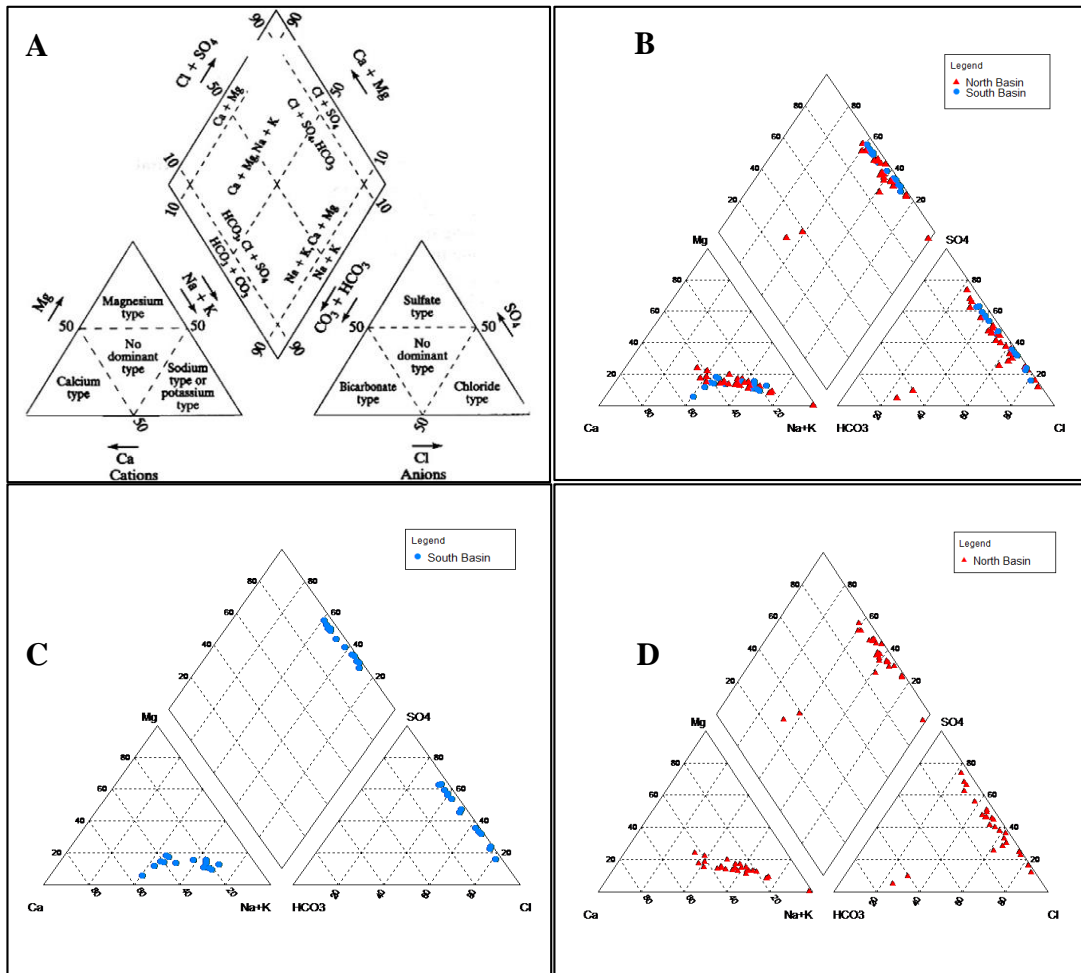


Figure 22. Piper Plot a. classification of Water Quality Types, b. Piper Plot for All GW Samples b. Piper Plot for South Basin Samples and c. Piper Plot for North Basin Samples.

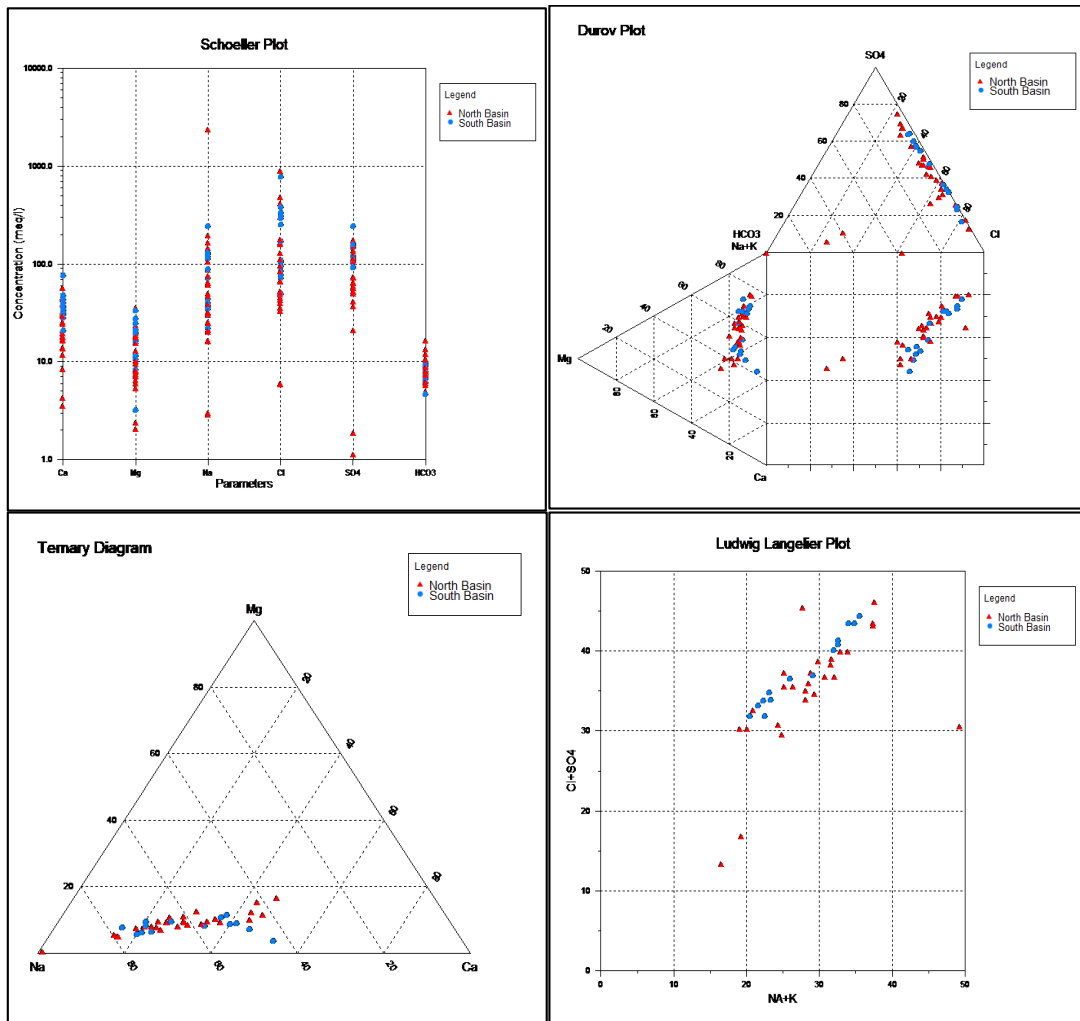


Figure 23. Hydro-geochemical plots for GW Samples a. Schoeller Plot, b. Durov Plot, c. Ternary Plot and d. Ludwig Langelier plot.

### Irrigation Water Quality & Irrigation Hazard Diagrams

The irrigation water problems, which are related to water quality, are salinity, trace elements, and a group of other miscellaneous problems such as nitrate. Othman, (2005) stated that the sodium absorption ratio (SAR) could be used to calculate sodium hazard. SAR measures the extent to which sodium in water substitute's adsorbed calcium ( $\text{Ca}^{2+}$ ) and magnesium ( $\text{Mg}^{2+}$ ) or sodium molarity over calcium plus magnesium molarity as shown in equation 25.

$$\text{SAR} = \frac{\text{Na}^+}{\sqrt{\frac{(\text{Ca}^{2+} + \text{Mg}^{2+})}{2}}} \quad (25)$$

Where, sodium, calcium, and magnesium levels are in milliequivalents/L.

Ranking of water suitability for irrigation can be done by using the irrigation hazard diagram (Wilcox plot) based on specific EC and SAR. The resulting four zones of alkalinity hazard are low sodium hazard water S1 ( $\text{SAR} < 10$ ), medium sodium hazard water S2 ( $10 < \text{SAR} < 18$ ), high sodium hazard water S3 ( $18 < \text{SAR} < 26$ ), and very high sodium hazard water S4 ( $\text{SAR} > 26$ ). While the resulting four zones of salinity hazard are low salinity C1 ( $\text{EC} < 250$ ), medium salinity C2 ( $250 < \text{EC} < 750$ ), high salinity C3 ( $750 < \text{EC} < 2250$ ) and very high salinity C4 ( $\text{EC} > 2250$ ).

The salinity problem causes the salts to accumulate in the crop root zone, decreases the osmotic of plants, hinders water from the plants, and causes a loss in yield (Machado & Serralheiro, 2017). Toxicity problems occur due to the high ion concentration that accumulates to significant levels and leads to crop damage or decreased yields. The level of damage depends on the absorbed amount and tolerability. Furthermore, toxicity commonly accompanies and complicates the salinity or water infiltration problem. Soil amendments might be needed for irrigation water with a high value of SAR to keep away the long-term soil degradation. Soil damage occurs due to  $\text{Na}^+$  ability in water to replace  $\text{Ca}^{2+}$  and  $\text{Mg}^{2+}$  in the soil. This will reduce the soil's ability to form stable aggregates and reduce the infiltration and permeability of the soil to water. However, sandy soils will have lower problems than clay soils (Sherif et al., 2011).

Samples in the irrigation hazard diagram (Wilcox plot) are grouped on the GW basins as shown in Figure 24. Notice that the irrigation hazard diagram is for specific electrical conductivity less than 5,000  $\mu\text{S}/\text{cm}$ . In the current study, only 16 samples (39 %) have EC less than 5,000  $\mu\text{S}/\text{cm}$ . The irrigation hazard analysis indicates that



irrigation use of 60.9% of the GW samples with specific electrical conductivity greater than 5,000  $\mu\text{S}/\text{cm}$  would not be expected since this would likely cause harm to agriculture. The high salinity is measured by specific electrical conductivity in the current study (mean values 5035  $\mu\text{S}/\text{cm}$ ) indicating that the GW with high salinity is not suitable for irrigation and it is only suitable for salt tolerance and semi tolerant crops. Wilcox plot shows 16 samples (34%) fall into the category of C4S2 and C4S3, indicating a very high salinity hazard and medium sodium hazard, and very high salinity hazard and high sodium hazard, respectively. The result shows that the irrigation hazard is always higher from salinity than from SAR. According to Ghalib (2017), C4 category GW samples are not suitable for irrigation for all soil types except for high permeable soil. Only two samples (4.8%) fell into high salinity and low alkalinity hazard (C3S1 category), which would not be expected to likely cause infiltration problems that the higher the salinity, the higher the SAR index so that the infiltration problems could happen. Using the S1 category for irrigation purposes is suitable for types of soil having slight risk or no risk of  $\text{Na}^+$  replacement, such as using coarse soil or organic soils with significant permeability (Adimalla & Venkatayogi, 2018). The C3 category might be used for irrigation semi-tolerant crops (Marghade et al., 2011). The SAR distribution for the study area shows high SAR values in the coastal areas.

The SAR plot only shows the impact of sodium on the stability of soil aggregates. However, high  $\text{K}^+$  and  $\text{Mg}^{2+}$  ion levels have also negative impacts on soil permeability. For example,  $\text{Mg}^{2+}$  in water impacts the soil by enhancing the alkalinity and reducing the crop yield. Another problem related to irrigation water quality occurs with high nitrate concentrations, which may cause extreme vegetable growth, lodging, and retarded crop maturity. High nitrate may indicate anthropogenic impact

from inorganic and organic fertilizers, slurry from animal production, and domestic effluents. El-Alfy et al., (2017) stated that boron occurs naturally in GW due to boron desorption by infiltrating rainwater from mineral surfaces. This might increase the boron levels by ion exchange, which is accompanied by Ca depletion and Na enrichment. The high boron concentrations are often caused by infiltrating wastewater, which has high boron from soaps and detergents.

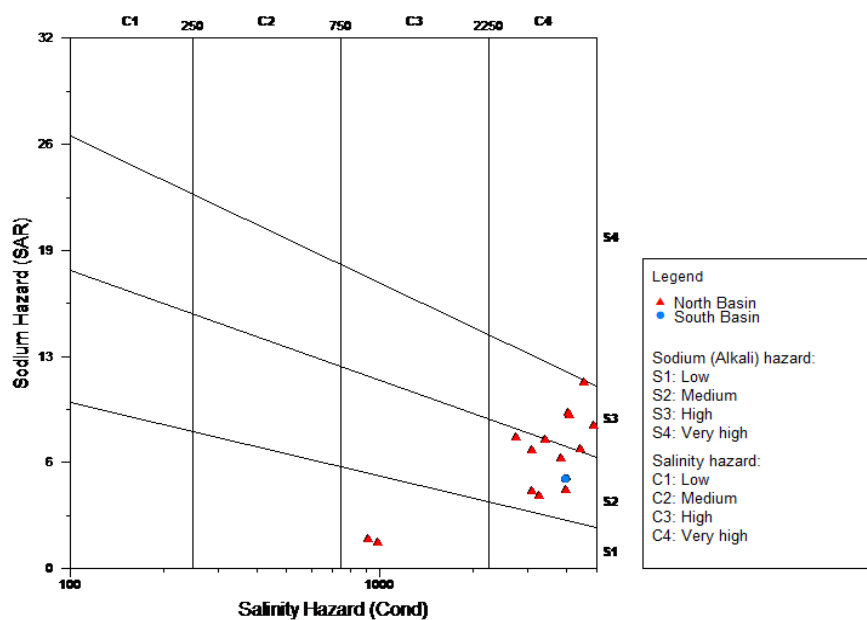


Figure 24. Wilcox plot for groundwater samples.

#### Hydrogeochemical Saturation Index (PHREEQC Analysis)

PHREEQC analysis was done to calculate saturation indices for various minerals, evaporite (gypsum, anhydrite, and halite), carbonate (calcite and dolomite), fluorite, and barite found in the aquifer to determine whether there is a tendency towards precipitation or dissolution. The summary of the statistical analysis using the PHREEQC and the calculated saturation indices (SI) of the collected GW samples

with respect to some common minerals are shown in Table 3. The geochemical modeling program PHREEQC, integrated with Aqua-Chem, is used to compute the saturation indices of common minerals. For the current study, the most relevant output of the geochemical modeling program PHREEQC is the mineral saturation indices, which express the tendency of a solution to dissolve or to precipitate minerals based on its chemical composition, pH, redox potential, and temperature. The saturation index was calculated for each mineral. If the saturation index values are in the range of -0.5 to +0.5; then this should pose no potential risk of dissolution or precipitation. If a negative value of the SI, which is less than -0.5, then this suggests that the solution is under-saturated with respect to the mineral and shows a tendency of the solution to dissolve the mineral if it is present in the aquifer. A positive SI, which is greater than +0.5, then indicates over-saturation, and the solution tends to precipitate the mineral. The SI of approximately 0 indicates equilibrium or saturation conditions between the solution and the mineral and no reaction is expected to occur. Figures 25A, 25B, and 25C illustrate the calculated SI for all GW samples, north basin samples, and south basin samples respectively. Under-saturation with respect to evaporites such as halite (NaCl), anhydrite (CaSO<sub>4</sub>), and gypsum (CaSO<sub>4</sub>·2H<sub>2</sub>O) were found. While over-saturation of carbonate like dolomite CaMg(CO<sub>3</sub>)<sub>2</sub>, fluorite (CaF<sub>2</sub>), and calcite (CaCO<sub>3</sub>) were shown. The areas with the most positive SI values would have the greatest potential for precipitation of these minerals; however, precipitation of dolomite (dolomitization) is not observed to occur, and dolomite is known to precipitate very slowly (SWS, 2009). These results indicate that the carbonate precipitation is significantly attributed to the evaporite dissolution. Adimalla & Venkatayogi (2018) stated significant levels of SO<sub>4</sub><sup>2-</sup> and Ca<sup>2+</sup> that might

precipitate to the soil, and  $\text{CaCO}_3$  saturation was observed in the semi-arid and arid area of sub-surface and surface water.

Table 3. *Saturation Indices Statistics Summary*

Mineral	Minimum (SI)	Maximum (SI)	Mean (SI)	Median (SI)
Anhydrite	-2.19	0.30	-0.30	-0.14
Barite	-0.45	0.34	0.04	0.05
Calcite	1.32	0.24	0.52	0.50
Dolomite	2.53	0.22	0.80	0.70
Fluorite	-0.54	1.10	0.20	0.21
Gypsum	-1.95	0.52	-0.05	0.09
Halite	-2.21	-6.48	-4.12	-4.21

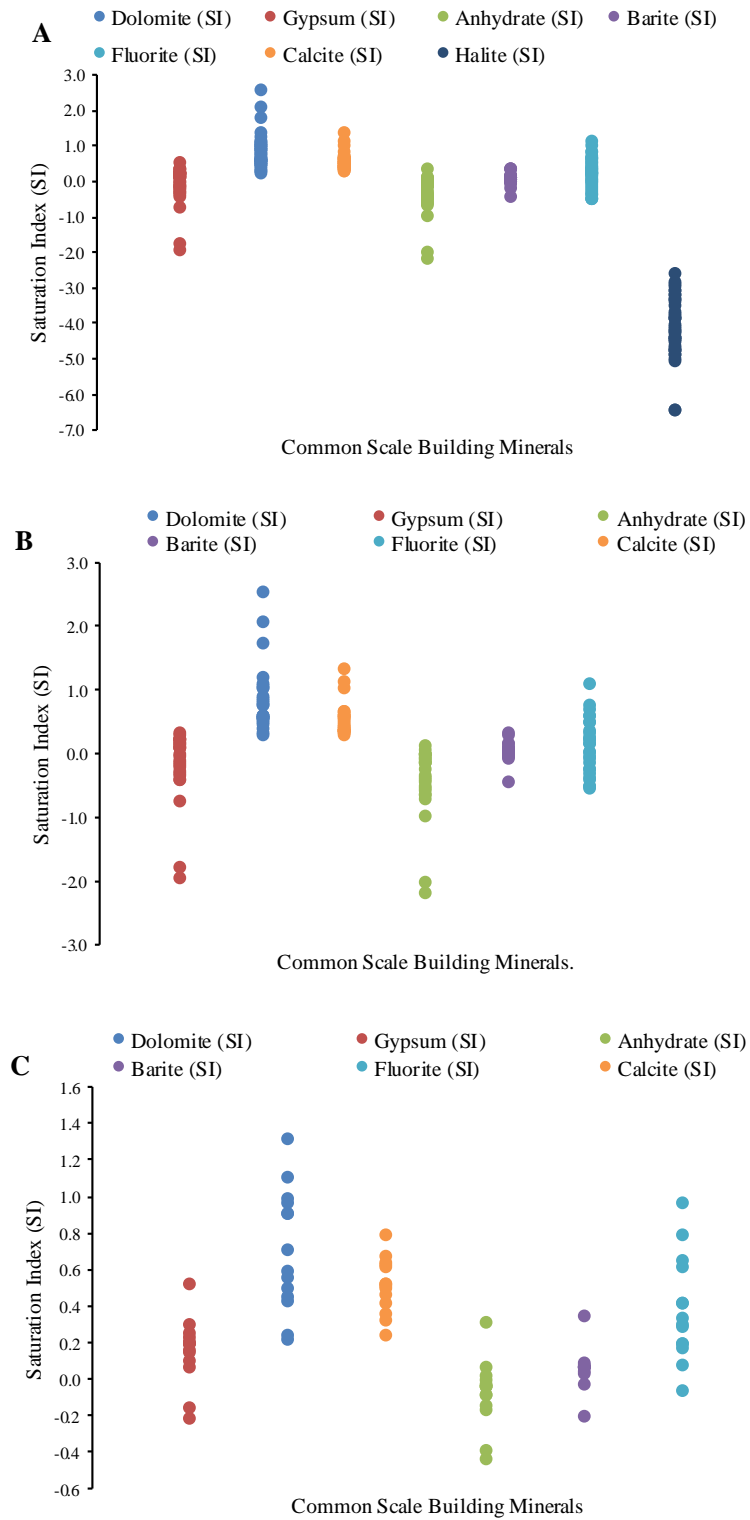


Figure 25. A. Saturation Indices (SI) for All Sample Locations, B. SI for North Basin, C. SI for South Basin.

The areas with the most negative halite, anhydrite, and gypsum SI values would have the greatest potential for dissolution of these minerals, which tend to be in the dissolved phases indicating an increase  $\text{Cl}^-$ ,  $\text{SO}_4^{2-}$  and salinity in GW with water flow. Calcite at first rapidly dissolves by rainwater in comparison with dolomite, then the GW is oversaturated by calcite as  $\text{Ca}^{2+}$ ,  $\text{CO}_3^{2-}$  and  $\text{HCO}_3^-$  levels increase. The permeability and porosity of an aquifer can be enhanced by the dissolution of these minerals causing fracture enlargement in the aquifer. This suggestion is consistent with the presence of karst formation in Qatar. The result of the saturation indices and the minerals trends are consistent with the sodium, chloride, calcium, and sulfate levels in GW as shown by the interpolation maps. The areas with higher calcium indices have a greater likelihood of well-scaling problems. Interpolated maps for anhydrite, barite, calcite, dolomite, fluorite, and gypsum are presented in Appendix B.

### Statistical Analysis

Descriptive statistics and correlation analysis were computed using the statistical package for the social sciences (SPSS). The physicochemical variables were analyzed for the 41 water samples. The summary of the statistical analysis (maximum, minimum, mean as well as standard deviation values) of the physicochemical characteristics of the GW samples. Outliers could be used as an indicator of potential agricultural activities such as fertilizer impacts, localized hydro-stratigraphic, geochemical conditions, or impacts from the well itself. For example, the highest specific electrical conductivity readings were in coastal areas, and the lowest readings were in central Qatar. Another example, fluoride, sulfate, strontium, selenium, and boron could be correlated with evaporite deposits, whereas nitrate could be correlated

with fertilizer impacts. If nitrogen levels in drinking water exceed the permissible limits, it can cause infant methemoglobinemia (blue-baby syndrome), birth malformations, goiter, gastric cancer, hypertension, metabolic disorder, and livestock poisoning. Furthermore, arsenic, iron, manganese, and Mo could be associated with a localized sedimentary depositional or hydrogeochemical environment.

To test the statistical differences between sample means in different locations, the wells were categorized according to the GW basins (north and south GW basin) and according to the hydrological basins. To compare means between north and south GW basin, t-tests were applied, while one-way ANOVA (complete randomized design) was used to test the hypothesis of equal mean between hydrological basins. The results show that TDS does not differ from the north basin to the south basin. The results show that for strontium, calcium, and sulfate, the p-value is  $< 0.05$ . The data provided sufficient evidence to support that there is a difference in strontium, calcium, and sulfate means between the north basin and south basin. According to SWS (2009), the hydrological basins categories were based on the surface water runoff in Qatar. These include 11 areas from A to K as shown in Table 4. Area K consists of the entire perimeter of the Qatar peninsula and includes most of the coastal. The well total depth was measured and the average well depths by hydrological basins are shown in Figure 26. The ANOVA results for the TDS, Li, boron, sodium, sulfate, fluoride, magnesium, calcium, strontium, and selenium are shown in Appendix C. The statistical ANOVA results for the TDS, Li, B, sodium, sulfate, fluoride, magnesium, calcium, strontium, and selenium showed that the p-value was less than 0.05 (t-tests & ANOVA Test). From the TDS homogenous subsets, the mean of hydrological basin B is not under the same column as the mean of hydrological basin K, which means they are not homogenous. Therefore, the mean

of hydrological basin K is significantly different from the mean of hydrological basin B at a 95 % confidence interval.

Table 4. Average Well Depth by Hydrological Basins

Hydrological Basin	Well 's Average Depth(m)
A	38.9
B	30.6
C	48.51
D	38.08
E	36.27
F	28.42
G	74.8
H	36.7
I	19.1
J	25.7
K	20.33



Figure 26. Hydrological Basin for the State of Qatar.



It was noticed that the Li interval values of the hydrological basin H versus the hydrological basin B (0.43, 199) did not contain zero and that the p-value was less than 0.05. Therefore, the mean of hydrological basin H is significantly different from the mean of hydrological basin B at a 95% confidence interval. Boron's mean of hydrological basin A is significantly different from the mean of hydrological basins B and F at a 95% confidence interval. The sodium mean of the hydrological basin k was significantly different from the mean of the hydrological basins A, B, C, E, and F at a 95% confidence interval. The sulfate mean-value of the hydrological basins A and B versus the hydrological basins C, K, F, E, and H and the hydrological basin at a 95% confidence interval. The fluoride mean of the hydrological basin B is significantly different from the mean of hydrological basin H at a 95% confidence interval. The magnesium mean of the hydrological basin B is significantly different from the mean of the hydrological basin H at a 95% confidence interval. The calcium mean value of the hydrological basin B was significantly different from the mean of the hydrological basins E, F, K, and H, at a 95% confidence interval. The strontium mean of hydrological basin H was significantly different from the mean of hydrological basin A and B, and the hydrological basin B versus the hydrological basin E, at a 95% confidence interval. The selenium mean of the hydrological basin A is significantly different from the mean of the hydrological basins E and H at a 95% confidence interval. The ANOVA results showed that TDS, Li, B, sodium, sulfate, fluoride, magnesium, calcium, strontium, and selenium are correlated with the GW depth.

Regression analysis and Pearson correlation were used to check the correlation between water physiochemical parameters such as temperature, pH, TDS, TOC, total hardness (TH), major cations and anions, and trace metals for different GW and topsoil samples. The term strongly correlation refers to  $r > 0.7$ , moderately correlation

refers to  $r = 0.5-0.7$  and weakly correlations refer to  $r < 0.5$ . The results of significant regression correlations are shown in Appendix C (t-tests & ANOVA).

The correlation and regression analysis showed that concentrations of the major anions and cations namely sodium, chloride, calcium, potassium, magnesium, fluoride, bromide and sulfate were a strong predictor for TDS in the GW. Also, the GW salinity was strongly correlated with the GW constituents which exceeded water quality guidelines, namely Li, B, Mo, strontium, uranium, chromium, selenium, and anions and cations namely sodium, chloride, calcium, potassium, magnesium, fluoride, bromide and sulfate with highly significant p-value and strong correlation with a correlation coefficient of 0.999. These correlations show that these are the main constituents that increase the GW salinity. The results of sulfate salts and evaporite minerals dissolution are consistent with (Mallick et al., 2018) such that they are more favorable by the highly saline GW, which causes the levels of  $Mg^{2+}$  and  $Ca^{2+}$  to increase.

Anions and cations namely sodium, chloride, calcium, potassium, magnesium, fluoride, bromide, and sulfate are strongly correlated to each other which contributes to the GW salinity and mineralization. The results were consistent with the SI calculated showing that the dissolution/precipitation caused the concurrent increase/decrease in the cations/anions (Al-Kalbani et al., 2015). For example, the correlation between  $Cl^-$  and  $Na^+$  was consistent with the dissolution of the halite;  $SO_4^{2-}$  correlated with  $Na^+$ ,  $Ca^{2+}$ , and  $Mg^{2+}$ ; indicating the dissolution of evaporite minerals. The correlation between  $Ca^{2+}$  and  $SO_4^{2-}$  contributed to gypsum dissolution, also the correlation between  $Ca^{2+}$  and  $Mg^{2+}$  infers the dolomite dissolution with low content of magnesium carbonate. A good correlation between  $Ca^{2+}$ ,  $Mg^{2+}$ ,  $Na^+$ , and  $K^+$  levels in the GW suggests a common source for the major cations. High fluoride

levels in GW are commonly dissolution by hydrolysis or removed by precipitation of calcite, which is consistent with (El-Alfy et al., 2017).

The correlation between the  $\text{Cl}^-$  and  $\text{SO}_4^{2-}$  with  $\text{Na}^+$ ,  $\text{K}^+$ ,  $\text{Ca}^{2+}$ , and  $\text{Mg}^{2+}$  is consistent with the hydro-chemical facies analysis as most of the GW samples were dominated by the combination of sodium-chloride-type and calcium-sulfate-type. The correlation between total hardness and the ions  $\text{Ca}^{2+}$ ,  $\text{Mg}^{2+}$ , and  $\text{Cl}^-$  showed that the hardness of the water was permanent in nature. The effect of the ion exchange process is indicated by the relations between  $\text{Na}^+$  and  $\text{K}^+$  with  $\text{Mg}^{2+}$  and  $\text{Ca}^{2+}$ .

The multiple regression analysis showed a highly significant correlation between Li and B and Mo, and a good correlation with a correlation coefficient of 0.601. Boron and Li in water did not show a significant correlation with B and Li in topsoil concentrations. The significant correlation was between sodium and chromium concentration in water with sodium and chromium concentrations in topsoil.

Figure 27 shows the PCA plot. It suggests three significant PCs, of Eigenvalues higher than one, explain 99% of the total variance of the dataset. All loadings, greater than 0.6, are considered in interpreting the analysis as a significant contributor. The first principal component (PC1) explains 49% of the total variance. PC1 showed a positive loading of Mg, Th, Sr, Ca, TDS,  $\text{SO}_4$ , Li, Cl, F, Br, Cd, K, Ba, Na, representing the factors, which are contributed to the high salinity of the GW due to the mineralization of rocks and soil. For example, the positive loadings of  $\text{Cl}^-$  and  $\text{SO}_4^{2-}$  indicate the dissolution of evaporite minerals (halite ( $\text{NaCl}$ ) and gypsum ( $\text{CaSO}_4 \cdot 2\text{H}_2\text{O}$ )) which is supported by water type classification and SI calculations.

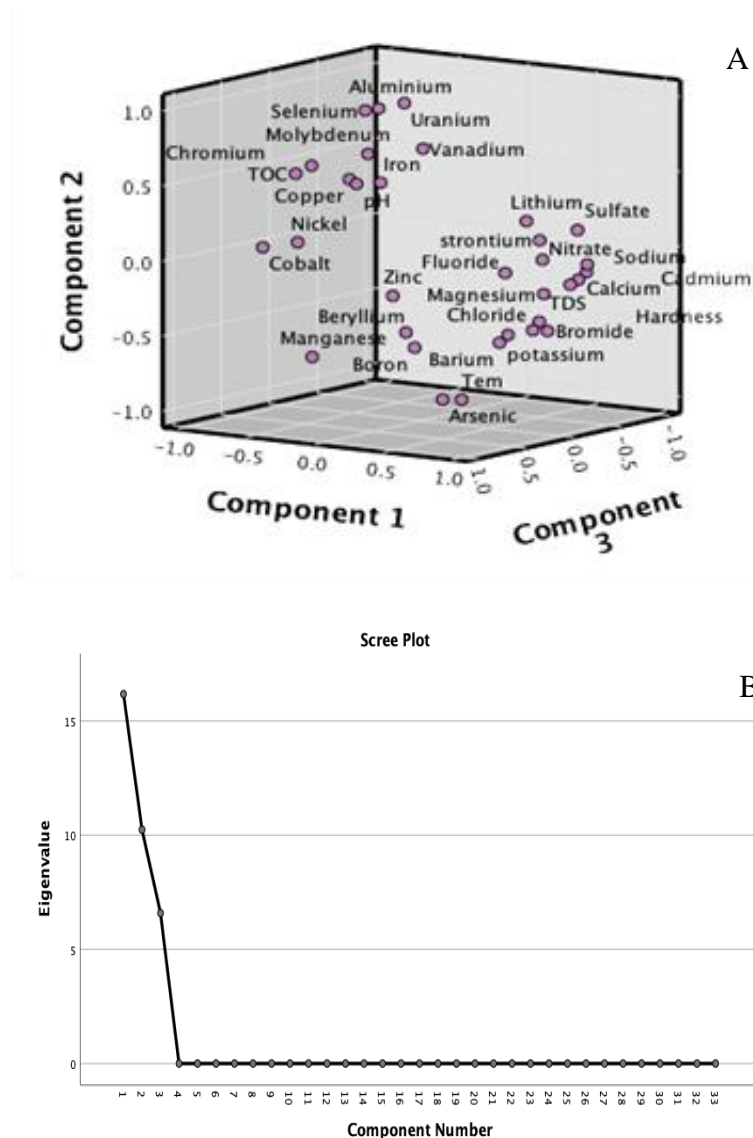


Figure 27. A. Principal Component Analysis Plot, B. Eigenvalues Loading plot.

Moreover, 31% of the total variance is explained by the second principal component (PC2). PC2 showed the negative loadings of U, Al, Se, Se, Mo, Mg, and temperature, which could be associated with localized sedimentary depositional or hydrogeochemical environment. The third principal component (PC3) accounts for 19.9% of the total variance. PC3 shows positive loadings of Ni, Zn, Be, pH, Cu, Co, Fe, B, V, TOC that indicate the dissolution and precipitation (reducing and oxidizing factor). Only  $\text{NO}_3^-$  in PC3 was shown a high negative loading, which might indicate

human influence from intense agricultural activities such as the utilization of potassium nitrate and phosphate fertilizers on quality of GW; particularly, potassium nitrate, which has high water solubility (El-Alfy et al., 2017). Therefore, there might be a vulnerability to anthropogenic pollution in a shallow aquifer. Knowing that B and Li are used as geothermal tracers (Al-Farraj et al., 2013). The positive loadings of B and Li might indicate geothermal activity and mineral weathering. This is consistent with the high-significant positive regression correlation between sodium with B and Li.

#### Comparisons with Standard and Guidelines

The summary of the analytical results of the general water quality parameters, major cations, and anions, and inorganic chemical concentrations are compared with the US environmental protection agency (US-EPA), the world health organization (WHO), and the Gulf standardization organization (GSO) drinking water and irrigation guidelines and standards. The mean values of the EC, TDS, hardness, cations, and anions namely  $\text{Ca}^{2+}$ ,  $\text{Mg}^{2+}$ ,  $\text{K}^+$ ,  $\text{Na}^+$ ,  $\text{Cl}^-$ ,  $\text{F}^-$  and  $\text{SO}_4^{2-}$  exceeded the drinking and irrigation guidelines. All other means of water quality variables are within the guidelines. The interpolation maps for B, Li, Mo, strontium, chromium, and selenium are presented in Appendix B.

Boron levels in eight samples exceeded the WHO, GSO, and Qatar drinking water guidelines. The presence of boron in GW can be natural or due to anthropogenic sources. Natural sources are igneous rocks weathering and leaching from sedimentary boron-bearing salt deposits. Another natural boron source in the coastal regions due to its high volatility is rainfall containing sea salt from ocean spray. Anthropogenic sources are landfill leachate, drainage from coal mines and mining industry, glass

industry, semiconductor manufacture, fly ash, petroleum products, using fertilizers or pesticides in agricultural, and sewage effluents due to use of sodium perborate in detergents and cosmetics (Hasenmueller & Criss, 2013). In the current study, the anthropogenic sources of boron could be from the petroleum industry, using fertilizers or pesticides in agricultural, and sewage effluents. When boron amount is higher than required, toxic effects appear such as yellow tips of leaves, spots on fruits, spoil, and drop of unripe fruit, further it may cause the death of plants. Boron level less than 1 mg/L should be used in irrigation water for sensitive crops, and of a level of 0.5 mg/L for long-term irrigation (Voutsas et al., 2009). Boron forms complexes with other toxic metals such as lead, cadmium, or nickel, which may enhance the toxicity (Al-Ghouti et al., 2017).

Mo levels in nine samples exceeded the WHO, GSO, and Qatar drinking water guidelines, and 23 samples exceeded the US-EPA lifetime health advisory. Mainly Mo compounds are low soluble in water, while when Mo-bearing minerals react with oxygen and water, they produce molybdate ion is less soluble. Acute exposure to elevated Mo levels causes adverse health effects such as diarrhea, anemia, and gout; while chronic exposure causes weakness, fatigue, lack of appetite, anorexia, liver dysfunction, joint pain, osteoporosis, Cu deficiencies, and pneumoconiosis (WHO, 2011). Mo is an important alloying agent, which strengthens the steel and decreases its weight (Henckens et al., 2018). A potential source of Mo in Qatar's GW could be from the oil and gas-processing sector as mainly the local natural gas is a sulfur-containing as Mo is used as a catalyst in the desulfurization process (Kuiper et al., 2015). According to the international Mo association, Mo is also used in the manufacturing of pigments, corrosion inhibitors, smoke suppressants, lubricants, and fertilizers (IMOA, 2018).

Li levels in 39 samples exceeded the GSO and Qatar (Kahramaa) requirements for the water quality distribution systems in Qatar. Li is a naturally occurring alkali metal with an atomic number of three, it is found in many igneous rocks and several natural brines (Weil & Ziemann, 2014). The main sources of Li are Li -containing wastes such as produced petroleum water (Isupov et al, 1999). Li is an alkali metal that is characterized by high electrochemical activity due to the quick loss of electrons; thus, Li is a significant producer of electric current (Wang et al., 2016).

Strontium in 40 samples exceeded the US-EPA lifetime health advisory, the GSO, and the Qatar drinking water guidelines. Strontium commonly occurs in nature. It is primarily used in television cathode ray tubes. Strontium is used in glow-in-the-dark toys, red firework, and strontium chloride is used in toothpaste for sensitive teeth. Strontium in the human body is absorbed like it the lighter congener calcium due to the chemical similarity. In children, strontium can substitute calcium and thus lead to bone growth issues. Uranium levels in one sample exceeded the WHO, GSO, and Qatar drinking water guidelines and one sample exceeded the US-EPA drinking water guidelines. Boron levels in 39 samples exceeded the USEPA guidelines for short-term use of irrigation water, 20 exceeded the USEPA guidelines for long-term use of irrigation water and three samples exceeded the Qatar irrigation guidelines. Mo levels in 40 samples exceeded the USEPA guidelines for short-term use of irrigation water, 18 exceeded USEPA guidelines for long-term use of irrigation water. Selenium levels in one sample exceeded the US-EPA irrigation guidelines. Chromium levels in two samples exceeded the Qatar irrigation guidelines.

### Comparing Interpolation Methods

In this study, different values of powers and neighborhoods were examined using standard neighborhood type (or nearest neighbor) then the RMSE values were obtained (Balakrishnan, 2011), as shown in Tables 5, 6, and 7. The best-fit interpolated model for the input data representation is the one with the least RMSE value (Arslan & Turan 2015). Similarly, Falivene et al., (2010) have shown that interpolation smoothing is primarily controlled by the number of neighbors averaged and by the model parameters. Table 5 shows RMSE for IDW parameters, with the lowest RMSE value and the best parameters. Tables 6 and 7 show the optimized RBFS parameters and the optimized kriging parameters respectively. Some cross-validation statistics such as RMSE, average standard error, mean standardized, and root mean square standardized values were also shown. The result shows that the SK model performed better than IDW and RBFs models for pH, chloride, selenium, strontium, potassium, SAR, Mo, Li, and nitrate data. While the RBFs model was the best for sodium and calcium. IDW model worked better for TDS, boron, sulfate. Nevertheless, RMSE values between IDW and RBF are not significantly different. In this study, RMSE values were generally high; one possible explanation is the uneven distribution of the data configuration as large spacing intervals between sample locations generated high RMSE values. Another possible explanation is the presence of outliers in the original data. In the current study, the sampling points are not well distributed, and the sample intensity is low due to the limitation to access the private farms that contained some GW wells. This resulted in high spatial variation in some attribute data. Thus, to enhance the performance of spatial interpolation and to allow estimation of short-range variance, the sample size needs to be increased.



Table 5. *RMSE values obtained by the IDW interpolation method for different parameters.*

Attribute Variable	Power	Sector type (circular)	Number of Neighbors		Root Mean Square	Mean Square
			Minimum	Maximum		
pH	1	8	10	15	0.2466	-0.018
TDS	1	4	10	15	3278	-80.54
TOC	2	8	10	15	6.43	-0.237
Hardness	1	4	10	15	939.22	18.25
SAR	1	1	10	15	7.68	-0.08
Boron	2	1	10	15	645.66	65.58
Sodium	1	1	10	15	1188.10	9.99
Lithium	1	1	10	15	51.48	-0.519
Molybdenum	1	4	10	15	47.10	-1.18
Selenium	2	1	10	15	3.98	-0.36
Uranium	1	1	10	15	5.04	-0.128
Chromium	1	4	10	15	3.28	-0.16
Strontium	1	1	10	15	4097.7	112.48
Potassium	1	1	10	15	57.69	-1.52
Calcium	1	1	10	15	237.92	12.87
Magnesium	1	4	10	15	91.07	-1.8
Fluoride	1	1	10	15	1.47	-0.054
Chloride	1	4	10	15	6883.93	-237.6
Bromide	1	8	10	15	5.22	-0.17
Nitrate	1	8	10	15	28.03	1.33
Sulfate	1	1	10	15	2000.98	191.78

Table 6. *RMSE values obtained by RBFs interpolation method for different parameters.*

Attribute Variable	Kernel parameter	Sector type (circular)	Number of Neighbors		Root Mean Square	Mean
			Minimum	Maximum		
pH	0.0090	1	10	15	0.256	-0.011
TDS	0.0090	1	10	15	3348.49	-121.3
TOC	0.0013	1	10	15	6.45	-0.020
Hardness	0.0090	1	10	15	957.94	-2.06
SAR	0.0090	1	10	15	7.84	-0.15
Potassium	0.0090	1	10	15	58.44	-2.08
Strontium	0.0090	1	10	15	4235.2	-40.47
Chromium	0.0090	1	10	15	3.35	-0.146
Uranium	0.0090	1	10	15	5.15	-0.051
Molybdenum	0.0090	1	10	15	48.15	-0.585
Selenium	0.0020	1	10	15	3.88	-0.125
Lithium	0.0090	1	10	15	52.35	-0.717
Sodium	0.0090	1	10	15	1216.37	-10.28
Boron	0.0090	1	10	15	633.76	25.806
Calcium	0.0090	1	10	15	239.37	3.53
Magnesium	0.0090	1	10	15	94.87	-2.64
Fluoride	0.0090	1	10	15	1.49	-0.049
Chloride	0.0090	1	10	15	7039.93	-319.4
Bromide	0.0090	1	10	15	5.45	-0.23
Nitrate	0.0090	1	10	15	29.72	1.53
Sulfate	0.0090	1	10	15	1982.7	92.73

Table 7. RMSE values and prediction indices obtained by the SK interpolation method for different parameters.

Attribute Variable	Number of Neighbors		Mean	Root Mean Square	Average Standard Error	Mean Standardized	Root Mean Square Standardized
	Min	Max					
pH	2	5	-0.007	0.238	0.239	-0.030	0.994
TDS	2	5	66.76	3228.9	3566.5	0.025	0.917
TOC	2	5	0.038	6.22	6.72	0.009	0.940
Hardness	2	5	4.16	929.18	927.46	-0.000	1.029
SAR	2	5	0.10	8	9.08	0.022	0.865
Potassium	2	5	-1.68	56.44	50.72	-0.034	1.12
Strontium	2	5	-78.1	4416.35	4003.23	-0.007	1.13
Chromium	2	5	-0.10	3.27	3.39	-0.028	0.95
Uranium	2	5	-0.418	4.86	2.64	-0.244	2.25
Molybdenum	2	5	-2.59	45.46	36.19	-0.07	1.27
Selenium	2	5	-0.128	4.18	4.37	-0.006	0.96
Lithium	2	5	-0.093	50.5	50.66	-0.093	0.98
Sodium	2	5	14.02	1187.56	1227.66	0.021	0.95
Boron	2	5	53.42	635.56	668.92	0.066	0.96
Calcium	2	5	6.64	236.65	235.63	0.012	1.05
Magnesium	2	5	0.140	90.25	91.43	0.000	0.99
Fluoride	2	5	-0.018	1.42	1.27	-0.039	1.14
Chloride	2	5	-350.79	6676.94	6058.41	-0.05	1.09
Bromide	2	5	0.048	4.86	4.97	0.011	0.97
Nitrate	2	5	0.926	27.12	27.08	0.021	1.01
Sulfate	2	5	78.88	1943	1921.67	0.029	1.11

The current study showed that each of the three spatial interpolation methods has unique advantages and produced different output surfaces. The SK produced smooth and relatively continuous surfaces that contained irregular changes in the data because SK is an unbiased interpolator that has fitted a semi-variogram model. SK provides the measurement of prediction uncertainty. However, SK is an inexact interpolator, as the output data did not include the exact input values. Being exact interpolators, IDW and RBF have output surface values exactly equal to that of the input data values. Therefore, IDW and RBF models gave better interpolation maps that help to visualize the location of GW within and above the guidelines. However, the IDW model is better than RBF as it does not produce values above or below the range of the measured values. Furthermore, the smoothness of the output surface is also an important factor for assessing the performance of the interpolation methods. It was noticed that RBFs gave smoother interpolation maps than IDW and kriging methods. The inferior smoothness of the interpolated maps is due to the uneven distribution of sample points and some extreme value points.

#### Spatial Variability Analysis

Appendix B shows the interpolated map for pH using the SK method. The pH values are changed within a range of 6.8 to 7.9 with an average of 7.3, which meets the WHO standard (6.5-8.5) revealing geochemical equilibrium (WHO, 2017). Only two samples were slightly acidic (pH = 6.9 and 6.8) that could be correlated to the use of the fertilizer in the farms. The spatial variation of TDS was done using the IDW method. EC ranged from 0.92 S/cm to 0.92 - 22.33 S/cm, and the average was 7.29 S/cm. TDS ranged from 598 mg/L to 15633 mg/L, and the average was 5038 mg/L. EC is grouped to low saline (EC = 1500  $\mu$ S/cm), medium saline (1500 -3000  $\mu$ S/cm)

and high saline ( $EC > 3000 \mu S/cm$ ) (Ghalib, 2017). Using this classification, there were no samples with  $EC < 500 \mu S/cm$  which is similar to freshwater EC. Only two samples are characterized as low salinity, one sample as moderately saline, and 38 samples as highly saline, which is considered unfit for drinking and irrigation (WHO, 2017) (FAO, 1994). High TDS and EC enhance the corrosion and salinity of the GW. Using salty GW for irrigation over the long term reduces soil fertility (Elumalai et al., 2017). The spatial variation in TDS maps is due to the type of aquifer rock and the residence time of the GW, in addition to the extreme weather condition such as high temperature and low rainfall (Alsuhami et al., 2019). In the current study, the high EC and the high salinity values are attributed to the aridity of Qatar due to the low rainfall and high evaporation. Also, some agricultural activities like the use of the high salinity GW for irrigation that causes salts leaching. In addition, overexploitation of GW caused the intrusion of the deep brackish GW or the seawater. High TDS values are shown along with the coastal areas due to the seawater intrusion, while high EC in south areas due to low rainfall and deep brackish GW intrusion. The high TDS problem with GW is also stated in the study of Hadi & Al-Ruwaith (2008), in Kuwait, where TDS ranged from 200 mg/L to 800 mg/L and it revealed 14500 mg/l in some locations; While in Saudi, TDS ranged from 13- to 6000 mg/L (Abdel-Satar et al., 2017). Saltwater intrusion from coastal areas is also reported by other studies such as the study by Nwankwo et al., (2020).

The interpolated map of  $Na^+$  was done using the RBFs method.  $Na^+$  ions were found as the most dominant cation, the range of the ions was (64.2 mg/L - 5547 mg/L), with an average of 1466 mg/L. The natural source of  $Na^+$  in the GW is the weathering minerals such as halite and feldspar minerals.  $Na^+$  high levels more than the natural levels are mainly correlated to anthropogenic sources such as sewage effluent and

leaching from landfills and saltwater intrusion (Ghalib, 2017). Sodium levels above 200 mg/L in water are inappropriate for domestic use and can result in severe health problems in the human body, such as hypertension, congenital diseases, kidney disorders, nervous disorders, circulatory and cardiac problems (WHO, 2017). 39 samples were inappropriate for drinking due to high  $\text{Na}^+$  concentration ( $\text{Na}^+ > 200$  mg/L).  $\text{Cl}^-$  ions were the most dominant anion ranging from 203.6 to 30806 mg/L with an average of 6289 mg/L. The interpolated map of  $\text{Cl}^-$  using the SK method shows high  $\text{Cl}^-$  in drinking water results in a salty taste (Adimalla & Venkatayogi, 2018). The spatial distribution of sodium and chloride in GW is similar to the distribution of TDS, which increases from inland to coast as shown by the interpolation maps. Thus, TDS can be used as a surrogate for sodium and chloride.  $\text{SO}_4^{2-}$  ions ranged from 53.4 mg/L to 11596 mg/L with an average of 4977 mg/L. The gypsum ( $\text{CaSO}_4 \cdot 2\text{H}_2\text{O}$ ) and anhydrite ( $\text{CaSO}_4$ ) are a natural source of metallic sulfate. The interpolation map of  $\text{SO}_4^{2-}$  ions illustrates that the highest levels are in the south of the study area due to the dissolution of gypsum and anhydrite, and leached water from agriculture activities (Alsuhaime et al., 2019). Water with high  $\text{Cl}^-$  and  $\text{SO}_4^{2-}$  result in hypertension, laxative effect, diarrhea, asthma, dehydration, and gastrointestinal irritation (WHO 2004).  $\text{NO}_3^-$  ions ranged from 5.2 mg/L to 113.3 mg/L with an average of 37.2 mg/L. The interpolation map for  $\text{NO}_3^-$  is produced using the SK method.  $\text{NO}_3^-$  ions are important for plant growth as a main nutrient. Fertilizers, agricultural/municipal waste, and leaching of sewage might contribute to high  $\text{NO}_3^-$  in the GW (Mallick et al., 2018). The high concentration of nitrate in drinking water results in methemoglobinemia in infants, furthermore, it has also been stated that it causes cyanosis, goiter, oral cancer, cancer of the colon, gastrointestinal cancers, lymphoma (WHO, 2017). The average value of  $\text{NO}_3^-$  in the GW was 36.32

mg/L. The interpolation map shows the highest values of  $\text{NO}_3^-$  in the northern and central of Qatar. High  $\text{NO}_3^-$  in the current study is related to inorganic and organic fertilizers, manure application in the private farms, especially in the shallow GW, and domestic effluents (Shomar, 2015).

Twenty metals are analyzed in this study, namely B, Li, Se, U, Al, As, Ba, Be, Cd, Cr, Co, Cu, Fe, Pb, Mn, Mo, Ni, P, Sr, V, Zn, and Ag. The mean concentrations of these metals were below the permissible WHO guidelines for drinking water (WHO, 2017). B, Li, Mo, strontium, chromium, and selenium exceeded in some samples. Boron ranged from 0.38 mg/L to 3.8 mg/L with an average of 1.8 mg/L, and selenium ranged from 0.0015 mg/L to 0.02 mg/L with an average of 0.008 mg/L. Interpolated maps for boron and selenium interpolated maps respectively. Boron in 8 samples was higher than the WHO, GSO, and Qatar drinking water guidelines. Mo ranged from 0.0078 mg/L to 0.29 mg/L with an average of 0.053 mg/L. The interpolation map for Mo is produced using the SK method. Boron in 8 samples was higher than the WHO, GSO, and Qatar drinking water guidelines (WHO, 2017; GSO, 2008; Kahramaa, 2016). Mo concentrations in 9 samples exceeded the WHO, GSO, and Qatar drinking water guidelines and 23 samples were higher than the US-EPA lifetime health advisory. In the current study, high Mo levels can be attributed to the oil and gas industry (Kuiper et al., 2015). In addition, Mo is an alloying agent, corrosion inhibitors, smoke suppressants, and it is used in some fertilizer and pigments manufacturing (IMOA, 2018). Li ranged from 0.02 mg/L to 0.23 mg/L with an average of 0.12 mg/L. Li ion in 39 samples was higher than Qatar's guideline in Qatar (Kahramaa, 2016). Strontium ranged from 3.5 mg/L to 20.2 mg/L with an average of 13.2 mg/L. The interpolated maps for strontium using the SK method. Strontium in 40 samples was higher than the US-EPA lifetime health advisory (US-EPA, 2018), the

GSO, and the Qatar drinking water guidelines (WHO, 2017; GSO, 2008; Kahramaa, 2016). Strontium is used in the manufacturing of television cathode ray tubes, glow-in-the-dark items, and fireworks. In children, strontium can replace calcium as the mineral of the growing bones and cause health problems.

Using GIS spatial methods in studying the suitability of land for agriculture activities is a significant tool (Abdel-Rahman and Arafat, 2020; Masoud, 2020). Using salty GW for irrigation over the long term reduces soil fertility and hinders crop yield (Elumalai et al., 2017). Irrigation with high salinity GW results in salt accumulation in the crop root zone and reduces the osmotic ability of plants (Machado and Serralheiro, 2017). Only 16 samples (39%) have EC less than 5000  $\mu\text{S}/\text{cm}$ , which is not used in the irrigation hazard diagram. The irrigation hazard analysis shows that 60.9% of the GW samples with EC > 5000  $\mu\text{S}/\text{cm}$  should not be used for irrigation. The GW found to be with high salinity, and EC GW in the study is inappropriate for irrigation, and it could be used to irrigate salt tolerance and semi tolerant crops. If the soil is irrigated with water of high SAR, then the soil will need amendments. Ghalib (2017) stated that GW samples falling into the C4 category are inappropriate for irrigation of all soil types, they are only appropriate for high permeable soil, which is not the case in Qatar. The spatial distribution of SAR is produced using the SK method. The high SAR values in the coastal areas are due to seawater intrusion. A study by Al-Omran (2018), showed that SAR in Saudi Arabia ranged from 0.79 to 10 and TDS was higher than the drinking water standard in Saudi Arabia (GSO, 2008).

Boron levels in 39 samples are higher than the USEPA guidelines for short-term use as irrigation water, 20 are higher than the USEPA guidelines for irrigation water (USEPA, 2018). In a study by El-Alfy (2016), boron was found to reach a high concentration of 2.8 mg/L in Egypt. Mo levels in 40 samples are higher than the



USEPA guidelines for short-term use as irrigation water, 18 are higher than USEPA guidelines for long-term use as irrigation water (US-EPA, 2018). High Mo (mean 26.9  $\mu\text{g/L}$ ; max 103  $\mu\text{g/L}$ ) was observed in Qatar's GW (Kuiper et al., 2015). High Mo concentration (0.07 mg/L-1.44 mg/L with an average of 98  $\mu\text{g/L}$ ) was also reported by Al-Kuisi et al. (2015), in Jordan that exceeded WHO guidelines for Mo. In this study, selenium levels in one sample are found to be higher than the US-EPA irrigation guidelines. Chromium levels in the two samples are higher than the Qatar irrigation guidelines. In Jordan, selenium concentration exceeded the permitted level of 10  $\mu\text{g/L}$  (Al-Taani, 2012).

#### Physical and Chemical Characteristics of Adsorbates

The adsorption relies on the adsorption of the metal ions from the solutions onto the adsorbent's surfaces (Shafiq et al., 2019). Metal ions of larger electronegativity would adsorb easily, and the metal ions of larger hydrolysis constants would increase adsorptive capacity, while metal ions with higher ionic radius have a lower charge density and a lower electrostatic attraction, which decreases the adsorption (Minceva et al., 2008). The attractive forces between adsorbate and the solid surface of adsorbent are chemical bonding, hydrogen bonding, weak Van der Waals forces, dipole-dipole interaction, dipole-induced dipole interaction, induced dipole-induced dipole interaction, and ion exchange (Ahmad et al., 2011). Furthermore, electrostatic chemical bonding between the adsorbate and adsorbent forms in a monolayer and it is an irreversible process. The electrostatic interaction is a site specific and relies on the high temperature. In contrast, the physisorption is mono or multilayer, reversible process and it decreases with high temperature such that very high temperatures are required for desorption (Shafiq et al., 2019). In order to find a possible attractive site

between adsorbate ions (B, Mo, and Li) and adsorbents, characteristic properties such as crystal radius and equilibrium constants for adsorbate ions are shown in Table 8.

Table 8. *Crystal Radius, Hydrolysis Constant and Electronegativity for Adsorbate Ions*

Adsorbate	Crystal radius $r_{\text{cryst}}$ (Å) (Shannon, 1976; Corti, 1980)	Hydration radius $r_s$ (Å) (Wang & Weinstock, 2012; Yizhak, 1989).	Hydrolysis constant pKa (Miessler, 2014; Wulfsberg, 1995; Nagul, 2015)	Pauling electronegativity (Daniel & Harris, 2011)
$B(OH)_4^-$	2.44	2.61	Boric acid $B(OH)_3$ 9.24 (Weakly acidic cation)	2.051 for boron
$MoO_4^{2-}$	2.70	4.06	Molybdic acid ( $MoO_3$ or $MoO_3(OH)_3$ ) 0.9 (Strongly acidic cation)	2.16 for molybdenum
$Li^+$	0.68	2.38	13.6 (Feebly acidic cation)	0.912

### *Lithium*

The physicochemical properties of Li are shown in Appendix E. Li is a naturally occurring alkali metal with an atomic number of three, it is found in many igneous rocks and several natural brines (Weil & Ziemann, 2014). The main sources of Li are Li-containing wastes such as produced petroleum water (Isupov et al, 1999). Such as all alkali metals that are characterized by high electrochemical activity, Li atoms give up electrons very easily, making them highly efficient producers of electric current (Huang, 2018). Li is a light element, thus; it is used in lightweight alloys such as steel and aluminum industry (Jackson, 2007). Li is used in many commercial applications

such as batteries, glass, ceramics, and chemicals industries (Visco, 2015). Li salts have proven to be useful as a mood-stabilizing drug in the treatment of bipolar disorder in humans (Jackson, 2007). The high demand for Li in many commercial applications has increased research on its recovery from brine for the past decades (Sun et al., 2018). Ion exchange adsorption is an efficient technique for removing Li ions from solutions due to the high selectivity such as manganese-type Li-ion sieves and titanium-type Li-ion sieves (Wang et al., 2018). Aluminum hydroxide could be used as sorbent of Li salts from brines such that the total dynamic exchange capacity (TDEC) reached 6 mg/g, (Isupov et al, 1999). Another study by Özmal & Erdoğan (2015) showed that Li ions adsorption from the borogypsum solution using a spinal type of manganese oxides gave 98.54% of adsorption yield. The surface of AC can adsorb Li-ions due to oxygen-containing functional groups so that Li ions are adsorbed by the electrostatic interaction of positive and negative charges; ion exchange, the core of adsorption is dipole interaction, which belongs to physical adsorption (Zhang et al. 2017). However, there is a lack of thermodynamics and kinetics of Li adsorption in the aqueous phase (Zhang et al. 2017).

### *Boron*

The physicochemical properties of boron are shown in Appendix E. Boron is semimetal; it is found in the block P (group 13) in the periodic table (metalloids); It has a high melting point and quite low vapor pressure. Boron is a widely spread natural occurring element and normally it presents in compounds such boric acid or borate salts with oxidation states of +3, +1, 0, or less than 0 (Köse et al., 2011; Wolska & Bryjak, 2013). Boron is concentrated by the water-solubility of the borate minerals. Boron is an essential trace element for plant growth; however, boron

deficiency levels are close to toxicity levels (Hilal & Somerfield, 2011). When boron amount is higher than required, toxic effects appear such as yellow tips of leaves, spots on fruits, spoil and drop of unripe fruit, further it may cause death of the plant. Boron level of <1 mg/L in irrigation water is needed for sensitive crops and of 0.5 mg/L for long-term irrigation (Wang et al., 2014; Voutsas, 2009). Boron forms complexes with other heavy metals such as lead, cadmium, or nickel, which may enhance the toxicity (Al-Ghouti, 2018). In freshwater boron levels are usually from less than 0.01 mg/L to 1.5 mg/L. Boron forms a very weak monobasic acid in aqueous solution. Boric acid is a solid substance soluble in the water with a solubility of 55 g/L at 25 °C; Tetrahydroxyborate is the conjugate base of boric acid in an aqueous solution, which has a strong attraction to hydrogen ions (Wolska & Bryjak, 2013; Karahan et al., 2006). WHO proposed a guideline of 2.4 mg/L in drinking water (WHO, 2011). There are natural and anthropogenic sources of boron in GW. Natural sources are weathering igneous rocks and leaching from sedimentary boron-bearing salt deposits. Another natural boron source in coastal regions due to its high volatility is rainfall containing sea salt from ocean spray. Anthropogenic sources are landfill leachate, drainage from coal mines and mining industry, glass industry, semiconductor manufacture, fly ash, petroleum products, using fertilizers or pesticides in agricultural, and sewage effluents due to use of sodium perborate in detergents and cosmetics (Hasenmueller & Criss, 2013).

### *Molybdenum*

The physicochemical properties of Mo are shown in Appendix E. Mo has an atomic number of 42 and an atomic weight of 95.94 g/mol. It is a transition metal and an essential nutrient; adults need from 75 µg/day to 250 µg/day which mainly can be

taken from drinking water and some foods. Mo is detected in trace amounts (1-10 mg/kg) in most rocks and soil and less than (10 µg/L) in most freshwater (Henckens et al., 2018). Mo has different oxidation states (-2 to +6) which enable various redox reactions; generally, Oxidation states (+6) such as Molybdate ( $\text{Mo(VI)O}_4^{2-}$ ) ion is found in oxygenated natural waters whereas the reduced forms ( $\text{HMoO}_4^-$  and  $\text{H}_2\text{MoO}_4$ ) is found in low pH/Eh conditions (Smedley & Kinniburgh, 2017). Most Mo compounds have low solubility in water, but when Mo-bearing minerals react with oxygen and water, they produce a molybdate ion that is little soluble. Acute exposure to elevated Mo levels causes adverse health effects such as diarrhea, anemia, and gout; while chronic exposure causes weakness, fatigue, lack of appetite, anorexia, liver dysfunction, joint pain, osteoporosis, Cu deficiencies, and pneumoconiosis (WHO, 2011). In 1993, the WHO set a drinking water guideline for Mo as 70 µg/L. The use of Mo is increasing very rapidly. Mo is an important alloying agent, which strengthens the steel and decreases its weight (Henckens et al., 2018). A potential source of Mo in Qatar's GW (mean = 26.9 µg/L; max = 103 µg/L) could be from the oil and gas processing sector as mainly the local natural gas is sulfur-containing and Mo is used as a catalyst in the desulfurization process (Kuiper et al., 2015). Mo is also used in the manufacturing of pigments, corrosion inhibitors, smoke suppressants, lubricants, and fertilizers (International Mo Association (IMOA), 2018). Mobilization of Mo and the other anions/oxyanions ( $\text{HCO}_3$ , As, B, F, V, U) mainly occurs in the oxic and neutral to alkaline aquifers; Mo movement is also controlled by Sulphur content in water since it is chalcophile (sulfur-loving) and forms precipitation with Sulphur (Smedley & Kinniburgh, 2017).

#### Physical and chemical characterization of the Adsorbents

An efficient adsorbent should be of a low cost; available, high surface area and pore

volume, mechanical, chemical, and thermal stability, ease to desorb and reuse, fast kinetics, and high adsorption capacity (Singh et al., 2018). Thus, it is essential to study the physicochemical properties of adsorbents to better understanding the adsorption process and have insight into the governing mechanisms of adsorption. The surface modification of adsorbents can be done by using different methods such as thermal and chemical treatments with acids, bases, ozone, biological modification, microwave and ultrasound treatments. In the current study, a proper surface modification method for the cost-efficient, green, and energy-saving adsorption processes is adopted.

The modification steps are shown in Figure 28. The first modification step is  $\text{H}_2\text{SO}_4$ -modification to open the polymer rings, the second step is  $\text{NaOH}$ -modification to add hydroxyl functional groups, while the last step is mercaptoacetic acid ( $\text{C}_2\text{H}_2\text{O}_2\text{S}$ ) modification to change the abundant hydroxyl groups to mercapto groups, also known as a thiol group or a sulfhydryl group ( $-\text{SH}$ ), which showed significant metal removal from water (Shafiq et al., 2019; Amin et al., 2016; Yadav et al. (2013). The surface morphology of the prepared RDPs and the MDPs are analyzed by SEM and the chemical characterization of the functional group of the sample's surface was performed by FTIR (FT-IR/FT-NIR Spectrometer- Spectrum 400). BET (model Aim Sizer-AM301) was used for the analysis of the surface area and pore size distribution of the adsorbents.

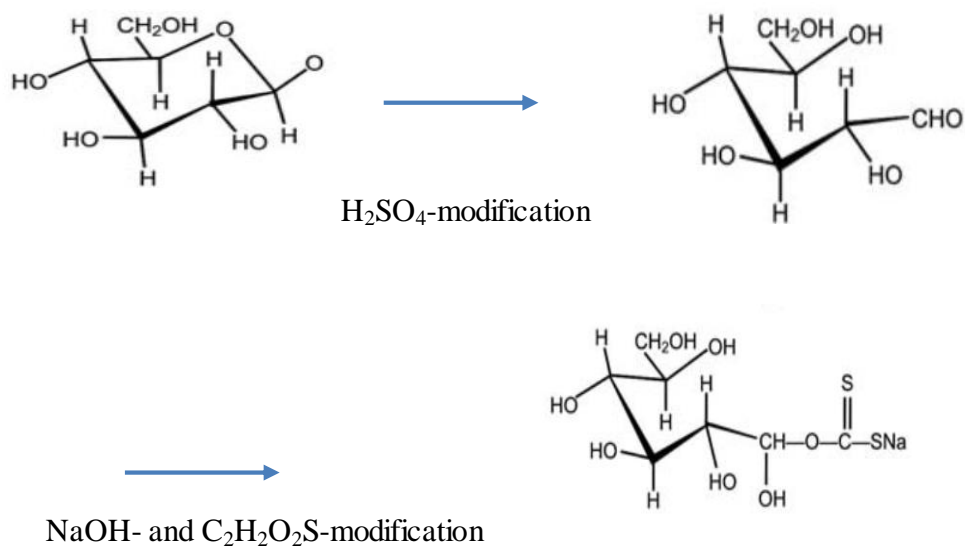


Figure 28. Scheme of Date pits modification Methodology.

#### *Brunauer Emmett Teller (BET) Analysis*

Surface area parameters for different adsorbents are conducted using BET using nitrogen physisorption. Table 9 shows the obtained results such as surface area and pore size for different adsorbents. The order of surface area for the adsorbent is shown as AC > bentonite > MDPs > RDPs. AC shows the highest surface area of 178.79 m<sup>2</sup>/g while RDPs show the lowest surface area of 2.84 m<sup>2</sup>/g. The pore volume for different adsorbents is ordered as bentonite > AC > RDPs > MDPs. AC shows the highest pore volume (0.187 cm<sup>3</sup>/g), while RDPs show the lowest pore volume (0.0837 cm<sup>3</sup>/g). The adsorption microporous volume follows the order AC > bentonite > RDPs > MDPs, with AC, has the highest microporous volume (0.078 cm<sup>3</sup>/g), while RDPs show the lowest microporous volume (0.0100 cm<sup>3</sup>/g). The order of average pore radius for different adsorbent are as bentonite > MDPs > RDPs > AC. Bentonite has mesopores diameters which is the highest average pore radius (10.81 nm), MDPs and RDPs have mesopores diameters of 5.7 nm and 6.31 nm respectively, while AC

shows micropores diameters such that the average pore radius is the lowest (1.88 nm). Comparative results to the current results are shown by other studies. Al-Ghouti et al., (2017) stated that the total surface area and cumulative pore volume of RDPs were 99.76 m<sup>2</sup>/g and 0.14 cm<sup>3</sup>/g respectively, and the study of Alhamed, (2009) found that the total surface area and cumulative pore volume of RDPs were 1.2 m<sup>2</sup>/g and 0.23 cm<sup>3</sup>/g respectively. While the total surface area for AC was 359 m<sup>2</sup>/g in the study of Djlani et al., (2015). Besides, the study of Andrade et al. (2018) showed that the total surface area and cumulative pore volume of bentonite were 28 m<sup>2</sup>/g.

Table 9. *Brunauer Emmett Teller (BET) Surface Area Parameters for Different Adsorbents*

Parameters	Activated Carbon	Bentonite	Roasted Date Pits	Modified Roasted Date Pits
Surface Area (m <sup>2</sup> /g)	179	34.7	28.4	29.7
Single Point Total Pore Volume (cm <sup>3</sup> /g)	0.165	0.187	0.0837	0.0980
Single Point Adsorption Microporous Volume (cm <sup>3</sup> /g)	0.0780	0.0146	0.0100	0.0140
Single Point Average Pore Radius (nm)	1.88	10.8	5.7	6.31

#### *The Fourier Transform Infrared Spectroscopy (FTIR) Analysis*

FTIR analysis is conducted using Perkin Elmer 400 spectrum instrument universal attenuated total reflectance (UATR). The absorbance spectra are obtained in the 4000–400 cm<sup>-1</sup> range by 100 scans at 1.0 cm<sup>-1</sup> resolution, and the signal-to-noise ratio



was 45000:1. Figures 29, 30, 31, and 32 show the peaks that are approximately assigned for different functional groups for AC, bentonite, and RDPs and MDPs that are present 1  $\mu\text{m}$  near the surface of internal reflection. The identification of functional group from the absorbance spectra are adopted from the study by Socrates, (2015) and Ewen and Geoffrey, (2019). The main is approximately assigned functional found in different AC, bentonite, RDPs, MDPs are stated in Tables 10, 11, 12 and 13, respectively, where  $\nu$  is stretching,  $\beta$  is in-plane bending and  $\gamma$  is out-of-plane bending. Figure 29 shows that AC is characterized by different hydroxyl groups such as  $\beta(\text{OH})$  at  $1440\text{ cm}^{-1}$  and  $\nu(\text{OH})$  at  $2887\text{ cm}^{-1}$  and  $3650\text{ cm}^{-1}$ , in addition to oxygenated groups such as at  $2349\text{ cm}^{-1}$   $1205\text{ cm}^{-1}$ . Bentonite is characterized by hydroxyl groups like  $\nu(\text{OH})$  at  $3620\text{ cm}^{-1}$  and  $3650\text{ cm}^{-1}$ , in addition to oxygenated groups such as at  $2349\text{ cm}^{-1}$   $1117\text{ cm}^{-1}$  as shown in figure 30. RDPs are characterized by hydroxyl groups such as  $\nu(\text{OH})$  at  $3356\text{ cm}^{-1}$  and  $3560\text{ cm}^{-1}$ , in addition to oxygenated groups such as at  $1374\text{ cm}^{-1}$   $1744\text{ cm}^{-1}$  as shown in figure 31. Figure 32 shows that the modification of date pits has different new functional groups. The MDPs have oxygen groups, mainly carbonyl, alcohol, and aromatic groups such as at  $1370\text{ cm}^{-1}$  which is assigned to the (S=O) and at  $1703\text{ cm}^{-1}$  t which is assigned to stretching vibrations of  $\nu(\text{C=O})$  ester groups, suggesting that mercapto-acetate functions with thiol groups are presented. Furthermore, the peak at  $650\text{ cm}^{-1}$  and  $650\text{ cm}^{-1}$  implied the weak absorbance of  $\nu(\text{S-H})$  groups, which represent the thiol group. A similar finding of adding sulfur functional group at peaks  $613\text{ cm}^{-1}$ ,  $1014\text{ cm}^{-1}$  and  $1075\text{ cm}^{-1}$  after date pits modification is found by Al-Ghouti et al., (2019). As shown in figure 33, thiol groups were introduced into the adsorbent date pits, in addition to hydroxyl groups such as  $\nu(\text{OH})$  at  $2921\text{ cm}^{-1}$  and  $3650\text{ cm}^{-1}$ . The availability of these functional groups on the surface of the different adsorption will significantly enhance

the adsorption process. Cellulose and hemicellulose are the main constituents of the date pits, thus different oxygenated functional groups such as hydroxyl, ether, and carbonyl are located on the surface of the date pits (AlGhouthi et al., 2017). The results of the available functional groups on the surface of the date pits such as (alcohol O-H), (aldehyde, ketone, ester C=O), and (alcohol, ester C-O) are comparative with the reported study by (AlGhouthi et al., 2010; AlGhouthi et al., 2017).

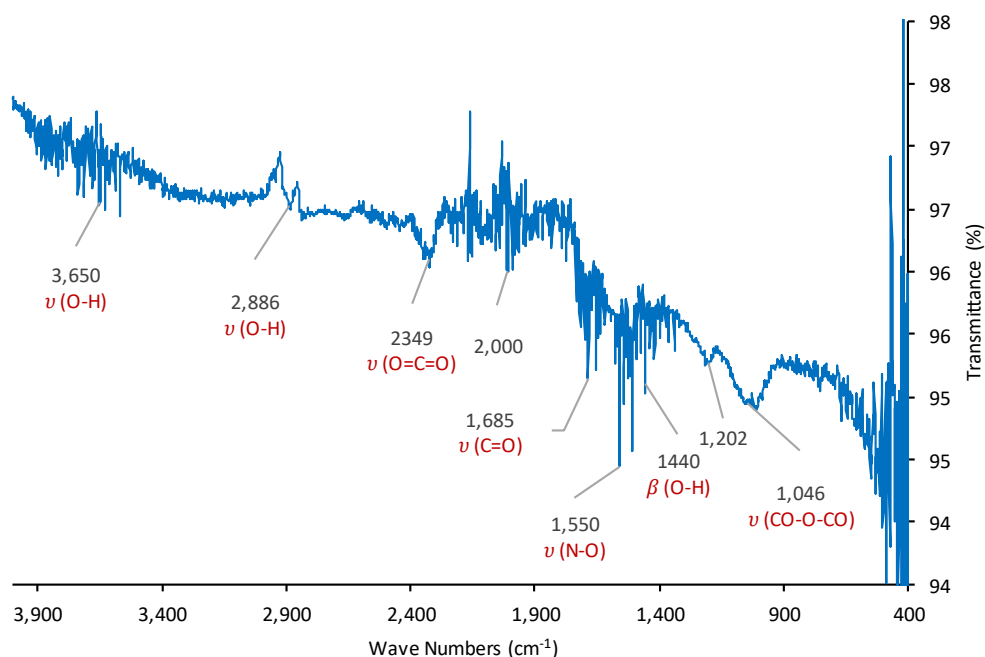


Figure 29. FTIR for activated carbon.

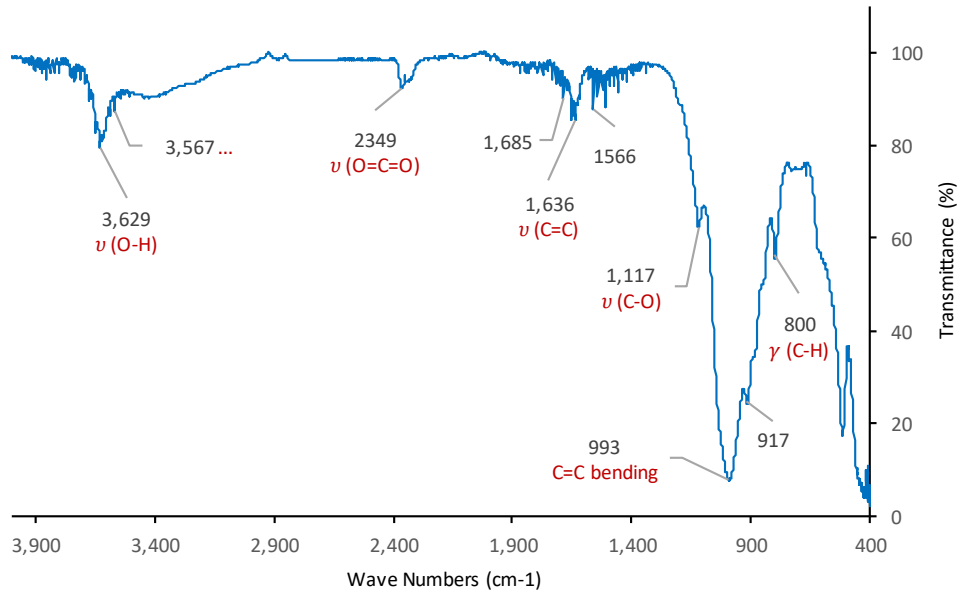


Figure 30. FTIR for bentonite.

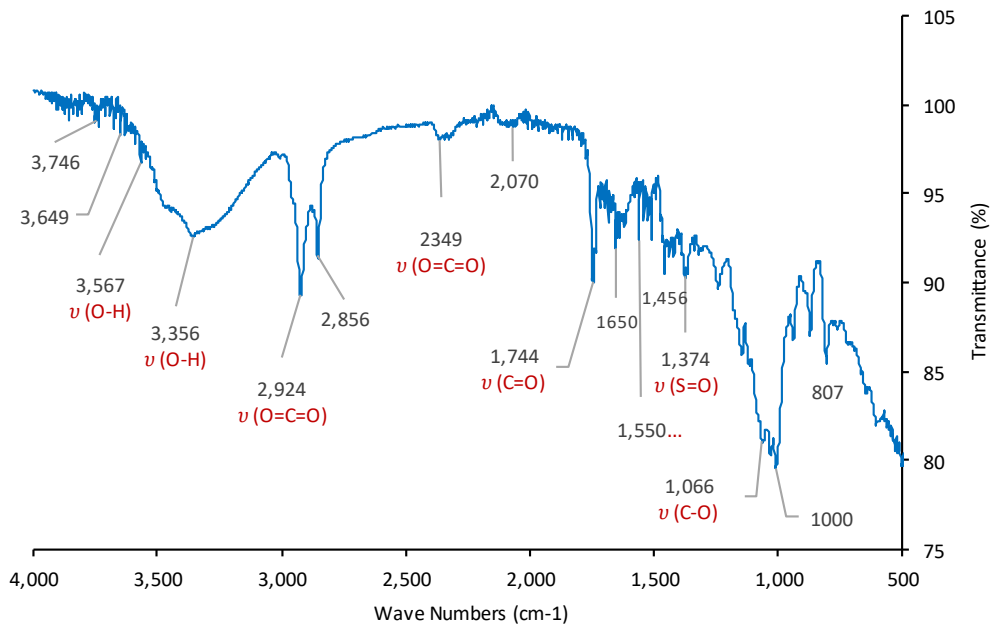


Figure 31. FTIR for RDPs.

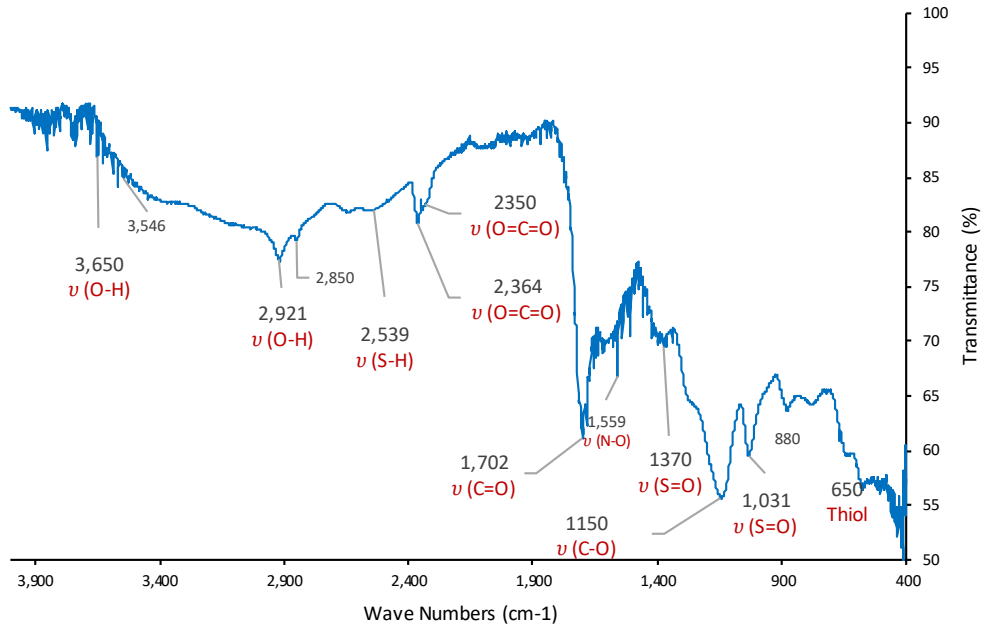


Figure 32. FTIR for MDPs.

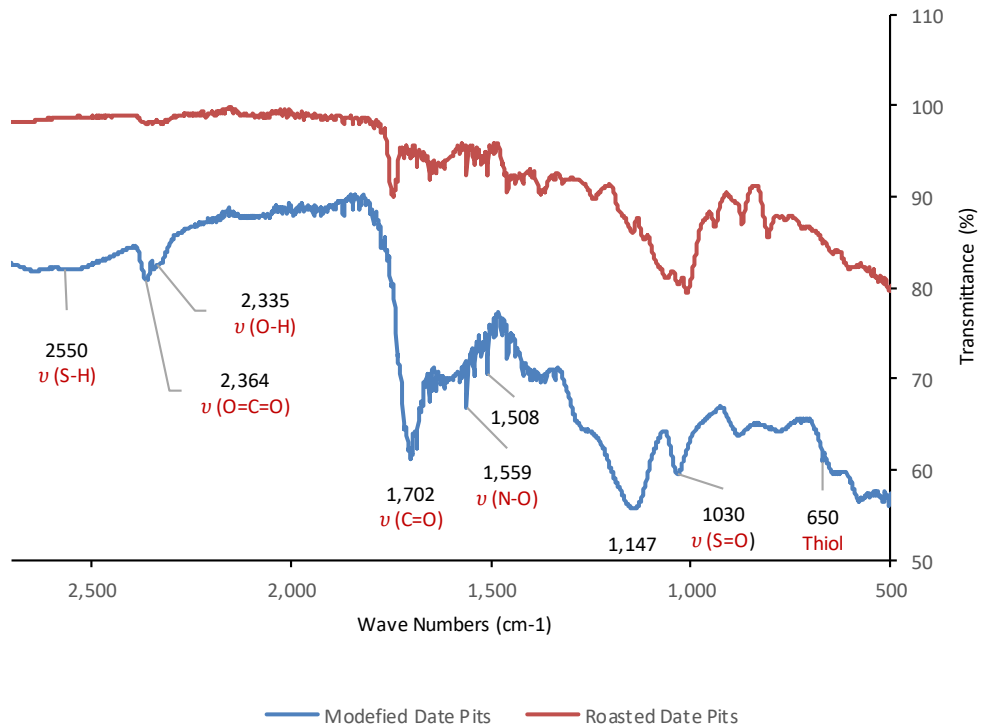


Figure 33. Comparison FTIR between MDPs and RDPs

Table 10. *Functional Groups on Activated Carbon (Socrates, 2015; Ewen and Geoffrey, 2019).*

Wave numbers (cm <sup>-1</sup> )	Appearance	Approximate Functional Groups
750	strong	$\gamma$ (C-H)
757	strong	$\beta$ (C=C)
985	strong	$\beta$ (C=C)
1046	strong, broad	$\nu$ (CO-O-CO)
1205	strong	$\nu$ (C-O)
1310	strong	$\nu$ (C-O)
1440	medium	$\beta$ (O-H)
1500	strong	$\nu$ (N-O)
1550	strong	$\nu$ (N-O)
1650	medium	$\nu$ (C=C)
1685	strong	$\nu$ (C=O)
2000	medium	$\nu$ (C=C=C)
2349	strong	$\nu$ (O=C=O)
2840	medium	$\nu$ (C-H)
2887	weak, broad	$\nu$ (O-H)
3560	medium, sharp	$\nu$ (O-H)
3650	medium, sharp	$\nu$ (O-H)

Table 11. *Functional Groups on Bentonite (Socrates, 2015; Ewen and Geoffrey, 2019).*

Wave numbers (cm <sup>-1</sup> )	Appearance	Approximate Functional Groups
800	strong	$\gamma$ (C-H)
995	strong	Silicate ion, C=C bending
1117	strong	$\nu$ (C-O)
1566	medium	$\nu$ (C=C)
1636	medium	$\nu$ (C=C)
2349	strong	$\nu$ (O=C=O)
3560	medium, sharp	$\nu$ (O-H)
3620	Medium, sharp	$\nu$ (O-H)

Table 12. *Functional Groups on RDPs (Socrates, 2015; Ewen and Geoffrey, 2019).*

Wave numbers (cm <sup>-1</sup> )	Appearance	Approximate Groups	Functional
810	strong	$\gamma$ (C-H)	
869	strong	C=C bending	
1000	strong	C=C bending	
1066	strong	$\nu$ (C-O)	
1147	strong	$\nu$ (C-O)	
1241	strong	$\nu$ (C-O)	
1374	strong	$\nu$ (S=O)	
1456	strong	$\beta$ (C-H)	
1550	strong	$\nu$ (N-O)	
1650	medium	$\nu$ (C=C)	
1744	strong	$\nu$ (C=O)	
2349	strong	$\nu$ (O=C=O)	
2856	medium	$\nu$ (C-H)	
2924	strong	$\nu$ (O-H)	
3356	strong, broad	$\nu$ (O-H)	
3567	medium	$\nu$ (O-H)	

Table 13. *Functional Groups on MDPs (Socrates, 2015; Ewen and Geoffrey, 2019).*

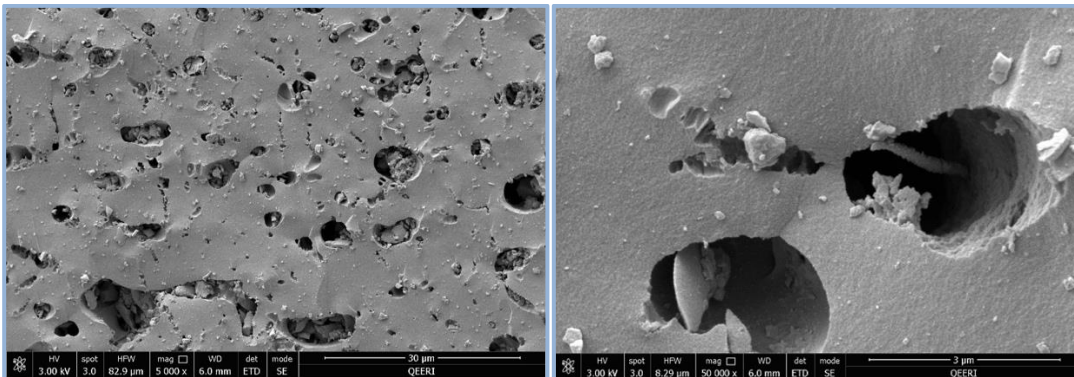
Wave numbers (cm <sup>-1</sup> )	Appearance	Approximate Functional Groups
650	medium	Thiol or thioether, CH <sub>2</sub> -S- $\nu$ (C-S)
880	medium	$\gamma$ (C-H)
1030	strong	$\nu$ (S=O)
1370	strong	$\nu$ (S=O)
1150	strong	$\nu$ (C-O)
1559	strong	$\nu$ (N-O)
1702	strong	$\nu$ (C=O)
2350	strong	$\nu$ (O=C=O)
2550	weak	$\nu$ (S-H)
2850	medium	$\nu$ (C-H)
2921	weak, broad	$\nu$ (O-H)
3650	medium, sharp	$\nu$ (O-H)

### *The Scanning Electron Microscopy (SEM) Analysis*

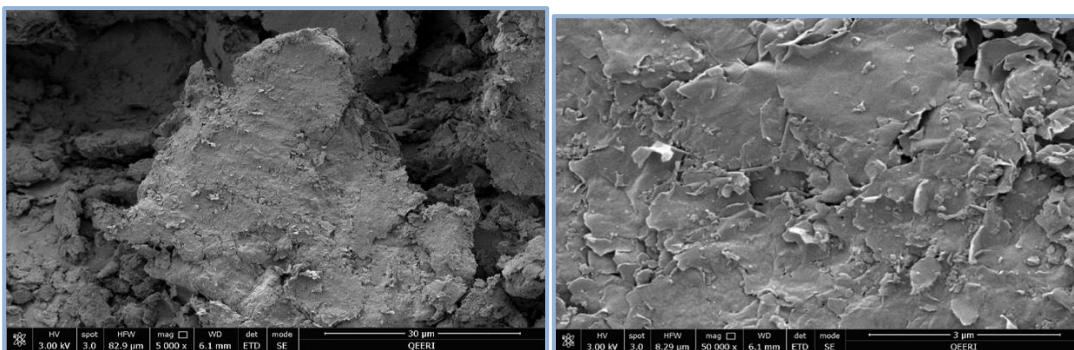
SEM is a very significant tool that is extensively used to analyze the surface morphology of the adsorbent. Figure 34 shows SEM images that demonstrate the morphology, pore structure, and homogeneity of AC, bentonite, RDPs, and MDPs.

All adsorbents showed irregular shapes and sharp edges due to the preparation method and mechanical grinding. The bentonite surface structure was less rough and smoother than other adsorbents. The surface structure of the adsorbent of chemical treatment (AC and MDPs) had a rougher surface and more pores and edges than bentonite and RDPs. Thus, the chemical modification increased the surface area of the adsorbents that further enhances the adsorption capacity. AC and MDPs have diverse pore sizes and shapes that are narrow and confined which facilitate capturing the different adsorbates. The very tiny pores that characterized AC are mainly due to the activation process and the successive release of volatile organic species. While RDPs show larger pores with a random arrangement that facilitates the adsorption on the surface. These findings are in support of the BET surface area results. The presence of fine particles residing at the outer surface of the adsorbent solids is also shown. The presence of such debris could be attributed to impurities found in the original RDPs. Heat treatment and roasting may have facilitated the removal of such organic impurities and hence their appearance is less on MDPs surface. The morphology of the AC and RDPs particles was similar to that observed in the study by (Al-Ghouti, 2017). After adsorption images for adsorbent are shown in Figures 35, 36 and 37 for Li, mixture solution of Li, Mo and B, Mo, and B respectively. It is clear that AC and MDPs have a high number of pores that indicate a significant capacity for trapping adsorbates. It is also shown that the structure of the adsorbent is changed, as the small pores are reduced, while the large pores are increased which indicates a possibility of different adsorption mechanisms. Also, the structure is smoothed for AC, RDPS, and MDPs after the adsorption process comparing with the relatively rough and irregular surfaces before the adsorption. The rough and irregular surfaces indicated a higher adsorption capacity by trapping the adsorbate.

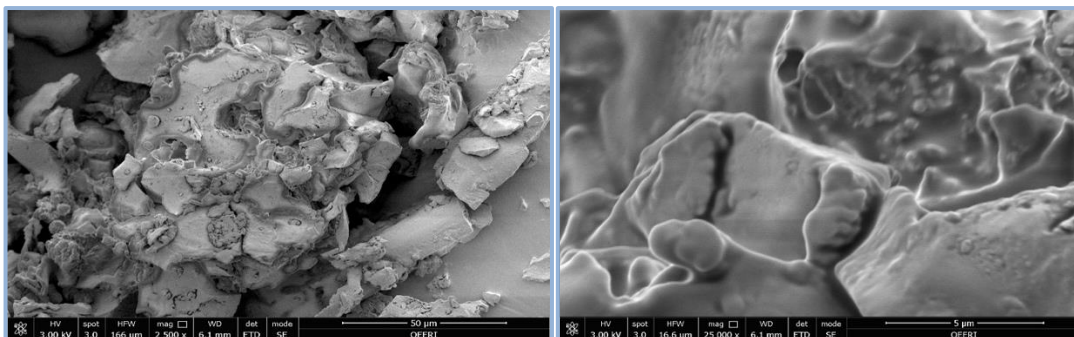
AC



Bentobite



RDPs



MDPs

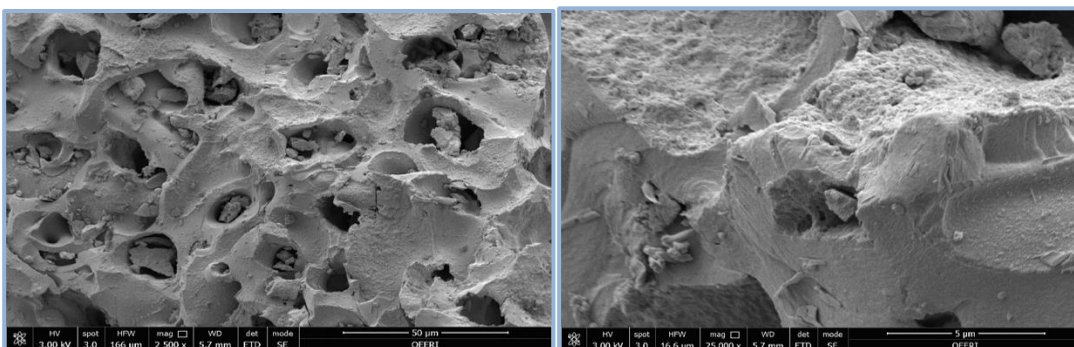
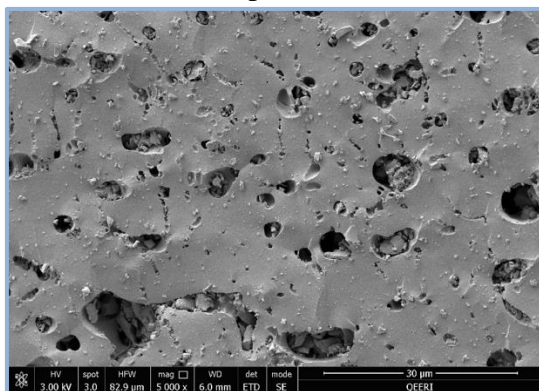


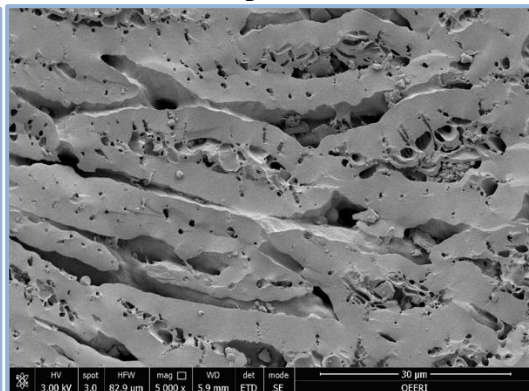
Figure 34. Morphology characteristic of AC, RDPs and MDPs adsorbents.



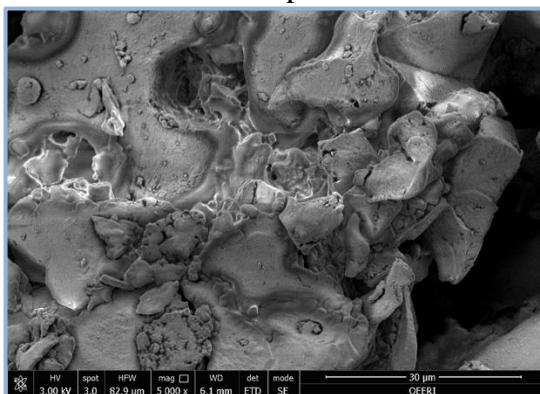
AC before the adsorption



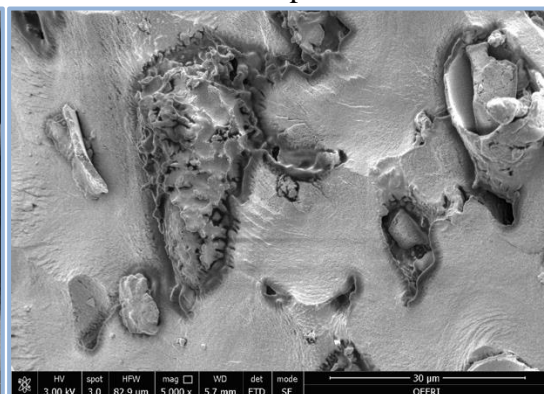
AC after the adsorption



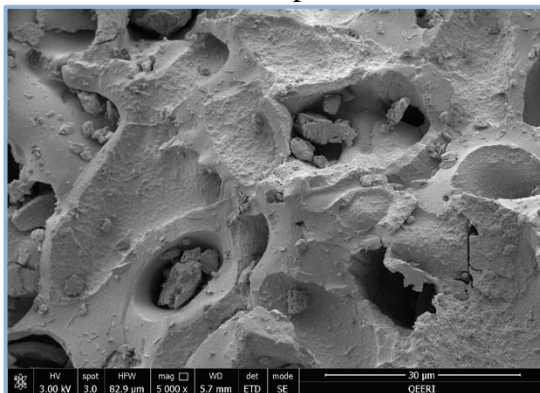
RDPs before the adsorption



RDPs after the adsorption



MDPs before the adsorption



MDPs after the adsorption

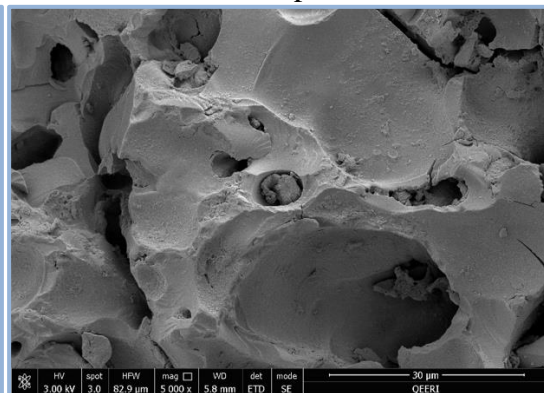
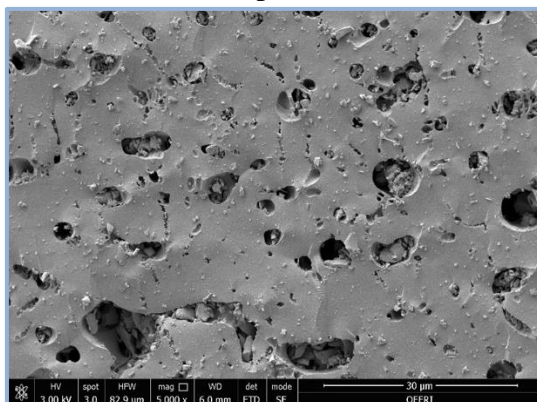
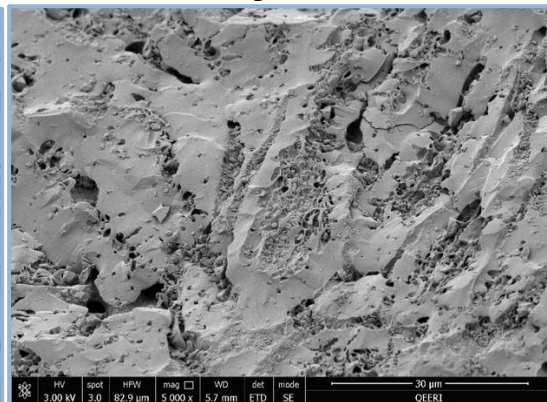


Figure 35. Morphology characteristic of AC, RDPs and MDPs before and after the adsorption of Li.

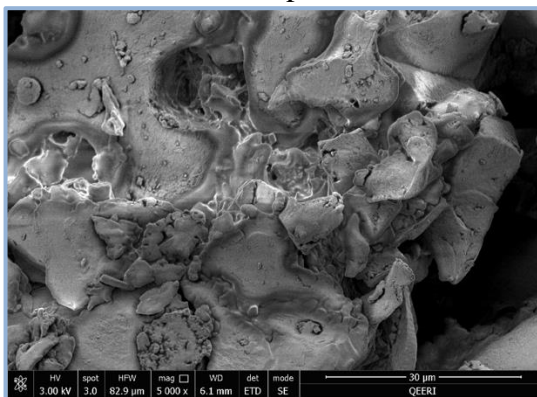
AC before the adsorption



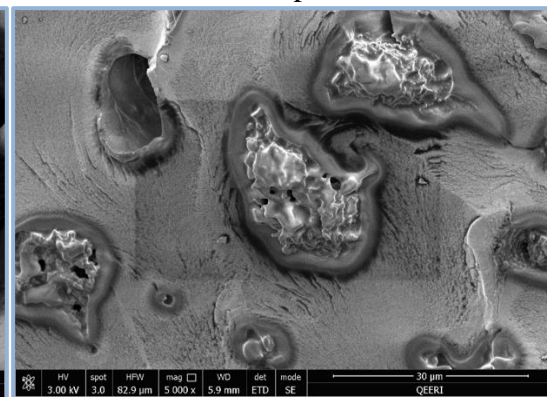
AC after the adsorption



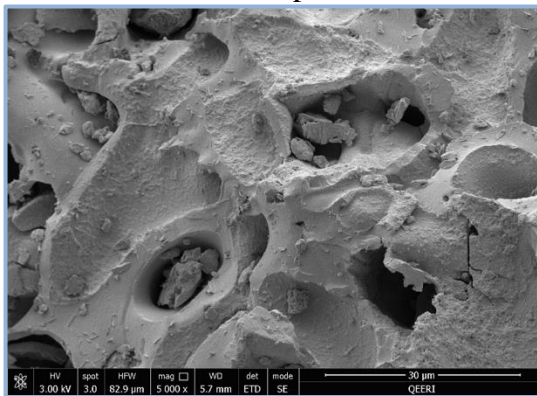
RDPs before the adsorption



RDPs after the adsorption



MDPs before the adsorption



MDPs after the adsorption

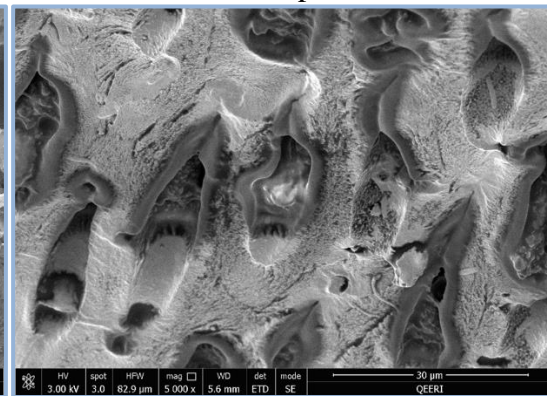
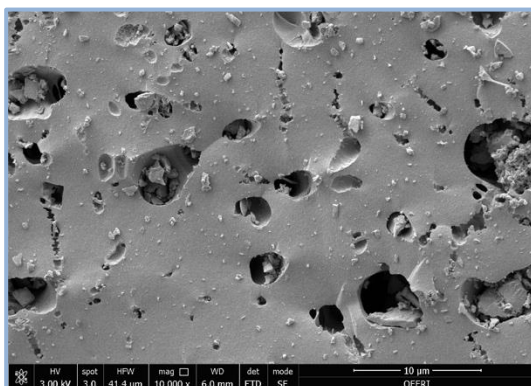
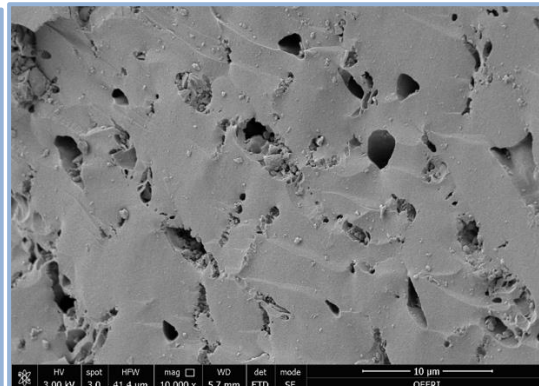


Figure 36. Morphology characteristic of AC, RDPs and MDPs before and after the adsorption of the mixture of Li, Mo and B.

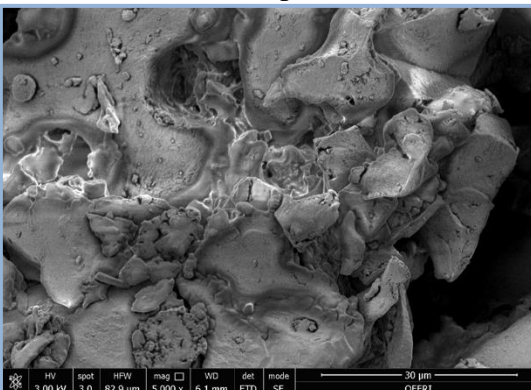
AC before the adsorption



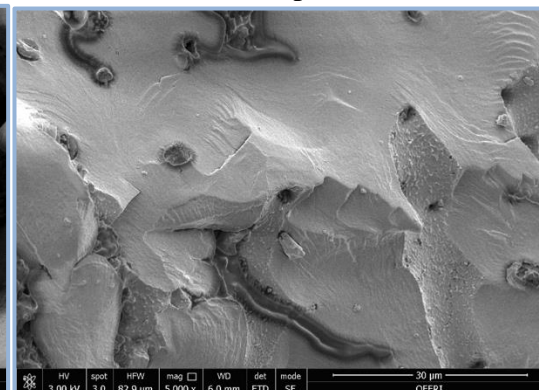
AC after the adsorption



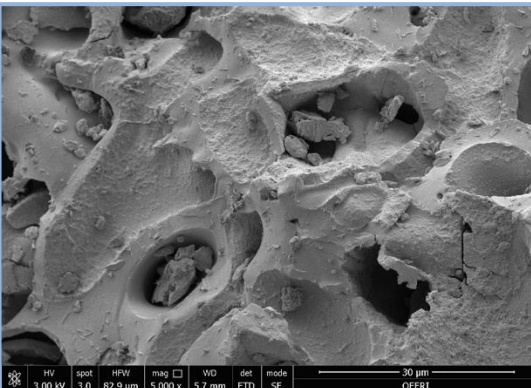
RDPs before the adsorption



RDPs after the adsorption



MDPs before the adsorption



MDPs after the adsorption

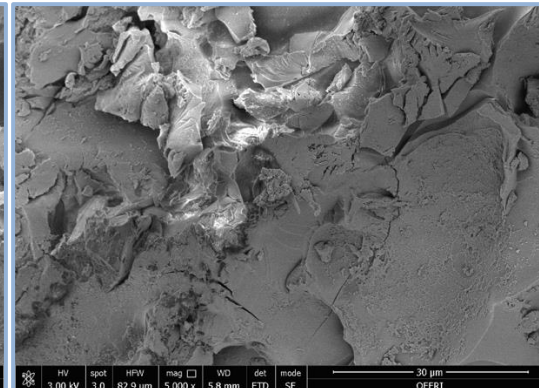
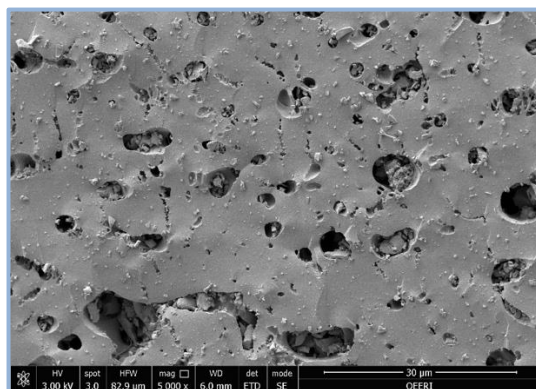
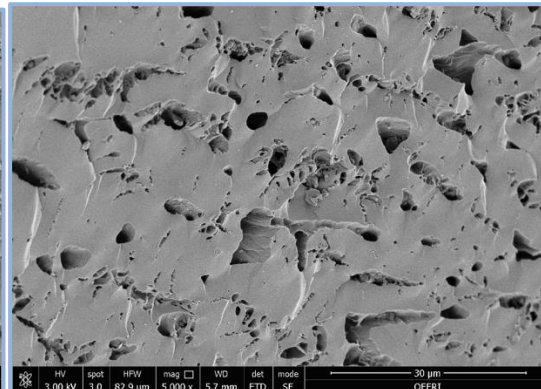


Figure 37. Morphology characteristic of AC, RDPs and MDPs before and after the adsorption of Mo.

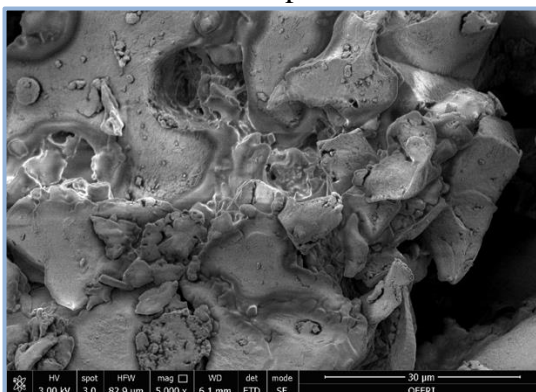
AC before the adsorption



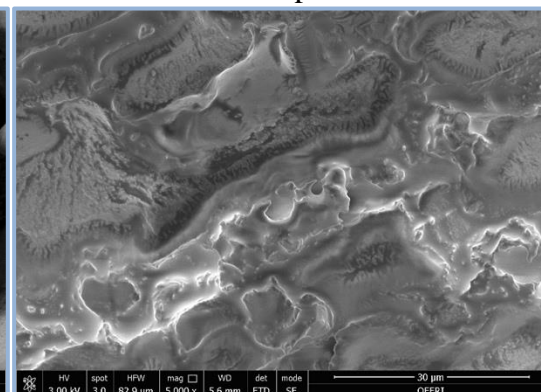
AC after the adsorption



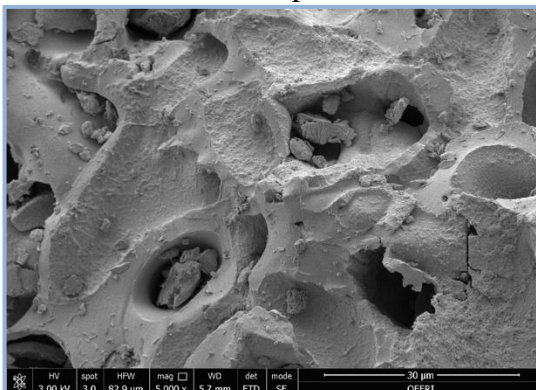
RDPs before the adsorption



RDPs after the adsorption



MDPs before the adsorption



MDPs after the adsorption

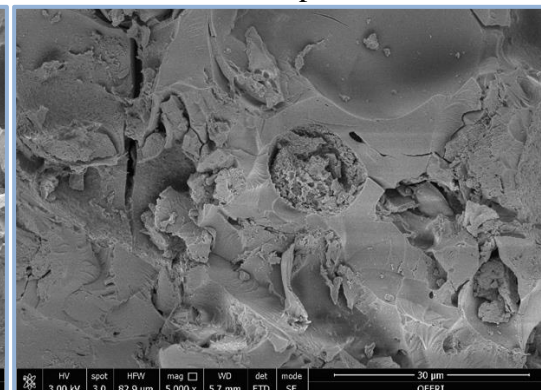


*Figure 38. Morphology characteristic of AC, RDPs and MDPs before and after the adsorption of B.*

### Study the effect of pH on the Adsorption process

The adsorption of metal ions from aqueous solutions is highly dependent on the solution pH as it determines the hydrogen and hydroxyl ion concentrations (Al-Ghouti et al., 2017). In this study, batch adsorption experiments are carried out in pH 2, 4, 6,

8, and 10 to study the effect of pH on Li, Mo, and B adsorption. Changing pH values alters the charge of the functional groups on the surface of the adsorbent, hence affects the adsorption capacity. Thus, at a  $\text{pH} < \text{pH}_{\text{pzc}}$ , the adsorbent accepts protons, and the surface becomes positively charged; hence the surface adsorbs the anions and repels the cations. While at  $\text{pH} > \text{pH}_{\text{pzc}}$ , the adsorbent donates protons, and the surface becomes negatively charged; hence the surface adsorbs the cations and repels the anions.

The effect of pH on the Li adsorption efficiency onto AC, RDP, MDP, and bentonite were investigated, and the results are shown in Figure 39. It is illustrated that the maximum percentage removal of Li was at pH 6 for RDP, pH 8 for MDP, pH 4 for AC, and pH 2 and pH 8 for bentonite. It can be observed that the maximum removal efficiency of Li by bentonite and AC was 12.65% and 14.05% under acidic conditions at pH 2 and pH 4, respectively. However, the maximum adsorption percentage of Li by RDP, MDP under alkaline conditions at pH 6 and pH 8 with removal percentage of 15.45%, and 14.6% respectively, also bentonite removal efficiency was and 12.2 % at pH 8. This can be explained by the fact that increases in the pH values raise the number of hydroxyl ions in the solution and the density of the negative charged binding sites that electrostatically attract  $\text{Li}^+$  cations. While the decrease of Li adsorption onto RDP, MDP at low pH could be explained by the competition between  $\text{H}^+$  ions and Li-ions for the adsorption sites, thus the adsorbed capacity of Li decreases. However, the increase of Li adsorption by AC and bentonite at low pH could be explained by the attraction between the chloride ions at the adsorption sites with Li-ions. While the decrease of Li adsorption by AC at high pH could be explained by the electrostatic repulsion between the negatively charged species and the adsorbent surface.

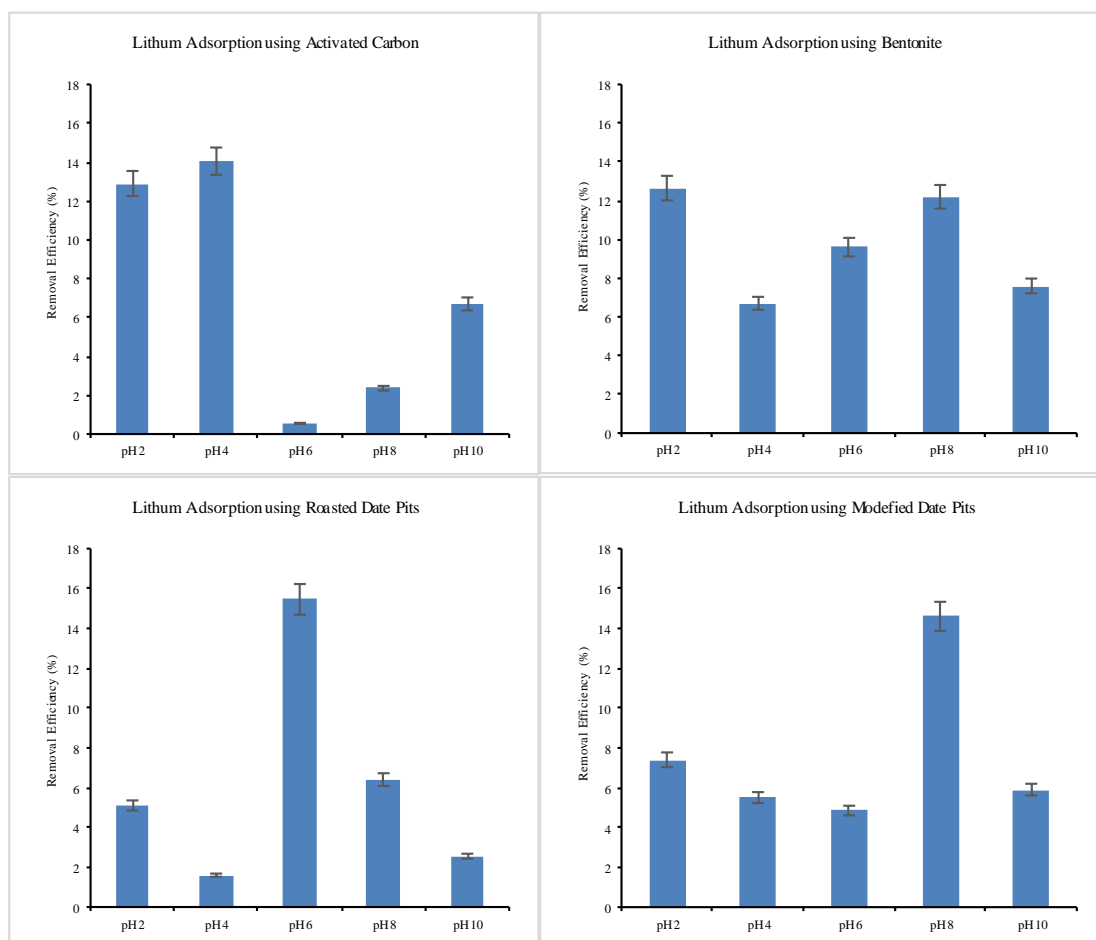


Figure 39. Study the effect of pH on lithium adsorption using activated carbon, bentonite, RDPs, and MDPs.

Figure 40 shows the tendency of Mo adsorption over AC, bentonite, RDPs, and MDPs at different pH values. The results show clearly that the pH dependency of Mo removal is critical at the investigated pH values. The Mo adsorption is affected by the surface characteristics of the adsorbent and Mo species present in the aqueous solution. In alkaline and neutral solutions, the  $H^+$  ions concentration is very small, so the dominant Mo species is monomeric Mo(VI) like  $[MoO_4]^{2-}$  ions ( Lee et al., 2011). As the pH is lowered, more  $H^+$  ions are available and the anion molybdate species becomes protonated. Whether it polymerizes to hepta- or octa-molybdate depends on

the pH and the Mo concentration, as at pH 5-6 the dominant species are heptamolybdate ions  $[\text{Mo}_7\text{O}_{24}]^{6-}$  and at pH 3-5 the dominant species is octa-molybdate ions  $[\text{Mo}_8\text{O}_{26}]^4$  (Zhao et al. 2012). The neutral species  $\text{H}_2\text{MoO}_4$  begins to form as the pH is further decreased. While in more acidic solutions, the concentration of hydrogen ions is high, so complexes with positive charges begin to form, and the  $[\text{MoO}_2]^{2+}$  ions are the dominant species.

It is noted that the removal capacity is decreased with enhancing pH and showed a maximum removal value at pH 2. This is possible due to the electrostatic attraction of Mo species  $[\text{MoO}_2]^{2+}$  by the anion groups on the adsorbent surface. At higher pH, the adsorption of Mo decreased due to the competition for the adsorption sites between negatively charge molybdate species and hydroxyl ions (Zhao et al. 2012). Additionally, the negative charge molybdate species are electrostatically repulsed from the negative adsorption site. A similar favorable Mo adsorption with pH levels was found in other adsorbent's studies such as Tu et al., (2014) stated that the maximum Mo adsorption (30.59 mg/g) was found at pH 2.75. In the current study, when adsorption conditions were set at pH 2, Mo removal capacities observed in this study were about 60.6%, 55.9%, 70.72%, and 49.57% using MDP, RDP, bentonite, and AC respectively. However, low Mo removal efficiencies are observed when the pH was in high alkaline conditions.

Figure 41 shows that boron adsorption efficiency under different pH values. The maximum boron adsorption efficiency was about 31.65% for bentonite at pH 6, about 31.6% for AC at pH 6, and about 31.8% for MDP at pH8, 30.75%, and 29.35 % at pH 2 and pH 6 respectively for RDP. The result indicates that a weak acid solution (pH 6) was efficient for boron adsorption because boron adsorption is affected by pH conditions that could change the surface characteristics of the adsorbent and the

dominant boron species available in the aqueous solution. Boric acid is a weak acid with a pKa value of 9.24, so at pH less than 9, boric acid  $B(OH)_3$  is the dominant species whereas at pH more than 9, borate  $B(OH)_4^-$  is the dominant species (Al-Ghouti et al., 2018). Borate is negatively charged; it is electrostatically attracted with hydrogen ions, while it is electrostatically repulsed with hydroxyl ions. It is well known that the changes in pH conditions affect the ionization degree and the adsorbents' surface charge. Hence, boron adsorbent could have different mechanisms such as coordination, ion exchange, electrostatic interactions, and other chemical bindings besides the physical adsorption. As mentioned above at weak acidic conditions, AC offered a higher adsorption efficiency in comparison to RDPs and MDPs. While in a neutral environment it only reaches around 30% removal efficiency. A strong acidic conditions pH 2, the removal efficiency is decreased using MDPs due to the electrostatic repulsion between the boric acid  $B(OH)_3$  with the protonation hydroxyl and carbonyl functional groups (Al-Ghouti et al., 2010). Additionally, the presence of chloride ions which competes with boron ions on the positive adsorption sites. While the high removal efficiency of boron at low pH is due to the presence of excess  $Cl^-$  ions that could interact with the anion functional groups on the adsorbent surface hence  $Cl^-$  attracting boric acid  $B(OH)_3$ . The increase of boron adsorption by AC and MDPs with the increase of the pH of the solution could be explained by a complexation reaction between the borate  $B(OH)_4^-$  and  $OH^-$  on the adsorbent's surface. On the other hand, the decrease of the adsorption capacity at higher alkalinity conditions is attributed to the competition for the active adsorption sites between the dominant species of boron (borate)  $B(OH)_4^-$  and hydroxyl ions.



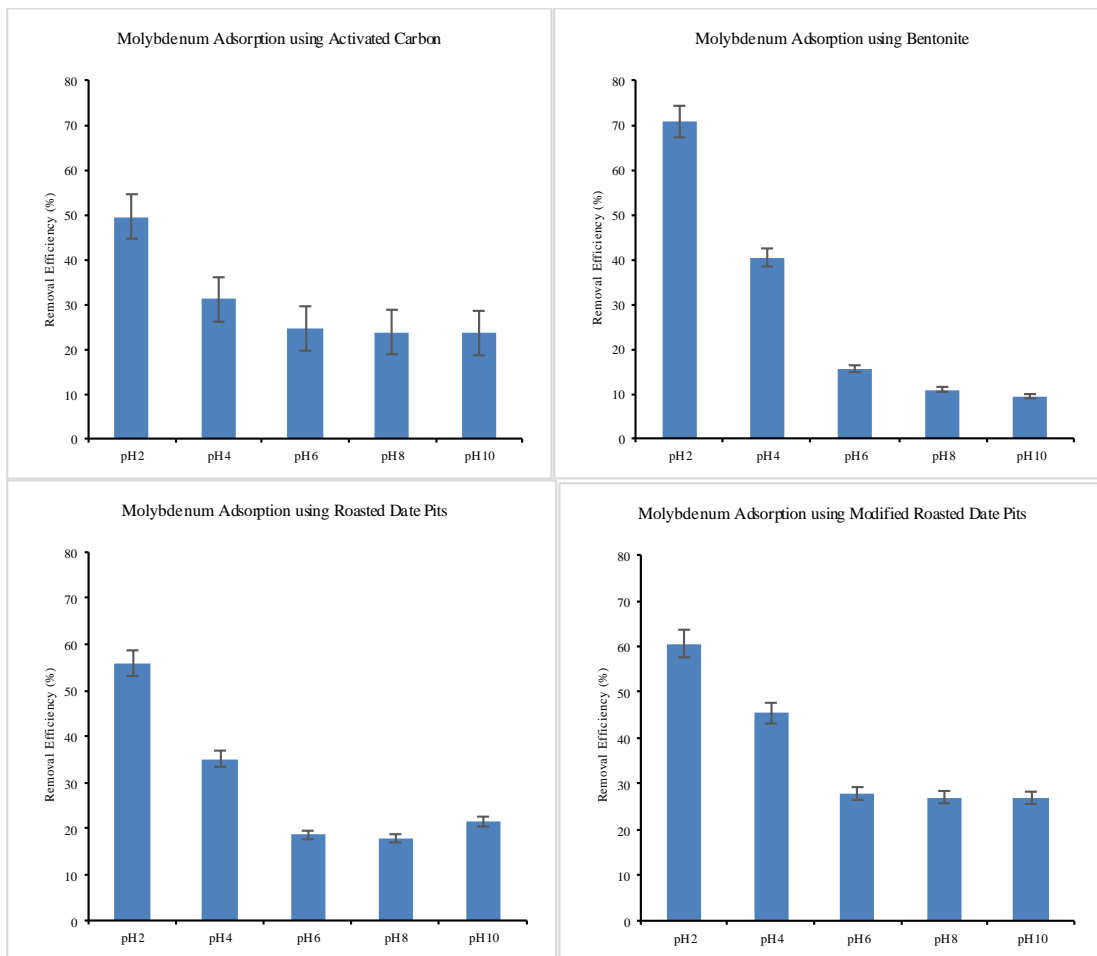


Figure 40. Study the effect of pH on molybdenum adsorption using activated carbon, bentonite, RDPs and MDPs.

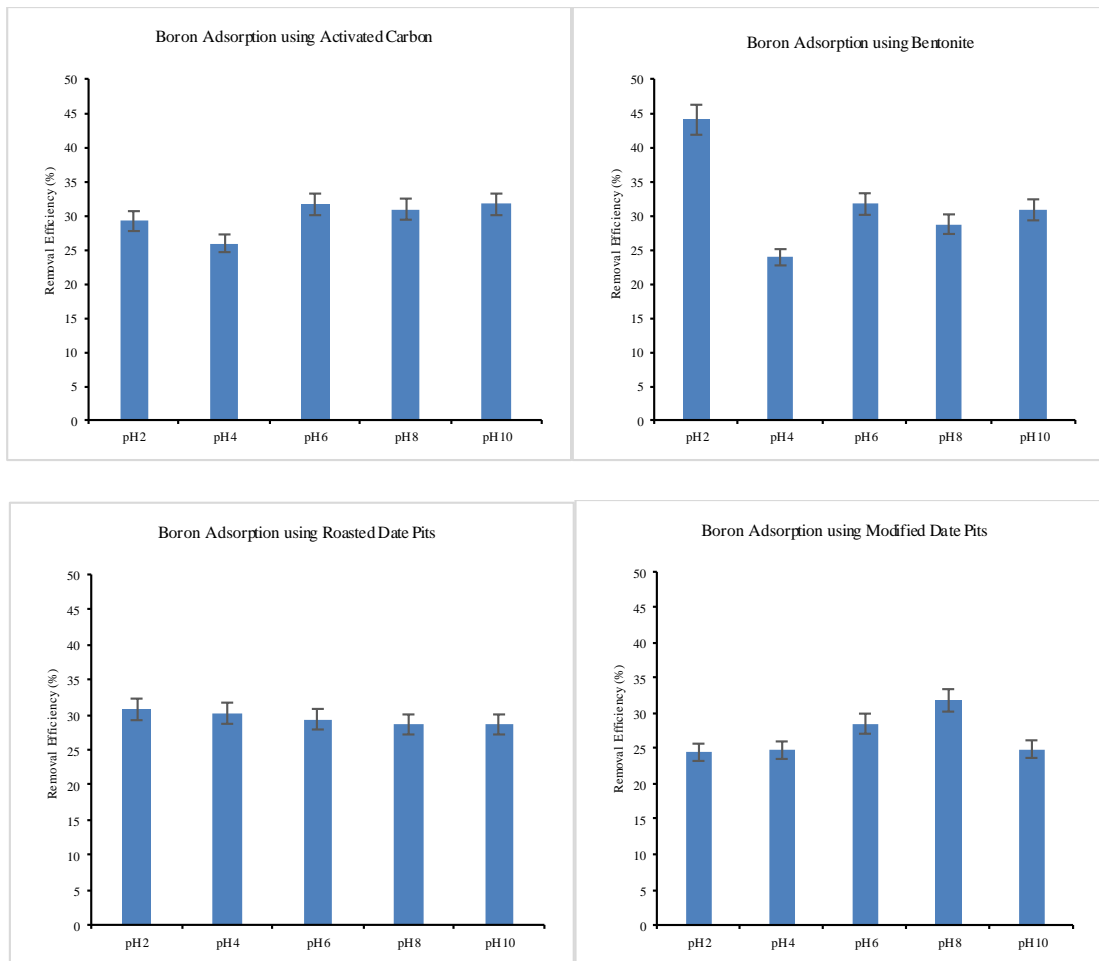


Figure 41. Study the effect of pH on Boron adsorption using activated carbon, bentonite, RDPs and MDPs.

#### Study the Effect of Initial Adsorbate Concentration on Adsorption Process

Figure 42 shows the effect of the initial concentration of Li on the adsorption process using different adsorbents such as AC, bentonite, RDPs, and MDPs. The highest removal efficiency of Li was about 64 % when the initial Li concentration was 80 ppm using AC, followed by about 59 % using MDPs when the initial Li concentration was 50 ppm, about 35 % when the initial Li concentration was 20 ppm using bentonite, and about 25% when the initial Li concentration was 20 ppm using RDPs. The increase in initial Li concentration enhanced the adsorption capacity due to the increase of the concentration of Li per unit weight of adsorbent. Also, the increase of

the Li concentration increased the Li diffusion into pores. The decreasing of the adsorption efficiency at 100 ppm concentration is related to the limited availability of vacant adsorption sites. While the high adsorption capacity at low concentration is attributed to the presence of unoccupied active adsorption sites. Similar results were observed by Al-Ghouti et al. (2019), as the concentration of mercury increases the adsorption capacity also increases on RDP and sulfur-modified- RDP. The fluctuations trend of increasing and decreasing Li removal efficiencies with the increase of the initial concentration are due to the heterogeneity of the adsorption process and potential chemical bindings, besides the availability of different oxygenated functional groups such hydroxyl, ether, and carbonyl that considerably influence the adsorption mechanisms.

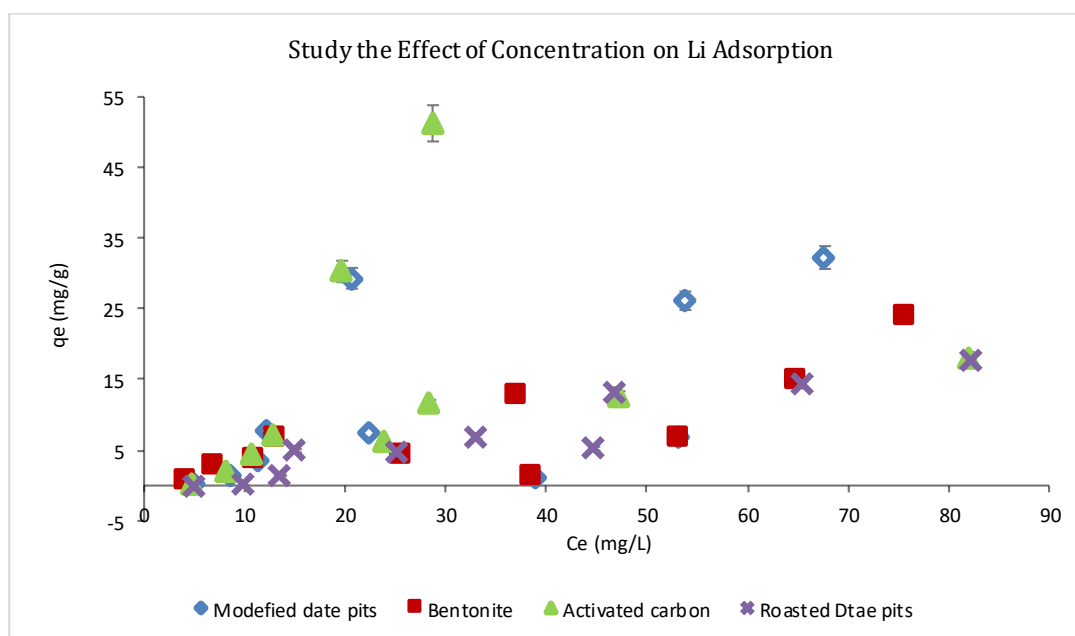


Figure 42. Study the effect of concentration on lithium adsorption.

Figure 43 shows that the effect of the initial concentration of Mo on the adsorption process using different adsorbents such as AC, bentonite, RDPs, and MDPs. The highest removal efficiency of Mo was about 64 % when the initial Mo concentration

was 100 ppm using MDPs. The adsorption of Mo increases with the increase of the initial Mo concentration, which indicates a positive correlation due to the availability of different adsorption mechanisms and more pores after the modification of date pits. While the highest removal efficiency of Mo was 58 % using RDPs when the initial Mo concentration was 20 ppm, 51 % at 20 ppm using AC, and 32% when the initial Mo concentration was 100 ppm using bentonite. It is shown that the increase in initial Mo concentration increased the adsorption capacity due to the increase of the Mo concentration per unit weight of adsorbent, Mo diffusion into the internal layer, besides the availability of various functional groups on the surface of the adsorbents. The decreasing of the adsorption efficiency at high concentrations is related to the limited availability of vacant adsorption sites. While the high adsorption capacity at low concentration is attributed to the availability of unoccupied active adsorption sites.

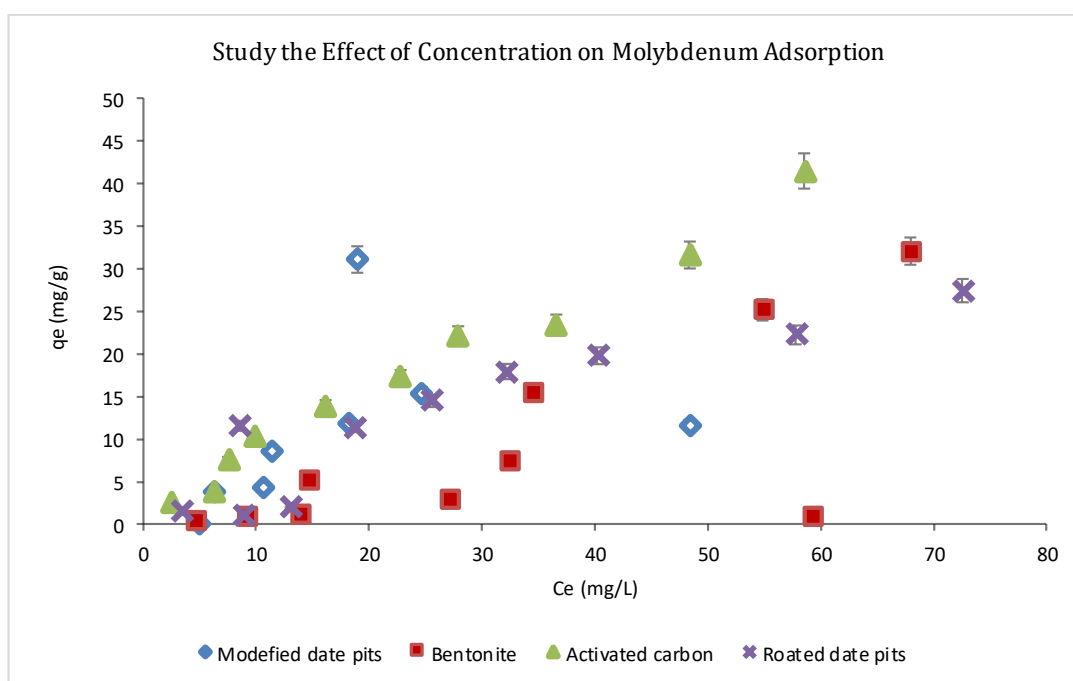


Figure 43. Study the effect of concentration on molybdenum adsorption.

Figure 44 shows that the effect of the initial concentration of boron on the adsorption process using different adsorbents such as AC, bentonite, RDPs, and MDPs. The adsorption of boron is decreased when the initial concentration is 100 ppm for all adsorbents due to the unavailability of vacant adsorption sites. The highest removal efficiency of boron was about 36 % when the initial boron concentration was 30 ppm using MDPs, while it was 50 % using RDPs when the initial boron concentration was 40 ppm, 18 % when the initial boron concentration was 10 ppm using AC, and 54% when the initial boron concentration was 30 ppm using bentonite. The high adsorption capacity at low concentrations is attributed to the availability of unoccupied adsorption sites. The increase in initial B concentration increases the removal efficiency. This is predictable due to the increase of the B concentration per unit weight of adsorbent. In addition, increasing the B concentration increased the B diffusion into internal pores. Also, it is shown that there is a fluctuations trend of increasing and decreasing the adsorption capacity due to the heterogeneity of adsorption active sites and potential chemical bindings such as surface complexation and/or mono-, di, and tri- coordination of B. The surface of the adsorbents had various functional groups such as hydroxyl, ether, and carbonyl; hence, considerably influence the adsorption mechanisms. The fluctuation trend of increasing and decreasing bromide ions adsorption by RDPs was also observed by Al-Ghouti et al., (2017).

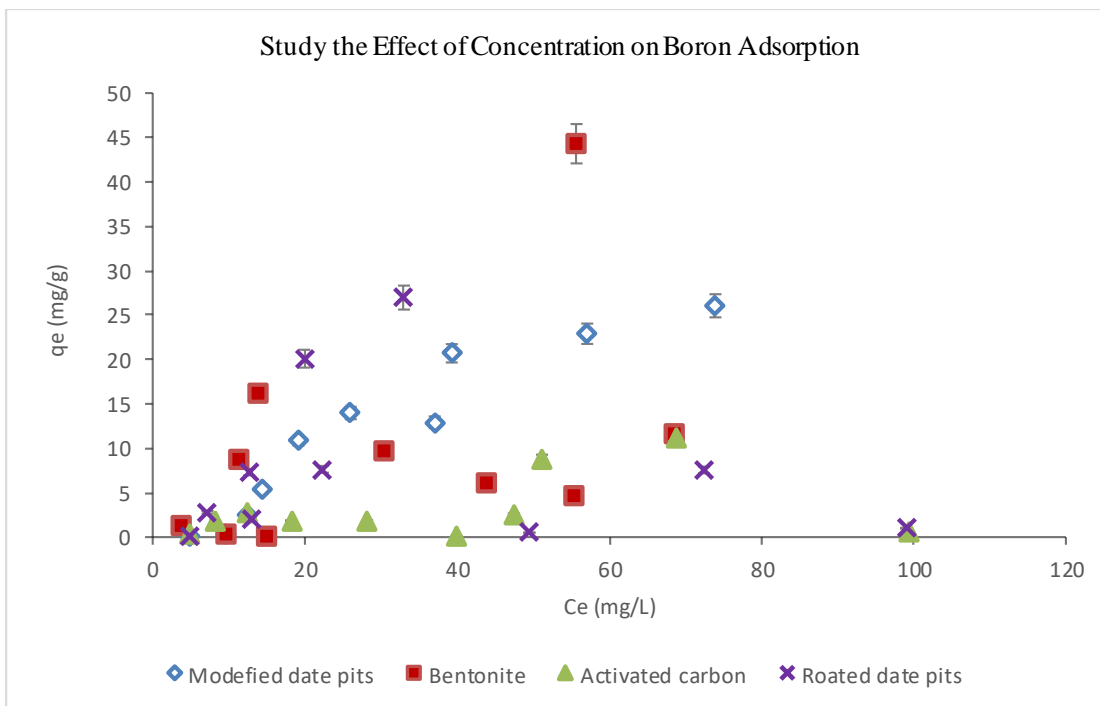


Figure 44. Study the effect of concentration on boron adsorption.

#### Study the Effect of Temperature on Adsorption Process

Tables 14, 15 and 16 show the effect of temperature on the adsorption of Li and Mo and boron respectively using AC, bentonite, RDPs, and MDPs. Figure 45 shows the effect of temperature values 25 °C, 35 °C and 45 °C on Li adsorption using AC, bentonite, RDPs, and MDPs respectively. Overall, the adsorption efficiency of Li increases at 35 °C using the four adsorbents. At 35 °C, the maximum adsorption efficiency reached 95% for AC, 94% using MDPs, 63% using bentonite, and 38% using RDPs. The increasing of adsorption efficiency with temperature is attributed to the increasing viscosity that enhances the mobility of metals. In addition to the swelling effect that facilitates the intra-particle diffusion and enables metals to further enter the internal pores hence increasing the adsorption capacity. While the removal efficiency decreasing at 45 °C due to the high kinetic energy and mobility of Li that cause a collision and prevent it from adsorption to active adsorption sites. Another

reason for decreasing the adsorption that high temperature could break down the adsorption bonds with active sites. At 45 °C, the maximum adsorption efficiency reached 86% for AC, 83% using MDPs, 57% using bentonite and 29 % using RDPs. The fluctuation trend of increasing and decreasing adsorption capacity indicates the possibility of reversible adsorption and different diffusion mechanisms such as intra-particle diffusion and complex formation (Al-Ghouti et al., 2010; Al-Ghouti et al., 2017). Besides, the fluctuation trend of increasing and decreasing adsorption capacity indicates that intra-particle diffusion governed the adsorption process more than the external diffusion (Hawari et al., 2014).

Figure 46 shows the effect of temperature values 25 °C, 35 °C and 45 °C on Mo adsorption using AC, bentonite, RDPs, and MDPs respectively. It was shown that the adsorption efficiency of Mo increases at 35 °C using AC and RDPs. The maximum adsorption efficiency reached 48% for AC and 50% for RDPs. The increasing of adsorption efficiency with temperature is attributed to the increasing viscosity. However, the removal efficiency was decreasing at 45 °C due to the mobility of Mo that could prevent it from adsorption at active adsorption sites. At 45 °C, the adsorption efficiency decreased to 40% for AC and 47% using RDPs. While the adsorption efficiency decreases at 35 °C using the MDPS and bentonite adsorbents. The maximum adsorption efficiency reached 38% using MDPs and 32% using bentonite. However, the removal efficiency was increasing at 45 °C. As at 45 °C, the maximum adsorption efficiency increased to 50% using MDPs and 33% using bentonite.

Figure 47 shows the effect of temperature values 25 °C, 35 °C and 45 °C on boron adsorption using AC, bentonite, RDPs, and MDPs respectively. The adsorption efficiency of boron increases at 45 °C using AC, RDPs, and MDPs. The maximum

adsorption efficiency reached 91% for AC, 72% for MDPs, and 46% for RDPs. While the adsorption efficiency of boron increases at 35 °C using bentonite that reached the maximum adsorption efficiency of 66%. The increasing of adsorption efficiency with temperature is attributed to the increasing of viscosity. However, the removal efficiency decreasing at 25 °C due to lower mobility of boron than at higher temperature that could prevent it from adsorption at active adsorption sites. At 25 °C, the adsorption efficiency decreased to 18% for AC, and 36% using MDPs. While the adsorption efficiency decreases to 40% at 35 °C using the RDPS.

Table 14. *The Effect of Temperature on Lithium Adsorption*

Adsorbent	Removal Efficiency %		
	at 25 °C	at 35 °C	at 45 °C
AC	64.07	95.16	86.42
Bentonite	35.24	63.83	57.90
RDPs	24.51	38.04	29.19
MDPs	58.66	94.17	83.43

Table 15. *The Effect of Temperature on Molybdenum Adsorption*

Adsorbent	Removal Efficiency %		
	at 25 °C	at 35 °C	at 45 °C
AC	51.01	48.05	39.60
Bentonite	32.04	32.20	32.55
RDPs	57.60	49.60	47.49
MDPs	64.33	38.55	49.40

Table 16. *The Effect of Temperature on Boron Adsorption*

Adsorbent	Removal Efficiency %		
	at 25 °C	at 35 °C	at 45 °C
AC	18.00	55.38	91.25
Bentonite	54.16	66.10	59.85
RDPs	44.96	40.13	45.58
MDPs	36.18	56.17	71.69



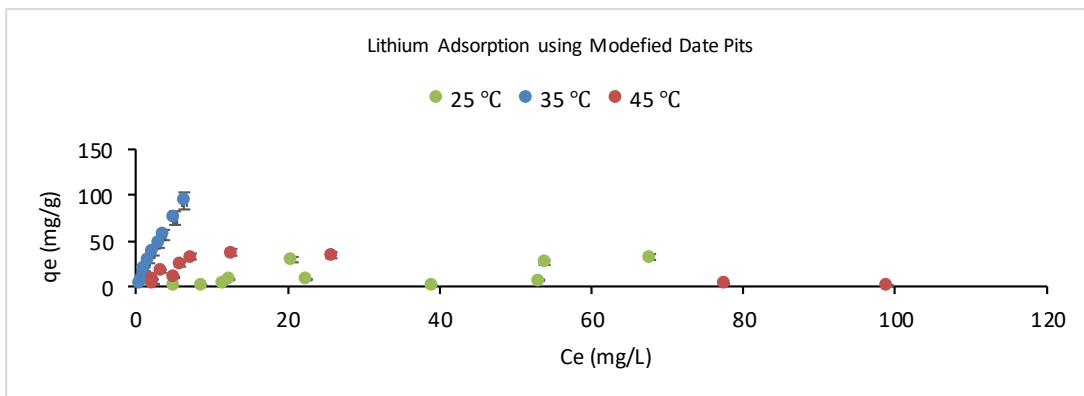
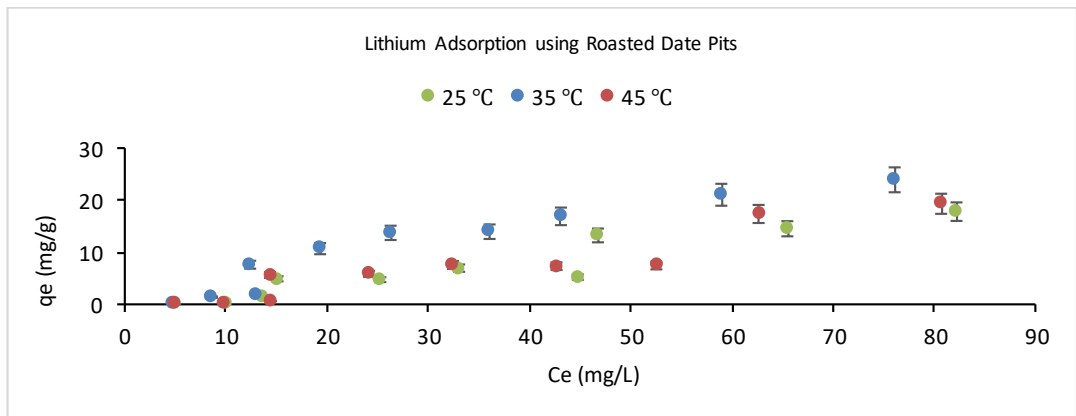
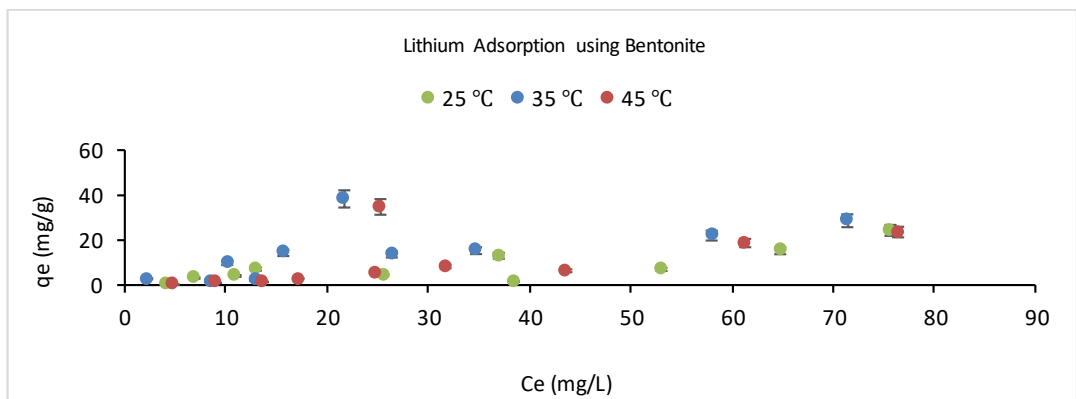
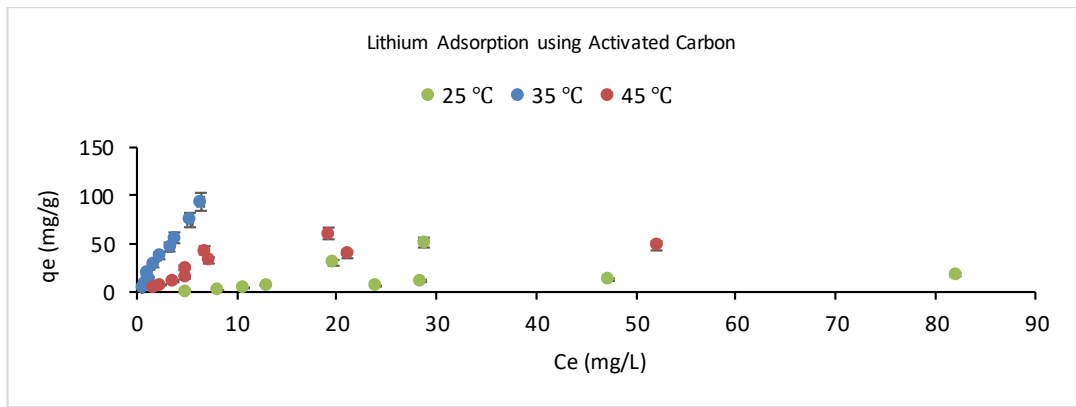


Figure 45. Study the effect of temperature on lithium adsorption using activated carbon, bentonite, RDPs, and MDPs.

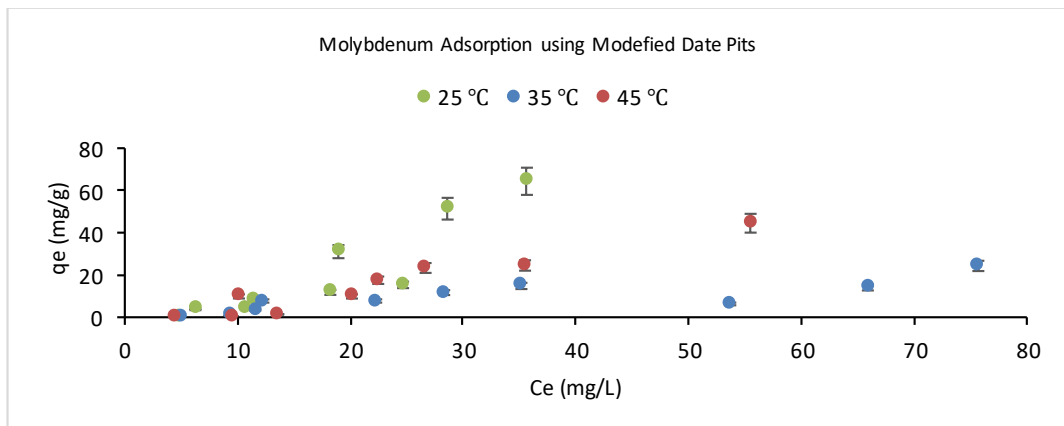
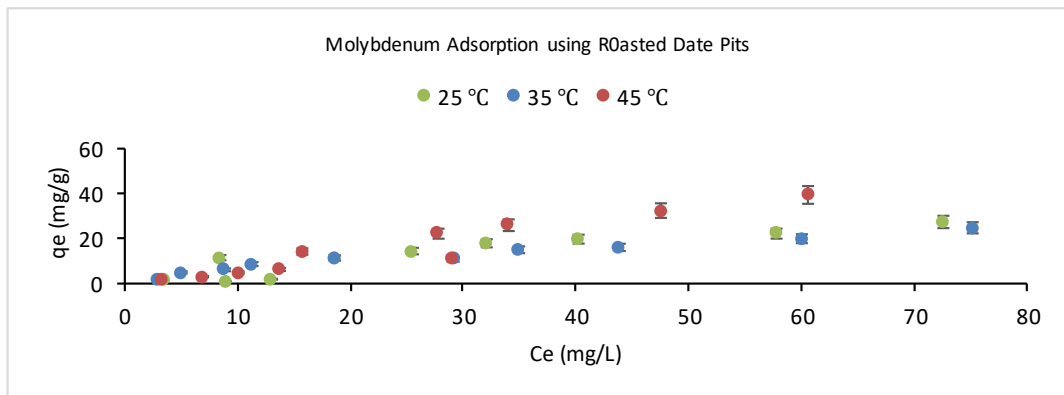
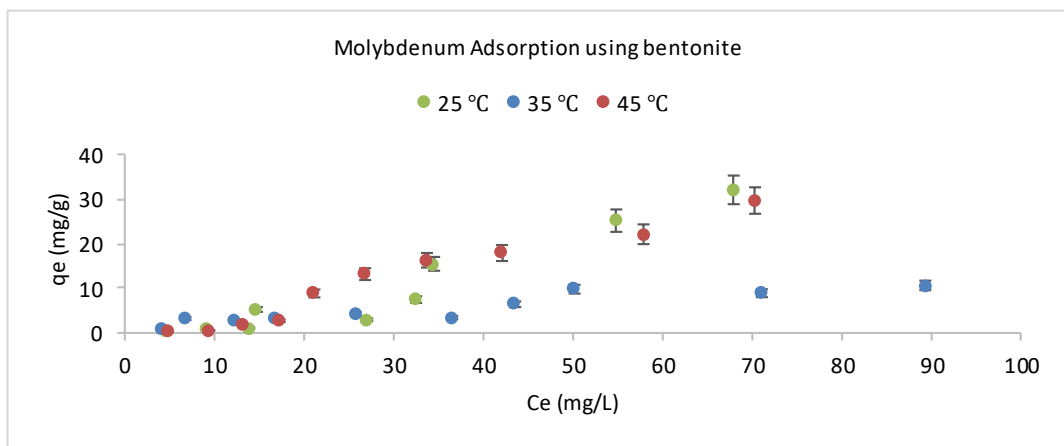
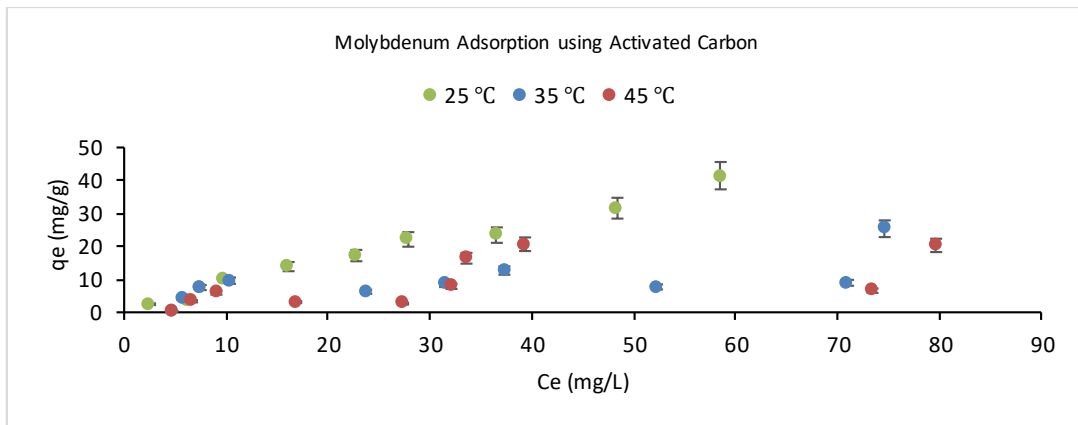


Figure 46. Study the effect of temperature on molybdenum adsorption using activated carbon, bentonite, RDPs, and MDPs.

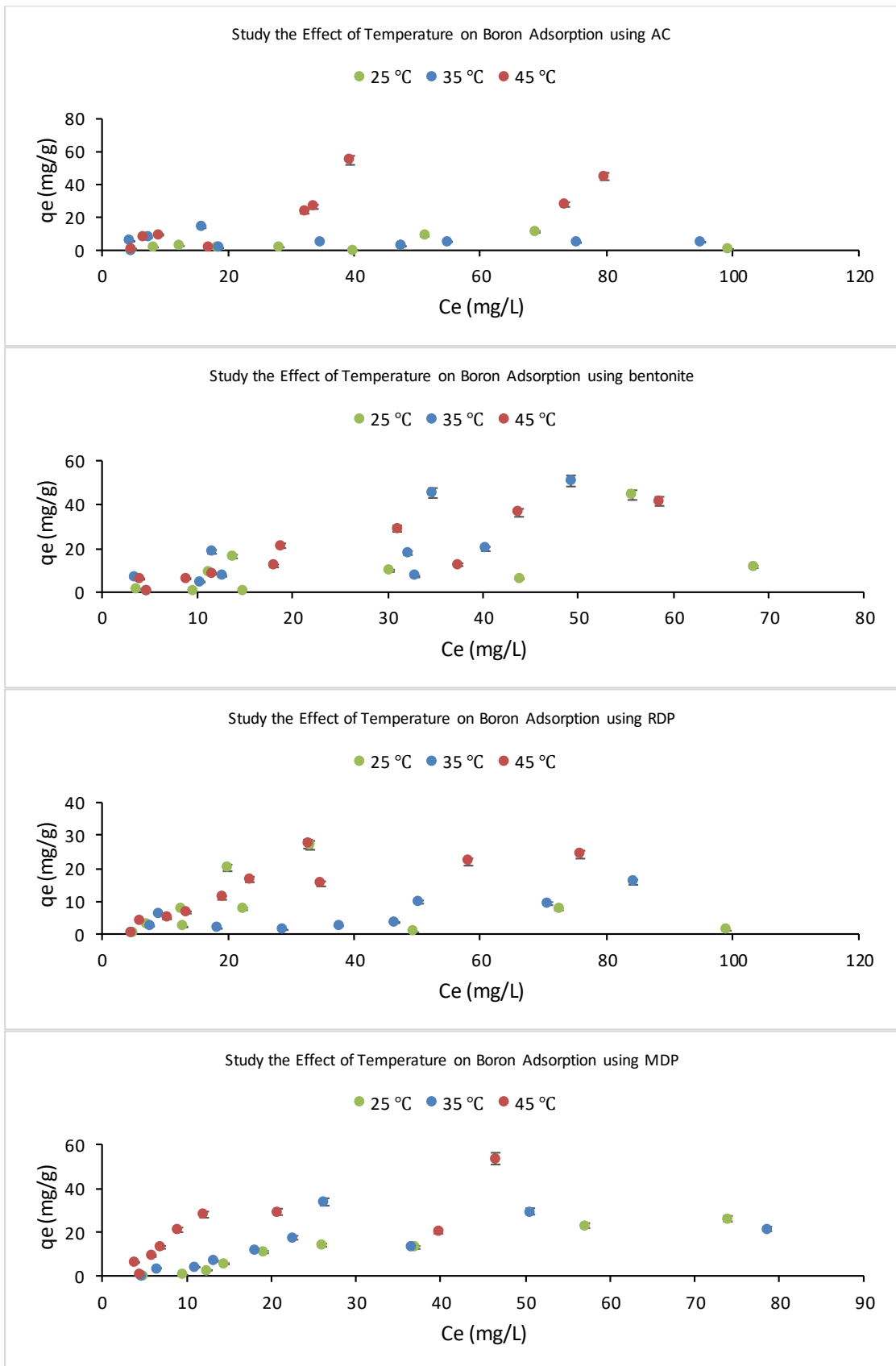


Figure 47. Study the effect of temperature on Boron adsorption using activated carbon, bentonite, RDPs, and MDPs.

## The Adsorption Models

In the current study, four adsorption models, namely Langmuir, Dubinin-Radushkevich, Freundlich, and Temkin are applied to investigate the adsorption process as shown in Appendix F. Adsorption isotherm models use the equilibrium data that is reached after the adsorbate moves from the aqueous phase to the solid phase, this equilibrium data is used to describe the interaction between the adsorbent and adsorbate at a constant temperature. For example, if there is an electron transfer between the adsorbent and adsorbate, this implies chemical adsorption of high energy about 40 to 800 kJ/mol (Al-Ghouti & Da'ana, 2020). Hence, the desorption process is difficult, while the adsorption process is irreversible and happens in monolayer. In chemical adsorption, the possible interactions are mainly ionic or covalent bonds. Therefore, if there is no electron transfer between the adsorbent and adsorbate, this implies physical adsorption of low energies about 5 kJ/mol to 40 kJ/mol. Hence the desorption process is easy, while the adsorption process is reversible and happens in multilayer. In physical adsorption, the different possible interactions are electrostatic, hydrogen bonds, London forces, Van der Waals, or dipole-dipole (Al-Ghouti & Da'ana, 2020). The summary of the adsorption parameters of the four adsorption isotherm models in the current study is shown in Tables 17, 18, 19, and 20 using AC, bentonite, RDPs, and MDPs respectively. The best-fit models for the experimental data are selected based on the coefficient determination  $R^2$  and chi-square  $\chi^2$ . The coefficient of determination  $R^2$  and  $X^2$  is calculated for each model using equations 26 and 27 respectively.

$$R^2 = 1 - \frac{\sum_{i=1}^n (q_{i,exp} - q_{i,mod})^2}{\sum_{i=1}^n (q_{i,exp} - q_{i,exp,mean})^2} = 1 - \frac{SSE}{SST} \quad (26)$$

$$\chi^2 = \sum_{i=1}^n \frac{(q_{i,exp} - q_{i,mod})^2}{q_{i,mod}} \quad (27)$$

Where  $q_{i,exp}$  and  $q_{i,mod}$  are the equilibrium capacity (mg/g) taken from the experimental (observed) and model (predicted) data respectively, n is the number of sample size, SST is the sum of square of total deviation and SSE is the sum of square error (Bonilla-Petriciolet et al., 2019).

The  $R^2$  value is sensitive to outliers, which could mislead in fitting the model. Thus,  $\chi^2$  is also used for the determination of the good fit model. Critical Chi (p-value) for n=10 is 18.31 at  $\alpha = 0.05$  and 23.21 at  $\alpha = 0.01$ , if the  $\chi^2$  statistic is lower than the p-value, the null hypothesis is not rejected, and it is concluded that there is no sufficient evidence to that the experimental value is different from the model value.

#### *Monolayer Adsorption and the Langmuir Isotherm*

It is found that the Langmuir model describes well the adsorption of Mo by AC at 25 °C ( $R^2 = 0.94$  and  $\chi^2 = 4.8$ ), the adsorption of Mo by Bentonite at 35 °C ( $R^2 = 0.84$  and  $\chi^2 = 3.8$ ), the adsorption of Li by Bentonite at 45 °C ( $R^2 = 0.88$  and  $\chi^2 = 13$ ), the adsorption of Mo by RDPs at 35 °C ( $R^2 = 0.99$  and  $\chi^2 = 12$ ), the adsorption of Mo by RDPs at 45 °C ( $R^2 = 0.98$  and  $\chi^2 = 10$ ), and the adsorption of boron by bentonite at 45 °C ( $R^2 = 0.84$  and  $\chi^2 = 11$ ). According to the Langmuir model, monolayer uptake of Mo and Li occurs in these experiments. This indicates homogenous adsorption in which the adsorption energies are uniform. Langmuir adsorption constant (b) is associated with increased attraction between the adsorbate and adsorbent, the high b value suggested the presence of strong binding while the lower b values suggest the lower binding. Whereas the non-fitted plot of Langmuir model for Li and B adsorption using AC and RDPs, and for Li and Mo using MDPs showed two different

linear lines; one line is at low concentrations, and the other is at high concentrations. This indicates the heterogeneous adsorption in which the highest adsorption energy sites are adsorbed first, and then the second adsorption energies are created allowing more adsorption at high concentrations. The creation of the second adsorption sites is explained by the high concentration of adsorbate that creates pressure on the adsorbent surface and forces the adsorbates into the internal surface and pores. In addition, it could be explained by the formation of new adsorption sites due to the pressure force that removes blocks that hinder the adsorbates from entering the pores (Al-Ghouti et al., 2010).

#### *Temkin Isotherm*

The Temkin isotherm model is the best fit to describe the adsorption of Mo by AC at 25 °C ( $R^2 = 0.87$  and  $\chi^2 = 6$ ), the adsorption of Li by AC at 35 °C ( $R^2 = 0.93$  and  $\chi^2 = 9.5$ ), the adsorption of Li by AC at 45 °C ( $R^2 = 0.75$  and  $\chi^2 = 23$ ), the adsorption of Mo by bentonite at 25 °C ( $R^2 = 0.78$  and  $\chi^2 = 15.31$ ), the adsorption of Mo by bentonite at 35 °C ( $R^2 = 0.77$  and  $\chi^2 = 8.23$ ), the adsorption of Mo by bentonite at 45 °C ( $R^2 = 0.87$  and  $\chi^2 = 0.97$ ), the adsorption of Li by RDPs at 25 °C ( $R^2 = 0.80$  and  $\chi^2 = 4.3$ ), the adsorption of Mo by RDPs at 25 °C ( $R^2 = 0.81$  and  $\chi^2 = 10.2$ ), the adsorption of Mo by RDPs at 35 °C ( $R^2 = 0.91$  and  $\chi^2 = 7.6$ ), the adsorption of Li by RDPs at 35 °C ( $R^2 = 0.93$  and  $\chi^2 = 0.7$ ), the adsorption of Mo by RDPs at 45 °C ( $R^2 = 0.80$  and  $\chi^2 = 2.8$ ), the adsorption of Li by RDPs at 45 °C ( $R^2 = 0.75$  and  $\chi^2 = 6.8$ ), the adsorption of Mo by MDPs at 35 °C ( $R^2 = 0.68$  and  $\chi^2 = 12.7$ ), the adsorption of Li by MDPs at 35 °C ( $R^2 = 0.91$  and  $\chi^2 = 8.4$ ), the adsorption of boron by bentonite at 45 °C ( $R^2 = 0.73$  and  $\chi^2 = 19$ ), the adsorption of boron by MDPs at 35 °C ( $R^2 = 0.91$  and  $\chi^2 = 3.5$ ), and the adsorption of boron by RDPs at 45 °C ( $R^2 = 0.83$  and  $\chi^2 = 9.3$ ).

Temkin model indicates the heat of adsorption and the interaction between the adsorbate and adsorbent. Temkin isotherm equation assumes that the heat of adsorption affects the adsorbate concentration, which is decreases linearly with the layer coverage onto a heterogeneous surface. The other assumption is that the adsorption binding energies are a uniformly distributed until it reaches maximum binding energy.  $A_T$  is Temkin isotherm equilibrium binding constant (L/g),  $(\frac{RT}{bT})$  is the constant related to the heat of adsorption (J/mol). When the heat of adsorption,  $b_t$  decreased as the temperature increased, it indicates that the adsorption is exothermic.

#### *Freundlich Isotherm*

The Freundlich isotherm model describes well the adsorption of Mo by AC at 25 °C ( $R^2 = 0.97$  and  $\chi^2 = 1.9$ ), the adsorption of Li by AC at 35 °C ( $R^2 = 0.95$  and  $\chi^2 = 9.2$ ), the adsorption of Mo by bentonite at 35 °C ( $R^2 = 0.83$  and  $\chi^2 = 3.2$ ), the adsorption of Mo by bentonite at 45 °C ( $R^2 = 0.94$  and  $\chi^2 = 22$ ), the adsorption of Mo by RDPs at 35 °C ( $R^2 = 0.94$  and  $\chi^2 = 1.7$ ), the adsorption of Mo by RDPs at 45 °C ( $R^2 = 0.94$  and  $\chi^2 = 8.7$ ), the adsorption of Li by MDPs at 35 °C ( $R^2 = 0.98$  and  $\chi^2 = 5.4$ ), and the adsorption of boron by MDPs at 35 °C ( $R^2 = 0.86$  and  $\chi^2 = 42$ ).

According to the Freundlich model, multilayer uptake of Mo and Li happens in these experiments, which indicates heterogeneous adsorption energy. Thus, both chemisorption and physisorption are proposed adsorption mechanisms. It is also noticed that the values of Freundlich adsorption constant ( $K_f$ ) increase with increasing the temperature at 35 °C; While it is decreased at a greater temperature at 45 °C. The value of  $1/n$  is the intensity of the adsorption indicating the surface heterogeneity and the distribution of binding energy. When the value ( $1/n$ ) is greater than zero ( $0 < 1/n < 1$ ) the adsorption is favorable, while if the value of ( $1/n$ ) is greater than 1, the

adsorption process is unfavorable, and if  $1/n$  is equal to 1, the adsorption process is irreversible. For example, the value ( $1/n$ ) is 0.893 in the adsorption of Mo by AC at 25 °C, which is favorable indicating 89% of the active sites have the same adsorption energy. The adsorption of Mo by bentonite at 35 °C, and RDPs at 35 °C, are also favorable; While the adsorption process is unfavorable for the adsorption of Li by AC at 35 °C, the adsorption of Mo by bentonite at 45 °C, the adsorption of Mo by RDPs at 45 °C, and the adsorption of Li by MDPs at 35 °C are unfavorable. Consequently, ( $n$ ) value near one indicates a homogeneous surface.

#### *Dubinin–Radushkevich (D-R) Isotherm*

Dubini-Radushkevich isotherm model is best fit to describe the adsorption of Mo at 35 °C by MDP ( $R^2 = 0.92$ ).  $K$  is the adsorption energy constant,  $\varepsilon$  is Polanyi adsorption potential, which is the amount of energy, required to desorb the adsorbate from its adsorption site. The Dubinin-Radushkevich model is temperature-dependent and when the value of low mean free energy ( $E$ ) indicates physisorption.

Table 17. *Langmuir, Dubini-Radushkevich, Freundlich Parameters for the Adsorption Process by Activated Carbon.*

Model	Temperature	Parameter	Li	Mo	B
Langmuir	25	$Q_0$ (mg/g)	-0.54	74	-34
		$b$ (L/mg)	-0.043	0.013	-0.0018
		$R^2$	0.69	<b>0.93</b>	0.57
		$X^2$	102	<b>4.8</b>	34
	35	$Q_0$ (mg/g)	-49	-3.3	57
		$b$ (L/mg)	-0.18	-0.023	0.0022
		$R^2$	0.91	0.44	0.28
		$X^2$	936	170	178
	45	$Q_0$ (mg/g)	-51	-2.9	6.1
		$b$ (L/mg)	-0.044	-0.026	0.38
		$R^2$	0.90	0.60	0.038
		$X^2$	792	50	159
Freundlich	25	$1/n$	1.58	0.89	0.73



Model	Temperature	Parameter	Li	Mo	B	
		$K_f$ (mg/g)(L/mg) <sup>1/n</sup>	0.060	1.05	0.16	
		$R^2$	0.58	<b>0.96</b>	0.19	
		$X^2$	257	<b>1.9</b>	40	
	35	1/n	1.1	0.76	0.28	
		$K_f$ (mg/g)(L/mg) <sup>1/n</sup>	12	0.62	1.48	
		$R^2$	<b>0.94</b>	0.45	0.084	
	45	$X^2$	<b>9.2</b>	30	57	
		1/n	0.74	0.99	0.53	
		$K_f$ (mg/g)(L/mg) <sup>1/n</sup>	4.97	0.24	2.3	
	Dubini-Radushkevich	25	$R^2$	0.72	0.55	0.13
			$X^2$	69	41	146
			1/n	0.74	0.99	0.53
		35	$q_s$ (mg/g)	18	26	2.07
			K (mol <sup>2</sup> /kJ <sup>2</sup> )	-3E-05	-1E-05	-9E-06
			$R^2$	0.89	0.88	0.16
45		$X^2$	119	213	67	
		$q_s$ (mg/g)	61	12	4.8	
		K (mol <sup>2</sup> /kJ <sup>2</sup> )	-4E-07	-1E-05	-4E-06	
Temkin		25	$R^2$	0.81	0.70	0.16
			$X^2$	34	24	43
			1/n	0.74	0.99	0.53
		35	$q_s$ (mg/g)	39	10	22
			K (mol <sup>2</sup> /kJ <sup>2</sup> )	-2E-06	-1E-05	-8E-07
			$R^2$	0.86	0.69	0.14
	45	$X^2$	88	37	382	
		B (J/mol)	8.63	11	1.6	
		$b_t$	286	213	1545	
		25	At (L/mg)	0.26	0.27	0.27
			$R^2$	0.21	<b>0.87</b>	0.17
			$X^2$	105	<b>6</b>	23
		35	B (J/mol)	34	0.43	-0.213
			$b_t$	72	596	-11636
			At (L/mg)	1.58	4.1	6E-08
45		$R^2$	<b>0.92</b>	0.42	0.016	
		$X^2$	<b>9.5</b>	60	-	
		B (J/mol)	15	5.21	5.07	
45		$b_t$	160	474	488	
		At (L/mg)	0.89	0.23	4.2	
		$R^2$	<b>0.74</b>	0.44	0.093	
			$X^2$	<b>23</b>	25	112

Table 18. Langmuir, Dubini-Radushkevich, Freunlich Parameters for the Adsorption Process by Bentonite.

Model	Temperature	Parameter	Li	Mo	B
Langmuir	25	$Q_0$ (mg/g)	14.61	-5.133	0.083
		b (L/mg)	0.021	-0.012	0.027
		$R^2$	0.583	0.782	0.50
		$X^2$	49	90	2200
	35	$Q_0$ (mg/g)	8.86	15.197	-9.8
		b (L/mg)	0.151	0.018	-0.015
		$R^2$	0.206	<b>0.839</b>	0.22
		$X^2$	256	<b>3.8</b>	359
	45	$Q_0$ (mg/g)	-1.15	-1.266	222
		b (L/mg)	-0.031	-0.030	0.0033
		$R^2$	<b>0.881</b>	0.944	<b>0.84</b>
		$X^2$	<b>13</b>	34	<b>11</b>
Freundlich	25	1/n	0.72	1.78	0.55
		$K_f$ (mg/g)(L/mg) <sup>1/n</sup>	0.55	0.017	1.4
		$R^2$	0.51	0.90	0.32
		$X^2$	25	34	116
	35	1/n	0.81	0.67	1.1
		$K_f$ (mg/g)(L/mg) <sup>1/n</sup>	0.92	0.49	0.36
		$R^2$	0.54	<b>0.83</b>	0.50
		$X^2$	78	<b>3.2</b>	125
	45	1/n	1.70	1.97	1.2
		$K_f$ (mg/g)(L/mg) <sup>1/n</sup>	0.020	0.010	0.27
		$R^2$	0.80	<b>0.93</b>	0.62
		$X^2$	190	<b>22</b>	54
Dubini-Radushkevich	25	$q_s$ (mg/g)	7.8	6.3	11
		K (mol <sup>2</sup> /kJ <sup>2</sup> )	-7E-06	-2E-05	-5E-06
		$R^2$	0.46	0.44	0.28
		$X^2$	54	195	336
	35	$q_s$ (mg/g)	24	5.9	15
		K (mol <sup>2</sup> /kJ <sup>2</sup> )	-3E-05	-6E-06	-5E-06
		$R^2$	0.63	0.66	0.27
		$X^2$	45	10	185
	45	$q_s$ (mg/g)	9.3	11	19
		K (mol <sup>2</sup> /kJ <sup>2</sup> )	-2E-05	-2E-05	-9E-06
		$R^2$	0.70	0.71	0.49
		$X^2$	137	61	91
Temkin	25	B (J/mol)	5.1	14	6.1
		$b_t$	483	166	402
		At (L/mg)	0.21	0.081	0.24
		$R^2$	0.48	<b>0.78</b>	0.20
		$X^2$	25	<b>15</b>	83
	35	B (J/mol)	7.9	2.9	12

Model	Temperature	Parameter	Li	Mo	B
		$b_t$	311	853	198
		At (L/mg)	0.36	0.25	0.24
		$R^2$	0.45	<b>0.76</b>	0.46
		$X^2$	34	<b>8.12</b>	22
	45	B (J/mol)	7.1	11	12
		$b_t$	346	217	191
		At (L/mg)	0.11	0.11	0.22
		$R^2$	0.62	<b>0.87</b>	<b>0.73</b>
		$X^2$	98	<b>0.97</b>	<b>19</b>

Table 19. Langmuir, Dubini-Radushkevich, Freundlich Parameters for the Adsorption Process by RDPs.

Model	Temperature	Parameter	Li	Mo	B
Langmuir	25	$Q_o$ (mg/g)	-0.18	45	-0.38
		b (L/mg)	-0.029	0.010	-0.034
		$R^2$	0.87	0.64	0.56
		$X^2$	205	39	32
	35	$Q_o$ (mg/g)	-1.7	21	-23
		b (L/mg)	-0.033	0.037	-0.0043
		$R^2$	0.84	<b>0.94</b>	0.61
		$X^2$	53	<b>12</b>	36
	45	$Q_o$ (mg/g)	-0.440	-100	-2.8
		b (L/mg)	-0.030	-0.005	-0.035
		$R^2$	0.883	<b>0.978</b>	0.62
		$X^2$	108	<b>10</b>	376
Freundlich	25	1/n	2.2	1.04	0.66
		$K_f$ (mg/g)(L/mg) <sup>1/n</sup>	0.0016	0.36	1.0
		$R^2$	0.80	0.67	0.28
		$X^2$	41	29	51
	35	1/n	1.5	0.67	0.80
		$K_f$ (mg/g)(L/mg) <sup>1/n</sup>	0.061	1.34	0.24
		$R^2$	0.840	<b>0.94</b>	0.50
		$X^2$	27	<b>1.7</b>	30
	45	1/n	1.9	1.1	1.2
		$K_f$ (mg/g)(L/mg) <sup>1/n</sup>	0.006	0.39	0.21
		$R^2$	0.84	<b>0.93</b>	<b>0.76</b>
		$X^2$	30	<b>8.7</b>	<b>31</b>
Dubini-Radushkevich	25	$q_s$ (mg/g)	6.1	23	6.4
		K (mol <sup>2</sup> /kJ <sup>2</sup> )	-3E-02	-5E-05	-2E-05
		$R^2$	0.72	0.89	0.46
		$X^2$	-	6.5E06	36

Model	Temperature	Parameter	Li	Mo	B	
Temkin	35	$q_s$ (mg/g)	13	13	5.0	
		$K$ (mol <sup>2</sup> /kJ <sup>2</sup> )	-2E-02	-4E-06	-1E-05	
		$R^2$	0.83	0.79	0.46	
		$X^2$	-	15	42	
	45	$q_s$ (mg/g)	7.1	16	18	
		$K$ (mol <sup>2</sup> /kJ <sup>2</sup> )	-2E-02	-5E-06	-1E-05	
		$R^2$	0.73	0.58	<b>0.89</b>	
		$X^2$	-	74	<b>41</b>	
	25	$B$ (J/mol)	6.2	8.6	1.2	
		$b_t$	398	285	2004	
		$A_t$ (L/mg)	0.12	0.22	21	
		$R^2$	<b>0.79</b>	<b>0.81</b>	0.017	
		$X^2$	<b>4.3</b>	<b>10</b>	692	
		35	$B$ (J/mol)	9.0	6.2	3.2
			$b_t$	274.94	396.70	764
			$A_t$ (L/mg)	0.158	0.360	0.20
$R^2$			<b>0.93</b>	<b>0.91</b>	0.43	
45		$X^2$	<b>0.7</b>	<b>7.6</b>	23	
		$B$ (J/mol)	6.405	13.03	9.2	
		$b_t$	386.96	190.26	268	
	$A_t$ (L/mg)	0.123	0.189	0.21		
45	$R^2$	<b>0.75</b>	<b>0.80</b>	<b>0.83</b>		
	$X^2$	<b>6.8</b>	<b>2.8</b>	<b>9.3</b>		

Table 20. Langmuir, Dubini-Radushkevich, Freunlich Parameters for the Adsorption Process by MDPs.

Model	Temperature	Parameter	Li	Mo	B
Langmuir	25	$Q_0$ (mg/g)	-0.28	-71	-1.0
		$b$ (L/mg)	-0.040	-0.0076	-0.035
		$R^2$	0.67	0.78	<b>0.90</b>
		$X^2$	261	157	<b>63</b>
	35	$Q_0$ (mg/g)	-59	-0.28	-2.2
		$b$ (L/mg)	-0.15	-0.038	-0.038
		$R^2$	0.97	0.72	0.67
		$X^2$	105	290	33
	45	$Q_0$ (mg/g)	-3.6E-05	0.58	-6.39
		$b$ (L/mg)	-0.027	-14	-0.046
		$R^2$	0.96	0.62	0.29
		$X^2$	42286	598	1.9E05

Model	Temperature	Parameter	Li	Mo	B
Freundlich	25	1/n	1.5	1.1	1.8
		$K_f$ (mg/g)(L/mg) <sup>1/n</sup>	0.037	0.53	0.017
		$R^2$	0.48	0.52	<b>0.86</b>
		$X^2$	201	123	<b>42</b>
	35	1/n	1.1	1.6	1.3
		$K_f$ (mg/g)(L/mg) <sup>1/n</sup>	12	0.023	0.17
		$R^2$	<b>0.97</b>	0.68	0.72
		$X^2$	<b>5.4</b>	54	68
	45	1/n	0.87	0.19	1.1
		$K_f$ (mg/g)(L/mg) <sup>1/n</sup>	3.3	0.72	0.92
		$R^2$	0.62	0.44	0.54
		$X^2$	362	2192	84
Dubini-Radushkevich	25	$q_s$ (mg/g)	12	35	25
		K (mol <sup>2</sup> /kJ <sup>2</sup> )	-3E-05	-4E-05	-7E-05
		$R^2$	0.733	0.53	<b>0.97</b>
		$X^2$	119	173	<b>45</b>
	35	$q_s$ (mg/g)	57	12	19
		K (mol <sup>2</sup> /kJ <sup>2</sup> )	-4E-07	-3E-05	-2E-05
		$R^2$	0.76	0.91	<b>0.88</b>
		$X^2$	118	9997	<b>26</b>
	45	$q_s$ (mg/g)	55	0.72	37
		K (mol <sup>2</sup> /kJ <sup>2</sup> )	-0.0025	-0.19	-8E-06
		$R^2$	0.74	0.44	0.66
		$X^2$	-	-	52
Temkin	25	B (J/mol)	8.4	27	10
		$b_t$	294	89	234
		At (L/mg)	0.18	0.14	0.13
		$R^2$	0.35	0.67	<b>0.91</b>
	35	$X^2$	63	71	<b>3.5</b>
		B (J/mol)	34	6.6	9.9
		$b_t$	72	370	248
		At (L/mg)	1.52	0.17	0.21
	45	$R^2$	<b>0.91</b>	<b>0.68</b>	0.61
		$X^2$	<b>8.4</b>	<b>12.7</b>	25
		B (J/mol)	13	1.6	16
		$b_t$	179	1469	146
	At (L/mg)	0.77	0.11	0.33	
	$R^2$	0.75	0.49	0.62	
	$X^2$	124	1120	15	

## Thermodynamic Study

Tables 21, 22, and 23 show the thermodynamic parameters for Li, Mo and B adsorption respectively. Thermodynamic parameters are essential to understand the adsorption process. Thermodynamic studies estimate standard Gibbs free energy change ( $\Delta G^\circ$ ), standard enthalpy change ( $\Delta H^\circ$ ), and standard entropy change ( $\Delta S^\circ$ ). These parameters help to verify if the adsorption is favorable, spontaneous, endothermic, or exothermic. Also, it helps to investigate the adsorption nature, as physical adsorption or chemical adsorption (Al-Ghouti & Da'ana, 2020). Physical adsorption is an exothermic process that is characterized by the heat of adsorption lower than 20 kJ/mol for van der Waals, and it is from 20 kJ/mol to 80 kJ/mol for electrostatic interaction, while it is from 80 kJ/mol to 450 kJ/mol for chemical adsorption (Bonilla-Petriciolet et al., 2017). The potential energy is the sum of all interactions between the adsorbate and the active sites on the surface of the adsorbent. Thus, if the adsorption process is spontaneous, there is a decrease in Gibbs free energy, such that  $\Delta G^\circ$  is less than zero. Further, according to thermodynamics, the entropy increases, and  $\Delta H^\circ$  decreases, and hence heat is released (Noll et al., 1990). The estimation of the adsorption thermodynamic parameters is found by plotting  $(1/T)$  versus  $(\ln b)$ , where  $(b)$  Langmuir isotherm constant, or  $\ln (K_f)$ , where  $(K_f)$  is Freundlich isotherm constant, depending on the applicability of the models as shown in Figures 48, 49, 50 and 51, the graph is known as the Van't Hoff plot. The adsorption of Li on AC and MDP at 35 °C and 45 °C, beside the adsorption of boron on AC at 25°C, 35 °C and 45 °C showed negative values for free energy that indicates a spontaneous and favorable adsorption process. The value of  $\Delta G^\circ$  is increased for higher temperature showing more favorable and spontaneous adsorption at high temperature. However, the positive value of  $\Delta H^\circ$  inferred that experiment favored

endothermic pathway, and the magnitude of  $\Delta H^\circ$  from 150 kJ/mol to 180 kJ/mol can give an idea that electrostatic interaction and chemical adsorption occur between the adsorbent and adsorbate. In relation to the positive entropy values that suggest dissociative adsorption and the possibility of some structural changes or readjustments in the adsorbate–adsorbent that forms an active complex. Finally, ( $T\Delta S^\circ$ ) contributes more than  $\Delta H^\circ$ , thus the adsorption is an entropy-controlled process.

Table 21. *Thermodynamic Parameters of Lithium Adsorption*

Adsorbent	Temperature °C	ln b or ln $K_f^*$	$\Delta G^\circ$ (kJ/mol)	$\Delta H^\circ$ (kJ/mol)	$\Delta S^\circ$ (J/mol.K)
AC	25	-2.8	4.5	180	580
	35	2.5	-1.3		
	45	1.6	-7.0		
Bentonite	25	-3.9	8.0	-0.22	-28
	35	-1.9	8.3		
	45	-4.0	8.5		
RDP	25	-6.4	14	55	140
	35	-2.8	12		
	45	-5.1	11		
MDP	25	-3.2	5.4	181	590
	35	2.5	-0.47		
	45	1.2	-6.4		

\* Langmuir isotherm constant (b) or Freundlich isotherm constant ( $K_f$ ) depend on the applicability of the models.

Table 22. *Thermodynamic Parameters of Molybdenum Adsorption*

Adsorbent	Temperature °C	ln b or ln $K_f^*$	$\Delta G^\circ$ (kJ/mol)	$\Delta H^\circ$ (kJ/mol)	$\Delta S^\circ$ (J/mol.K)
AC	25	-4.4	8.9	120	360
	35	-0.47	5.2		
	45	-1.4	1.6		
Bentonite	25	-4.0	9.8	-18	-93
	35	-4.0	11		
	45	-4.5	12		
RDP	25	-4.6	12	144	444
	35	-3.3	7.4		
	45	-0.93	3.0		

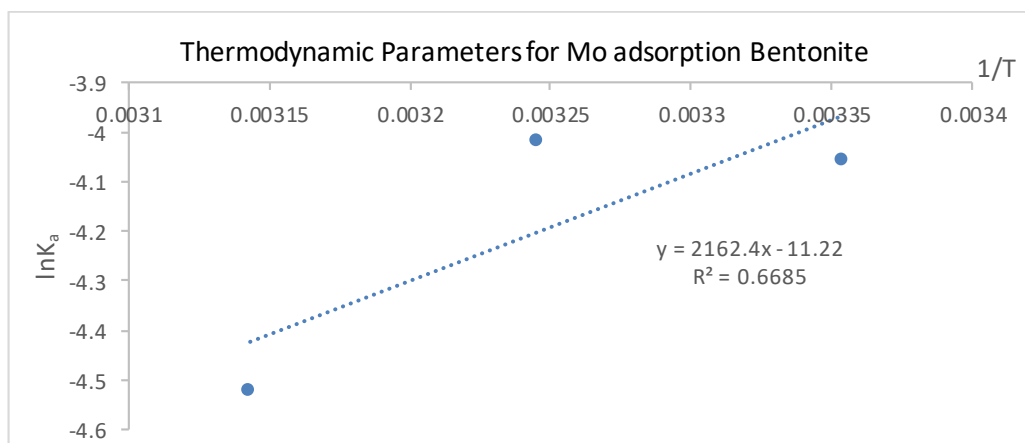
MDP	25	-0.63	4.2	10	19
	35	-3.8	4.0		
	45	-0.31	3.8		

\* Langmuir isotherm constant (b) or Freundlich isotherm constant (Kf) depend on the applicability of the models.

Table 23. Thermodynamic Parameters of Boron Adsorption

Adsorbent	Temperature °C	ln b or ln K <sub>f</sub> *	ΔG° (kJ/mol)	ΔH° (kJ/mol)	ΔS° (J/mol.K)
AC	25	-1.8	-25	150	580
	35	4.0	-30		
	45	1.8	-36		
Bentonite	25	-2.5	5.5	47	140
	35	-1.0	4.1		
	45	-1.3	2.7		
RDP	25	0	-0.49	-61	-203
	35	-0.2	1.5		
	45	-1.5	3.5		
MDP	25	-4.0	9.9	160	495
	35	-1.8	4.9		
	45	-0.31	0.015		

\* Langmuir isotherm constant (b) or Freundlich isotherm constant (Kf) depend on the applicability of the models.





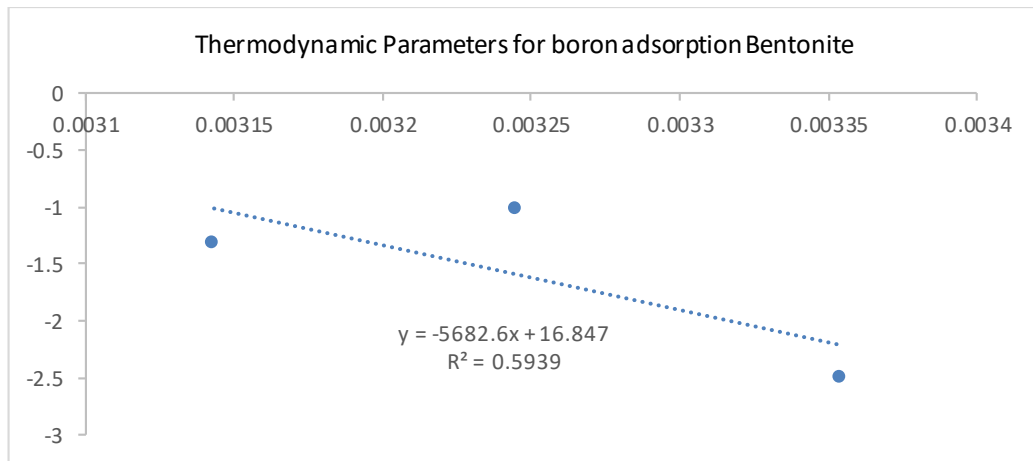
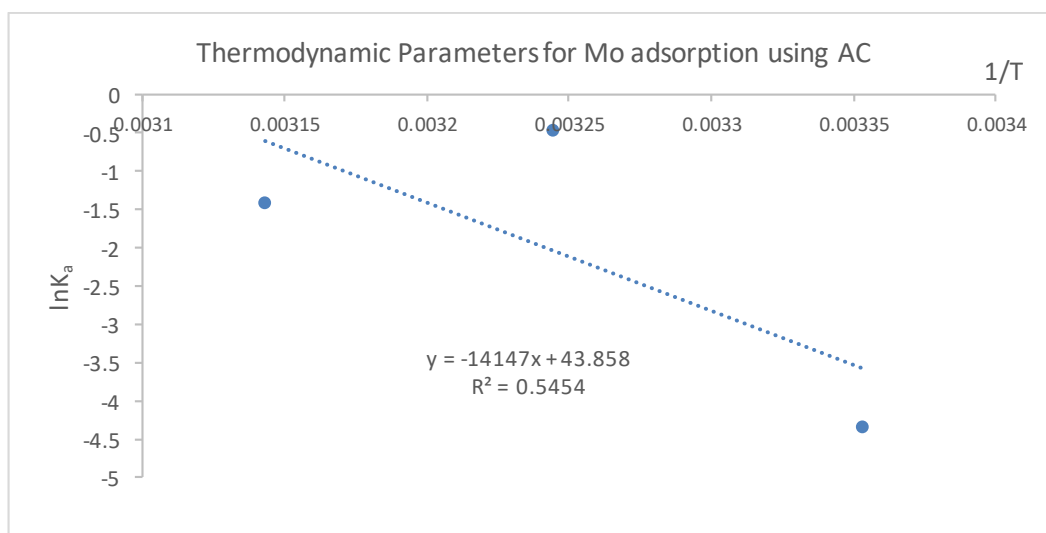
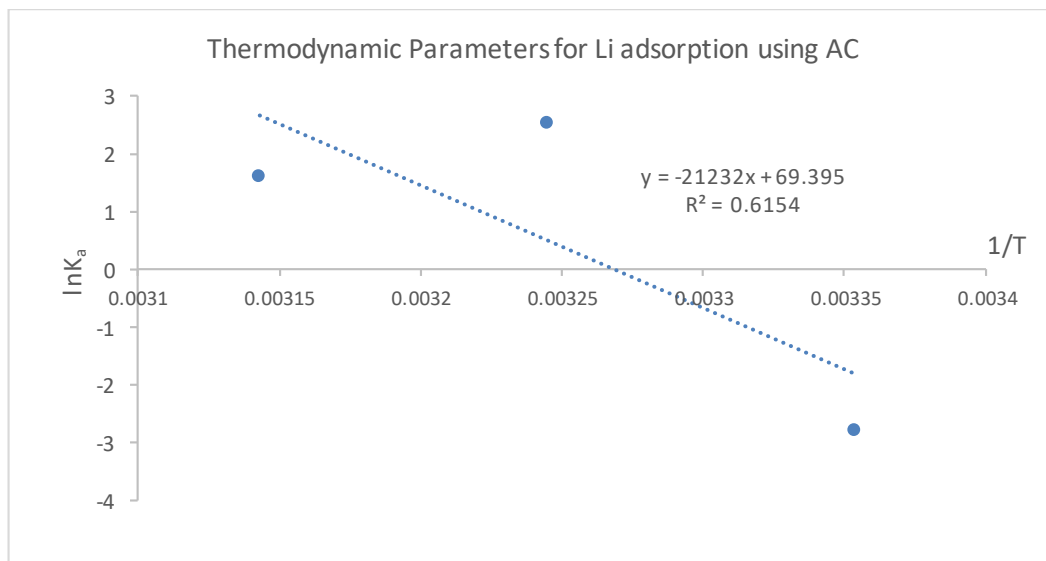


Figure 48. Van't Hoff plot for adsorption process using bentonite.



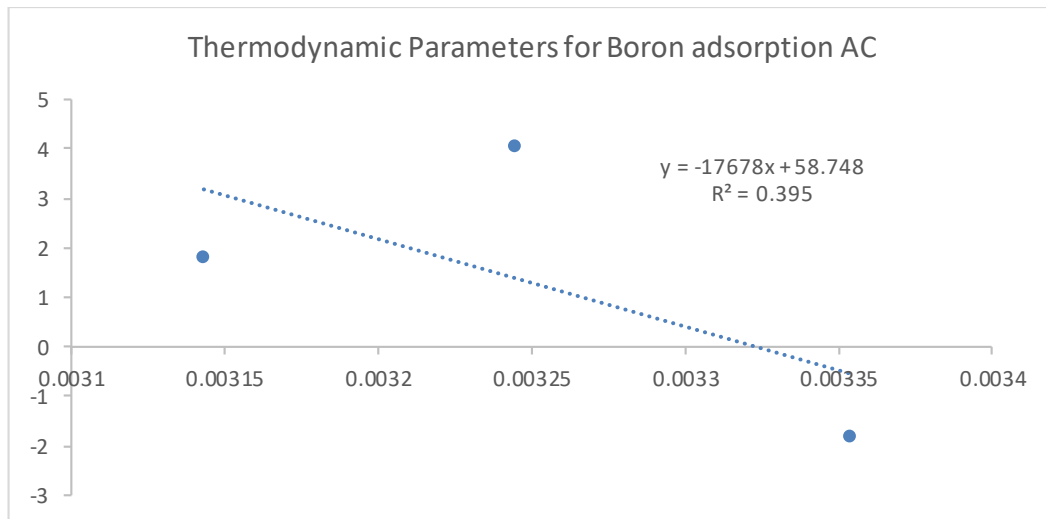


Figure 49. Van't Hoff plot for adsorption process using activated carbon.

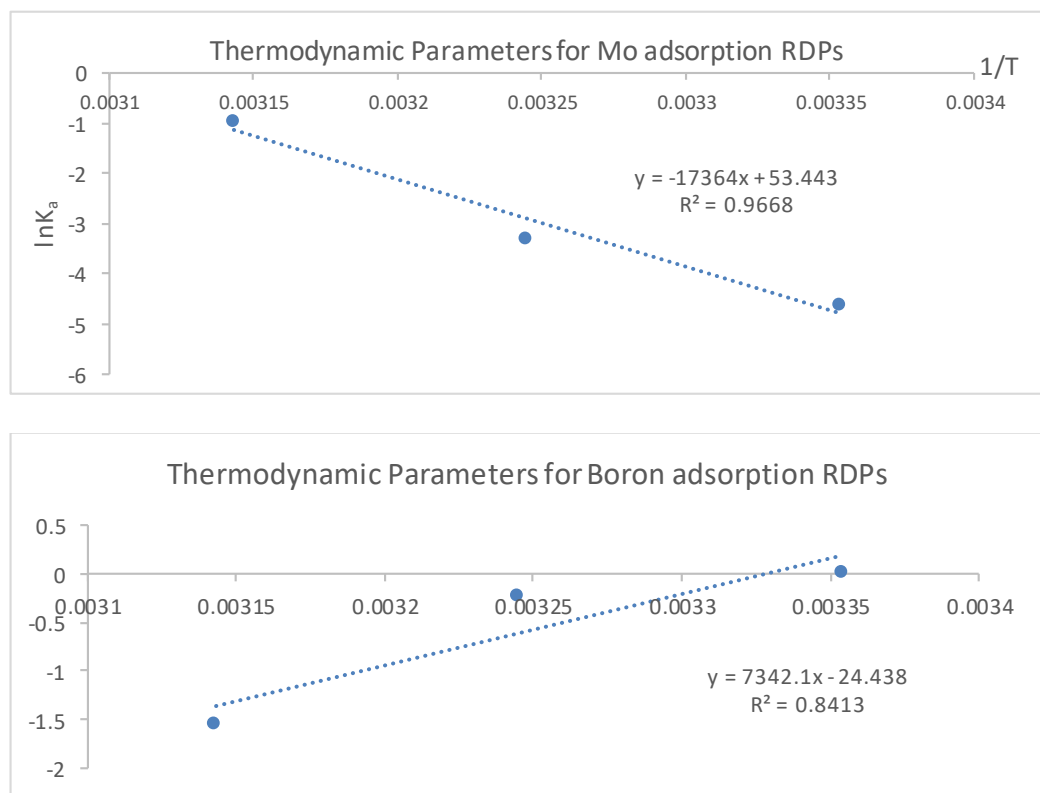


Figure 50. Van't Hoff plot for adsorption process using RDPs.

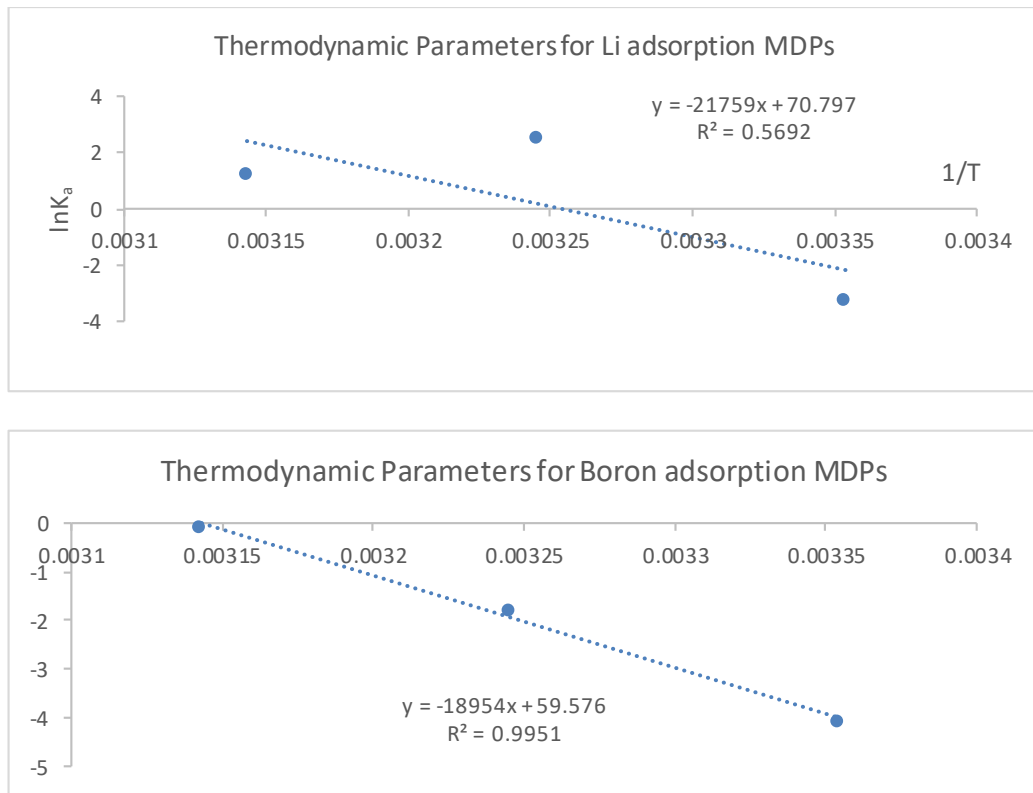


Figure 51. Van't Hoff plot for adsorption process using MDPs.

#### Mixture Solutions Adsorption Experiments

The mixture of five solutions were prepared to study the effect of the concentration of a mixture solution of Li, Mo, and B on the adsorption process. The concentrations of Li, Mo, and B in each mixture solution are shown in Table 24. The adsorption experiment is conducted at pH 7 to compare the result with the real water pH mean value of (7.3), and it was the optimum pH value for the adsorption of Li, Mo, and B.

Table 24. The effect of the concentration of a mixture solution of lithium, molybdenum, and boron on the adsorption process

	Initial Concentration $C_o$ (mg/L)		
	Molybdenum	Lithium	Boron
Mixture 1	5	5	5
Mixture 2	10	10	10
Mixture 3	20	20	20
Mixture 4	30	30	30
Mixture 5	5	10	20

The adsorption experiment of a mixture of adsorbates in GW is more complicated than the single compound adsorption. This is due to the interaction between the adsorbate that could be synergic, antagonistic or no interaction could happen, that is related to many factors such as the physicochemical properties of the adsorbates, and their concentrations, GW properties such as temperature and pH, and the physicochemical properties of the adsorbent. The complex physicochemical nature of some pollutants in GW challenges the adsorption processes treatment. In the current study, efforts are focused to improve the different phases of the adsorption process for removing pollutants.

In general, as shown in Figure 52, the adsorption of boron is increased with the increase of boron concentration in mixtures 1, 2, and 3, and then it is decreased in mixture 4 because all the active sites are occupied by the adsorbates. The highest percent of boron removal is 68% using AC as an adsorbent in the mixture 3 using 20 mg/L of B, Li, and Mo concentrations due to lower competition for the active sites than the highest concentrations in the mixture 4. The use of MDPs and bentonites gave a percent of boron removal of 67%, which is close to AC percent of boron removal for the same mixture, followed by 66% percent of boron removal using RDPs. However, the percent of boron removal is reduced in mixture 4 using 20 mg/L

boron, 10 mg/L Li, and 5 mg/L Mo concentrations because Li and boron ions compete with boron ions on the adsorption sites.

Figures 53 and 54 shows that the adsorption of Li and Mo in mixture 1 using the lowest concentrations is higher than the adsorption of boron. The percent of Li removal is the highest in mixture 3, while the highest percent of Mo removal was at the lowest mixture concentration. The adsorption of Li is increased with the increase of the mixture concentration because Li-ions compete with Mo and B ions on the active sites that allow more Li ions to adsorb. The highest percent of Li removal was 59% using bentonite in mixture 3 using 20 mg/L of B, Li, and Mo concentrations due to lower competition for the active sites than the mixture 4 with the highest concentrations, followed by percent of Li removal 57% by the use of AC, and 56% by the use of date pits and MDPs. MDPs showed the highest percent of Mo removal in the mixtures 1, 2 and 3, and the highest percent of Mo removal was 48% at mixture 1 with the lowest concentrations. While in mixture 4 bentonite showed the highest Mo adsorption that the percent of Mo removal reached 38.4 % followed by 28% using MDPs.

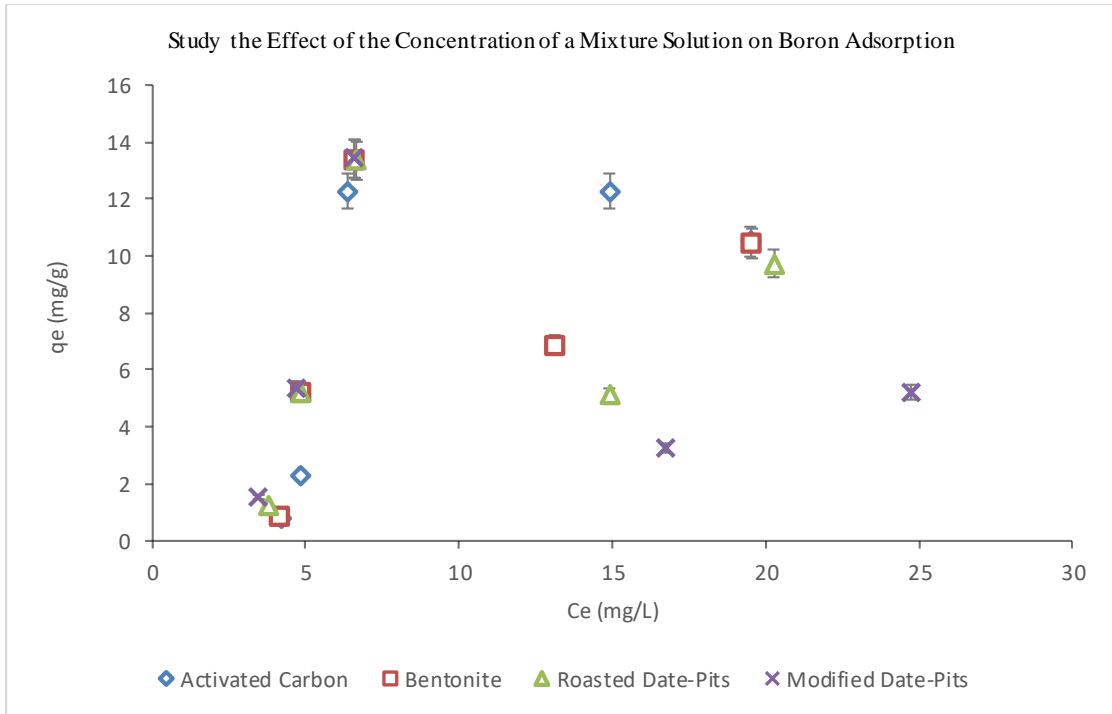


Figure 52. The effect of the concentration of a mixture solution in boron adsorption.

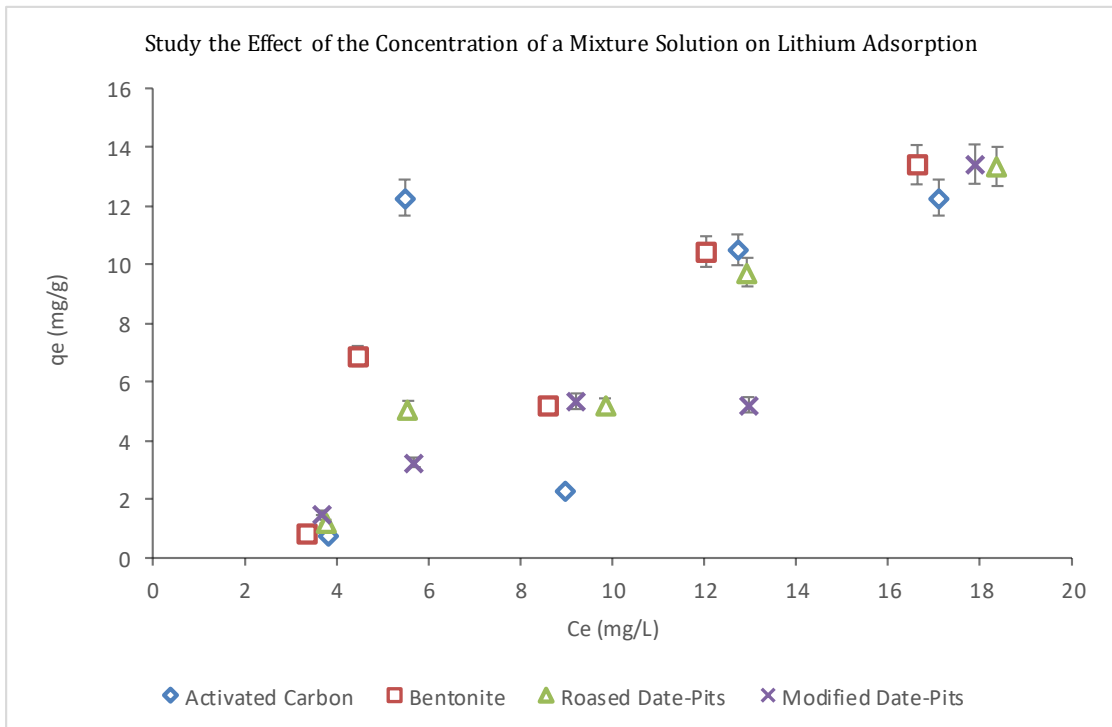


Figure 53. The effect of the concentration of a mixture solution in lithium adsorption.

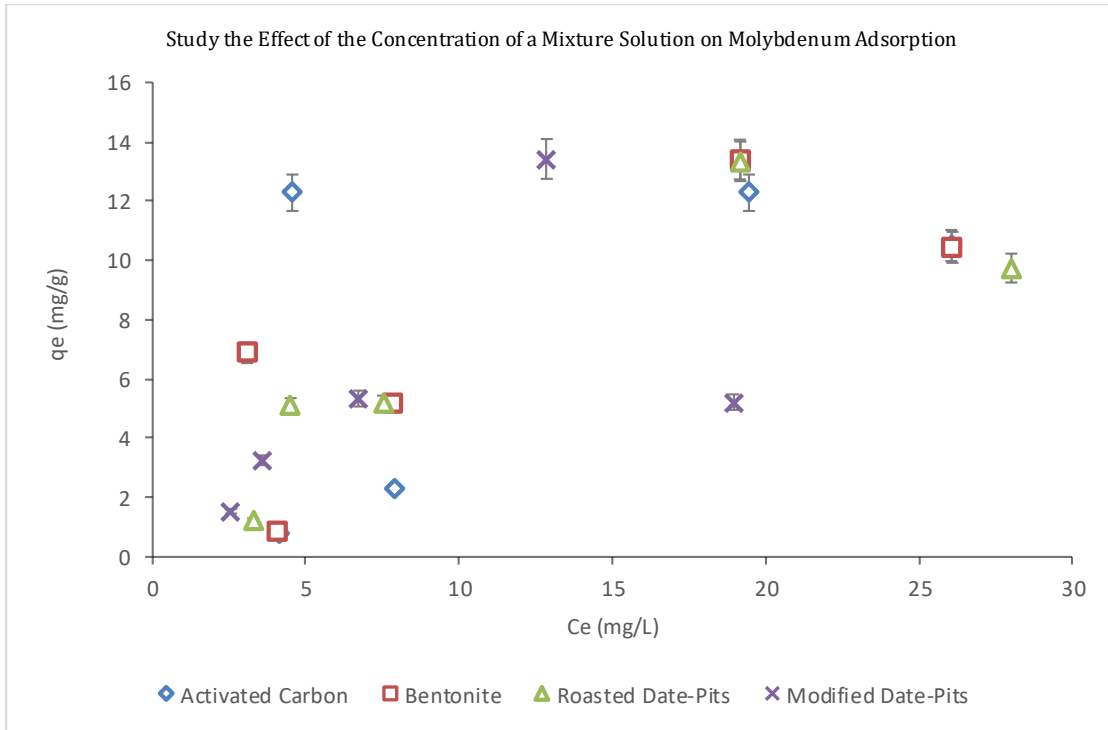


Figure 54. The effect of the concentration of a mixture solution in molybdenum adsorption.

#### Real GW Adsorption Experiments

Three real GW samples are used to study the adsorption of B, Li, and Mo using the four adsorbents, namely AC, bentonite, RDPs, and MDPs. The effect of temperature was also studied at 25 °C as shown in Figures 55, 56, and 57, and at 35°C as shown in Figures 58, 59, and 60. The concentrations of B, Li, and Mo on the three studied GW samples are shown in Table 25. The adsorption of boron decreased with the increase in boron concentration in GW samples due to the compete with Li and Mo ions on the active sites. The highest percent of boron removal is in GW sample 3 due to the availability of active sites for boron adsorption. The maximum percent of boron removal at 25 °C is 44% using RDPs followed by bentonite, AC, and MDPs with 42%, 40%, and 39% respectively. The adsorption of boron decreases at 35°C in the samples that have low boron concentration, while it increases at 35°C for high

concentration samples due to increasing boron ions mobility that bombarded with some adsorbed ions and hence restructure the adsorption ions. The maximum percent of boron removal at 35 °C is 40% using MDPs followed by RDPs, AC, and bentonite with 38%, 37%, and 36% respectively.

The adsorption of Li was decreased with the increase in the Li concentration due to competition with the high boron concentrations on the active sites. The percent of Li removal is the same for all adsorbents, and it reached the percent of Li removal of only 9% in GW sample 3. The adsorption of Li increased with the temperature at 35 °C due to the mobility of adsorbate, which rearranges the adsorption process and allows more Li to adsorb. All adsorbents, namely MDPs, RDPs, AC, and bentonite showed the same maximum percent of Li removal that reached 19% in GW sample 3. Similar behavior is also noticed with Mo adsorption.

In general, MDPs showed the highest adsorption of Mo in all GW samples. The adsorption of Mo increased with the increase in Mo concentrations, and the maximum Mo removal at 25 °C is 80% in sample 1 followed by 78% in sample 3 by using MDPs followed by RDPs, bentonite, and AC, with 75%, 71%, and 68% percent of Mo removal respectively. The adsorption of Mo increases with the increase in the temperature, the maximum percent of Mo removal at 35 °C reached 92% in sample 3 and 80% in sample 2 using MDPs followed by AC with 75% percent of Mo removal in sample 3, then 73% percent of Mo removal in sample 1 that has the lowest Mo concentration using MDPs and RDPs, and 71% percent of Mo removal using bentonite in sample 3.



Table 25. The Concentration of lithium, molybdenum and boron on the three studied GW samples.

	Initial Concentration $C_o$ ( $\mu\text{g/L}$ )		
	Molybdenum	Lithium	Boron
GW Sample 1	75	209	4523
GW Sample 2	77	465	4101
GW Sample 3	142	99	1502

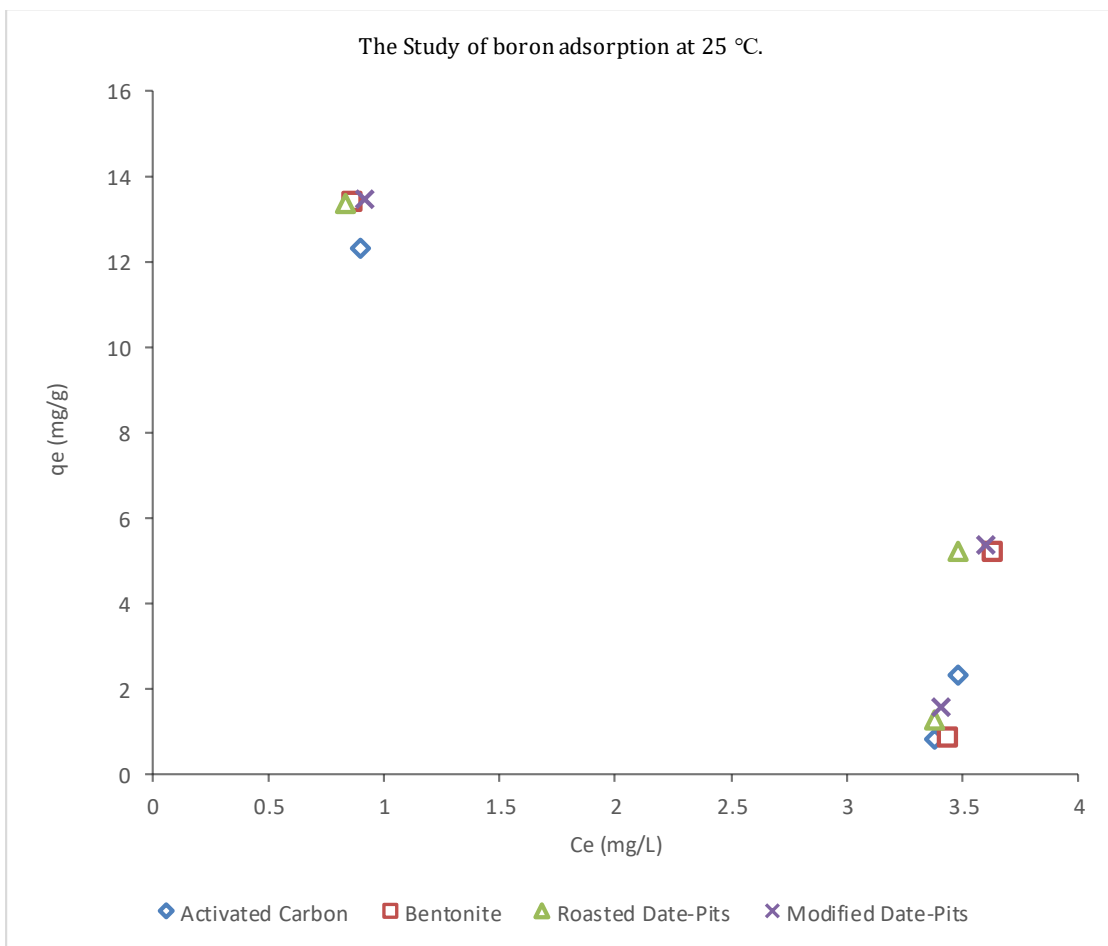


Figure 55. The Study of boron adsorption from GW Samples at 25 °C.

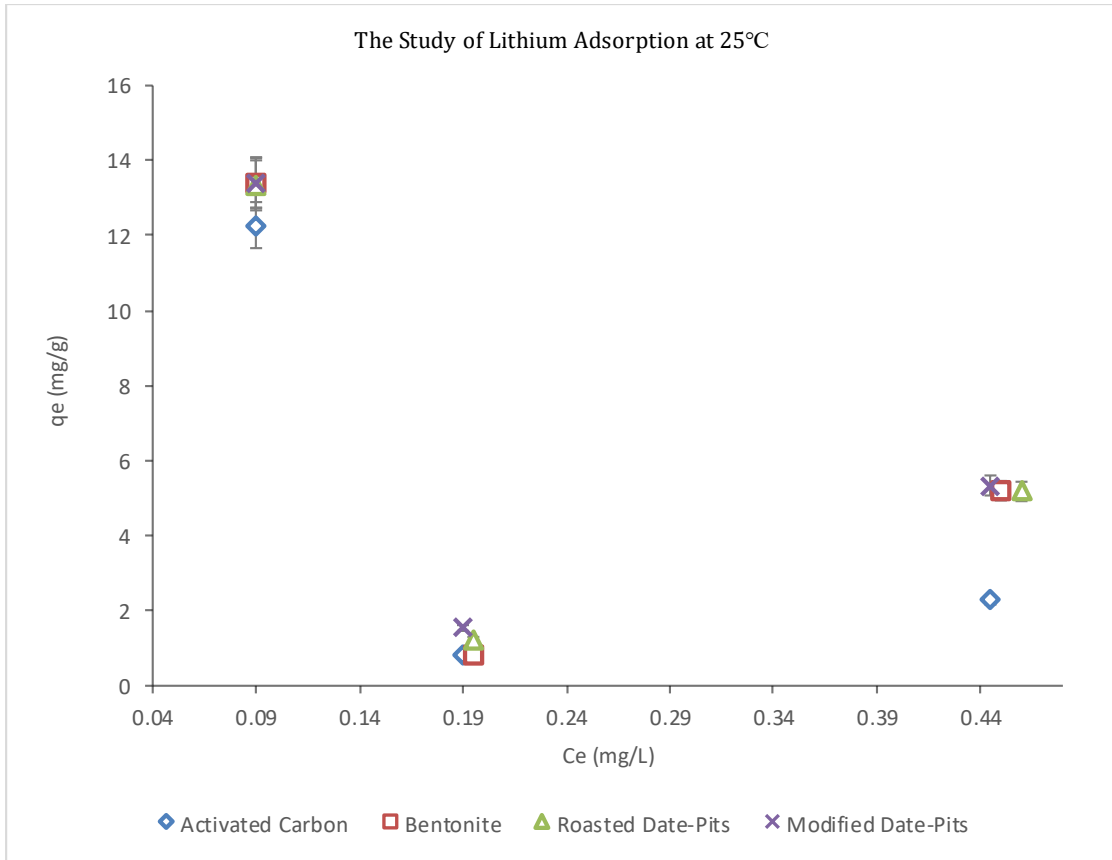


Figure 56. The Study of Lithium adsorption from Real GW Samples at 25 °C.

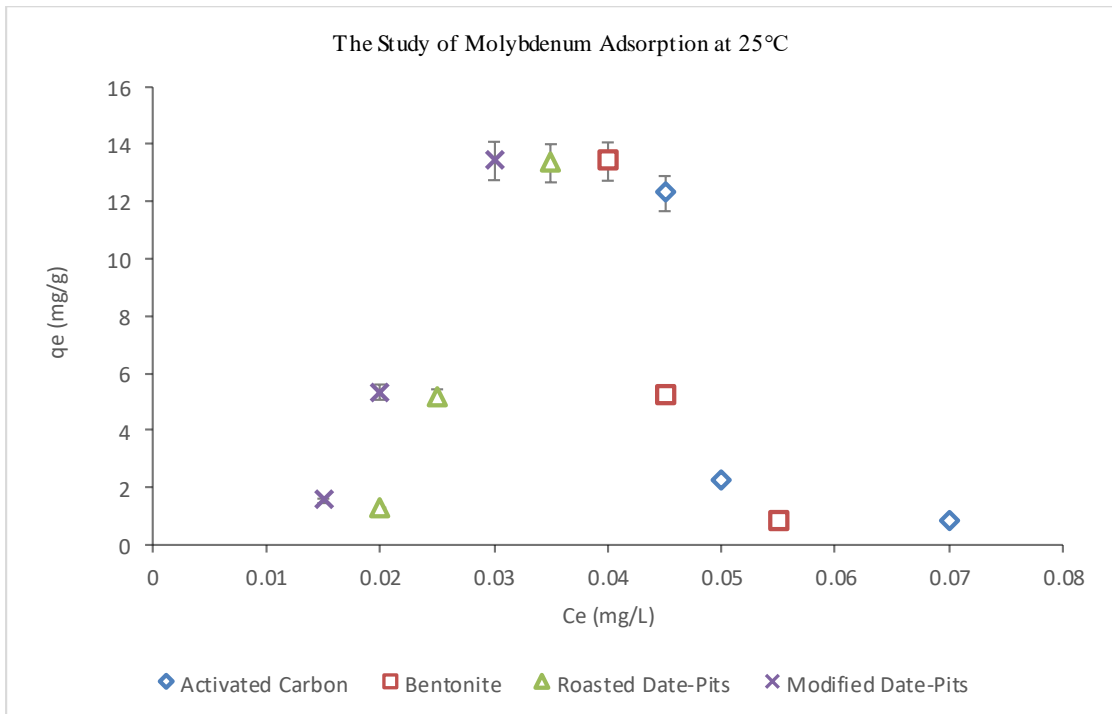
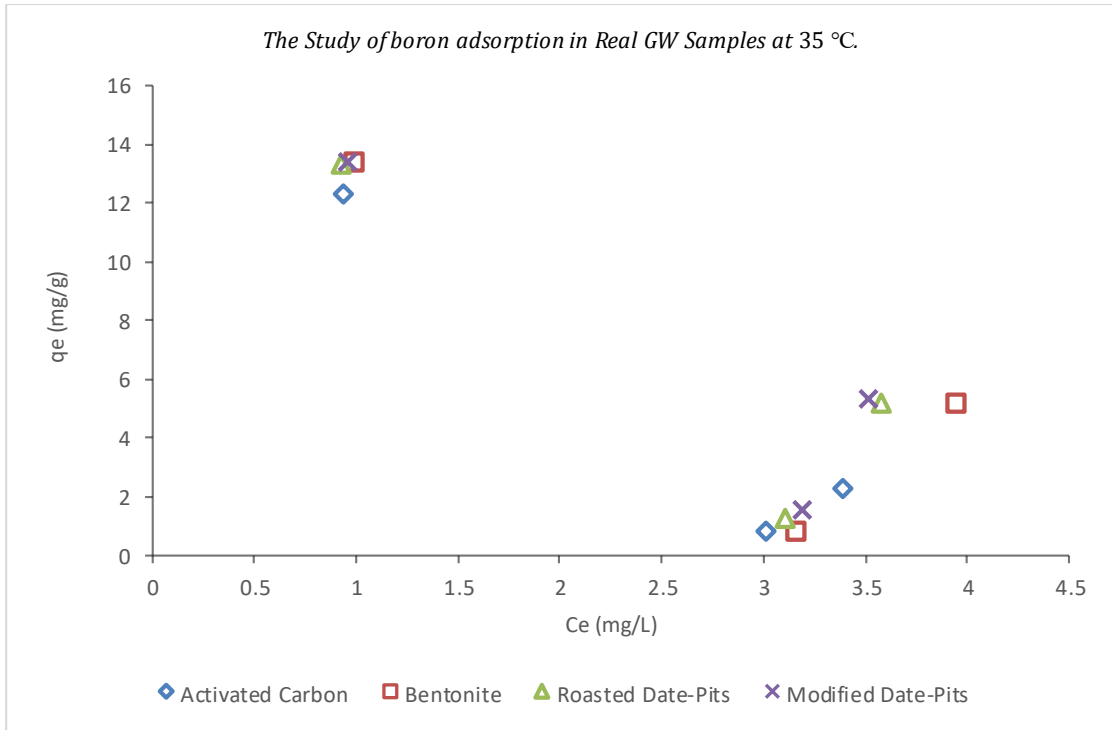
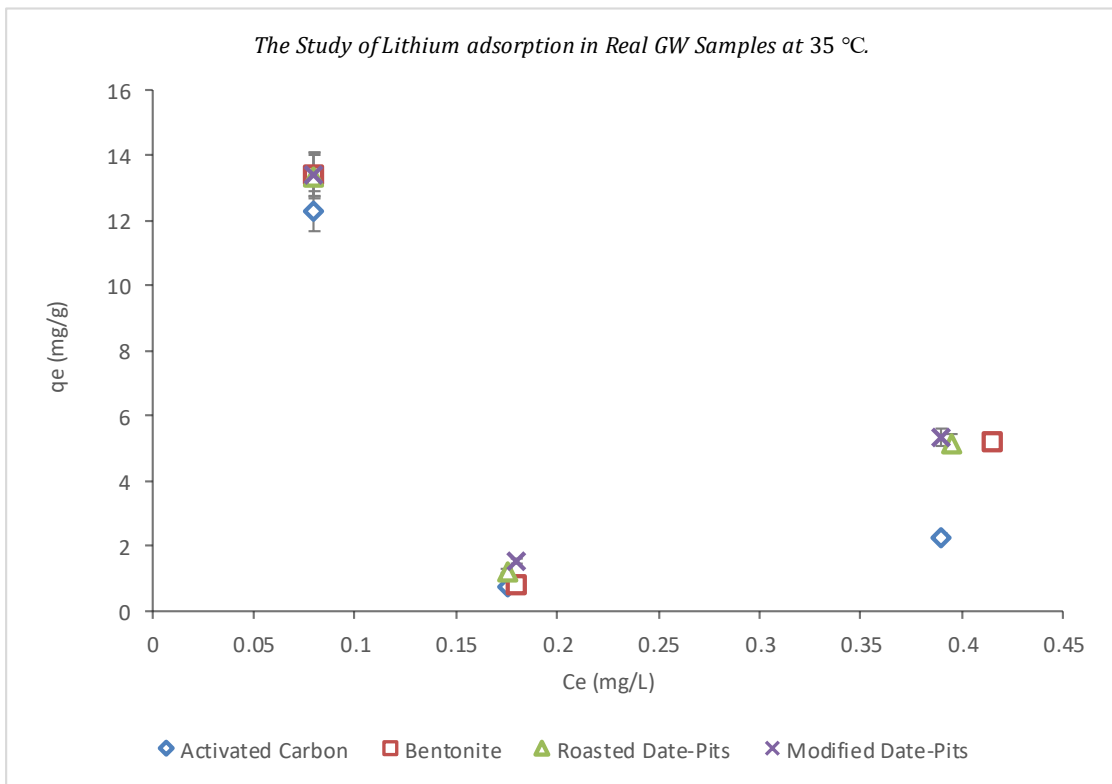


Figure 57. The Study of Molybdenum adsorption from GW Samples at 25 °C.



*Figure 58. The Study of boron adsorption from GW samples at 35 °C.*



*Figure 59. The Study of lithium adsorption from GW samples at 35 °C.*

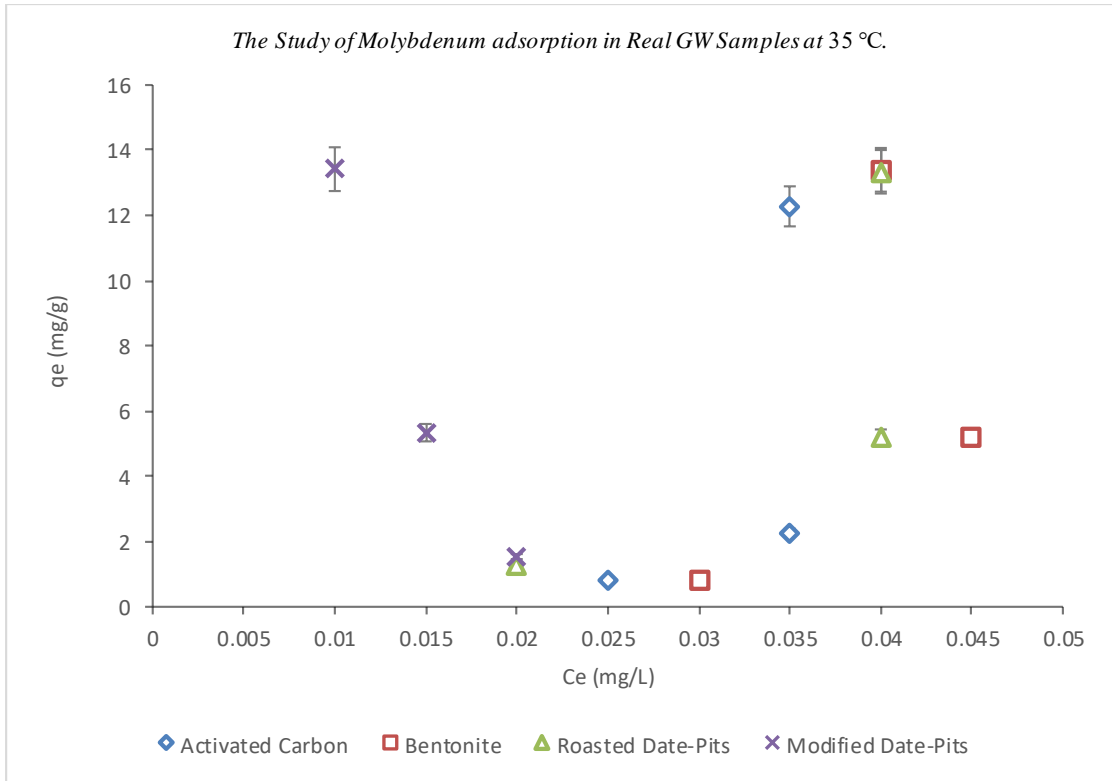


Figure 60. The Study of molybdenum adsorption from GW samples at 35 °C.

### Statistical Analysis for Adsorption Experiments

The results of statistical analysis for the adsorption experiment are shown in Appendix G. The experimental design of the experiments was factorial and completely randomized design (CRD). Thus, ANOVA single factor is used to study the effect of pH on the adsorption capacity of Li, B, and Mo ions since the temperature and initial concentration were constant through the experiment. While ANOVA two-factor with replication is used to test the relationship between initial boron concentration and temperature.

The ANOVA single factor test was conducted to test the effect of pH on Li, B, and Mo adsorption using AC, bentonite, RDPs, and MDPs. There is not a significant difference between the adsorbate concentrations and pH value as the  $F < F_{\text{Critical}}$ , and

p- value  $\geq 0.05$ , and the null hypothesis of equal means is not rejected.

The two-factor ANOVA with replication test was conducted to test the relation between temperature and concentration using AC, bentonite, RDPs and MDPs. The two-way ANOVA test showed a high significant difference between Mo concentration and temperature as the  $F > F_{\text{Critical}}$ , and p- value  $\leq 0.05$ , thus the null hypothesis of equal means is rejected. However, there is not significant difference between (column) the adsorbents namely AC, bentonite, RDPs, and MDPs concentration. Boron concentration is not significantly different between different temperatures because p-value  $\geq 0.05$ . The two-way ANOVA test showed a highly significant difference between Li concentration and temperature as the  $F > F_{\text{Critical}}$ , and p-value  $\leq 0.05$ , thus the null hypothesis of equal means is rejected. In addition, there is a highly significant difference between (column) the adsorbents namely AC, bentonite, RDPs and MDPs as the  $F > F_{\text{Critical}}$ , and p-value  $\leq 0.05$ .

The ANOVA single factor test was performed for the effect of a mixture concentration on Li, B and Mo adsorption using AC, bentonite, RDPs and MDPs. The results were not significantly different between the adsorbate concentrations with the changing in the mixture concentrations as the  $F < F_{\text{Critical}}$ , and p-value  $\geq 0.05$ , thus the null hypothesis of equal means is not rejected.

The two-way ANOVA test showed a highly significant difference between Mo concentration and temperature in the adsorption experiment using GW samples as the  $F > F_{\text{Critical}}$ , and p-value  $\leq 0.05$ , thus the null hypothesis of equal means is rejected. In addition, there is a highly significant difference between (column) the adsorbents namely AC, bentonite, RDPs and MDPs as the  $F > F_{\text{Critical}}$ , and p-value  $\leq 0.05$ .

## Comparative Adsorption Study

Tables 26, 27, and 28 show the comparison of Li, Mo, and B adsorption respectively in different solutions such as single adsorbate solution, the mixture of the adsorbate's solution, and real GW solution at 25 °C. The adsorption of Li from mixture solution that contains is highest for MDPs (26% percent of removal), while the adsorption decreases in real GW solutions than the adsorption from Li and mixture solutions because Li concentration in real GW is very low. Besides, Li ions could not compete with the other ions present in the solution to the active sites. Thus, the ionic strength of the solution affects the adsorbent-adsorbate electrostatic interactions (Wong et al., 2003).

The adsorption capacity of Mo from the solution that contains 5 ppm Mo is highest by using MDPs (80% percent of removal). The adsorption of Mo increases significantly in real GW solutions than the adsorption in Mo solution and mixture solution because Mo concentration in GW is very low and Mo ions have a higher capacity to adsorb onto the active sites than other ions. This indicates that the adsorption of Mo onto MDPs surface has various adsorption mechanisms such as electrostatic interaction, ion change and complex formation onto the active sites, besides possible intra-diffusion into pores.

Furthermore, the adsorption capacity of boron is highest in real GW solution (37% percent of removal). The adsorption of B increases in real GW solutions than the adsorption in B solution and mixture solution that indicates possible facilitating of the adsorption mechanisms onto the active sites and intra-diffusion that enhance the adsorption capacity.

Table 26. Comparative Study for Lithium Adsorption at 25 °C

Adsorbent	Removal Efficiency %		
	Li Solution (5 ppm Li)	Mixture Solution (5 ppm Li)	Real GW (0.465 ppm Li)
AC	19	23	9
Bentonite	19	33	7
RDPs	10	24	7
MDPs	14	26	9

Table 27. Comparative Study for Molybdenum Adsorption at 25 °C

Adsorbent	Removal Efficiency %		
	Mo Solution (5 ppm)	Mixture Solution (5 ppm)	Real GW (0.143 ppm)
AC	49	17	68
Bentonite	8	19	27
RDPs	32	34	73
MDPs	37	49	80

Table 28. Comparative Study for Boron Adsorption at 25 °C

Adsorbent	Removal Efficiency %		
	B solution (5 ppm B)	Mixture Solution (5 ppm B)	Real GW (4.5 ppm B)
AC	17	16	25
Bentonite	27	17	24
RDPs	18	25	25
MDPs	28	31	37

Mo and B do not form simple ions in aqueous solution; while Li form  $\text{Li}^+$  cations. In a slightly alkaline aqueous solution, the dominant Mo species are molybdate anions  $\text{MoO}_4^{2-}$  as +6 is the most stable oxidation state for Mo. While the dominant species of boron are borate anions  $\text{B(OH)}_4^-$  as shown by the equilibrium reaction equation 28.

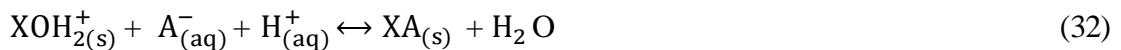


Date pits consist of about 17.5 % hemicellulose, 11.0 % lignin, and 42.5 % cellulose (Al-Ghouti et al, 2010). Lignin is considered as the cementing matrix that holds cellulose and hemicellulose units together; while cellulose and hemicellulose contain oxygenated functional groups such as hydroxyl, ether, and carbonyl (Hawari et al., 2014). This is supported by the FTIR results that showed the availability of the different oxygenated functional groups such as hydroxyl, carboxyl, and thiol groups that indicate the possibility of chemical adsorption mechanisms besides the physical adsorption. Physical adsorption is supported by the physical analysis results using SEM and BET that showed the high surface area and the pores volume of AC and MDPs adsorbents that enhanced the adsorption capacity. While the availability of the negative active functional groups indicates chemical adsorption mechanisms such as hydrogen bond, electrostatic interaction, and/or complexation. Thus, the proposed adsorption mechanisms onto MDPs active sites are dispersion forces known as van der Waal's forces, electrostatic interaction, hydrogen bond and/or complexation. This is supported by the thermodynamic results that the adsorption of Li on AC and MDP at 35 °C and 45 °C, beside the adsorption of boron on AC at 25°C, 35 °C and 45 °C showed negative values for free energy  $\Delta G^\circ$  that is increased for higher temperature, while the magnitude of  $\Delta H^\circ$  from 150 to 180 that indicates electrostatic interaction and chemical adsorption.

In an alkaline solution, the surface functional groups such as carboxylic and phenolic acids are deprotonated, and the surface charge becomes negatively charged. Thus,  $\text{Li}^+$  cations electrostatically interact with the negative functional groups. Also,  $\text{Li}^+$  could interact with borate ions because Li is alkali earth metal that form metallic complexes such as  $[\text{LiB}(\text{OH})_4]^+$ , and  $[\text{Li}_2\text{MoO}_4]^{2+}$ . Al-Ghouti & Salih (2018) showed that magnesium ion reacted with borate ion to form the complex  $[\text{Mg B}(\text{OH})_4]^+$  at a basic



solution. On the other hand,  $\text{MoO}_4^{2-}$  and  $\text{B(OH)}_4^-$  anions are repelled with negatively charged functional groups. Shan et al. (2012) showed that  $\text{MoO}_4^{2-}$  adsorbed by ion exchange with hydroxyl ions or neutral water molecules available in the solution around adsorbent that is made from orange peels. Thus, the proposed mechanisms for  $\text{MoO}_4^{2-}$  and  $\text{B(OH)}_4^-$  adsorption is that cellulose and/or lignin captures free proton during complexing of borate and molybdate by functional groups such as hydroxyl which then interact with borate ion through a covalent attachment and form a coordination complex as shown in Figure 61 and 62. A similar mechanism is shown by Wolska & Bryjak (2013) that described the formation of mono-, di, and tri coordination of boron complexation by tertiary amine groups. The possible surface complexation (mono-, di-, and tri-coordination) onto MDPs between surface hydroxyls (XOH) and adsorbate ions (A) such as  $\text{Li}^+$  cations ( $\text{A}^+$ ), and  $\text{MoO}_4^{2-}$  and  $\text{B(OH)}_4^-$  anions ( $\text{A}^-$ ) are described in reaction equations 29, 30, 31 and 32.



Furthermore, the intra-diffusion within the pores is also proposed as SEM and BET results showed the high surface area and the pores volume for the adsorbents that enhanced the removal efficiency. In addition, as stated earlier in Table 8 that Mo and B have almost the same Pauling electronegativity, which is higher than Li electronegativity thus, they adsorb on the surface more readily. After that they could migrate into the pores, however, the high electronegativity may hinder them from migrating into the pores and keeping them adsorb onto the surface. While the lower ionic radius and hydration radius for Li than for Mo and B indicated that Li has the

ability for external and internal adsorption because Li could migrate into the pores easier than Mo and B. Another parameter that affects the adsorption is that Li is a strongly hydrated ion while  $\text{B(OH)}_4^-$  is neither that of a strongly hydrated ion nor that of hydrophobic ions (Corti & Crovetto, 1980). It is also indicated from the fluctuation trend of increasing and decreasing adsorption capacity indicates that intra-particle diffusion governed the adsorption process more than the external diffusion.

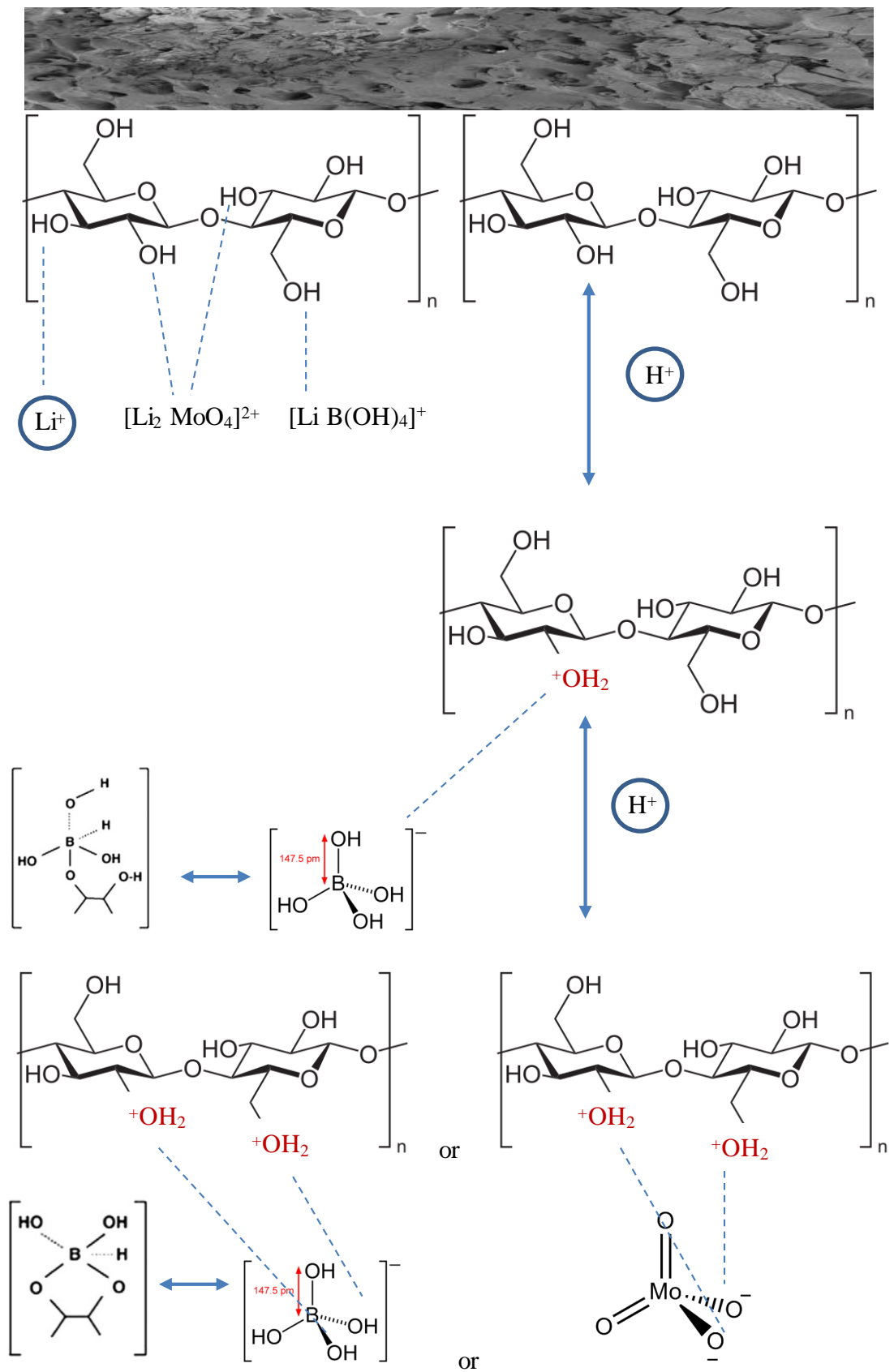


Figure 61. Schematic diagram of adsorption onto cellulose structure.

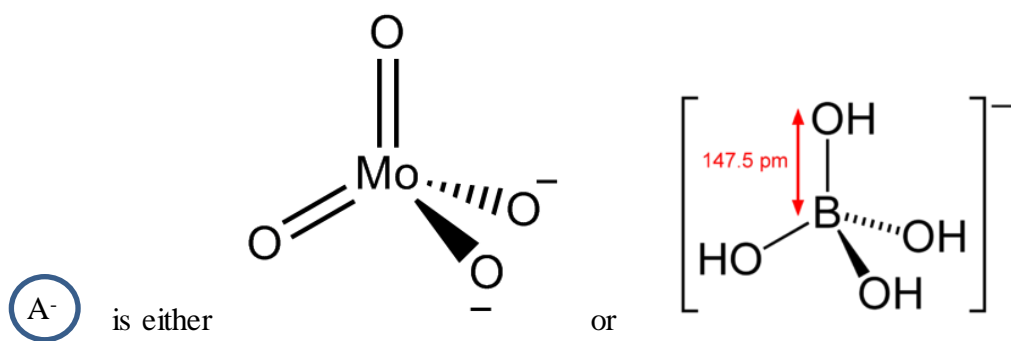
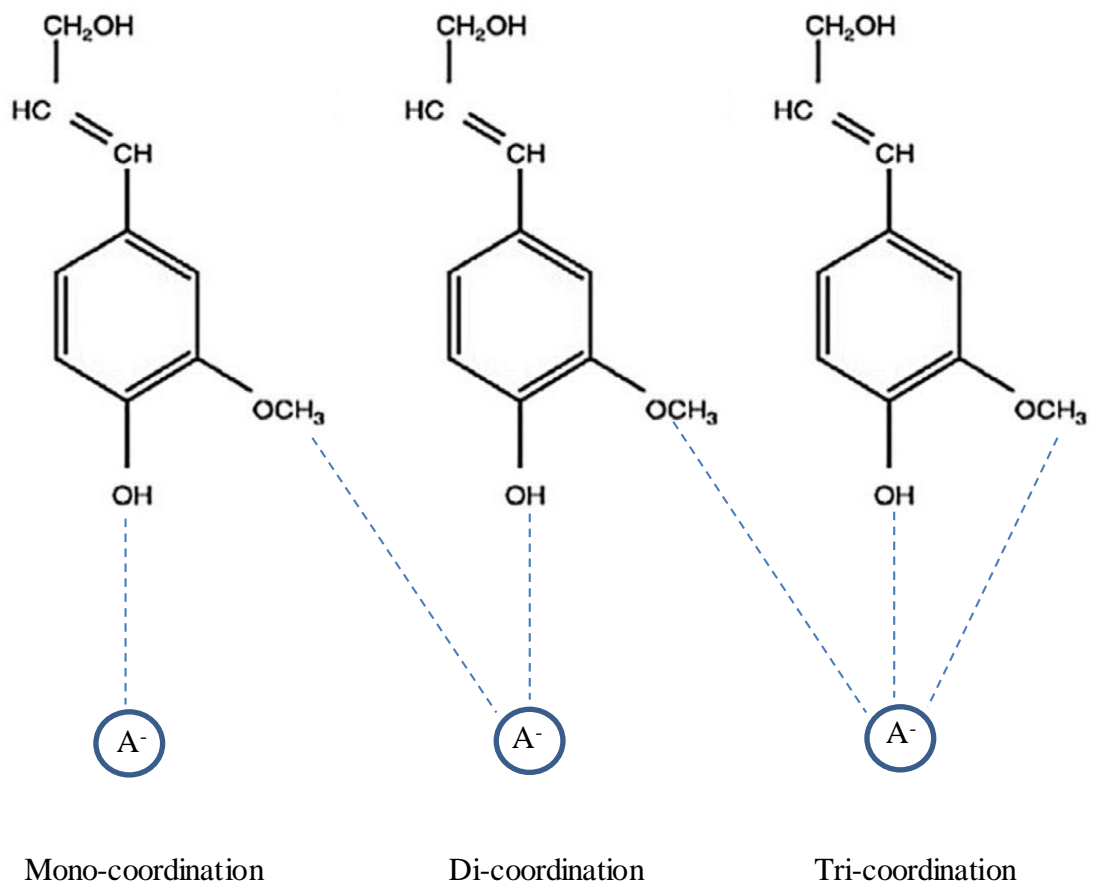
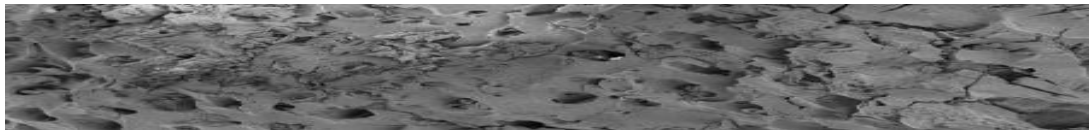


Figure 62. Schematic diagram of adsorption onto Phenylpropanoid units found in lignin.

## CHAPTER 5: CONCLUSION

The GW in Qatar is mainly used for agricultural use. The significant increases in the population and agricultural activities have driven the high extraction of the GW that negatively impacts its quantity and quality. Salinity is the most GW quality concern. The high salinity of the analyzed samples may be the result of climate conditions of high temperature and low rainfall, high evaporation, increasing agricultural activities, and the intrusion of brackish water from deep aquifers or with seawater intrusion. Most exceedances of the drinking water standards pertained to aesthetic qualities rather than health-based concerns. The results showed that  $\text{Na}^+ > \text{Ca}^{2+} > \text{Mg}^{2+} > \text{K}^+$  was the sequence of major cations and  $\text{Cl}^- > \text{SO}_4^{2-} > \text{HCO}_3^- > \text{NO}_3^-$  is the order of the main anions. The hydrogeochemical facies and Piper plots further confirmed that most of the analyzed GW samples were falling in the field of  $\text{SO}_4\text{-Cl}$  and  $\text{Ca-Mg}$  (permanent hardness); calcium chloride type and  $\text{SO}_4\text{-Cl}$  and  $\text{Na-K}$  (saline); sodium-chloride-type of water type indicating the permanent (non-carbonate) hardness in the majority of the analyzed samples. This result suggests halite dissolution, ion exchange, and seawater mixing. The GW hydrochemistry results revealed high levels of nitrate might be due to the agricultural activities and leakage of un-rehabilitated sewage systems. Based on the geochemical PHREEQC modeling results, the chemical equilibrium and saturation indices showed oversaturation of calcite, dolomite, while anhydrite, gypsum, and halite show under-saturation. Principal component analysis reveals three main components that explain > 99% of the total variance. The result showed the dissolution of evaporite minerals halite and gypsum, localized sedimentary depositional or hydrogeochemical environment, irrigation return flows, and nitrate fertilizers. The results showed that most of the analyzed anions and cations quality parameters in the GW are higher than the regional and

international guidelines for drinking water. The irrigation hazard analysis indicates that 60.9 % of the GW samples, with specific electrical conductivity greater than 5,000  $\mu\text{S}/\text{cm}$ , would likely cause harm to agriculture, and only salt-tolerant crops are suitable. The 34% of the irrigation water was C4S2 and C4S3 of very high salinity hazard and medium sodium hazard, and very high salinity hazard and high sodium hazard respectively, indicating that the irrigation hazard is always higher from salinity than from SAR, thus it is not suitable for irrigation in almost all soils, except soils with high permeability.

A clear understanding of the spatial distribution of GW quality parameters is the key issue for agricultural and environmental management. In the current analysis, unsampled points are interpolated by three interpolation methods using Arc-GIS along with the mapping of spatial variability. SK predicts values at unsampled points and assesses the uncertainty associated with the predicted value. However, IDW and RBFS do not make explicit predictions about the statistical properties of the input data. Most of the analyzed GW samples in Qatar are characterized by high salinity due to the climate conditions including low rainfall and high temperature. Besides, overexploitation of the GW caused saltwater intrusion from seawater or the deep brackish GW. The northern parts of the study area have the lowest salinity, while the highly saline locations are within the coastal areas due to seawater intrusion and within some south inland farms due to the mixing with deep brackish water. GW with high nitrate is found in some farms that might intensively use nitrogen fertilizers intensively. Thus, the interpolated maps show two types of distributions of analytes as distributions consistent with salinity, and clustered distributions independent of salinity that could be related to localizing hydro-stratigraphic, geochemical conditions, anthropogenic causes, such as fertilizer impacts.

This study confirmed that using MDPs to remediate B, Li, and Mo from GW is an effective adsorption method. Date pits are agricultural waste; thus, it has environmental and economic benefits to use it as adsorbents. Different parameters were studied to optimize the efficiency of the adsorbent process such as pH, initial adsorbates concentration, and temperature. It was found that pH 6 plays a significant role in the process of adsorption because it affects the interaction of the adsorbate's ions and the surface of the adsorbent. In addition to this, the adsorption process MDPs was favorable indicating a spontaneous and an endothermic process. FTIR analysis confirmed the presence of different oxygenated functional groups that are responsible for adsorbates adsorption onto MDPs. Hence, this study proved that MDPs are valuable for remediating B, Li and Mo from GW. The negative values for free energy indicate a spontaneous and favorable adsorption process that is more favorable and spontaneous of the adsorption at high temperatures. The positive entropy values that controlled the adsorption process suggest the possibility of some structural changes or readjustments in the adsorbate–adsorbent complex. A better understanding of the adsorption of MDPs can be achieved by further modification or chemical activation in future studies. Besides further studies to investigate the effect of kinetic reaction time on the adsorption process, besides the study of the desorption process.

This study assists managers and decision-makers to manage the GW and improve water quality used for irrigation. The obtained results illustrated that 95% of the GW was just suitable for irrigation certain tolerable crops in high permeability soil. Therefore, the following recommendations should be implemented according to the results of this study. Salinity reduction could be achieved by mixing saline water with low salinity water. The mixing process was already conducted by the national water supplier as they mix GW with treated wastewaters. The development of a low-cost

treatment technique that can efficiently and simultaneously remove undesirable elements in the GW is highly recommended. This will help to enhance water security at the national level to yield a GW with superior quality and quantity. Additionally, the GW managers should supervise and optimize the quantity of irrigation water to prevent further deterioration of the GW quality. The current irrigation practices use flood irrigation, which enhances evaporation and thus increases the salt level in soil that could be leached to the GW. Thus, the farmer's awareness of the importance of GW conservation should be increased. Farmers should be encouraged to use alternative agricultural practices such as using modern irrigation techniques like drip and sprinkler irrigation, use salt-tolerant and low water demand crops, and reduce the application of chemical fertilizers and pesticides.

To achieve sustainable use and management of the GW in Qatar, supply and demand management practices should be adopted. The major GW consumption is for agricultural activities. Therefore, a management plan should focus on these activities. For demand management, educating the agricultural sector of the consequences of GW mining, encouraging the use of alternative sources of water, and the use of efficient irrigation techniques to lower GW extraction is highly recommended. For example, farmers should be encouraged to use desalinated seawater and treated sewage effluent (TSE) for irrigation rather than abstraction GW. In addition, farmers are encouraged to adopt developed irrigation and agronomic practices such as using water-efficient irrigation methods (sprinkler and drip irrigation systems) and replacing water-intensive crops with water-efficient crops, in addition to developing reliable and cost-efficient treatment techniques for low GW quality. The supply management should include developed monitoring systems, managed storage, recovery projects, and artificial recharge by recharge wells and lagoons using treated wastewater and



desalinated seawater. Recently, the full GW characterizations and measurement by using advanced technology in data analysis, remote sensing, and modeling generate significant data and knowledge to decision-makers with lower uncertainty. To protect the GW quality, the monitoring strategy should also include vulnerability maps using geostatistical analysis and interpolation models. In addition, the classification of aquifer systems should be developed. GIS-linked monitoring systems could be used for easier and faster determination of the GW quality. It can be inferred from the analysis that GW in Qatar requires treatment before being used for irrigation. Regulations and GIS-based monitoring systems should be implemented to control GW exploitation and to monitor water quality improvement for better future planning.

## REFERENCES

- Abdel-Gawad, E. A., Al Azab, M., & Lotfy, M. M. (2007). Assessment of organic pollutants in coastal sediments, UAE. *Environmental Geology*, 54(5), 1091-1102. doi:10.1007/s00254-007-0880-x
- Abdel-Rahman, M.A.E., Arafat, S.M (2020). An Approach of Agricultural Courses for Soil Conservation Based on Crop Soil Suitability Using Geomatics. *Earth Syst Environ* 4, 273–285. <https://doi.org/10.1007/s41748-020-00145-x>
- Abdel-Salam, O. E., Reiad, N. A., & ElShafei, M. M. (2011). A study of the removal characteristics of heavy metals from wastewater by low-cost adsorbents. *Journal of Advanced Research*, 2(4), 297-303. doi:10.1016/j.jare.2011.01.008
- Abdel-Satar, A. M., Al-Khabbas, M. H., Alahmad, W. R., Yousef, W. M., Alsomadi, R. H., & Iqbal, T. (2017). Quality assessment of groundwater and agricultural soil in Hail region, Saudi Arabia. *The Egyptian Journal of Aquatic Research*, 43(1), 55-64. doi:10.1016/j.ejar.2016.12.004
- Acosta, J., Jansen, B., Kalbitz, K., Faz, A., & Martínez-Martínez, S. (2011). Salinity increases mobility of heavy metals in soils. *Chemosphere*, 85(8), 1318–1324. doi: 10.1016/j.chemosphere.2011.07.046
- Adimalla, N., & Venkatayogi, S. (2018). Geochemical characterization and evaluation of groundwater suitability for domestic and agricultural utility in semi-arid region of Basara, Telangana State, South India. *Applied Water Science*, 8(1). doi: 10.1007/s13201-018-0682-1
- Ahmad, T., Danish, M., Rafatullah, M., Ghazali, A., Sulaiman, O., Hashim, R., & Ibrahim, M. N. (2011). The use of date palm as a potential adsorbent for wastewater treatment: A review. *Environmental Science and Pollution Research*,

- 19(5), 1464-1484. doi:10.1007/s11356-011-0709-8
- Akpomie, K. G., & Dawodu, F. A. (2015). Potential of a low-cost bentonite for heavy metal abstraction from binary component system. *Beni-Suef University Journal of Basic and Applied Sciences*, 4(1), 1-13. doi:10.1016/j.bjbas.2015.02.002
- Al-Ameri, A. A., Al-Qurainy, F., Gaafar, A. Z., Khan, S., & Nadeem, M. (2016). Molecular identification of sex in phoenix dactylifera using inter simple sequence repeat markers. *BioMed Research International*, 2016, 1-5. doi:10.1155/2016/4530846
- Al-Farraj, A. S., Al-Wabel, M. I., El-Saeid, M. H., El-Naggar, A. H., & Ahmed, Z. (2013). Evaluation of Groundwater for Arsenic Contamination Using Hydrogeochemical Properties and Multivariate Statistical Methods in Saudi Arabia. *Journal of Chemistry*, 2013, 1–9. doi: 10.1155/2013/812365
- Al-Ghouti, M., Al Disi, Z., Alkaabi, N., Khraisheh, M. (2017). Mechanistic Insights into The Remediation of Bromide Ions from Desalinated Water Using Roasted Date Pits. *Chemical Engineering Journal*, doi: 10.1016/j.cej.2016.09.091
- Al-Ghouti, M. A., & Da'ana, D. A. (2020). Guidelines for the use and interpretation of adsorption isotherm models: A review. *Journal of Hazardous Materials*, 393, 122383. doi:10.1016/j.jhazmat.2020.122383
- Al-Ghouti, M. A., Da'ana, D., Abu-Dieyeh, M., & Khraisheh, M. (2019). Adsorptive removal of mercury from water by adsorbents derived from date pits. *Scientific Reports*, 9(1). doi:10.1038/s41598-019-51594-y
- Al-Ghouti, M. A., & Khan, M. (2018). Eggshell membrane as a novel bio sorbent for remediation of boron from desalinated water. *Journal of Environmental Management*, 207, 405–416. doi: 10.1016/j.jenvman.2017.11.062
- Al-Ghouti, M. A., Li, J., Salamh, Y., Al-Laqtah, N., Walker, G., & Ahmad, M. N.

- (2010). Adsorption mechanisms of removing heavy metals and dyes from aqueous solution using date pits solid adsorbent. *Journal of Hazardous Materials*, 176(1-3), 510-520. doi:10.1016/j.jhazmat.2009.11.059
- Al-Ghouti, M. A., & Salih, N. R. (2018). Application of eggshell wastes for boron remediation from water. *Journal of Molecular Liquids*, 256, 599-610. doi:10.1016/j.molliq.2018.02.074
- Alhamed Y.A. (2009). Adsorption kinetics and performance of packed bed adsorber for phenol removal using activated carbon from dates' stones, *J. Hazard. Mater.* 170 (2009) 763–770.
- AlHaddabi, M., Ahmed, M., AlJebri, Z., Vuthaluru, H., Znad, H., & AlKindi, M. (2015). Boron removal from seawater using date palm (*Phoenix dactylifera*) seed ash, *Desalination and Water Treatment*, DOI: 10.1080/19443994.2014.1000385
- Al-Ithari, A. J. A. Sathasivan, R. Ahmed, H. B. Vuthaluru, W. Zhan, M. Ahmed. (2011). Superiority of date pits ash as an adsorbent over other ashes and ferric chloride in removing boron from seawater. *Water Treat.* 32 (2011) 324–328.
- Al-Jilil, S. A. (2015). Characterization and application of bentonite clay for lead ion adsorption from wastewater: Equilibrium and kinetic study. *Research Journal of Environmental Sciences*, 9(1), 1-15. doi:10.3923/rjes.2015.1.15
- Al-Kalbani, M. S., & Price, M. F. (2015). Sustainable Aflaj water management in Al Jabal Al Akhdar, Sultanate of Oman. *Water Resources Management VIII*. doi: 10.2495/wrm150031
- Al-Kuisi, M., Al-Hwaiti, M., Mashal, K., & Abed, A. M. (2015). Spatial distribution patterns of molybdenum (Mo) concentrations in Potable groundwater in Northern Jordan. *Environmental Monitoring and Assessment*, 187(3). doi:10.1007/s10661-015-4264-5

- Al-Maadheed, S., Goktepe, I., Latiff, A. B., & Shomar, B. (2019). Antibiotics in hospital effluent and Domestic wastewater treatment plants in Doha, Qatar. *Journal of Water Process Engineering*, 28, 60-68. doi:10.1016/j.jwpe.2019.01.005
- Al-Mahmoud, M. E., Al-Dous, E. K., Al-Azwani, E. K., & Malek, J. A. (2011). DNA-based assays to distinguish date palm (*Arecaceae*) gender. *American Journal of Botany*, 99(1). doi:10.3732/ajb.1100425
- Al-Naimi, L. S., & Mgbejedo, T. I. (2018). Hydrogeochemical Evaluation of Groundwater in Parts of Shamal, Northern Qatar. *Environmental Management and Sustainable Development*, 7(2), 181. doi:10.5296/emsd.v7i2.13046
- Al-Qahtani, K. M. (2016). Water purification using different waste fruit cortexes for the removal of heavy metals. *Journal of Taibah University for Science*, 10(5), 700-708. doi:10.1016/j.jtusci.2015.09.001
- Al-Rashed, M., Akber, A. (2015). Water security in the Gulf Cooperation Council (GCC) countries: challenges and opportunities. *Int. Assoc. Hydrol. Sci.* 366, 119–120.
- Al-Rashed, M. F., & Sherif, M. M. (2000). *Water Resources Management*, 14(1), 59-75. doi:10.1023/a:1008127027743
- Al-Saad, H. (2005). Lithostratigraphy of the Middle Eocene Dammam Formation in Qatar, Arabian Gulf: effects of sea-level fluctuations along a tidal environment. *Journal of Asian Earth Sciences*, 25(5), 781–789. doi: 10.1016/j.jseaes.2004.07.009
- Alsharhan, A.S., Rizk, Z.A., Nairn, A.E.M., Bakhit, D.W. and Alhajari, S.A. (2001). *Hydrogeology of an arid region: the Arabian Gulf and adjoining areas*. Elsevier, 2001.
- Al-Shidi, F. K. (2014). Study the Quality of Groundwater of Al-Zoroup Area in

- Mahdah State, The Sultanate of Oman. United Arab Emirate University. Theses and Dissertations paper 12. [https://scholarworks.uaeu.ac.ae/all\\_theses/114](https://scholarworks.uaeu.ac.ae/all_theses/114)
- Alsuhami, A. O., Almohaimidi, K. M., & Momani, K. A. (2019). Preliminary assessment for physicochemical quality parameters of groundwater in Oqdus Area, Saudi Arabia. *Journal of the Saudi Society of Agricultural Sciences*, 18(1), 22–31. doi: 10.1016/j.jssas.2016.12.002
- Al-Taani, A. A., Batayneh, A. T., El-Radaideh, Al-Momani, I., Rawabdeh, A., (2012). Monitoring of Selenium Concentrations in Major Springs of Yarmouk Basin, North Jordan. *World Applied Sciences Journal* 18 (5): 704-714, 2012. DOI: 10.5829/idosi.wasj.2012.18.05.3181
- Al-Yousef, M., (2003). Mineralogy, geochemistry and origin of quaternary sabkhas in the Qatar peninsula, Arabian Gulf; 437 pages. PhD Thesis, University of Southampton.
- Amin, M., Alazba, A., & Shafiq, M. (2016). Adsorption of copper ( $\text{Cu}^{2+}$ ) from aqueous solution using date palm trunk fibre: Isotherms and kinetics. *Desalination and Water Treatment*, 57(47), 22454-22466. doi:10.1080/19443994.2015.1131635
- Andrade, B., Giansi, c., Toffoli, S., Valenzuela-Díaz, Francisco. (2018). Adsorption and Surface Area of Modified Bentonite Used as Bleaching Clay. 10.1007/978-3-319-72484-3\_36.
- Apted, M., & Ahn, J. (2017). Multiple-barrier geological repository design and operation strategies for safe disposal of radioactive materials. *Geological Repository Systems for Safe Disposal of Spent Nuclear Fuels and Radioactive Waste*,3-28. doi:10.1533/9781845695422.1.3
- Arslan, H., & Turan, N. A. (2015). Estimation of spatial distribution of heavy metals in groundwater using interpolation methods and multivariate statistical techniques;

- its suitability for drinking and irrigation purposes in the Middle Black Sea Region of Turkey. *Environmental Monitoring and Assessment*,187(8). doi:10.1007/s10661-015-4725-x.
- Ashfaq, M. Y., Al-Ghouti, M. A., Qiblawey, H., Zouari, N., Rodrigues, D. F., & Hu, Y. (2018). Use of DPSIR framework to analyze water resources in Qatar and overview of reverse osmosis as an environment friendly technology. *Environmental Progress & Sustainable Energy*, 38(4), 13081. doi:10.1002/ep.13081
- Ashghal & Schlumberger, (2013). *Shallow Groundwater Monitoring in Greater Doha, Wakrah And Al Khor (Cp761). Final Hydrogeological Report.*
- Assubaie, F. N. (2015). Assessment of the levels of some heavy metals in water In Alahsa OASIS farms, Saudi Arabia, with analysis by atomic absorption spectrophotometry. *Arabian Journal of Chemistry*, 8(2), 240-245. doi:10.1016/j.arabjc.2011.08.018
- Ayanda, S. (2017). Water treatment technologies: Principles, applications, successes and limitations of bioremediation, membrane bioreactor and the advanced oxidation processes. doi:10.4172/978-1-63278-058-4-059
- Baalousha, H. M., Barth, N., Ramasomanana, F. H., & Ahzi, S. (2018). Estimation of groundwater recharge in arid regions Using Gis: A case study from Qatar. *Qatar Foundation Annual Research Conference Proceedings Volume 2018 Issue 1.* doi:10.5339/qfarc.2018.epp298
- Baalousha, H. M. (2016). Groundwater vulnerability mapping of Qatar aquifers. *Journal of African Earth Sciences*,124, 75-93. doi:10.1016/j.jafrearsci.2016.09.017
- Baeza, A., Salas, A., Legarda, F., (2008). Determining factors in the elimination of uranium and radium from groundwaters during a standard potabilization process.

- Sci. Total Environ. 406(1-2), 24-34.
- Babakhouya, N. S. Boughrara and F. Abad (2010). Kinetics and Thermodynamics of Cd (II) Ions Sorption on Mixed Sorbents Prepared from Olive Stone and Date Pit from Aqueous Solution. *American Journal of Environmental Sciences*, 6(5), 470-476. doi:10.3844/ajessp.2010.470.476
- Babel, S. (2003). Low-cost adsorbents for heavy metals uptake from contaminated water: A review. *Journal of Hazardous Materials*, 97(1-3), 219-243. doi:10.1016/s0304-3894(02)00263-7
- Babiker, E., Al-Ghouti, M. A., Zouari, N., & Mckay, G. (2019). Removal of boron from water using adsorbents derived from waste tire rubber. *Journal of Environmental Chemical Engineering*, 7(2), 102948. doi:10.1016/j.jece.2019.102948
- Bajjali, W., (2005). Model the effect of four artificial recharge dams on the quality of groundwater using geostatistical methods in GIS environment. *Oman. J. Spat. Hydrol. Fall*. 5(2):1–15
- Balakrishnan, P. (2011). Groundwater quality mapping using geographic information system (GIS): A case study of Gulbarga City, Karnataka, India. *African Journal of Environmental Science and Technology*, 5(12). doi:10.5897/ajest11.134
- Banat, F., Al-Asheh, S., & Al-Rousan, D. (2002). A comparative study of copper and zinc ion adsorption on to activated and non-activated date-pits. *Adsorption Science & Technology*, 20(4), 319-335. doi:10.1260/02636170260295515
- Barakat, M. (2011). New trends in removing heavy metals from industrial wastewater. *Arabian Journal of Chemistry*, 4(4), 361-377. doi:10.1016/j.arabjc.2010.07.019
- Bartram, J., Ballance, R., World Health Organization & United Nations Environment Programme. (1996). *Water quality monitoring: a practical guide to the design and*



- implementation of freshwater quality studies and monitoring programs / edited by Jamie Bartram and Richard Ballance. London: E & FN Spon.  
<https://apps.who.int/iris/handle/10665/41851>
- Bashir, B., & Fouli, H. (2015). Studying the spatial distribution of maximum monthly rainfall in selected regions of Saudi Arabia using geographic information systems. *Arabian Journal of Geosciences*,8(11), 9929-9943. doi:10.1007/s12517-015-1870-z\
- Bassioni, G., Ashraf, K., & Elhameed, A. A. (2015). Risk assessment using ICP-MS of heavy metals in groundwater in Upper Egypt. *Journal of Natural Resources and Development*, 65-70. doi:10.5027/jnrd.v5i0.09
- Bodzek, M. (2015). The removal of boron from the aquatic environment—state of the art. *Desalination and Water Treatment*, 57(3), 1107-1131. doi:10.1080/19443994.2014.1002281
- Bonilla-Petriciolet, A., Mendoza-Castillo, D. I., Dotto, G. L., & Duran-Valle, C. J. (2019). Adsorption in water treatment. Reference Module in Chemistry, Molecular Sciences and Chemical Engineering. doi:10.1016/b978-0-12-409547-2.14390-2
- Bonilla-Petriciolet, A., Mendoza-Castillo, D. I., & Reynel-Ávila, H. E. (2017). Introduction. *Adsorption Processes for Water Treatment and Purification*, 1-18. doi:10.1007/978-3-319-58136-1\_1
- Bourg, A. C. M. (1995). Speciation of Heavy Metals in Soils and Groundwater and Implications for Their Natural and Provoked Mobility. *Heavy Metals*, 19–31. doi:10.1007/978-3-642-79316-5\_2
- Brown, J., Das, P., & Al-Saidi, M. (2018). Sustainable agriculture in the arabian/persian gulf region utilizing marginal water resources: Making the best of a bad situation. *Sustainability*, 10(5), 1364. doi:10.3390/su10051364

- Buzetzký, D., Nagy, N. M., & Kónya, J. (2020). Use of silver–bentonite in sorption of chloride and iodide ions. *Journal of Radioanalytical and Nuclear Chemistry*, 326(3), 1795–1804. doi:10.1007/s10967-020-07457-2
- Caridi, F., Messina, M., & D'Agostino, M. (2017). An investigation about natural radioactivity, hydrochemistry, and metal pollution in groundwater from Calabrian Selected areas, southern Italy. *Environmental Earth Sciences*, 76(19). doi:10.1007/s12665-017-7031-9
- Carvalho, F., Fernandes, S., Fesenko, S., Holm, E., Howard, B., Martin, P., Phaneuf, P., Porcelli, D., Pröhl, G., Twining, J. (2017). *The Environmental Behaviour of Polonium*. Technical reports series. 484. Vienna: International Atomic Energy Agency. p. 22. ISBN 978-92-0-112116-5. ISSN 0074-1914.
- Cheng, W.L., Saleem, A., Sadr, R. (2015). Recent warming trend in the coastal region of Qatar. *Theor. Appl. Climatol.* 128(1-2), 193–205.
- Chung, S. Y., Venkatramanan, S., Elzain, H. E., Selvam, S., & Prasanna, M. (2019). Supplement of Missing Data in Groundwater-Level Variations of Peak Type Using Geostatistical Methods. *GIS and Geostatistical Techniques for Groundwater Science*, 33–41. doi: 10.1016/b978-0-12-815413-7.00004-3
- Corti, Horacio & Crovetto, Rosa. (1980). Properties of the borate ion in dilute aqueous solutions. *J. Chem. Soc., Faraday Trans. 1.* 76. 10.1039/f19807602179.
- Crini, G., Lichtfouse, E., Wilson, L. D., & Morin-Crini, N. (2018). Conventional and non-conventional adsorbents for wastewater treatment. *Environmental Chemistry Letters*, 17(1), 195–213. doi: 10.1007/s10311-018-0786-8
- Czerewko, M., Cripps, J., Reid, J., & Duffell, C. (2003). Sulfur species in geological materials—sources and quantification. *Cement and Concrete Composites*, 25(7), 657–671. doi: 10.1016/s0958-9465(02)00066-5

- Daniel, C., Harris, W.H. (2011). *Quantitative Chemical Analysis*, eighth ed., Freeman and Company, 2011. ISBN-13: 978-1429263092
- Daniel, M., Lamki, M., Muhammad, D., Yaroubi, S., (2017). Boron content and sources in groundwater from Tertiary aquifers in the Sultanate of Oman. Sultan Qaboos University, College of Science, Earth Science, Muscat, Oman. General Assembly Conference Abstracts 2017-3180.
- Danielopol, D. L., & Griebler, C. (2008). Changing paradigms in groundwater ecology - from the 'living fossils' tradition to the 'new groundwater ecology'. *International Review of Hydrobiology*, 93(4-5), 565-577. doi:10.1002/iroh.200711045
- Darwish, M.A., Abdulrahim, H.K., Mohieldeen, Y., (2014). Qatar and GCC water security. *Desalin. Water Treat.* 55(9), 2302–2325.
- Davis, B. M. (1987). Uses and abuses of cross-validation in geostatistics. *Mathematical Geology*, 19(3), 241-248. doi:10.1007/bf00897749
- Dhawan, C., Kharb, P., Sharma, R., Uppal, S., & Aggarwal, R. K. (2013). Development of male-specific SCAR marker in date palm (*Phoenix dactylifera* L.). *Tree Genetics & Genomes*,9(5), 1143-1150. doi:10.1007/s11295-013-0617-9
- Djilani, C., Zaghdoudi, R., Djazi, F., Bouchekima, B. (2015). Adsorption of dyes on activated carbon prepared from apricot stones and commercial activated carbon, *Journal of the Taiwan Institute of Chemical Engineers*, Volume 53, Pages 112-121, ISSN 1876-1070, <https://doi.org/10.1016/j.jtice.2015.02.025>.
- Dodbiba, G., Ponou, J., Fujita, T., (2015). Biosorption of heavy metals. *Microbiology for Minerals, Metals, Materials and the Environment*, 427-444. doi:10.1201/b18124-20
- El-Alfy, M., Lashin, A., Abdalla, F., & Al-Bassam, A. (2017). Assessing the

- hydrogeochemical processes affecting groundwater pollution in arid areas using an integration of geochemical equilibrium and multivariate statistical techniques. *Environmental Pollution*, 229, 760-770. doi:10.1016/j.envpol.2017.05.052
- El-Hendawy, A. A. (2009). The role of surface chemistry and solution pH on the removal of Pb<sup>2+</sup> and Cd<sup>2+</sup> ions via effective adsorbents from low-cost biomass. *Journal of Hazardous Materials*, 167(1-3), 260-267. doi:10.1016/j.jhazmat.2008.12.118
- El-Maghraby, M. M., El Nasr, A. K., & Hamouda, M. S. (2013). Quality assessment of groundwater at South Al Madinah Al Munawarah area, Saudi Arabia. *Environmental Earth Sciences*, 70(4), 1525-1538. doi:10.1007/s12665-013-2239-9
- El-Messaoudi N., Lacherai A., El khomri M., Bentahar S., Dbik A. (2015). Modification of lignocellulosic biomass as agricultural waste for the biosorption of basic dye from aqueous solution. Laboratory of applied chemistry and environment, Department of Chemistry, Faculty of Science, University Ibn Zohr, BP 8106, 80000 Agadir, Morocco. *J. Mater. Environ. Sci.* 6 (10) (2015) 2784-2794  
ISSN: 2028-2508
- Elsaid, K., (2017). Development, modeling, analysis, and optimization of a novel inland desalination with zero liquid discharge for brackish groundwaters. UWSpace. PhD Dissertation, University of Waterloo, Ontario, Canada, p. 173.
- Elumalai, V., Brindha, K., Sithole, B., & Lakshmanan, E. (2017). Spatial interpolation methods and geostatistics for mapping groundwater contamination in a coastal area. *Environmental Science and Pollution Research*, 24(12), 11601-11617. doi:10.1007/s11356-017-8681-6
- Esmeray, Ertugrul & Aydin, Mehmet. (2008). Comparison of Natural Radioactivity Removal Methods for Drinking Water Supplies: A Review. *Journal of*

- International Environmental Application & Science. 3. 142-146.
- Etteieb, S., Cherif, S., & Tarhouni, J. (2015). Hydrochemical assessment of water quality for irrigation: a case study of the Medjerda River in Tunisia. *Applied Water Science*, 7(1), 469–480. doi: 10.1007/s13201-015-0265-3
- Ewen, S. and Geoffrey, D. (2019). *Modern Raman Spectroscopy a practical approach*. John Wiley & Sons Inc. ISBN: 978-1-119-44055-0. 256 Pages. 2000-2021
- Falivene, O., Cabrera, L., Tolosana-Delgado, R., & Sáez, A. (2010). Interpolation algorithm ranking using cross-validation and the role of smoothing effect. A coal zone example. *Computers & Geosciences*, 36(4), 512-519. doi:10.1016/j.cageo.2009.09.015
- FAO. (2016). AQUASTAT Main Database, Food and Agriculture Organization of the United Nations (FAO). Retrieved November 25, 2019
- FAO, (1992). The use of saline waters for crop production. FAO irrigation and drainage paper 48. Retrieved December 09, 2019.
- Feild, L., Pruchno, R. A., Bewley, J., Lemay, E. P., Jr., & Levinsky, N. G. (2006). Using probability vs. nonprobability sampling to identify hard-to-access participants for health-related research: costs and contrasts. *Journal of Aging and Health*, 18, 565–583.
- Fujinaga, A. (2016). Risk evaluation for remediation techniques to metal-contaminated soils. *Environmental Remediation Technologies for Metal-Contaminated Soils*, 231-254. doi:10.1007/978-4-431-55759-3\_11
- Galitskaya, I., Kostikova, I., Pozdnyakova, I., & Zhigalin, A. (2013). The role of rock in chemical and isotopic composition of groundwater in the vicinity of radioactive waste disposal site. *Procedia Earth and Planetary Science*, 7, 276-279. doi:10.1016/j.proeps.2013.03.072

- Ghalib, H. B. (2017). Groundwater chemistry evaluation for drinking and irrigation utilities in east Wasit province, Central Iraq. *Applied Water Science*, 7(7), 3447–3467. doi: 10.1007/s13201-017-0575-8
- Gidey, E., Dikinya, O., Sebege, R., Segosebe, E., & Zenebe, A. (2018). Modeling the Spatio-Temporal Meteorological Drought characteristics using the Standardized Precipitation Index (SPI) In Raya and Its Environs, Northern Ethiopia. *Earth Systems and Environment*, 2(2), 281-292. doi:10.1007/s41748-018-0057-7
- Griebler, C., & Avramov, M. (2015). Groundwater ecosystem services: A review. *Freshwater Science*, 34(1), 355-367. doi:10.1086/679903
- GSO, GCC Standardization Organization (2008). Unbottled drinking water standard. Retrieved from <https://www.gso.org.sa/en/>.
- Guan, Z., Lv, J., Bai, P., & Guo, X. (2016). Boron removal from aqueous solutions by adsorption — a review. *Desalination*, 383, 29-37. doi:10.1016/j.desal.2015.12.026
- Güler, M. (2014). Comparison of different interpolation techniques for modelling temperatures in Middle Black Sea region. – *Journal of Agricultural Faculty of Gaziosmanpasa University* 31(2): 61–71. DOI: 10.13002/jafag714.
- Gunaalan, K., Ranagalage, M., Gunarathna, M. H. J. P., Kumari, M. K. N., Vithanage, M., Saravanan, S., Warnasuriya, T. W. S. (2018). Application of geospatial techniques for groundwater quality and availability assessment: A case study in Jaffna Peninsula, Sri Lanka. *International Journal of Geo-Information* 7: 20. DOI: 10.3390/ijgi7010020.
- Gunarathna, M. H. J. P., Kumari, M. K. N., Nirmanee, K. G. S. (2016a). Evaluation of interpolation methods for mapping pH of groundwater. – *International Journal of Latest Technology in Engineering, Management and Applied Science* 5(3): 1–5.
- Gunarathna, M. H. J. P., Nirmanee, K. G. S., Kumari, M. K. N. (2016b). Are

- geostatistical interpolation methods better than deterministic interpolation methods in mapping salinity of groundwater? *International Journal of Research and Innovations in Earth Sciences* 3(3): 59–64.
- Hadi, k. m. & Al-Ruwaith, F. M. (2008). Geochemical evolution of the fresh groundwater in Kuwait desert. *Emirates journal for engineering research* 13 (3), 37-45.
- Hasenmueller, E. A., & Criss, R. E. (2013). Multiple sources of boron in urban surface waters and groundwaters. *Science of The Total Environment*, 447, 235–247. doi: 10.1016/j.scitotenv.2013.01.001
- Hashim, M., Mukhopadhyay, S., Sahu, J. N., & Sengupta, B. (2011). Remediation technologies for heavy metal contaminated groundwater. *Journal of Environmental Management*,92(10),2355-2388. doi:10.1016/j.jenvman.2011.06.009
- Hassan, I. Taimur, S. and T. Yasin (2017). Up cycling of polypropylene waste by surface modification using radiation-induced grafting. *Applied Surface Science*, 422, 720–730. <https://doi.org/10.1016/j.apsusc.2017.06.086>
- Hawari, A., Khraisheh, M., & Al-Ghouti, M. A. (2014). Characteristics of olive mill solid residue and its application in remediation of pb<sup>2+</sup>, cu<sup>2+</sup> and ni<sup>2+</sup> from aqueous solution: Mechanistic study. *Chemical Engineering Journal*, 251, 329-336. doi:10.1016/j.cej.2014.04.065
- Hazarika, N., & Nitivattananon, V. (2016). Strategic assessment of Groundwater resource Exploitation using DPSIR framework in Guwahati city, India. *Habitat International*, 51, 79-89. doi:10.1016/j.habitatint.2015.10.003
- Henckens, M., Driessen, P., & Worrell, E. (2018). Molybdenum resources: Their depletion and safeguarding for future generations. *Resources, Conservation and Recycling*, 134, 61–69. doi: 10.1016/j.resconrec.2018.03.002

- Hengl, T. (2007): A Practical Guide to Geostatistical Mapping of Environmental Variables. Office for Official Publication of the European Communities, Luxembourg.
- Hilal, N. M., Ahmed, I. A., & El-Sayed, R. E. (2012). Activated and nonactivated date pits Adsorbents for the removal of copper(ii) and Cadmium (II) from aqueous solutions. *ISRN Physical Chemistry*, 2012, 1-11. doi:10.5402/2012/985853
- Hilal, N., Kim, G., & Somerfield, C. (2011). Boron removal from saline water: A comprehensive review. *Desalination*, 273(1), 23-35. doi:10.1016/j.desal.2010.05.012
- Hossain, M. Z., Waly, M. I., Singh, V., Sequeira, V., & Rahman, M. S. (2014). Chemical composition of date-pits and its potential for developing value-added product - A review. *Polish Journal of Food and Nutrition Sciences*, 64(4), 215-226. DOI: 10.2478/pjfn-2013-0018
- Hoyer, M., Kummer, N., & Merkel, B. (2015). Sorption of Lithium on Bentonite, Kaolin and Zeolite. *Geosciences*, 5(2), 127-140. doi:10.3390/geosciences5020127
- Hoyos, I., Krakauer, N., Khanbilvardi, R., & Armstrong, R. (2016). A review of advances in the identification and characterization of groundwater dependent ecosystems using geospatial technologies. *Geosciences*, 6(2), 17. doi:10.3390/geosciences6020017
- Huang, F., Yi, F., Wang, Z., & Li, H. (2016). Sorptive removal of Ce(IV) from aqueous solution by Bentonite. *Procedia Environmental Sciences*, 31, 408-417. doi:10.1016/j.proenv.2016.02.073
- Hukoomi. (2019). Qatar government. Environment and agriculture. Retrieved December 09, 2019. <https://hukoomi.gov.qa/en/>
- Humphreys, W. F. (2008). Hydrogeology and groundwater ecology: Does each



- inform the other? *Hydrogeology Journal*, 17(1), 5-21. doi:10.1007/s10040-008-0349-3
- IAEA. (1999). *Technical options for the remediation of contaminated groundwater*. International Atomic Energy Agency, Vienna.
- IMOA. (2018). *Annual Review 2018/2019*. International molybdenum Association. Retrieved from <https://www.imoa.info/molybdenum-media-centre/downloads/annual-review.php>
- Isupov, V., Kotsupalo, N., Nemudry, A., & Menzeres, L. (1999). Aluminium hydroxide as selective sorbent of lithium salts from brines and technical solutions. *Studies in Surface Science and Catalysis Adsorption and Its Applications in Industry and Environmental Protection - Vol.I: Applications in Industry*, 621–652. doi: 10.1016/s0167-2991(99)80567-9
- Jackson, T. (2007). *Lithium*. New York: Marshall Cavendish Benchmark. ISBN 10 9780761421993
- Jafari, M., Bernardeau, F. (2019). 'Deep Injection Wells for Flood Prevention and Groundwater Management'. *World Academy of Science, Engineering and Technology, Open Science Index* 149, *International Journal of Geotechnical and Geological Engineering*, 13(5), 336 - 350.
- Jain, S. M. (2014). *Date palm biotechnology*. Place of publication not identified. Springer, 479 DOI 10.1007/978-94-007-1318-5\_23.
- Jakeman, A. J., Barreteau, O., Hunt, R. J., Rinaudo, J., Ross, A., Arshad, M., & Hamilton, S. (2016). Integrated groundwater management: An overview of concepts and challenges. *Integrated Groundwater Management*, 3-20. doi:10.1007/978-3-319-23576-9\_1
- Jaradat, A. A. (2013). *Date Palm: Production. Dates*, 29-55.

doi:10.1002/9781118292419.ch2

- Jolliffe, I. T., & Cadima, J. (2016). Principal component analysis: a review and recent developments. *Philosophical Transactions of the Royal Society A: Mathematical, Physical and Engineering Sciences*, 374(2065), 20150202. doi: 10.1098/rsta.2015.0202
- Kahramaa, (2016). Sustainability report 2016. Retrieved December 09, 2019, from <https://www.km.com.qa/MediaCenter/Pages/Publications.aspx?p=4>
- Kahramaa. (2018a). Supply and Installation of Advanced Flow Meters and Monitoring System for Groundwater Wells. Retrieved December 09, 2019, from <https://www.km.com.qa/Business/Pages/TenderDetails.aspx?ItemId=1243>
- Kahramaa. (2018b). Development of Rainfall Harvest (groundwater Recharge Wells) in Potable Wellfield Stations. Retrieved December 09, 2019, from <https://www.km.com.qa/Business/Pages/TenderDetails.aspx?ItemId=1126>
- Kagalou, I., Leonardos, I., Anastasiadou, C., & Neofytou, C. (2012). The DPSIR approach for an Integrated river management Framework. a preliminary application on a Mediterranean Site (kalamas River -nw greece). *Water Resources Management*, 26(6), 1677-1692. doi:10.1007/s11269-012-9980-9
- Kanagaraj, G., Elango, L., (2016). Hydrogeochemical processes and impact of tanning industries on groundwater quality in Ambur, Vellore district, Tamil Nadu, India. *Environ. Sci. Pollut. Res.* 23(23), 24364-24383.
- Karahan, S., Yurdakoç, M., Seki, Y., & Yurdakoç, K. (2006). Removal of boron from aqueous solution by clays and modified clays. *Journal of Colloid and Interface Science*, 293(1), 36-42. doi:10.1016/j.jcis.2005.06.048
- Karnib, M., Kabbani, A., Holail, H., & Olama, Z. (2014). Heavy metals removal using activated carbon, silica and silica activated carbon composite. *Energy*

- Procedia, 50, 113-120. doi:10.1016/j.egypro.2014.06.014
- Keranen, K., & Kolvoord, R. (2017). Making spatial decisions using ArcGIS Pro: a workbook. esri Press, 2017; 376 PAGES. PRICE \$69.99, Isbn 9781589484849.
- (2017). ISPRS International Journal of Geo-Information, 6(9), 279. doi:10.3390/ijgi6090279
- Khan, Q., Kalbus, E., Alshamsi, D. M., Mohamed, M. M., & Liaqat, M. U. (2019). Hydrochemical analysis of groundwater In Remah and Al Khatim REGIONS, United Arab Emirates. Hydrology, 6(3), 60. doi:10.3390/hydrology6030060
- Köse, T. E., Demiral, H., & Öztürk, N. (2011). Adsorption of boron from aqueous solutions using activated carbon prepared from olive bagasse. Desalination and Water Treatment, 29(1-3), 110-118. doi:10.5004/dwt.2011.2091
- Kuiper, N., Rowell, C., & Shomar, B. (2015). High levels of molybdenum in Qatar's groundwater and potential impacts. Journal of Geochemical Exploration, 150, 16-24. doi:10.1016/j.gexplo.2014.12.009
- Kul, A. R., & Koyuncu, H. (2010). Adsorption of Pb(II) ions from aqueous solution by native and activated bentonite: Kinetic, equilibrium and thermodynamic study. Journal of Hazardous Materials, 179(1-3), 332-339. doi:10.1016/j.jhazmat.2010.03.009
- Kumar, P., Bansod, B. K., Debnath, S. K., Thakur, P. K., & Ghanshyam, C. (2015). Index-based groundwater vulnerability mapping models using hydrogeological settings: A critical evaluation. Environmental Impact Assessment Review, 51, 38-49. doi: 10.1016/j.eiar.2015.02.001
- Kumar, S. K., Rammohan, V., Sahayam, J. D., & Jeevanandam, M. (2008). Assessment of groundwater quality and hydrogeochemistry OF Manimuktha river basin, Tamil Nadu, India. Environmental Monitoring and Assessment, 159(1-4),

- 341-351. doi:10.1007/s10661-008-0633-7
- Lee, M., Sohn, S., & Lee, M. (2011). Ionic equilibria and ion exchange of Molybdenum(VI) from strong acid solution. *Bulletin of the Korean Chemical Society*, 32(10), 3687-3691. doi:10.5012/bkcs.2011.32.10.3687
- Li, J., Heap, A D, (2011). A review of comparative studies of spatial interpolation methods in environmental sciences: performance and impact factors. *Ecol. Inf.* 6 (3–4), 228–241. <https://doi.org/10.1016/j.ecoinf.2010.12.003>
- Li, J., Hu, J., Sheng, G., Zhao, G., & Huang, Q. (2009). Effect of pH, ionic STRENGTH, foreign ions and temperature on the adsorption OF Cu(II) from aqueous solution To GMZ bentonite. *Colloids and Surfaces A: Physicochemical and Engineering Aspects*, 349(1-3), 195-201. doi:10.1016/j.colsurfa.2009.08.018
- Liu, Z. P., Shao, M. A., & Wang, Y. Q. (2012). Large-scale spatial interpolation of soil pH across the Loess Plateau, China. *Environmental Earth Sciences*, 69(8), 2731-2741. doi:10.1007/s12665-012-2095-z
- Lofrano, G., Meriç, S., Zengin, G. E., & Orhon, D. (2013). Chemical and biological treatment technologies for leather tannery chemicals and wastewaters: A review. *Science of The Total Environment*, 461-462, 265-281. doi:10.1016/j.scitotenv.2013.05.004
- Machado, R., & Serralheiro, R. (2017). Soil salinity: effect on vegetable crop growth. Management practices to prevent and mitigate soil salinization. *Horticulturae* 3 (2), 30. <https://doi.org/10.3390/horticulturae3020030>.
- Magesh, N., & Elango, L. (2019). Spatio-Temporal variations of fluoride in the Groundwater OF DINDIGUL DISTRICT, Tamil NADU, India: A Comparative Assessment using Two interpolation techniques. *GIS and Geostatistical Techniques for Groundwater Science*, 283-296. doi:10.1016/b978-0-12-815413-

7.00020-1

- Malassa, H., Hadidoun, M., Al-Khatib, M., Al-Rimawi, F., & Al-Qutob, M. (2014). Assessment of groundwater pollution with heavy metals in North West BANK/PALESTINE by ICP-MS. *Journal of Environmental Protection*, 05(01), 54-59. doi:10.4236/jep.2014.51007
- Mallick, J., Singh, C., Almesfer, M., Kumar, A., Khan, R., Islam, S., & Rahman, A. (2018). Hydro-Geochemical Assessment of Groundwater Quality in Aseer Region, Saudi Arabia. *Water*, 10(12), 1847. doi: 10.3390/w10121847
- Man, H. C. B., Akinbile, C. O., & Jun, C. X. (2015). Coconut Husk Adsorbent for the Removal of Methylene Blue Dye from Wastewater. *BioResources*, 10(2). doi: 10.15376/biores.10.2.2859-2872
- Manickum, T., John, W., Terry, S., & Hodgson, K. (2014). Preliminary study on the radiological and physicochemical quality of the Umgeni Water catchments and drinking water sources in KwaZulu-Natal, South Africa. *Journal of Environmental Radioactivity*, 137, 227-240. doi:10.1016/j.jenvrad.2014.07.015
- Mardiah, Fathoni, R. A., Pudyaningtyas, P., Gamu, H., & Rinaldy. (2018). Reuse of Newspaper as An Adsorbent for Cu (II) Removal by Citric Acid Modification. *MATEC Web of Conferences*, 156, 02012. doi: 10.1051/mateconf/201815602012
- Marghade, D., Malpe, D. B., & Zade, A. B. (2010). Geochemical characterization of groundwater from northeastern part of Nagpur urban, Central India. *Environmental Earth Sciences*, 62(7), 1419-1430. doi:10.1007/s12665-010-0627-y
- Marko, K., Al-Amri, N. S., & Elfeki, A. M. (2013). Geostatistical analysis using GIS for mapping groundwater quality: Case study in the Recharge area of Wadi USFAN, western Saudi Arabia. *Arabian Journal of Geosciences*, 7(12), 5239-5252. doi:10.1007/s12517-013-1156-2

- Maryam, Jaskani M. J., Awan F. S., Ahmad S., & Khan, I. A. (2016). Development of molecular method for sex identification in date palm (*Phoenix dactylifera* L.) plantlets using novel sex-linked microsatellite markers. *3 Biotech*, 6(1). doi:10.1007/s13205-015-0321-6.
- Masoud, M. (2020). Groundwater Resources Management of the Shallow Groundwater Aquifer in the Desert Fringes of El Beheira Governorate, Egypt. *Earth Systems and Environment*, Volume 4, Issue 1, p.147-165. DOI: 10.1007/s41748-020-00148-8
- Maxwell, O., Wagiran, H., Lee, S., Embong, Z., Ugwuoke, P., (2015). Radioactivity level and toxic elemental concentration in groundwater at Dei-Dei and Kubwa areas of Abuja, north-central Nigeria. *Radiat. Phys. Chem.* 107, 23-30.
- McCarthy, J. J., Canziani, O. F., Leary, N. A., Dokken D. J. and White K. S. (2001). *Climate change 2001: impacts, adaptation and vulnerability*, Contribution of Working Group II to the Third Assessment Report of the Intergovernmental Panel on Climate Change. Cambridge University Press, Cambridge, UK, and New York, USA, 2001. No. of pages: 1032. ISBN 0-521-01500-6 (paperback), ISBN 0-521-80768-9
- MDPS, Ministry of Development Planning and Statistics, (2016): National Development Strategy. Retrieved January 1, 2020, from <https://www.psa.gov.qa/ar/statistics1>
- MDPS, Ministry of Development Planning and Statistics (2018): Population Statistics in the State of Qatar 2018. Retrieved March 1, 2020, from <https://www.psa.gov.qa/ar/statistics1>
- MDPS, Ministry of Development Planning and Statistics (2017): Water Statistics in the State of Qatar 2018. Retrieved March 1, 2020, from

<https://www.psa.gov.qa/ar/statistics1>

- Miessler, G. L., Fischer, P. J., & Tarr, D. A. (2014). Inorganic chemistry. Harlow, Essex: Pearson. ISBN-13: 978-0321811059
- Minceva, M., Fajgar, R., Markovska, L., & Meshko, V. (2008). Comparative study of  $zn^{2+}$ ,  $cd^{2+}$ , and  $pb^{2+}$  removal from water solution using natural clinoptilolitic zeolite and commercial granulated activated carbon. equilibrium of adsorption. Separation Science and Technology, 43(8), 2117-2143. doi:10.1080/01496390801941174
- Missteart, B., Banks, D., & Clark, L. (2017). Water Wells and Boreholes. doi: 10.1002/9781119080176
- Mochida, I., Yoon, S., & Qiao, W. (2006). Catalysts in syntheses of carbon and Carbon precursors. Journal of the Brazilian Chemical Society, 17(6), 1059-1073. doi:10.1590/s0103-50532006000600002
- Mohamed N.B., Ngadi N., Lani N.S., Rahman R.A., (2017). Polyethylenimine modified sugarcane bagasse adsorbent for methyl orange dye removal, Chemical Engineering Transactions, 56, 103-108 DOI:10.3303/CET1756018
- Mojiri, A., Tajuddin, R. M., Ahmad, Z., Ziyang, L., Aziz, H. A., & Amin, N. M. (2017). Chromium (VI) and CADMIUM removal from aqueous solutions using THE BAZLSC/cockle SHELL CONSTRUCTED WETLAND SYSTEM: Optimization WITH RSM. International Journal of Environmental Science and Technology, 15(9), 1949-1956. doi:10.1007/s13762-017-1561-2
- Mousa KM, Taha AH. (2015). Adsorption of Reactive Blue Dye onto Natural and Modified Wheat Straw. J Chem Eng Process Technol 6: 260. doi:10.4172/2157-7048.1000260
- Myers, D. E. (1991). Interpolation and estimation with spatially located data.

- Chemometrics and Intelligent Laboratory Systems, 11(3), 209-228.  
doi:10.1016/0169-7439(91)85001-6
- Nagul, E. A., Mckelvie, I. D., Worsfold, P., & Kolev, S. D. (2015). The molybdenum blue reaction for the determination of orthophosphate revisited: Opening the black box. *Analytica Chimica Acta*, 890, 60-82. doi:10.1016/j.aca.2015.07.030
- Nas, B. (2009). Geostatistical approach to assessment of spatial distribution of groundwater quality. *Polish Journal of Environmental Studies. Pol. J. Environ. Stud.* 2009;18(6):1073–1082
- Njeban, H. S. (2018). Comparison and Evaluation of GIS-Based Spatial Interpolation Methods for Estimation Groundwater Level in AL-Salman District—Southwest Iraq. *Journal of Geographic Information System*, 10(04), 362–380. doi: 10.4236/jgis.2018.104019
- Noll, K. E., Gounaris, V., & Hou, W. (1990). Adsorption technology: For air and water pollution control. Chelsea: Lewis. ISBN: 0873713400
- Nriagu, J., Bhattacharya, P., Mukherjee, A., Bundschuh, J., Zevenhoven, R., & Loeppert, R. (2007). Arsenic in soil And Groundwater: An overview. *Trace Metals and Other Contaminants in the Environment*, 3-60. doi:10.1016/s1875-1121(06)09001-8
- Nwankwo, C.B., Hoque, M.A., Islam, M.A. et al. (2020). Groundwater Constituents and Trace Elements in the Basement Aquifers of Africa and Sedimentary Aquifers of Asia: Medical Hydrogeology of Drinking Water Minerals and Toxicants. *Earth Syst Environ* 4, 369–384. <https://doi.org/10.1007/s41748-020-00151-z>
- OECD. (1993). OECD Core Set of Indicators for Environmental Performance Reviews. A Synthesis Report by the Group on the State of the Environment. OECD, Paris. pp. 35



- Othman, A. K. (2005). Quantitative and Qualitative Assessment of Groundwater Resources in Al-Khatim Area, UAE. Theses. 68. [https://scholarworks.uaeu.ac.ae/all\\_theses/68](https://scholarworks.uaeu.ac.ae/all_theses/68)
- Özmal, F., & Erdoğan, Y. (2015). Li adsorption/desorption properties of lithium ion-sieves in aqueous solution and recovery of lithium from borogypsum. *Journal of Environmental Chemical Engineering*, 3(4), 2670-2683. doi:10.1016/j.jece.2015.09.024
- Pagnanelli, F., Ferella, F., De Michelis, I., & Vegliò, F. (2011). Adsorption onto activated carbon for molybdenum recovery from leach liquors of exhausted hydrotreating catalysts. *Hydrometallurgy*, 110(1-4), 67-72. doi:10.1016/j.hydromet.2011.08.008
- Pan, D., Fan, Q., Li, P., Liu, S., & Wu, W. (2011). Sorption of Th (IV) on Na-bentonite: Effects of pH, ionic strength, humic substances and temperature. *Chemical Engineering Journal*, 172(2-3), 898-905. doi:10.1016/j.cej.2011.06.080
- Paramasivam, C., & Venkatramanan, S. (2019). An introduction to various spatial analysis techniques. *GIS Geostat. Tech. Groundwater Sci.* 23–30. DOI: 10.1016/B978-0-12-815413-7.00003-1
- Parkinson, C. L., (2010). Coming climate crisis? Consider the past, beware the big fix. *Choice Reviews Online*, 48(02). doi:10.5860/choice.48-0883
- Poinssot, C., & Geckeis, H. (2012). Overview of radionuclide behaviour in the natural environment. *Radionuclide Behaviour in the Natural Environment*, 1-10. doi:10.1533/9780857097194.1
- Porcelli, D. (2008). Chapter 4 Investigating Groundwater processes using U- and Th-Series Nuclides. *Radioactivity in the Environment*, 105-153. doi:10.1016/s1569-4860(07)00004-6

- Porter, M.L., (2007). Subterranean biogeography: what have we learned from molecular techniques? *J. Cave. Karst. Stud.* 69, 179-186.
- Rajmohan, N., Niazi, B. A., & Masoud, M. H. (2019). Evaluation of a brackish Groundwater resource in the WADI Al-Lusub BASIN, western Saudi Arabia. *Environmental Earth Sciences*, 78(15). doi:10.1007/s12665-019-8441-7
- Rashed MN, Gad AA, Abd-Eldaiem AM. (2018). Preparation of low-cost adsorbent from waste glass for the removal of heavy metals from polluted water. *J Ind Environ Chem.*;2(2):7-18
- Ravikumar, P., & Somashekar, R. K. (2015). Principal component analysis and hydrochemical facies characterization to evaluate groundwater quality in Varahi river basin, Karnataka state, India. *Applied Water Science*, 7(2), 745–755. doi: 10.1007/s13201-015-0287-x
- Rehman, K., Fatima, F., Waheed, I., & Akash, M. S. (2017). Prevalence of exposure of heavy metals and their impact on health consequences. *Journal of Cellular Biochemistry*, 119(1), 157-184. doi:10.1002/jcb.26234
- Sadiq, A.M. and Nasir, S.J., (2002). Middle Pleistocene karst evolution in the State of Qatar, Arabian Gulf. *Journal of Cave and Karst Studies* 64(2): p.132-139.
- Saleh, I. A., & Balakrishnan, P. (2019). GIS Based Hotspot and Cold-spot Analysis for Primary Education in India. *Indian Journal of Science and Technology*, 12(45), 01-33. doi:10.17485/ijst/2019/v12i45/148448
- Santos, A., Alonso, E., Callejón, M., & Jiménez, J. (2002). Heavy metal content and speciation in groundwater of the Guadiamar river basin. *Chemosphere*, 48(3), 279–285. doi: 10.1016/s0045-6535(02)00083-8
- Sethi, R., & Molfetta, A. D. (2019). Remediation of Contaminated Groundwater. *Groundwater Engineering Springer Tracts in Civil Engineering*, 331–409. doi:

10.1007/978-3-030-20516-4\_17

- Seyedmohammadi, J., Esmaeelnejad, L., & Shabanpour, M. (2016). Spatial variation modelling of groundwater electrical conductivity using geostatistics and GIS. *Modeling Earth Systems and Environment*. doi:10.1007/s40808-016-0226-3
- Shafiq, M., Alazba, A. A., & Amin, M. T. (2019). Synthesis, characterization, and application of date palm leaf waste-derived biochar to remove cadmium and hazardous cationic dyes from synthetic wastewater. *Arabian Journal of Geosciences*, 12(2). doi:10.1007/s12517-018-4186-y
- Shah, K. H., Ayub, M., Fahad, M., Bilal, M., Amin, B. A. Z., & Hussain, Z. (2019). Natural dolomite as a low-cost adsorbent for efficient removal of As(III) from aqueous solutions. *Materials Research Express*, 6(8), 085535. doi: 10.1088/2053-1591/ab24f8
- Shamrukh, M. (2012). Exploring of deep groundwater in the southwest aquifer of Qatar. Department of water, ministry of environment, P.O. Box 7634, Doha, Qatar. DOI: 10.13140/2.1.3191.5521
- Shan, W., Fang, D., Zhao, Z., Shuang, Y., Ning, L., Xing, Z., & Xiong, Y. (2012). Application of orange peel for adsorption separation of molybdenum(vi) from re-containing industrial effluent. *Biomass and Bioenergy*, 37, 289-297. doi:10.1016/j.biombioe.2011.11.015
- Shannon, R. D. (1976). Revised effective ionic radii and systematic studies of interatomic distances in halides and chalcogenides. *Acta Crystallographica Section A*, 32(5), 751-767. doi:10.1107/s0567739476001551
- Sherif, M., Kacimov, A., Javadi, A., & Ebraheem, A. A. (2011). Modeling groundwater flow and seawater intrusion in the Coastal Aquifer of Wadi Ham, UAE. *Water Resources Management*, 26(3), 751-774. doi:10.1007/s11269-011-

- Shomar, B. (2015). Geochemistry of soil and groundwater in arid regions: Qatar as a case study. *Groundwater for Sustainable Development*, 1(1-2), 33-40. doi:10.1016/j.gsd.2015.12.005
- Shomar, B., Darwish, M., & Rowell, C. (2014). What does Integrated Water Resources Management from Local to Global Perspective Mean? Qatar as a Case Study, the Very Rich Country with No Water. *Water Resources Management*, 28(10), 2781–2791. doi: 10.1007/s11269-014-0636-9
- Shomar, B., & Hawari, J. (2017). Desalinated drinking water in the GCC countries – the need to address consumer perceptions. *Environmental Research*, 158, 203-211. doi:10.1016/j.envres.2017.06.018
- Singh, N., Nagpal, G., Agrawal, S., & Rachna. (2018). Water purification by Using Adsorbents: A review. *Environmental Technology & Innovation*, 11, 187-240. doi:10.1016/j.eti.2018.05.006
- Singh, P., & Verma, P. (2019). A Comparative Study of Spatial Interpolation Technique (IDW and Kriging) for Determining Groundwater Quality. *GIS and Geostatistical Techniques for Groundwater Science*, 43-56. doi:10.1016/b978-0-12-815413-7.00005-5
- Smedley, P.L., & Kinniburgh, D.G., (2017). Molybdenum in natural waters: A review of occurrence, distributions and controls. *Appl. Geochem.* 84, 387-432.
- Smith, J. W. N. (2005). *Groundwater-surface water interactions in the hyporheic zone*. Bristol: Environment Agency. ISBN: 1844324257
- Socrates, G. (2015). *Infrared and Raman Characteristic Group frequencies: Tables and Charts*. 3rd ed By George Socrates (the University of West London, Middlesex, U.k.). J. Wiley and SONS: Chichester. 2001. ISBN: 0-471-85298-8.

- (2002). *Journal of the American Chemical Society*, 124(8), 1830-1830.  
doi:10.1021/ja0153520
- Srinivasamoorthy, K., Gopinath, M., Chidambaram, S., Vasanthavigar, M., & Sarma, V. (2014). Hydrochemical characterization and quality appraisal of groundwater From Pungar SUB basin, tamilnadu, india. *Journal of King Saud University - Science*, 26(1), 37-52. doi:10.1016/j.jksus.2013.08.001
- Stahl, K., Moore, R. D., Floyer, J. A., Asplin, M. G., Mckendry, I. G. (2006). Comparison of approaches for spatial interpolation of daily air temperature in a large region with complex topography and highly variable station density. *Agricultural and Forest Meteorology* 139: 224–236. DOI: 10.1016/j.agrformet.2006.07.004.
- Sulyman, M. Al-Azabi, K.Y., Al-Marog, S., & Abukrain, A., 2018. New Approach for In-House Treatment of Colored Wastewater Using Olive-Waste Cake as an Alternative Adsorbent. *IOSR Journal of Environmental Science, Toxicology and Food Technology* ISSN: 2319-2399. Volume 10. DOI: 10.9790/2402-1012041931
- Sun, C., Liu, W., & Zou, W. (2016). Water poverty in urban and rural china considered through the harmonious and developmental ability model. *Water Resources Management*, 30(7), 2547-2567. doi:10.1007/s11269-016-1290-1
- Sun, D., Meng, M., Qiao, Y., Zhao, Y., Yan, Y., & Li, C. (2018). Synthesis of ion imprinted nanocomposite membranes for selective adsorption of lithium. *Separation and Purification Technology*, 194, 64–72. doi: 10.1016/j.seppur.2017.10.052
- Sundaram, B., Feitz, A. J., de Caritat, P., Plazinska, A., Brodie, R. S., Coram, J., Australia, G. (2009). *Groundwater sampling and analysis: A field guide*. Geoscience Australia. Retrieved from [http://ga.gov.au/image\\_cache/GA15501.pdf](http://ga.gov.au/image_cache/GA15501.pdf)

- Suursoo, S., Hill, L., Raidla, V., Kiisk, M., Jantsikene, A., Nilb, N., Isakar, K. (2017). Temporal changes in radiological and chemical composition of Cambrian-Vendian groundwater in conditions of intensive water consumption. *Science of The Total Environment*, 601-602, 679-690. doi:10.1016/j.scitotenv.2017.05.136
- Suzuki, S., Sazarashi, M., Akimoto, T., Haginuma, M., & Suzuki, K. (2008). A study of the mineralogical alteration of bentonite in saline water. *Applied Clay Science*, 41(3-4), 190-198. doi:10.1016/j.clay.2007.11.003
- SWS, Schlumberger Water Services, (2009). Studying and developing the natural and artificial recharge of the groundwater in aquifer in the State of Qatar. Department of Agriculture and Water Research (DAWR), Ministry of Environment, State of Qatar. Project final report.
- Syed, K. H., Goodrich, D. C., Myers, D. E., & Sorooshian, S. (2003). Spatial characteristics of thunderstorm rainfall fields and their relation to runoff. *Journal of Hydrology*, 271(1-4), 1-21. doi:10.1016/s0022-1694(02)00311-6
- Tamunobereton-Ari, I. (2011). Speciation of heavy metals (Cu, Pb, Ni) pollutants and the vulnerability of groundwater resource in Okrika of Rivers State, Nigeria. *American Journal of Scientific and Industrial Research*, 2(1), 69–77. doi: 10.5251/ajsir.2011.2.1.69.77
- Taylor, P. (2015). Physical, chemical, and biological treatment of groundwater at contaminated nuclear and norm sites. *Environmental Remediation and Restoration of Contaminated Nuclear and Norm Sites*, 237-256. doi:10.1016/b978-1-78242-231-0.00010-7
- Temesgen, T., Bui, T. T., Han, M., Kim, T., & Park, H. (2017). Micro and NANOBUBBLE technologies as a new horizon For Water-treatment techniques: A review. *Advances in Colloid and Interface Science*, 246, 40-51.

doi:10.1016/j.cis.2017.06.011

- Tenev, M. D., Farías, A., Torre, C., Fontana, G., Caracciolo, N., Boeykens, S. P. (2019). Cotton Industry waste as adsorbent for Methylene Blue, *J. sustain. dev. energy water environ. syst.*, 7(4), pp 667-677, 2019, DOI: <https://doi.org/10.13044/j.sdewes.d7.0269>
- Thapa, R., Gupta, S., Guin, S., & Kaur, H. (2018). Sensitivity analysis and mapping the potential groundwater vulnerability zones in Birbhum district, India: A comparative approach between vulnerability models. *Water Science*, 32(1), 44–66. doi: 10.1016/j.wsj.2018.02.003
- Tu, Y., You, C., Chang, C., Chan, T., & Li, S. (2014). Xanes evidence of molybdenum adsorption onto novel fabricated nano-magnetic  $\text{CuFe}_2\text{O}_4$ . *Chemical Engineering Journal*, 244, 343-349. doi:10.1016/j.cej.2014.01.084
- UNDP, United Nations Development Programme. (2013). *Water governance in the Arab region: managing scarcity and securing the future*. New York, NY. ISBN: 978-92-1-126366-4
- USDA, (2000). *Heavy Metal Soil Contamination*. Natural Resources Conservation Service. United States Department of Agriculture. Retrieved from [https://www.nrcs.usda.gov/Internet/FSE\\_DOCUMENTS/nrcs142p2\\_053279.pdf](https://www.nrcs.usda.gov/Internet/FSE_DOCUMENTS/nrcs142p2_053279.pdf)
- US-EPA. (2018). *Edition of the Drinking Water Standards and Health Advisories Tables*. Retrieved February 6, 2021, from <https://www.epa.gov/sites/production/files/2018-03/documents/dwtable2018.pdf>
- Uyan, M., Cay, T. (2013): Spatial analyses of groundwater level differences using geostatistical modeling. – *Environmental and Ecological Statistics* 20: 633–646. DOI: 10.1007/s10651-013-0238-3.
- Vargas-Guzmán, J.A. & Warrick, A. & Myers, Donald & Musil, S.A & Artiola, J.F.

- (2004). *Statistics and Geostatistics in Environmental Monitoring*. 10.1016/B978-012064477-3/50005-9.
- Vengosh, A., Gill, J., Lee Davisson, M., & Bryant Hudson, G. (2002). A multi-isotope (B, Sr, O, H, and C) and age dating ( $^3\text{H}$ – $^3\text{He}$  and  $^{14}\text{C}$ ) study of groundwater from Salinas Valley, California: Hydrochemistry, dynamics, and contamination processes. *Water Resources Research*, 38(1). doi:10.1029/2001wr000517
- Vhahangwele Masindi, Mugeru W. Gitari, Hlanganani Tutu & Marinda Debeer (2015): Removal of boron from aqueous solution using magnesite and bentonite clay composite, *Desalination and Water Treatment*, DOI: 10.1080/19443994.2015.1025849
- Vilardi, G., Palma, L. D., & Verdone, N. (2018). Heavy metals adsorption by banana peels micro-powder: Equilibrium modeling by non-linear models. *Chinese Journal of Chemical Engineering*, 26(3), 455–464. doi: 10.1016/j.cjche.2017.06.026
- Vinson, D. S., Tagma, T., Bouchaou, L., Dwyer, G. S., Warner, N. R., & Vengosh, A. (2013). Occurrence and mobilization of radium in fresh to saline coastal groundwater inferred from geochemical and isotopic tracers (Sr, S, O, H, Ra, Rn). *Applied Geochemistry*, 38, 161-175. doi:10.1016/j.apgeochem.2013.09.004
- Visco, Steven J. (2015). *Manufacturing of Protected Lithium Electrodes for Advanced Lithium-Air, Lithium-Water & Lithium-Sulfur Batteries*. United States. doi:10.2172/1226495.
- Voutsas, D., Dotsika, E., Kouras, A., Poutoukis, D., & Kouimtzis, T. (2009). Study on distribution and origin of boron in groundwater in the area of Chalkidiki, Northern Greece by employing chemical and isotopic tracers. *Journal of Hazardous Materials*, 172(2-3), 1264–1272. doi: 10.1016/j.jhazmat.2009.07.132



- Walsh, M., Wallner, G., & Jennings, P. (2014). Radioactivity in drinking water supplies in Western Australia. *Journal of Environmental Radioactivity*, 130, 56-62. doi:10.1016/j.jenvrad.2013.12.016
- Wang, F., Wu, X., Li, C., Zhu, Y., Fu, L., Wu, Y., & Liu, X. (2016). Nanostructured positive electrode materials for post-lithium-ion batteries. *Energy & Environmental Science*, 9(12), 3570–3611. doi: 10.1039/c6ee02070d
- Wang, B., Guo, X., & Bai, P. (2014). Removal technology of boron dissolved in aqueous solutions – A review. *Colloids and Surfaces A: Physicochemical and Engineering Aspects*, 444, 338-344. doi:10.1016/j.colsurfa.2013.12.049
- Wang, S., Hu, J., Li, J., & Dong, Y. (2009). Influence of pH, Soil humic/fulvic acid, ionic STRENGTH, foreign ions and ADDITION sequences on adsorption of Pb(II) ONTO GMZ bentonite. *Journal of Hazardous Materials*, 167(1-3), 44-51. doi:10.1016/j.jhazmat.2008.12.079
- Wang, S., Chen, X., Zhang, Y., Zhang, Y., & Zheng, S. (2018). Lithium adsorption from brine by iron-doped titanium lithium-ion sieves. *Particuology*, 41, 40–47. doi: 10.1016/j.partic.2018.02.001
- Wang, Y., & Weinstock, I. A. (2012). Polyoxometalate-decorated nanoparticles. *Chemical Society Reviews*, 41(22), 7479. doi:10.1039/c2cs35126a
- Wagner, P. D., Fiener, P., Wilken, F., Kumar, S., Schneider, K. (2012): Comparison and evaluation of spatial interpolation schemes for daily rainfall in data scarce regions. *Journal of Hydrology* 464–465: 388–400. DOI: 10.1016/j.jhydrol.2012.07.026.
- Weil, M., & Ziemann, S. (2014). Recycling of Traction Batteries as a Challenge and Chance for Future Lithium Availability. *Lithium-Ion Batteries*, 509–528. doi: 10.1016/b978-0-444-59513-3.00022-4

- WHO. (2011). Molybdenum in Drinking Water: Background Document for Development of WHO Guidelines for Drinking-water Quality (WHO/SDE/WSH/03.04/ 11/Rev/1). World Health Organization, Geneva, Switzerland.
- WHO. (2017). Guidelines for drinking-water quality: fourth edition incorporating the first addendum. Geneva: World Health Organization; 2017. Licence: CC BY-NC-SA 3.0 IGO. Retrieved from [https://www.who.int/water\\_sanitation\\_health/publications/drinking-water-quality-guidelines-4-including-1st-addendum/en/](https://www.who.int/water_sanitation_health/publications/drinking-water-quality-guidelines-4-including-1st-addendum/en/).
- WMO, World Meteorological Organization, (2013): World Weather Information Service. <http://www.worldweather.org/116/c00221.htm>.
- Wolska, J., & Bryjak, M. (2013). Methods for boron removal from aqueous solutions- A review. *Desalination*, 310, 18-24. doi:10.1016/j.desal.2012.08.003
- Wongsasuluk, P., Chotpantarat, S., Siriwong, W., & Robson, M. (2013). Heavy metal contamination and human health risk assessment in drinking water from shallow groundwater wells in an agricultural area in Ubon Ratchathani Province, Thailand. *Environmental Geochemistry and Health*, 36(1), 169-182. doi:10.1007/s10653-013-9537-8
- Wu, W., Tang, X., Ma, X., & Liu, H. (2015). A comparison of spatial interpolation methods for soil temperature over a complex topographical region. *Theoretical and Applied Climatology*, 125(3-4), 657-667. doi:10.1007/s00704-015-1531-x
- Wulfsberg, G. (1995). Principles of descriptive inorganic chemistry. Sausalito: University Science Books. ISBN-13: 978-0935702668
- Xiao, Y., Gu, X., Yin, S., Shao, J., Cui, Y., Zhang, Q., & Niu, Y. (2016). Geostatistical interpolation model selection based on ArcGIS and spatio-temporal

- variability analysis of groundwater level in piedmont plains, northwest China. Springer Plus, 5(1). doi: 10.1186/s40064-016-2073-0
- Xie, Y., Chen, T. B., Lei, M., Yang, J., Guo, Q. J., Song, B., Zhou, X. Y. (2011). Spatial distribution of soil heavy metal pollution estimated by different interpolation methods: Accuracy and uncertainty analysis. – Chemosphere 82: 468–476. DOI: 10.1016/j.chemosphere.2010.09.053.
- Xie, Y., Ren, L., Zhu, X., Gou, X., & Chen, S. (2018). Physical and chemical treatments for removal of perchlorate from water—a review. Process Safety and Environmental Protection, 116, 180-198. doi:10.1016/j.psep.2018.02.009
- Xu, M., & McKay, G. (2017). Removal of Heavy Metals, Lead, Cadmium, and Zinc, Using Adsorption Processes by Cost-Effective Adsorbents. Adsorption Processes for Water Treatment and Purification, 109-138. doi:10.1007/978-3-319-58136-1\_5
- Yadav, S. K., Singh, D. K., & Sinha, S. (2013). Adsorption study of lead(ii) onto xanthated date palm trunk: Kinetics, isotherm and mechanism. Desalination and Water Treatment, 51(34-36), 6798-6807. doi:10.1080/19443994.2013.792142
- Yang, S., Li, J., Lu, Y., Chen, Y., & Wang, X. (2009). Sorption of NI(II) on gmz bentonite: Effects of pH, ionic STRENGTH, FOREIGN ions, humic acid and temperature. Applied Radiation and Isotopes, 67(9), 1600-1608. doi:10.1016/j.apradiso.2009.03.118
- Yang, Z., Ma, X., & Tang, C. Y. (2018). Recent development of novel membranes for desalination. Desalination, 434, 37-59. doi:10.1016/j.desal.2017.11.046
- Ye, L., You, H., Yao, J., & Su, H. (2012). Water treatment technologies for perchlorate: A review. Desalination, 298, 1-12. doi:10.1016/j.desal.2012.05.006
- Yehia, M., Baghdady, A., Howari, F. M., Awad, S., & Gad, A. (2017). Natural radioactivity and groundwater quality assessment in the northern area of the

- Western desert of Egypt. *Journal of Hydrology: Regional Studies*, 12, 331-344.  
doi:10.1016/j.ejrh.2017.06.002
- Yizhak, M. (1989). Ionic radii in aqueous solutions. *ChemInform*, 20(17).  
doi:10.1002/chin.198917352
- Zhang, J., Huang, G., Liu, C., Zhang, R., Chen, X., & Zhang, L. (2018). Synergistic effect of microbubbles and activated carbon on the ozonation treatment of synthetic dyeing wastewater. *Separation and Purification Technology*, 201, 10-18.  
doi:10.1016/j.seppur.2018.02.003
- Zhang, W., Mou, Y., Zhao, S., Xie, L., Wang, Y. Chen J. (2017). Adsorption Materials for Lithium Ion from Brine Resources and Their Performances. *Progress in Chemistry*, 29(2/3): 231-240. *Progress in Chemistry*2017, Vol. 29, Issue (2/3): 231-240 DOI: 10.7536/PC161012
- Zhao, D. (2008). Adsorption of thorium (IV) on MX-80 bentonite: Effect of pH, ionic strength and temperature. *Applied Clay Science*,41(1-2), 17-23.  
doi:10.1016/j.clay.2007.09.012
- Zhao, Z., Xu, X., Chen, X., Huo, G., Chen, A., Liu, X., & Xu, H. (2012). Thermodynamics and kinetics of adsorption of molybdenum blue with d301 ion exchange resin. *Transactions of Nonferrous Metals Society of China*, 22(3), 686-693. doi:10.1016/s1003-6326(11)61232-6
- Zhou, Y. (2009). A critical review of groundwater budget myth, safe yield and sustainability. *Journal of Hydrology*, 370(1-4), 207–213. doi: 10.1016/j.jhydrol.2009.03.009

## APPENDIX

### Appendix A: Groundwater Physical and Chemical Analysis.

Table 1. Some International Concentrations of Groundwater Chemical Analysis.

Country	concentration (µg/L)													References
	Pb	Mo	Zn	Fe	Cd	As	Cu	Mn	Cr	Cl	F	NO3	SO4	
Qatar	76	103	14698	1904	8.67	71.6	-	-	-	1540000	1880	23600	1330000	(Shomar, 2015; Kuiper et al., 2015)
KSA (Hail and Al-Ahsa)	11-70	-	98-331	216	21	-	128-276	937	-	21300-3191000	-	4390	16800-1242000	(Abdel-Satar et al., 2017; Assubaie, 2015)
Oman (Al-Zorouf)	11	50	276	54	3	57	2	7	19	299800	-	62000	72500	(Al-Shidi, 2014)
UAE (Al-kathim)	-	-	8.2	-	429	-	-	-	5.5	1115500	-	315700	1512600	(Khan et al., 2019)
Egypt	30.04		490.2	1061.4	-	-	209.9	30.9	1271.2	930000	-	31000	995000	(Bassioni et al., 2015; Awad, 2019)
Palestine	45.8	11.3	11.8	-	1.17	-	143.6	112.6	56	104000	-	24000	3400	(Malassa et al., 2014; Shadeed, 2016)
Azerbaijan	0.79	-	49.33	-	6.55		16.23	-	3.41	3000-540000	-	2000-75000	18000-1270000	(Taghipour et al., 2012; Alakbarov, 2019)
India	-	-	-	-	<1	<1	-	-	-	517490	1310	28220	22220	(Mohankumar, 2016; Narsimha, 2012)
USA	0.07-480	1-4700	-	7.9-81000	<1-16	0.79-550	1-2000	7-28000	1.2-150	3280	3670	10000	5060	(Ayotte et al., 2011; DeSimone et al., 2014)

Table 2. Comparison the Results of General Water Quality Parameters with the National and International Standards and Guidelines.

Parameter	Number & frequency of detection	Min	Max	Mean	Number of exceedances	WHO (WHO, 2017)		USEPA		QATAR & GSO (GSO, 2008).	
						Drinking Water	Irrigation Water	Drinking Water (EPA, 2018)	Irrigation Water (EPA, 2004)	Drinking Water (Kahramaa, 2014)	Irrigation Water (FAO, 1994)
General Water Quality Parameters											
pH	41 100%	6.89	7.94	7.3	-	6.5-8.5	-	6.5-8.5	6.5-8.5	6.5-8.5	6-8.5
Electrical Conductivity (EC), $\mu\text{S}/\text{cm}$	41 100%	920	22330	7298.8	39 > 1200 38 > 3000	1200	-	-	-	-	3000
Total Dissolved Solid (TDS), mg/L	41 100%	598.87	15633.3	5109.16	41 > 500 39 > 1000 38 > 2000	1000	-	500	2000	1000	2000
Hardness, mg $\text{CaCO}_3/\text{L}$	41 100%	275.16	5393.01	2120.20	41 > 120 39 > 500	500 ***	-	-	-	-	120
Total Organic Carbon (TOC), mg/L	41 100%	1.27	35.50	14.62	-	-	-	-	-	-	75
Anions and Cations											
Calcium ( $\text{Ca}^{++}$ ), mg/L	41 100%	69.94	1497.85	570.16	40 > 80 35 > 300 29 > 400	300 ***	-	-	-	80 **	400
Magnesium ( $\text{Mg}^{++}$ ), mg/L	41 100%	24.41	420.19	169.13	39 > 30 38 > 60	-	-	-	-	30 mg/l **	60
Sodium ( $\text{Na}^+$ ), mg/L	41 100%	64.22	5547.10	1466.48	41 > 60 39 > 80 39 > 200 20 > 920	200 ***	-	60	-	80 **	920
Potassium ( $\text{K}^+$ ), mg/L	41 100%	16.36	320	90.18	41 > 2 41 > 4	-	-	-	-	4 **	2
Fluoride (F), mg/L	41 100%	1.59	8.77	3.81	41 > 1 41 > 1.5 14 > 4	1.5	-	4	1	1.5	15
Chloride ( $\text{Cl}^-$ ), mg/L	41 100%	203.68	30806.68	6289.48	41 > 80 35 > 300 39 > 1059	250	-	250	-	80 **	1059
Bromide ( $\text{Br}^-$ ), mg/L	41 100%	.37	21.98	4.32	41 > 0.1	-	-	-	-	0.1 **	-
Nitrate ( $\text{NO}_3^-$ ), mg/L	41 100%	.00	113.34	36.32	36 > 10 10 > 50	50	-	10	-	50	10

Sulfate (SO <sub>4</sub> <sup>-</sup> ), mg/L	41 100%	53.46	11596.33	4977.16	41 > 50 39 > 250 39 > 400	250 ***	-	250	-	50 **	400
Chemical Analyte											
Boron, mg/L	41 100%	0.388	3.819	1.884	39 > 0.75 20 > 2 8 > 2.4 3 > 3	2.4	-	6 *	2 Long term use 0.75 short term use	2.4	3
Lithium, mg/L	41 100%	0.023	0.236	0.1205	39 > 0.05	-	-	-	2.5	0.05	-
Molybdenum, mg/L	41 100%	0.0078	0.293	0.0538	9 > 0.07 23 > 0.04 18 > 0.05 40 > 0.01	0.07	-	0.04*	0.05 Long term use 0.01 short term use	0.07	-
Selenium, mg/L	41 100%	0.00154	0.022	0.0088	1 > 0.02	0.04	-	0.05	0.02	0.04	-
Uranium, mg/L	41 100%	0.00011	0.031	0.0016	1 > 0.02 1 > 0.03	0.03	-	0.02	-	0.03	-
Chromium, mg/L	41 100%	0.0001	0.0118	0.0039	2 > 0.01	0.05	-	0.1	1 Long term use 0.1 short term use	0.05	For crop 0.01 For grass 0.2
Strontium, mg/L	41 100%	3.53	20.27	13.22	40 > 4	-	-	4 *	-	4	-
Aluminum, mg/L	10 24%	0.00015	0.00761	0.0015	-	0.2	5	0.2 mg/L	20 Long term use 5 short term use	0.2 **	15
Copper, mg/L	41 100%	0.00008	0.0044	0.00137	-	2	-	1.3	5 Long term use 0.2 short term use	2	For crop 0.2 for grass 0.5
Cobalt, mg/L	41 100%	<di	0.00046	0.000071	-	-	-	-	5 Long term use 0.05 short term use	.002	0.2

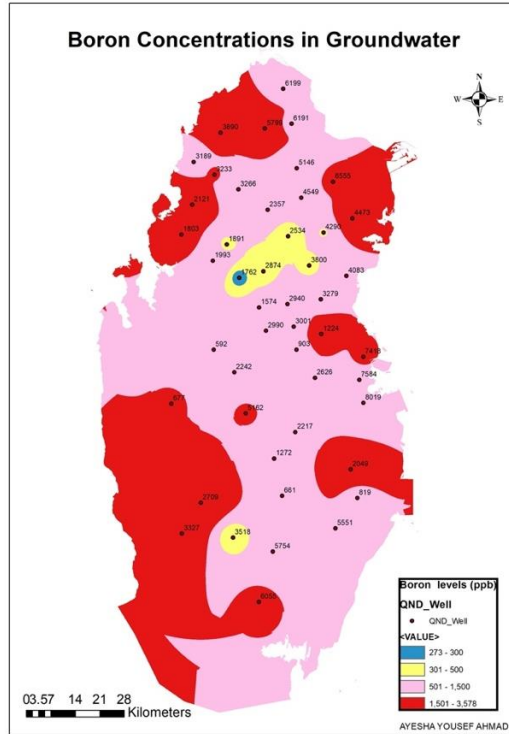
Iron, mg/L	38 29%	0.00001	0.118	0.0047	-	-	-	0.3	20 Long term use 5 short term use	0.3**	1
Manganese, mg/L	41 100%	<di	0.0049	0.001	-	0.4	-	0.05*	10 Long term use 0.2 short term use	0.4	0.05
Cadmium, mg/L	31 75%	<di	0.00049	0.000072	-	0.003	-	0.005	0.05 Long term use 0.01 short term use	0.003	.05
Lead, mg/L	0	<di	<di		-	0.01	-	0.015	10 Long term use 5 short term use	0.01	0.1
Barium, mg/L	41 100%	0.003	0.0246	0.01	-	1.3	-	2	-	0.7	2
Beryllium, mg/L	13 31%	<di	0.00014	0.000081	-	-	-	0.004	0.5 Long term use 0.1 short term use	0.004**	-
Silver, mg/L		<di	<di		-	-	-	0.1	-	0.1**	-
Arsenic, mg/L	41 100%	0.0006	0.005	0.002	-	0.01	.05	.01	2 Long term use 0.1 short term use	0.01	0.1
Nickel, mg/L	41 100%	0.00024	0.0116	0.0019	-	0.02	-	0.1*	2 Long term use 0.2 short term use	0.07 mg/l	For crop 0.2 for grass 0.5
Zinc, mg/L	20 48%	0.00003	0.0512	0.00588	-	3	-	5	2	3**	0.5

Note \* Life-time risk health advisory, \*\* KHHRAMAA requirements for water quality distribution system, \*\*\* Taste threshold.

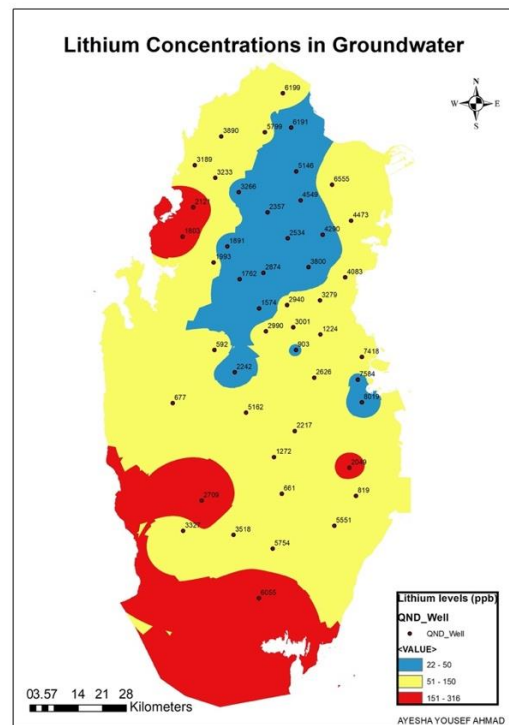


# Appendix B: Geostatistical Analysis

A.



B.



C.

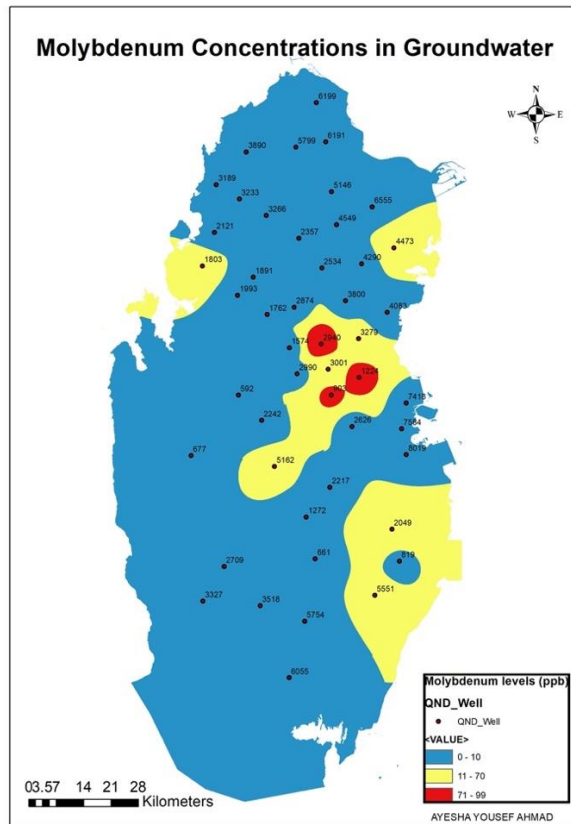


Figure 1. Maps generated for A. boron, B. lithium and C. Molybdenum concentrations in Qatar's groundwater using the interpolation technique.

Table 1. Interpolation methods Comparison (Li and Heap, 2014).

	<b>IDW</b>	<b>RBFS</b>	<b>Kriging</b>
<b>Class of interpolation</b>	Local deterministic interpolation	Local deterministic interpolation	Geostatistical interpolation
<b>Predicted values</b>	One prediction per location	One prediction per location	Prediction and measurement of the prediction uncertainty
<b>Modeling spatial autocorrelation</b>	Implicit: the model builds on the assumption of spatial autocorrelation in the data.	No	Yes
<b>Output type</b>	Prediction	Prediction	prediction, probability and prediction error
<b>Level of assumption / Complexity of the model</b>	Few	Intermediate: Normal distributed data	Many: data transformation (data originates from a stationary stochastic systems), trend removal and de-clustering
<b>Input data values</b>	Exact: the output surface contains exact values of the input data.	Exact: the output surface contains exact values of the input data.	Inexact: produces values which correspond to the input data value. If the measurement error is zero, then kriging is an exact interpolator
<b>Output surface</b>	Not smooth	Smooth	Intermediate
<b>Uncertainty of the prediction values</b>	No	No	Yes

## pH Levels in Groundwater

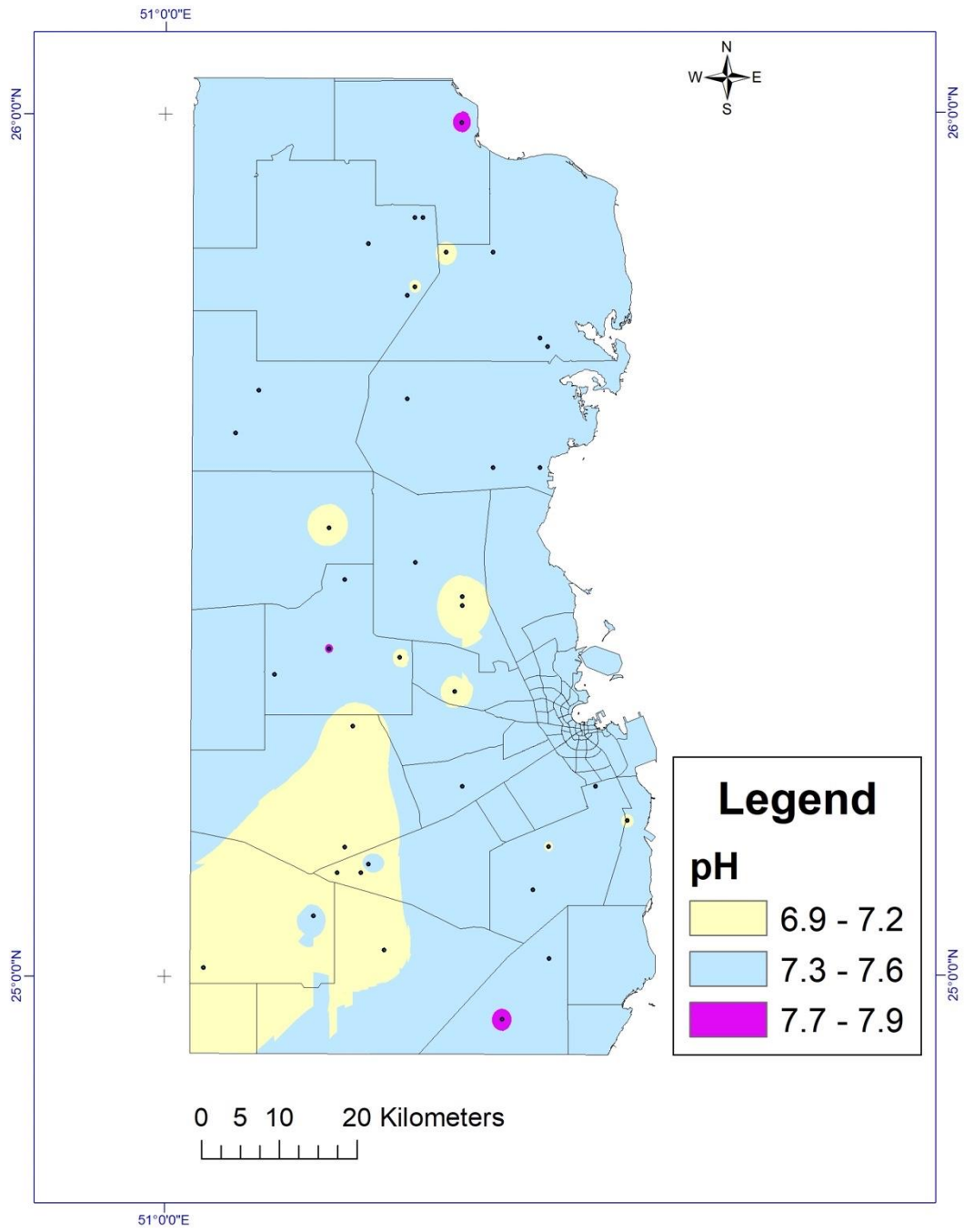


Figure 2. Spatial distribution of pH in the study area.

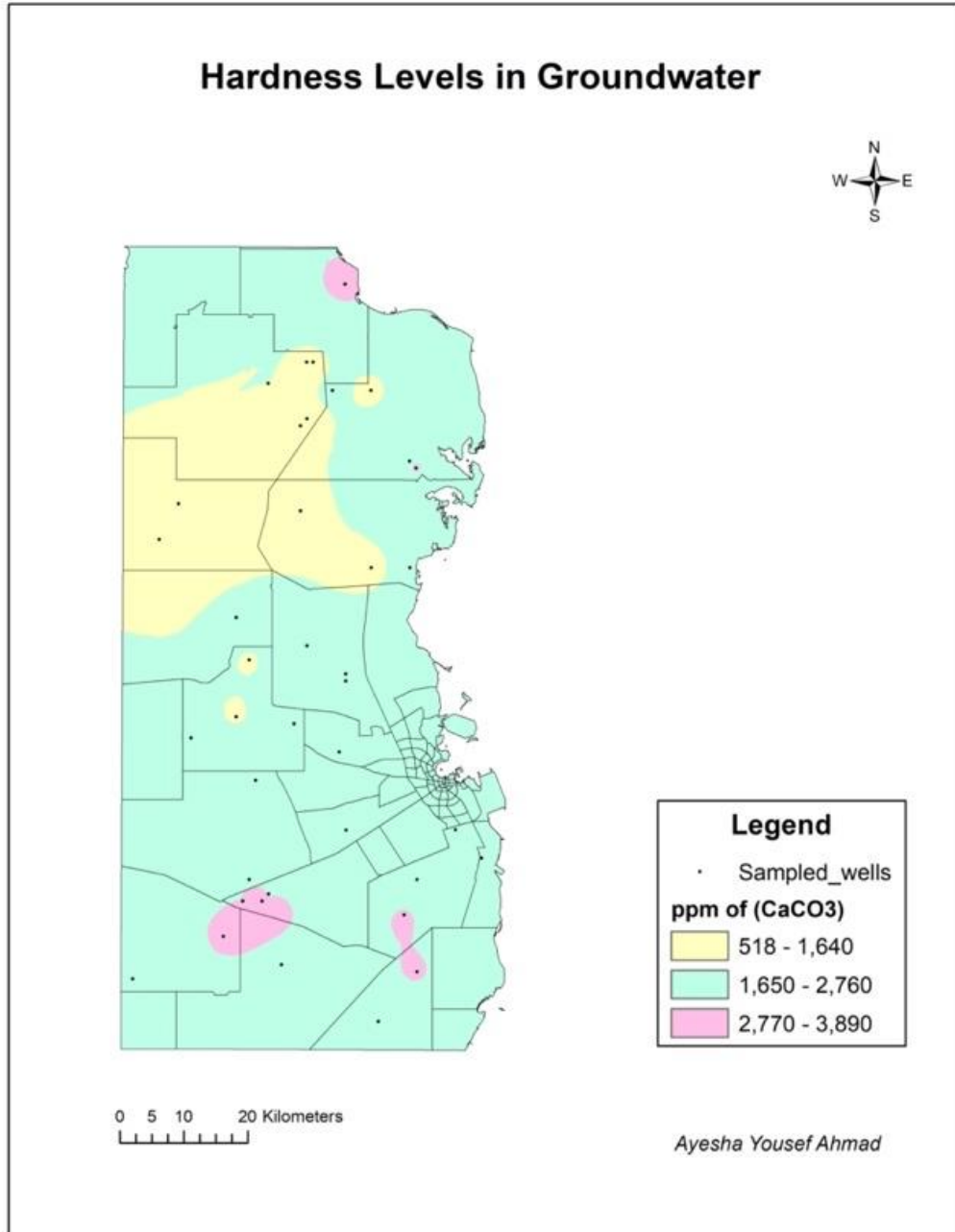


Figure 3. Spatial distribution of Hardness in the study area.

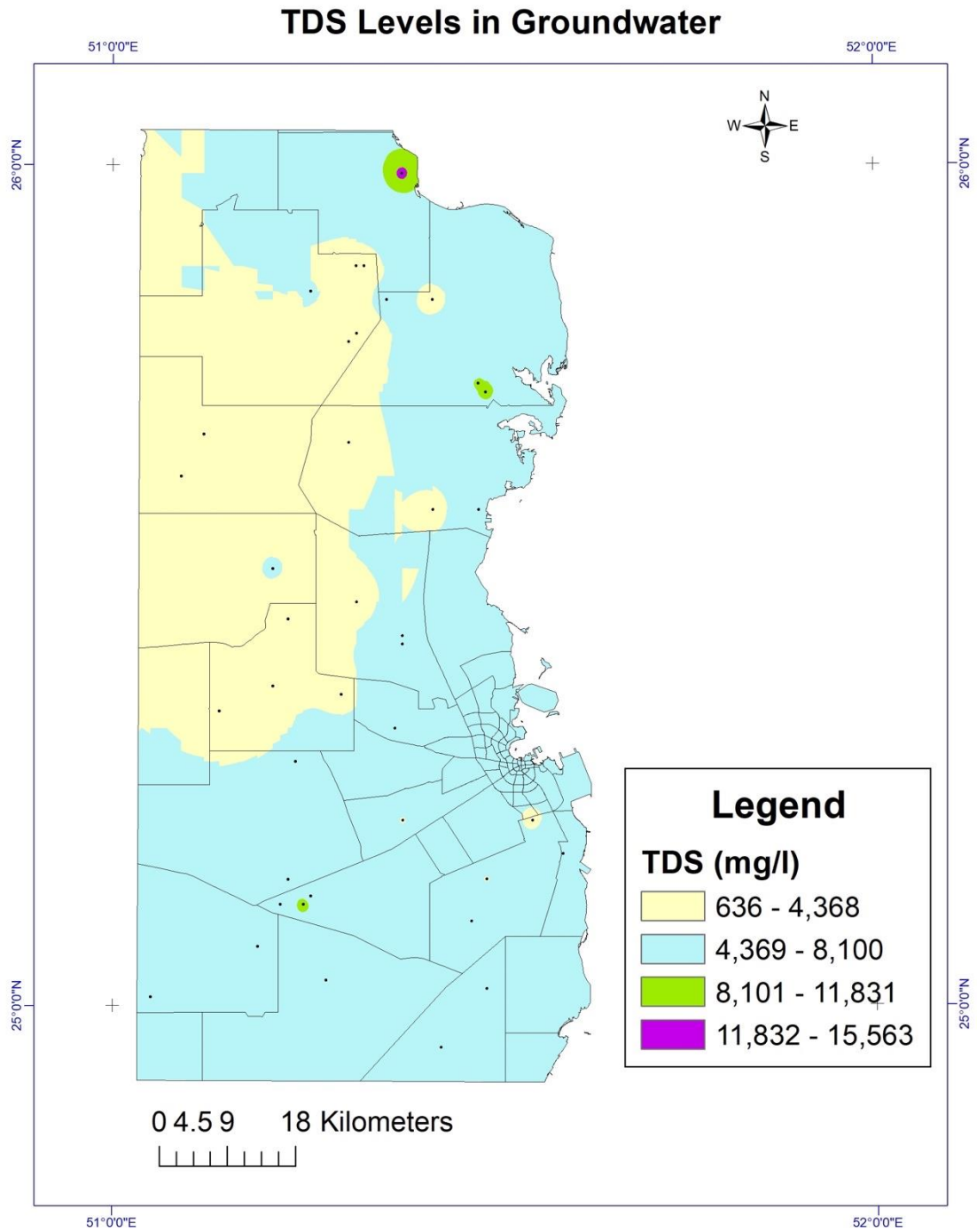


Figure 4. Spatial distribution of TDS in the study area.

## Sodium Levels in Groundwater

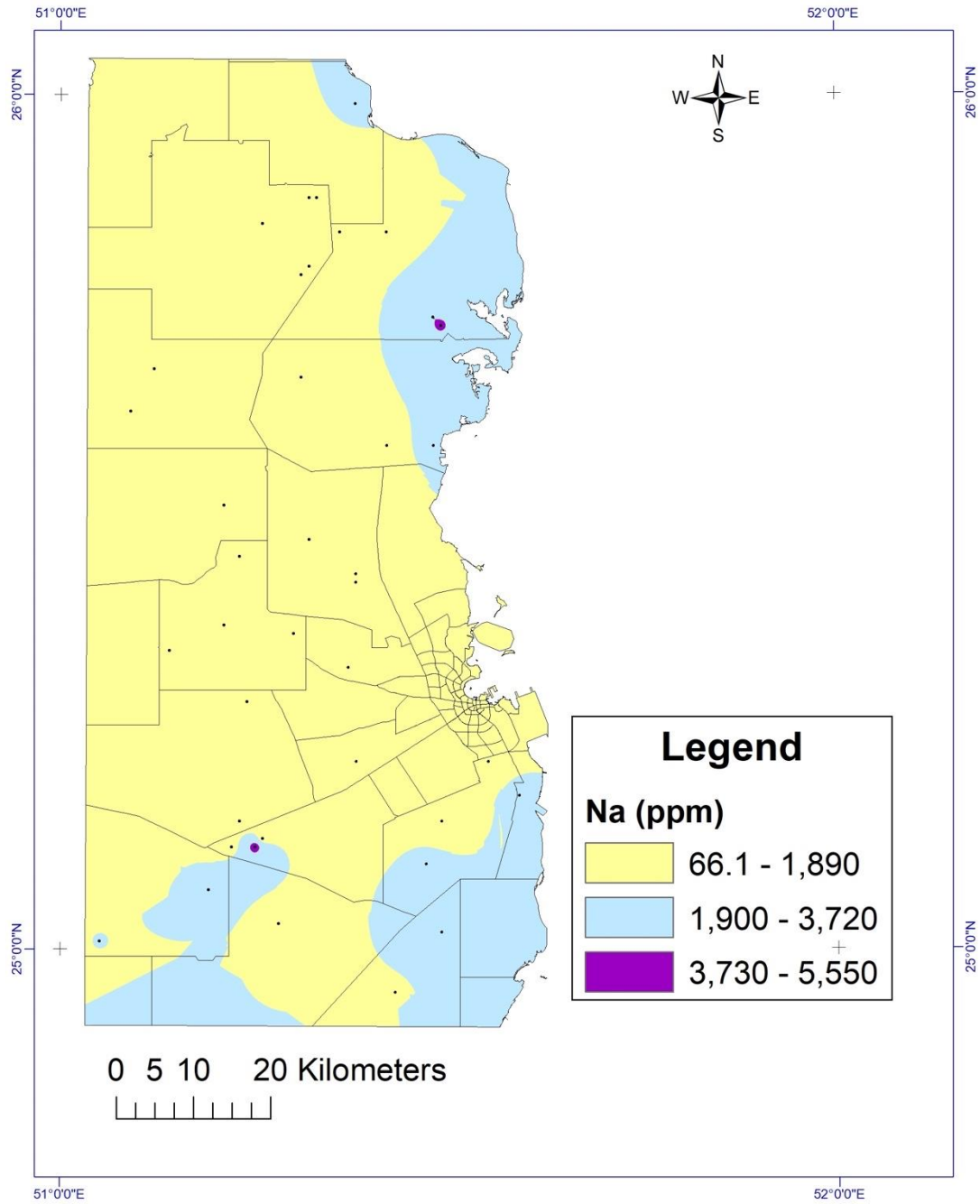


Figure 5. Spatial distribution of Sodium in the study area.

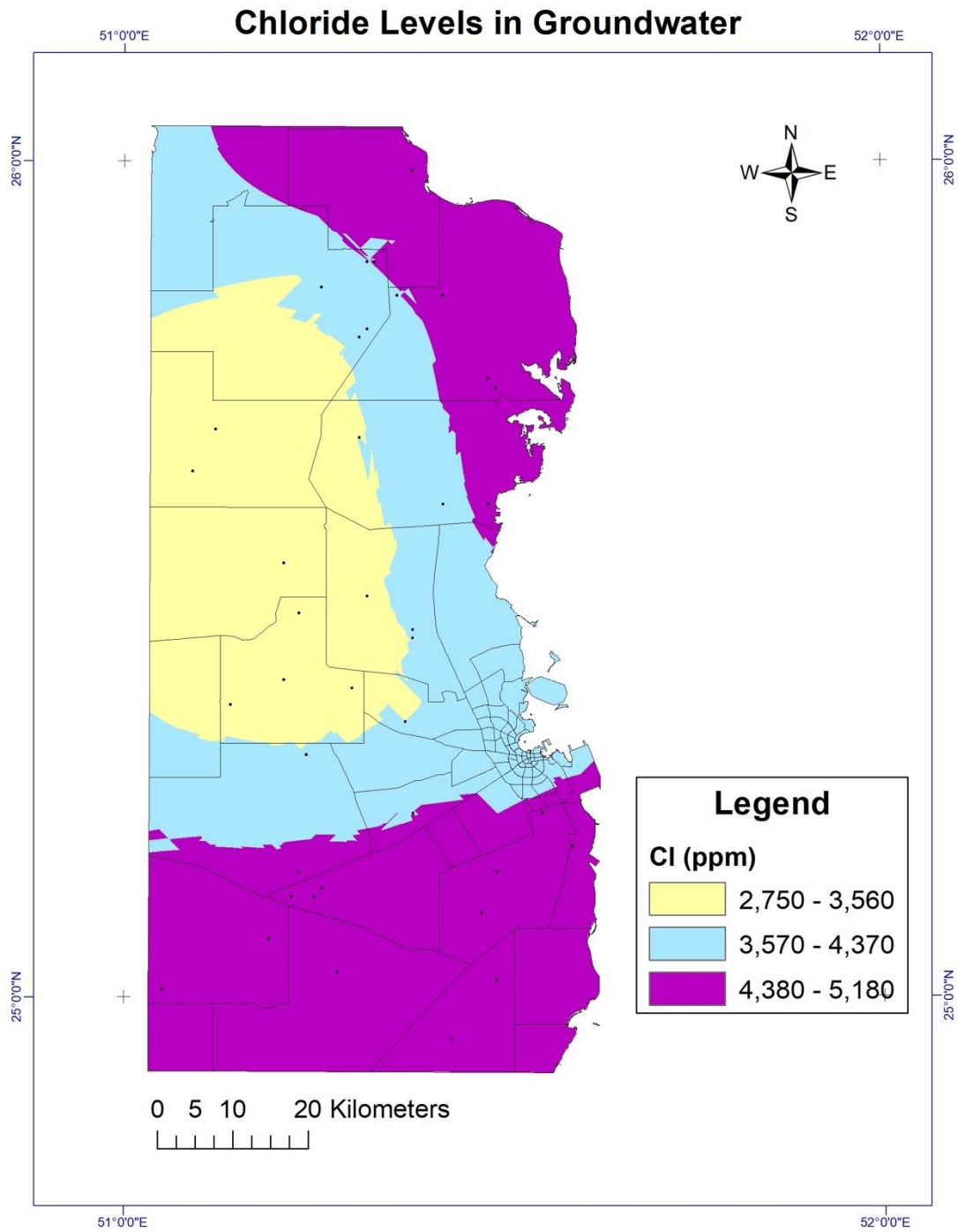


Figure 6. Spatial Distribution of Chloride in the study area.



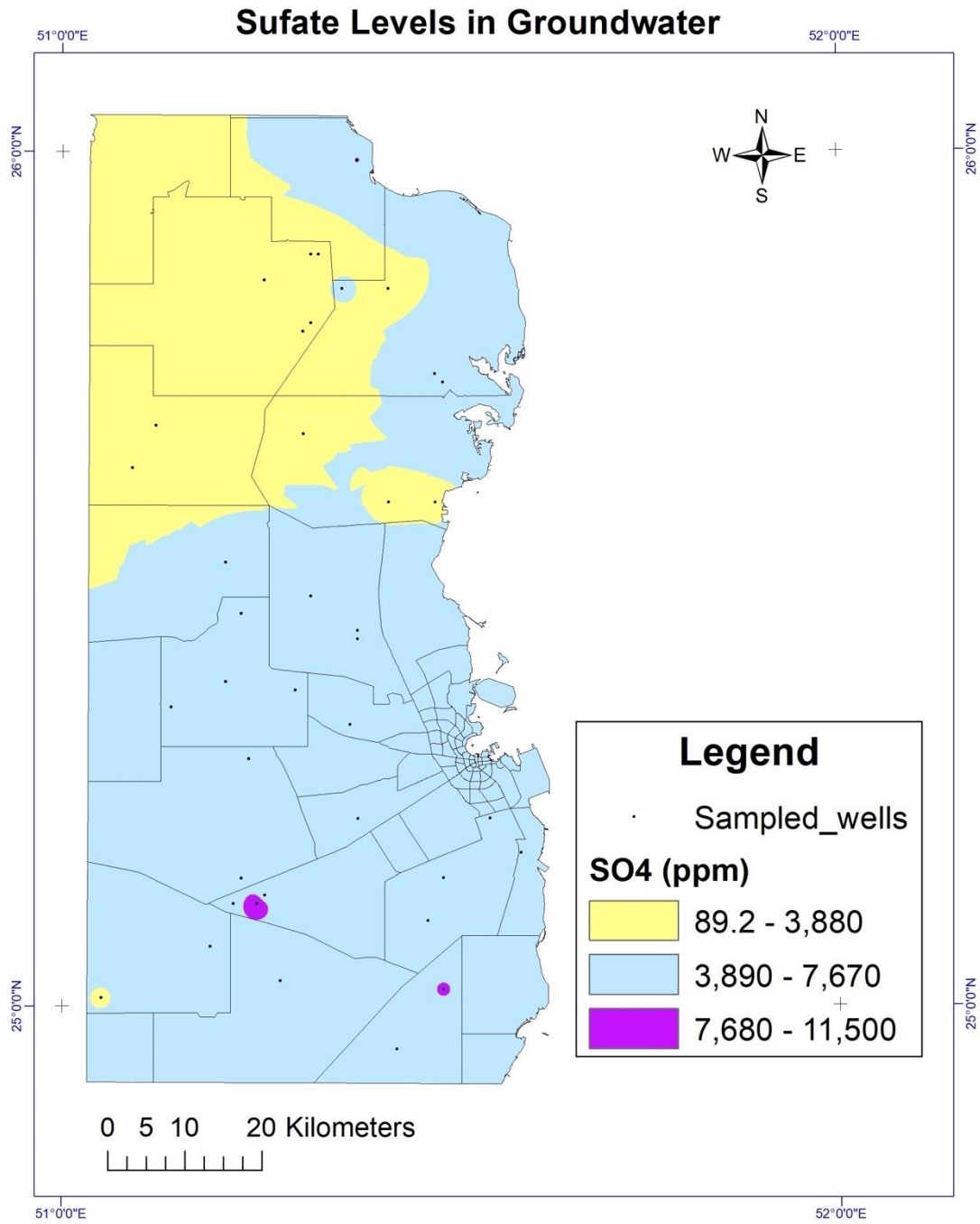


Figure 7. Spatial Distribution of Sulfate in the study area.

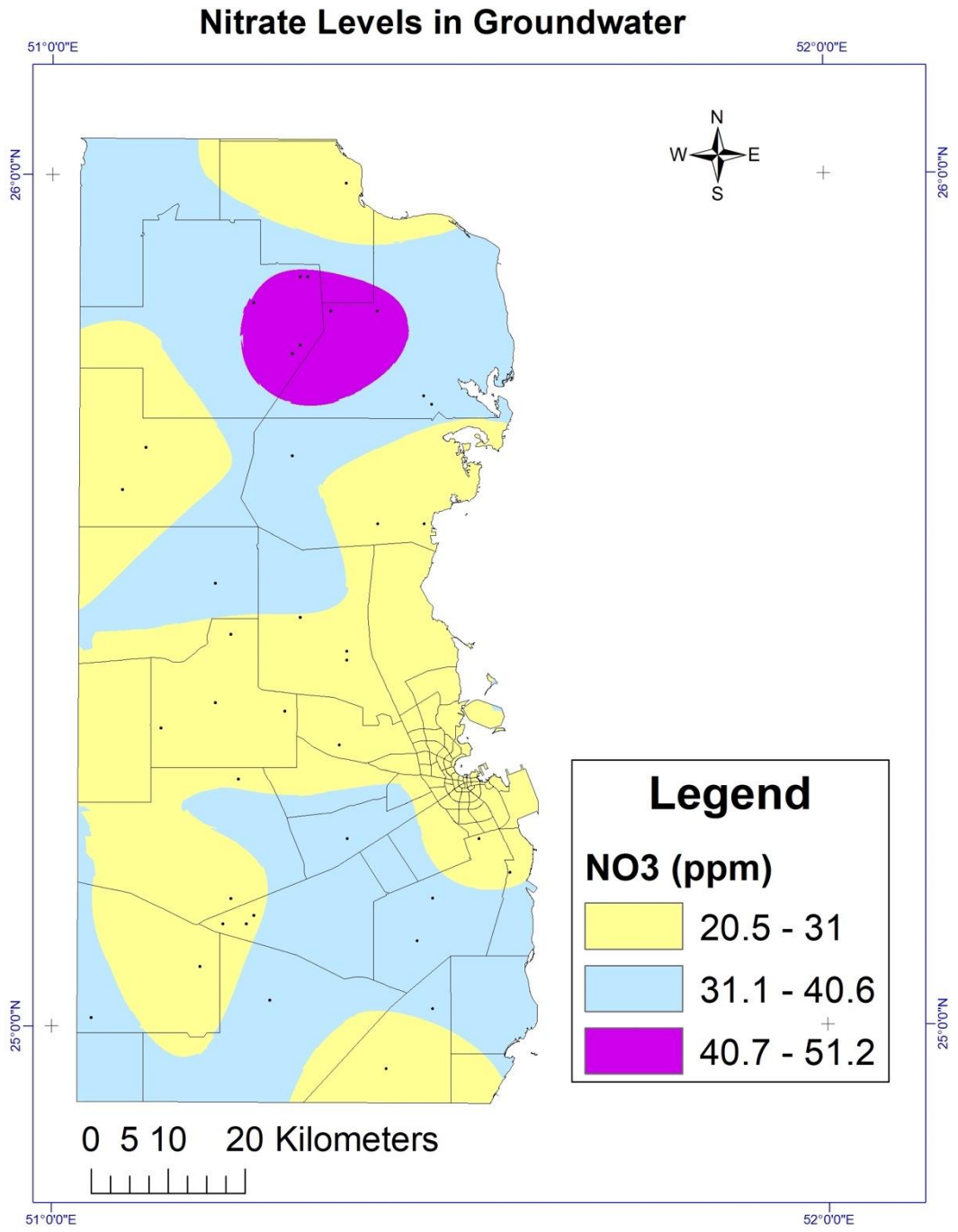


Figure 8. Spatial Distribution of Nitrate in the study area.

## Boron Levels in Groundwater

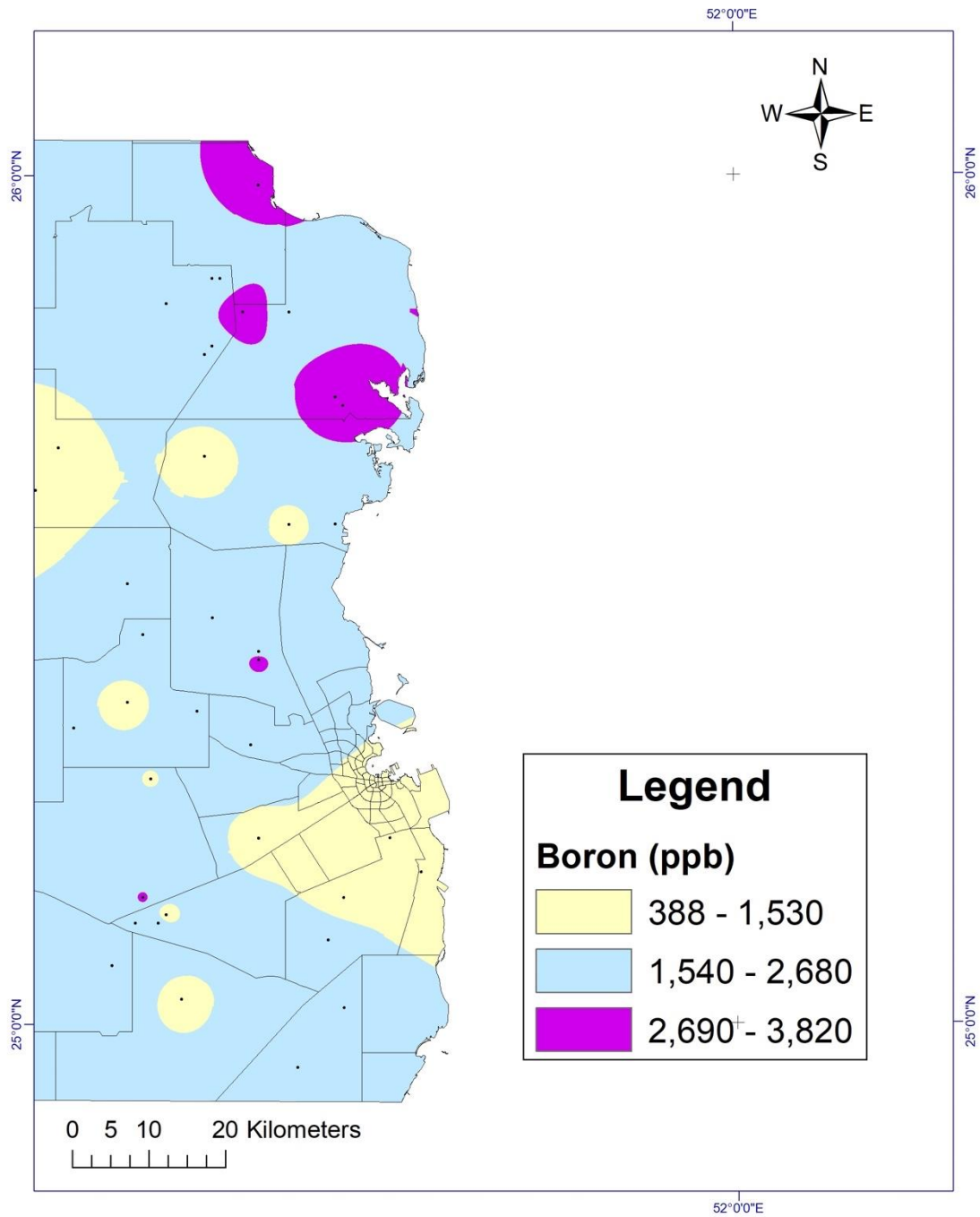


Figure 8. Spatial Distribution of Boron, in the study area.

## Selenium Levels in Groundwater

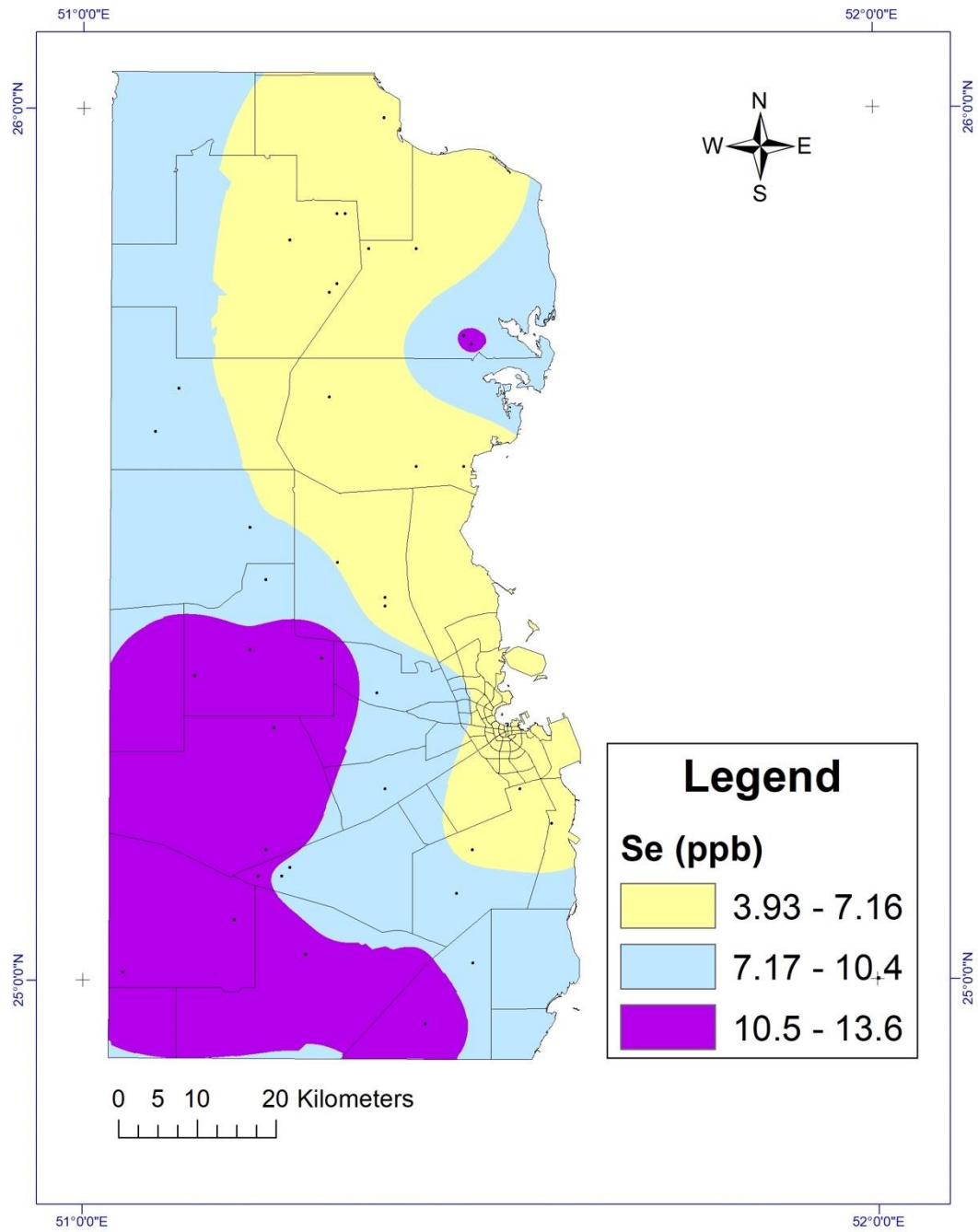


Figure 9. Spatial Distribution of Selenium, in the study area.

# Lithium Levels in Groundwater

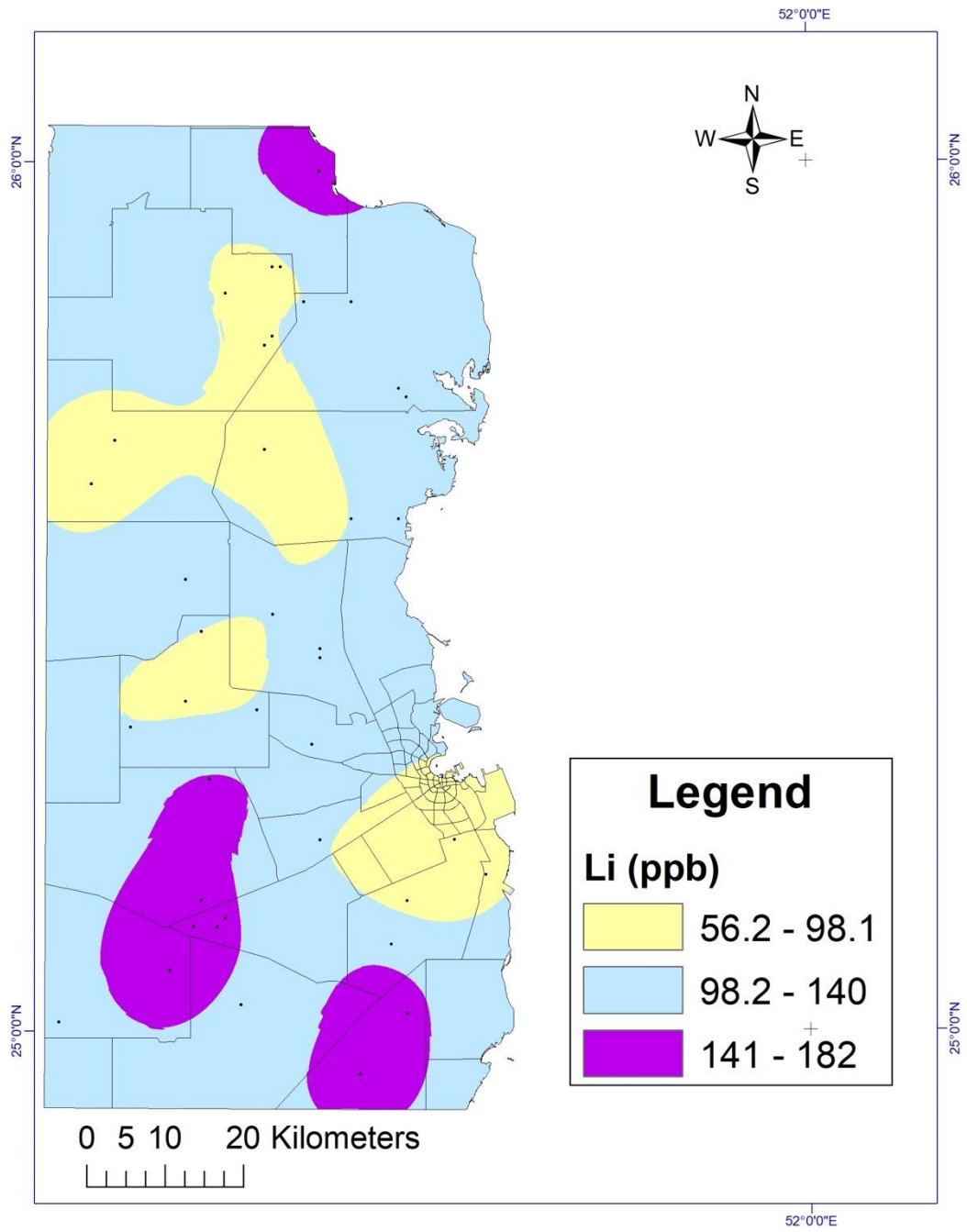


Figure 10. Spatial Distribution of Lithium, in the study area.

# Molybdenum Levels in Groundwater

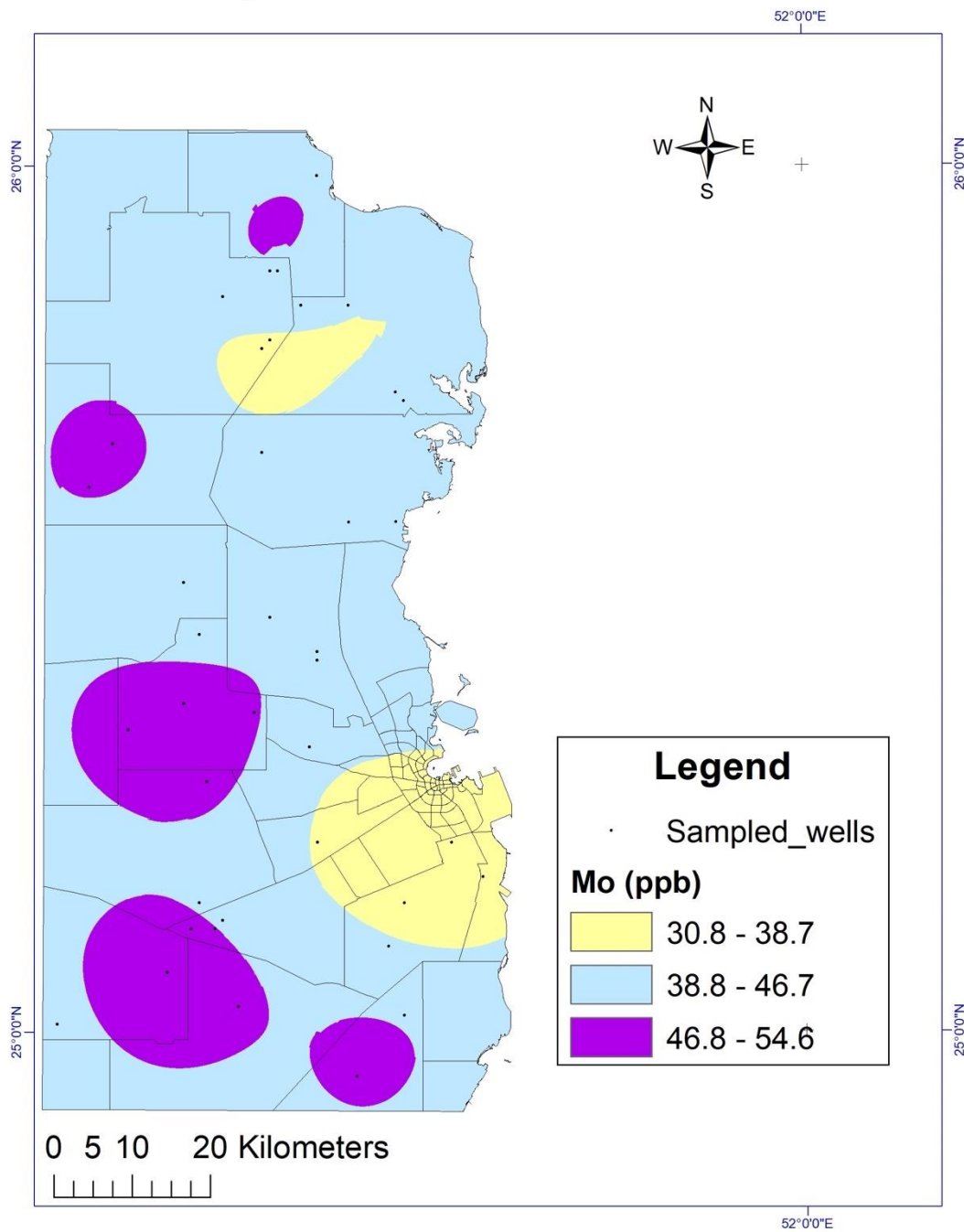


Figure 11. Spatial Distribution of Molybdenum in the study area.

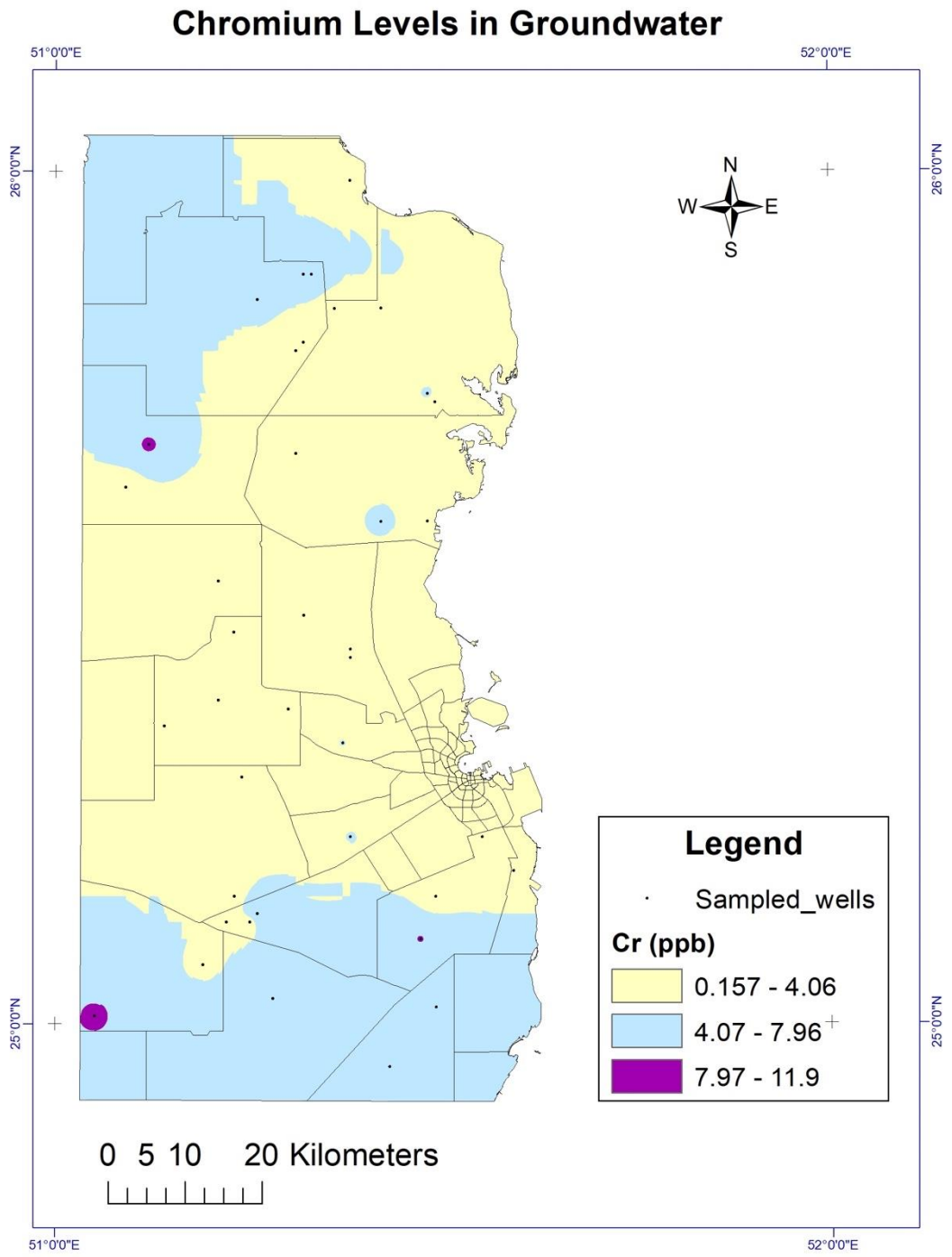


Figure 12. Spatial Distribution of Chromium, in the study area.

### Strontium Levels in Groundwater

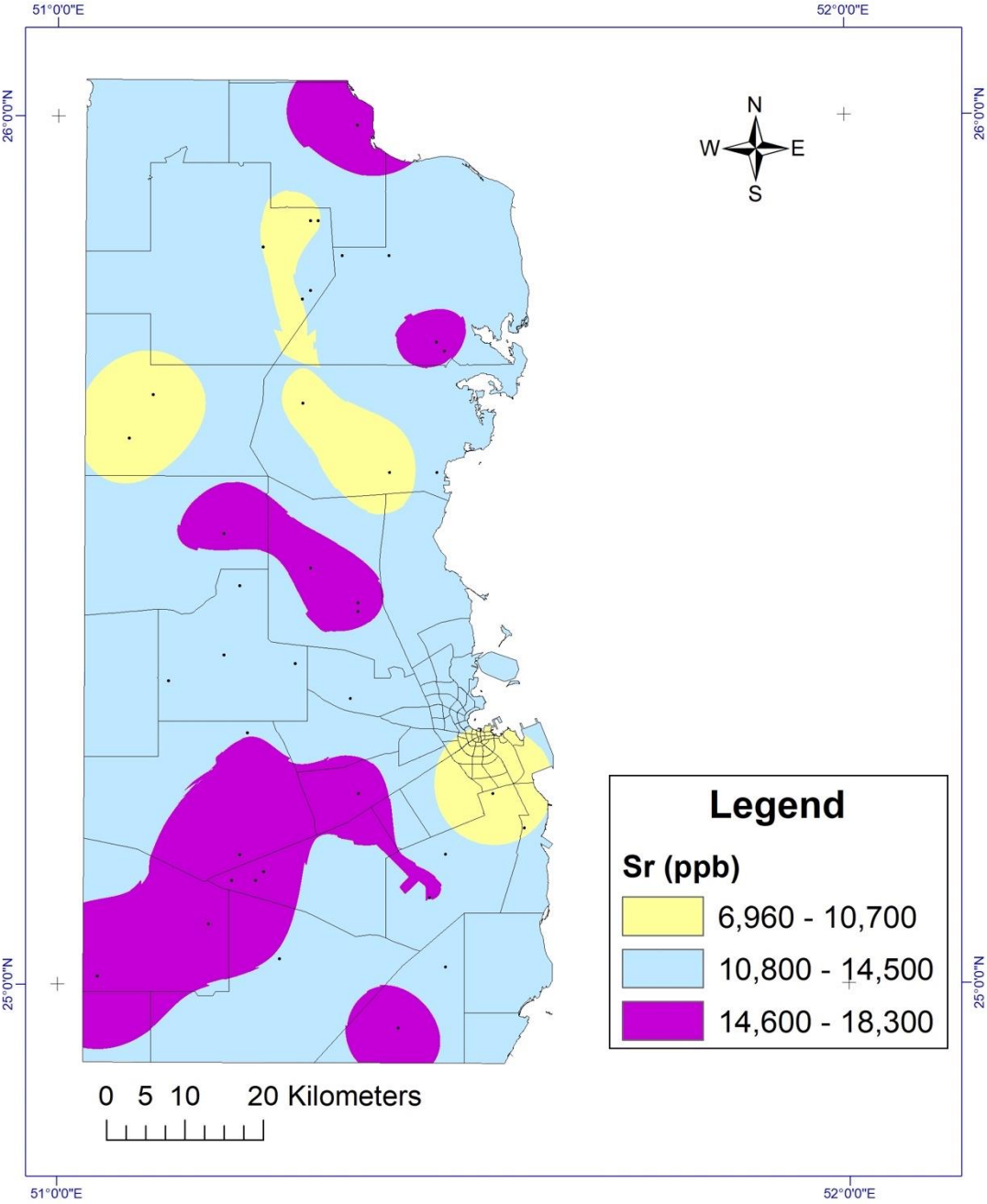


Figure 13. Spatial Distribution of Strontium in the study area.



# SAR Levels in Groundwater

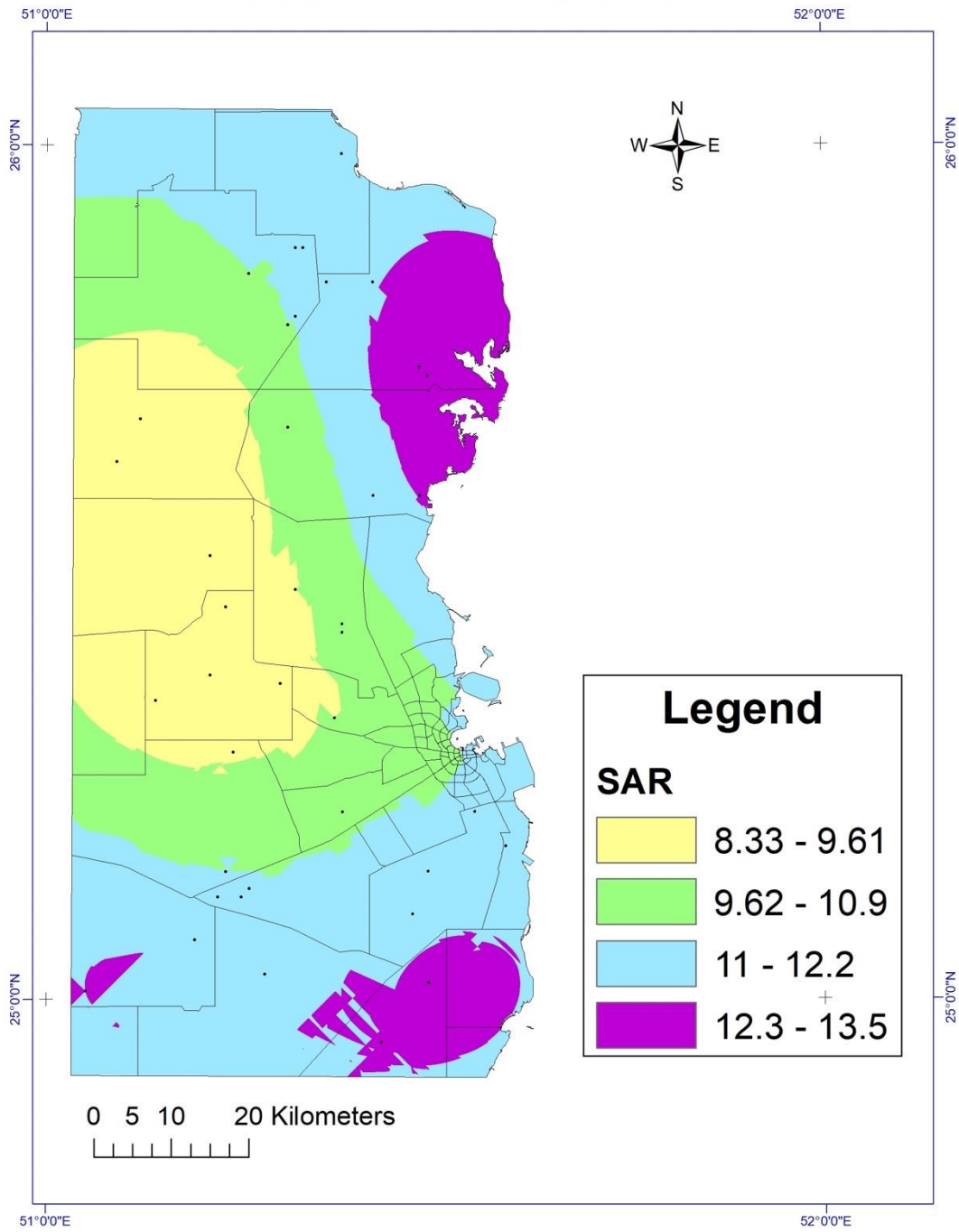


Figure 14. Spatial Distribution of SAR in the study area.

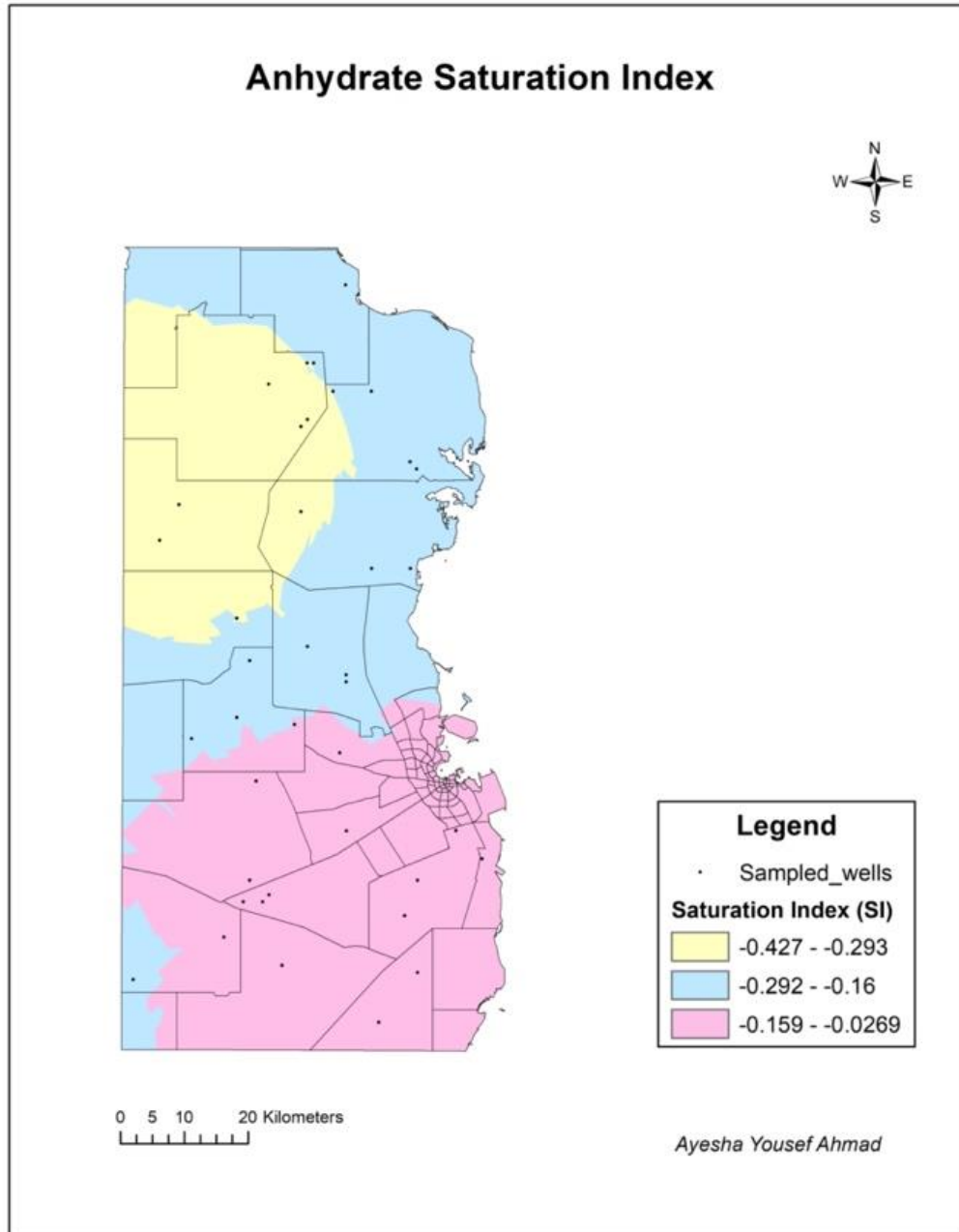


Figure 15. Interpolation maps for anhydrate in the study area.

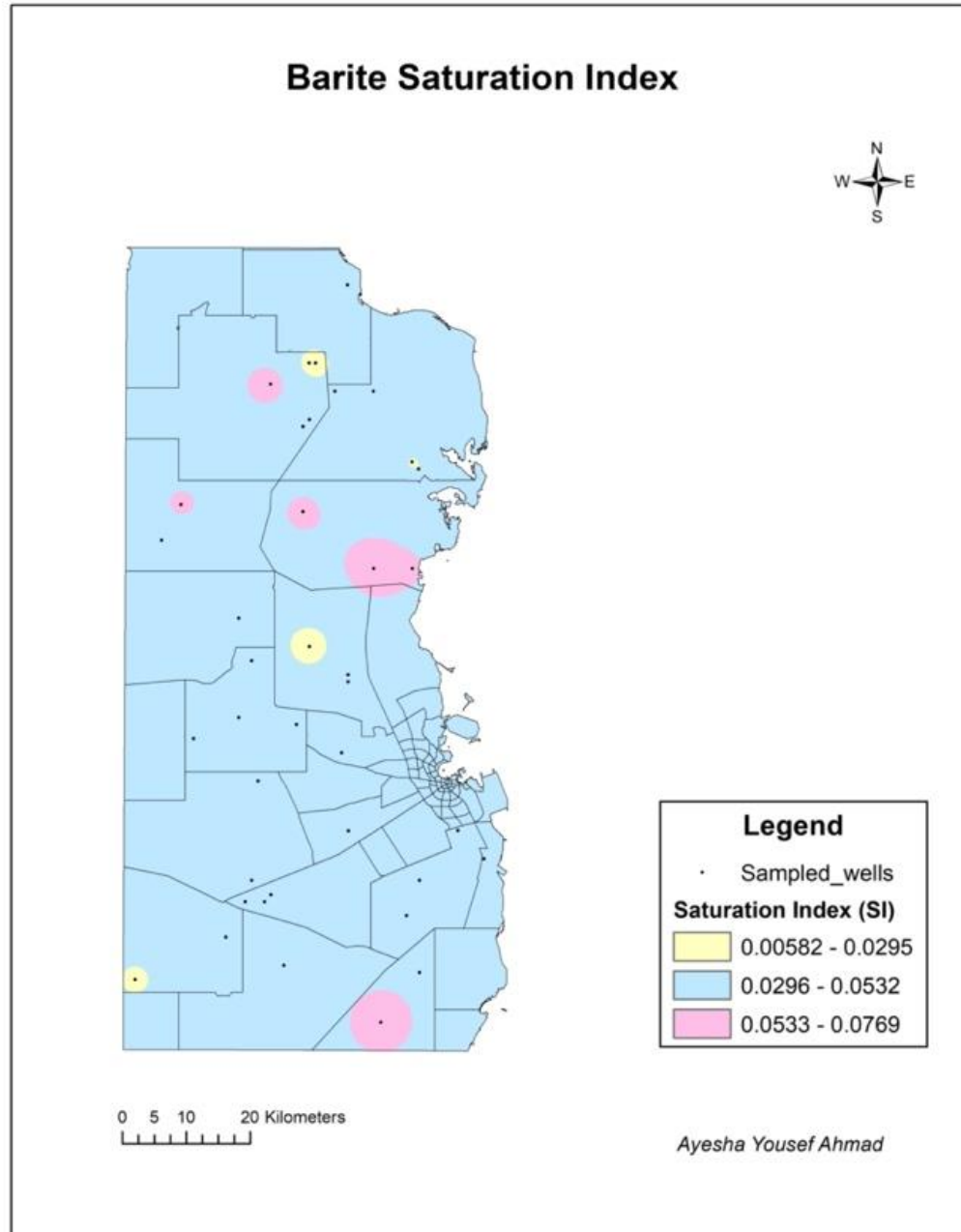


Figure 16. Interpolation maps for barite in the study area.

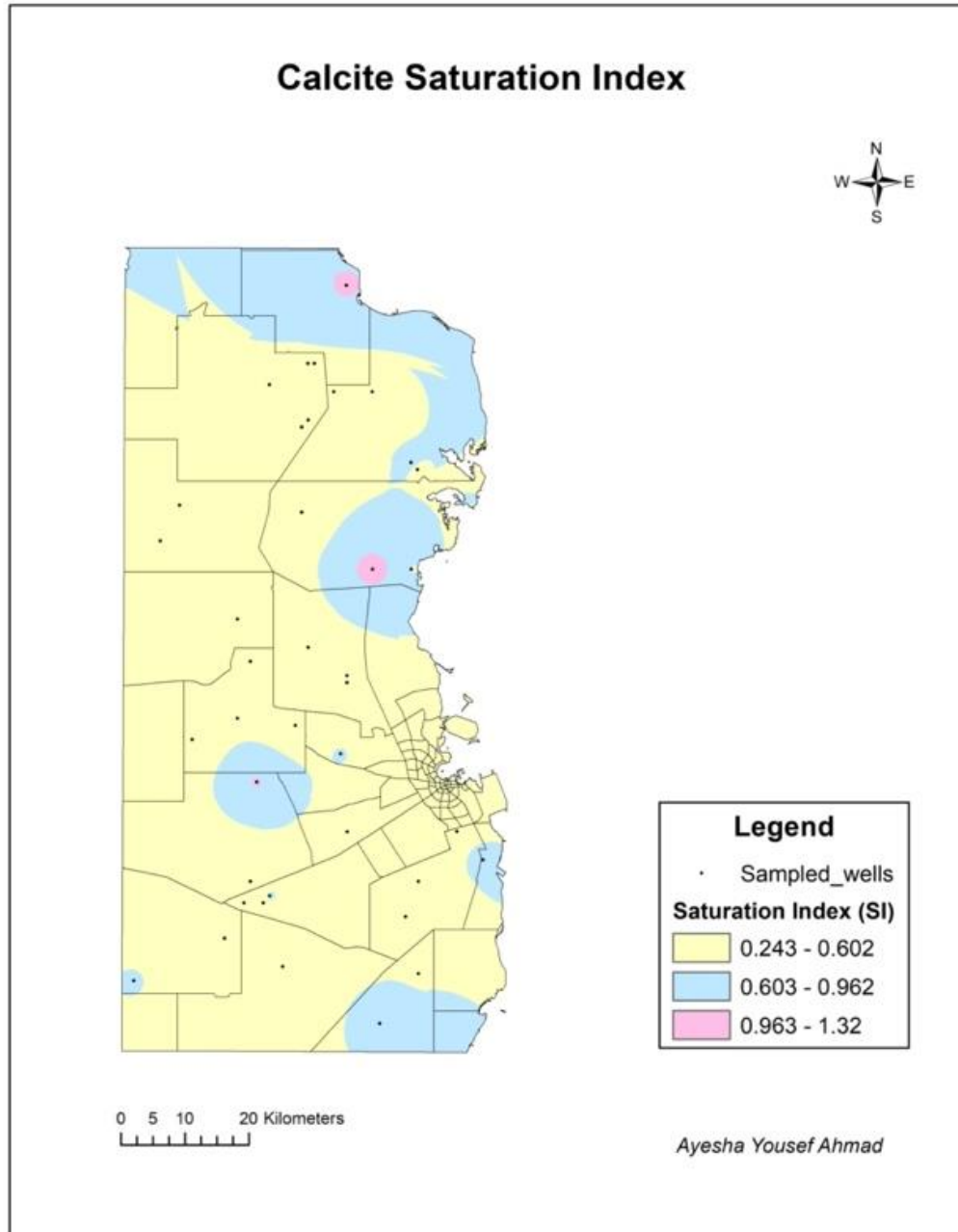


Figure 17. Interpolation maps for calcite in the study area.

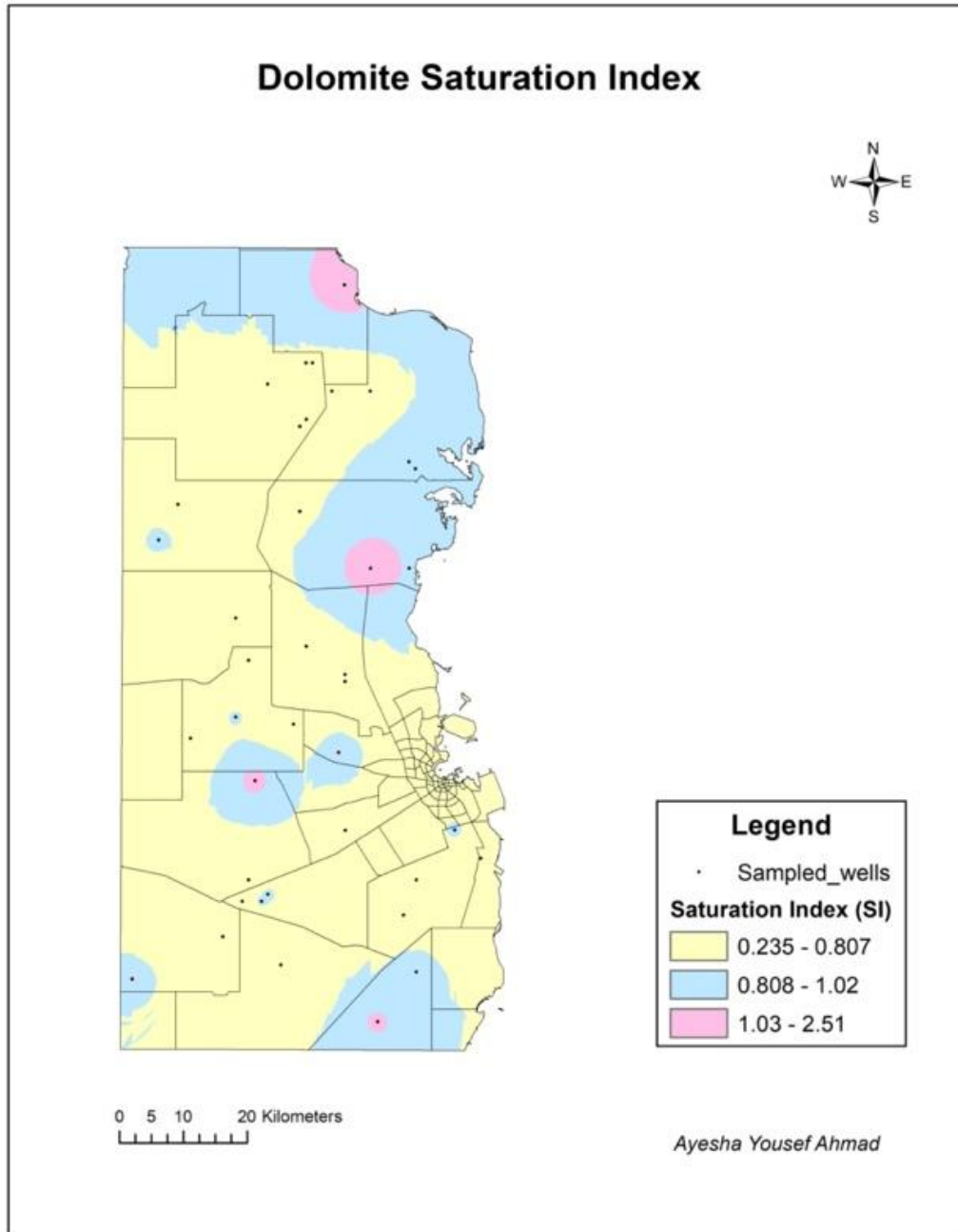


Figure 18. Interpolation maps for dolomite in the study area.

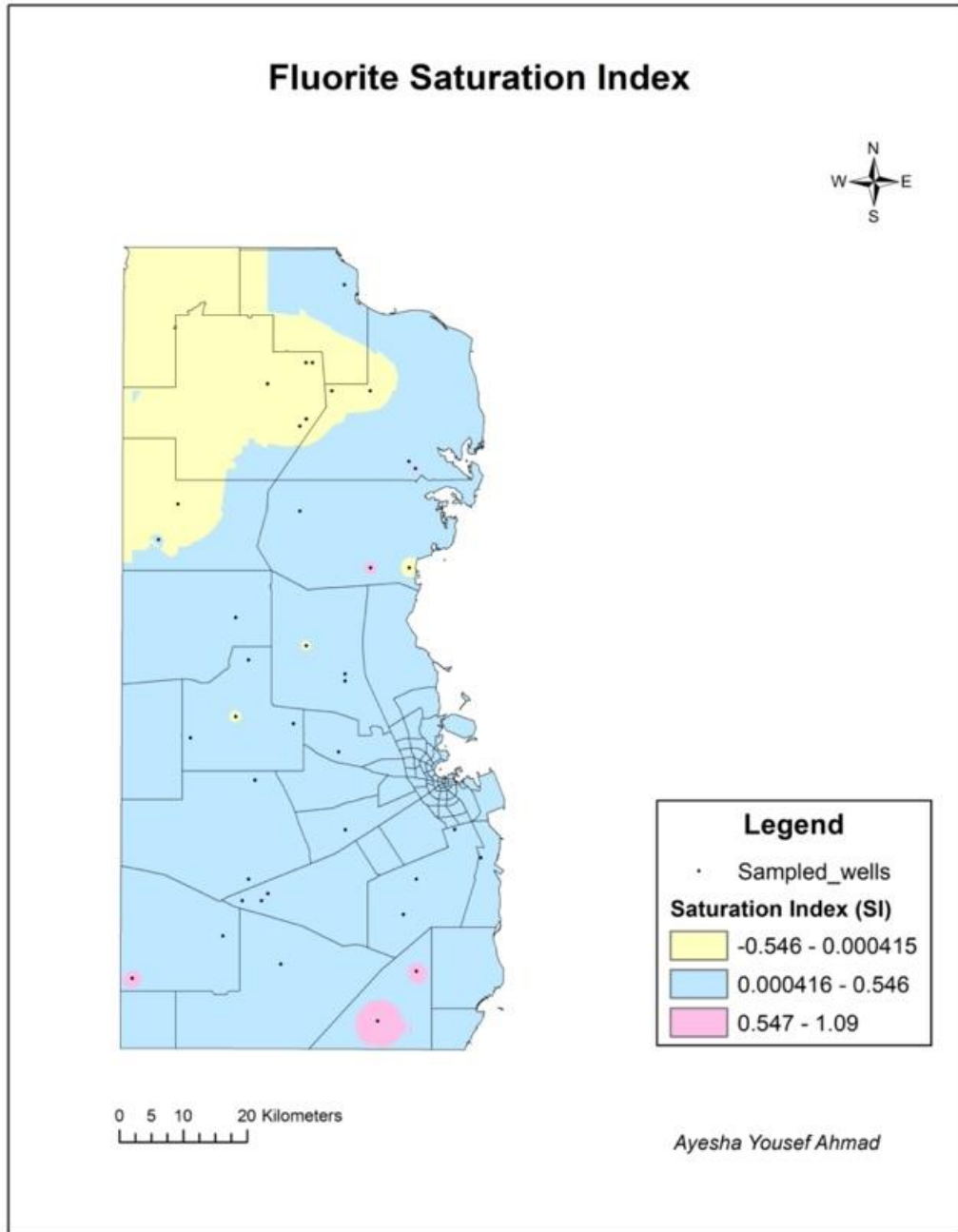


Figure 19. Interpolation maps for fluorite in the study area.

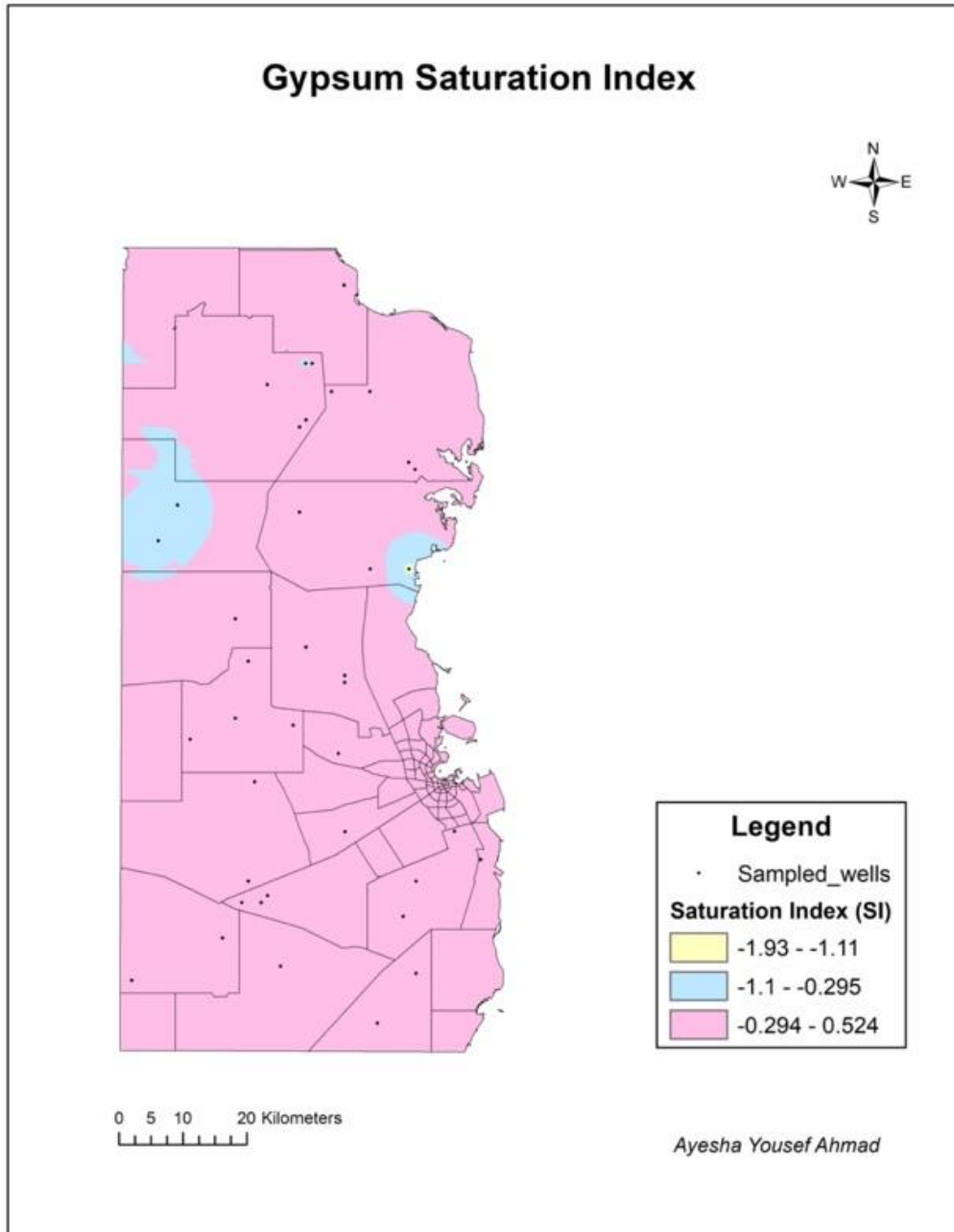


Figure 20. Interpolation maps for gypsum in the study area.

**Table 2.** RMSE values obtained by IDW interpolation method for different parameters.

Attribute Variable	Power	Sector type (circular)	Number of Neighbors		Root Mean Square	Mean
			Minimum	Maximum		
pH	1	8	10	15	0.2466	-0.018
TDS	1	4	10	15	3278	-80.54
TOC	2	8	10	15	6.43	-0.237
Hardness	1	4	10	15	939.22	18.25
SAR	1	1	10	15	7.68	-0.08
Boron	2	1	10	15	645.66	65.58
Sodium	1	1	10	15	1188.10	9.99
Lithium	1	1	10	15	51.48	-0.519
Molybdenum	1	4	10	15	47.10	-1.18
Selenium	2	1	10	15	3.98	-0.36
Uranium	1	1	10	15	5.04	-0.128
Chromium	1	4	10	15	3.28	-0.16
Strontium	1	1	10	15	4097.7	112.48
Potassium	1	1	10	15	57.69	-1.52
Calcium	1	1	10	15	237.92	12.87
Magnesium	1	4	10	15	91.07	-1.8
Fluoride	1	1	10	15	1.47	-0.054
Chloride	1	4	10	15	6883.93	-237.68
Bromide	1	8	10	15	5.22	-0.17
Nitrate	1	8	10	15	28.03	1.33
Sulfate	1	1	10	15	2000.98	191.78



**Table 3.** RMSE values obtained by RBFs interpolation method for different parameters.

Attribute Variable	Kernel parameter	Sector type (circular)	Number of Neighbors		Root Mean Square	Mean
			Minimum	Maximum		
pH	0.0090	1	10	15	0.256	-0.011
TDS	0.0090	1	10	15	3348.49	-121.31
TOC	0.0013	1	10	15	6.45	-0.020
Hardness	0.0090	1	10	15	957.94	-2.06
SAR	0.0090	1	10	15	7.84	-0.15
Potassium	0.0090	1	10	15	58.44	-2.08
Strontium	0.0090	1	10	15	4235.2	-40.47
Chromium	0.0090	1	10	15	3.35	-0.146
Uranium	0.0090	1	10	15	5.15	-0.051
Molybdenum	0.0090	1	10	15	48.15	-0.585
Selenium	0.0020	1	10	15	3.88	-0.125
Lithium	0.0090	1	10	15	52.35	-0.717
Sodium	0.0090	1	10	15	1216.37	-10.28
Boron	0.0090	1	10	15	633.76	25.806
Calcium	0.0090	1	10	15	239.37	3.53
Magnesium	0.0090	1	10	15	94.87	-2.64
Fluoride	0.0090	1	10	15	1.49	-0.049
Chloride	0.0090	1	10	15	7039.93	-319.46
Bromide	0.0090	1	10	15	5.45	-0.23
Nitrate	0.0090	1	10	15	29.72	1.53
Sulfate	0.0090	1	10	15	1982.7	92.73

**Table 4.** RMSE values and prediction indices obtained by SK interpolation method for different parameters.

Attribute Variable	Number of Neighbors		Mean	Root Mean Square	Average Standard Error	Mean Standardized	Root Mean Square Standardized
	Min	Max					
pH	2	5	-0.007	0.238	0.239	-0.030	0.994
TDS	2	5	66.76	3228.9	3566.5	0.025	0.917
TOC	2	5	0.038	6.22	6.72	0.009	0.940
Hardness	2	5	4.16	929.18	927.46	-0.000	1.029
SAR	2	5	0.10	8	9.08	0.022	0.865
Potassium	2	5	-1.68	56.44	50.72	-0.034	1.12
Strontium	2	5	- 78.1	4416.35	4003.23	-0.007	1.13
Chromium	2	5	-0.10	3.27	3.39	-0.028	0.95
Uranium	2	5	-0.418	4.86	2.64	-0.244	2.25
Molybdenum	2	5	-2.59	45.46	36.19	-0.07	1.27
Selenium	2	5	-0.128	4.18	4.37	-0.006	0.96
Lithium	2	5	-0.093	50.5	50.66	-0.093	0.98
Sodium	2	5	14.02	1187.56	1227.66	0.021	0.95
Boron	2	5	53.42	635.56	668.92	0.066	0.96
Calcium	2	5	6.64	236.65	235.63	0.012	1.05
Magnesium	2	5	0.140	90.25	91.43	0.000	0.99
Fluoride	2	5	-0.018	1.42	1.27	-0.039	1.14
Chloride	2	5	-350.79	6676.94	6058.41	-0.05	1.09
Bromide	2	5	0.048	4.86	4.97	0.011	0.97
Nitrate	2	5	0.926	27.12	27.08	0.021	1.01
Sulfate	2	5	78.88	1943	1921.67	0.029	1.11

## Appendix C: Statistical Analysis

Table 1. Summary statistics of physiochemical analysis for the GW samples.

	N	Range	Minimum	Maximum	Mean		Std. Deviation	Variance	Skewness		Kurtosis	
	Statistic	Statistic	Statistic	Statistic	Statistic	Std. Error	Statistic	Statistic	Statistic	Std. Error	Statistic	Std. Error
pH	41	1.05	6.89	7.94	7.30	0.037	0.238	0.057	0.795	0.369	0.714	0.724
Conductivity (mS/cm)	41	21.41	0.92	22.33	7.29	0.739	4.734	22.41	1.449	0.369	2.384	0.724
TDS (mg/l)	41	15034.46	598.87	15633.33	5038.09	525.93	3367.65	11341125	1.408	0.369	2.211	0.724
TOC (ppm)	41	34.23	1.27	35.50	14.62	1.20	7.726	59.695	0.370	0.369	-0.104	0.724
SAR	41	31.72	1.55	33.27	12.781	1.30	8.383	70.291	1.054	.369	0.310	0.724
Hardness	41	5117.85	275.16	5393.01	2120.20	163.88	1049.34	1101123.59	0.762	0.369	1.350	0.724
Potassium (ppm)	41	304.33	16.36	320.69	90.180	8.880	56.86	3233.75	2.231	.369	6.610	0.724
Magnesium (ppm)	41	395.78	24.41	420.19	169.135	14.85	95.093	9042.81	0.731	0.369	0.275	0.724
Calcium (ppm)	41	1427.91	69.94	1497.85	570.165	43.28	277.142	76807.99	0.784	0.369	1.994	0.724
Sodium (ppm)	41	5482.88	64.23	5547.11	1466.48	194.25	1243.86	1547198.65	1.438	0.369	1.899	0.724
Chloride (ppm)	41	30603.01	203.68	30806.68	6289.48	1053.78	6747.51	45528899.52	2.100	0.369	4.865	0.724
Fluoride (ppm)	41	7.18	1.59	8.77	3.81	.246	1.576	2.48	.974	0.369	1.049	0.724
Bromide (ppm)	41	21.61	0.37	21.98	4.32	.758	4.85	23.56	2.547	0.369	6.576	0.724
Nitrate (ppm)	41	113.34	.00	113.34	36.32	4.309	27.59	761.28	1.207	0.369	1.116	0.724
Sulfate (ppm)	41	11542.87	53.46	11596.33	4977.16	389.056	2491.17	6205964.66	.042	0.369	-.004	0.724
Lithium (ppb)	41	213.36	23.34	236.70	120.56	8.705	55.74	3107.28	.488	0.369	-.605	0.724
Boron (ppb)	41	3431.33	388.00	3819.33	1884.85	118.032	755.77	571194.89	.225	0.369	.066	0.724
Molybdenum (ppb)	41	286.12	7.83	293.95	53.878	7.042	45.095	2033.64	3.927	0.369	20.293	0.724
Selenium (ppb)	41	20.55	1.54	22.09	8.882	.773	4.95	24.52	.680	0.369	-.283	0.724
Strontium (ppb)	41	16739.66	3533.67	20273.33	13226.85	720.59	4614.05	21289539.33	-.294	0.369	-.925	0.724
Chromium (ppb)	41	11.79	0.10	11.89	3.9115	.534	3.419	11.69	.782	0.369	-.699	0.724
Uranium (ppb)	41	31.13	0.11	31.24	1.63	.746	4.77	22.82	6.248	0.369	39.625	0.724
Vanadium (ppb)	41	35.50	1.49	36.99	14.36	1.015	6.50	42.26	.603	0.369	2.701	0.724
Manganese (ppb)	41	4.98	0.01	4.99	1.009	0.216	1.38	1.92	1.862	0.369	2.786	0.724
Iron (ppb)	38	117.99	.01	118.00	4.72	3.068	18.91	357.83	6.119	0.383	37.618	0.750
Nickel (ppb)	41	11.38	.24	11.62	1.94	.305	1.95	3.83	3.450	0.369	14.910	0.724
Cobalt (ppb)	41	0.45	0.01	0.46	0.0712	.0136	0.08	0.008	3.481	0.369	12.874	0.724
Copper (ppb)	41	4.36	.08	4.44	1.37	.154	0.99	0.982	1.022	0.369	.911	0.724
Aluminum (ppb)	13	7.46	0.15	7.61	1.50	0.577	2.08	4.33	2.487	0.616	6.521	1.191
Beryllium (ppb)	19	0.14	0.00	0.14	.081	0.009	0.04	0.002	0.169	0.524	-0.868	1.014
Zinc (ppb)	20	51.25	0.03	51.28	5.88	2.51	11.23	126.25	3.820	0.512	15.760	0.992
Arsenic (ppb)	41	4.39	0.61	5.00	2.00	.153	0.98	0.971	0.770	0.369	0.622	0.724
Cadmium (ppb)	31	0.49	0.00	0.49	.0723	0.016	0.091	0.008	3.474	0.421	14.970	0.821
Barium (ppb)	41	21.55	3.07	24.62	10.20	0.671	4.30	18.497	1.239	.369	2.076	0.724

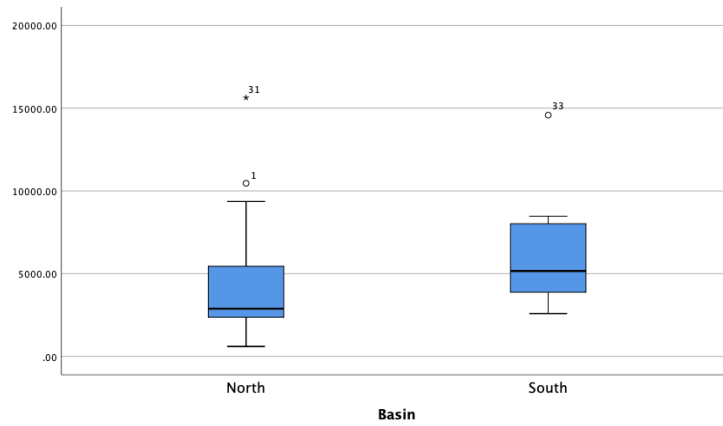


Figure 1. Means Difference between Groundwater Basins for TDS

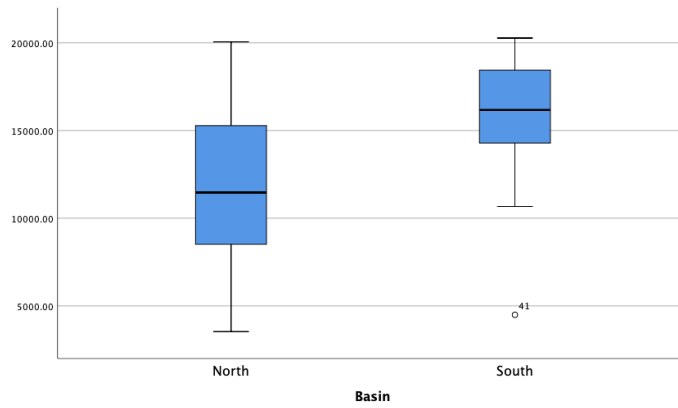


Figure 2. Means Difference between Groundwater Basins for Strontium

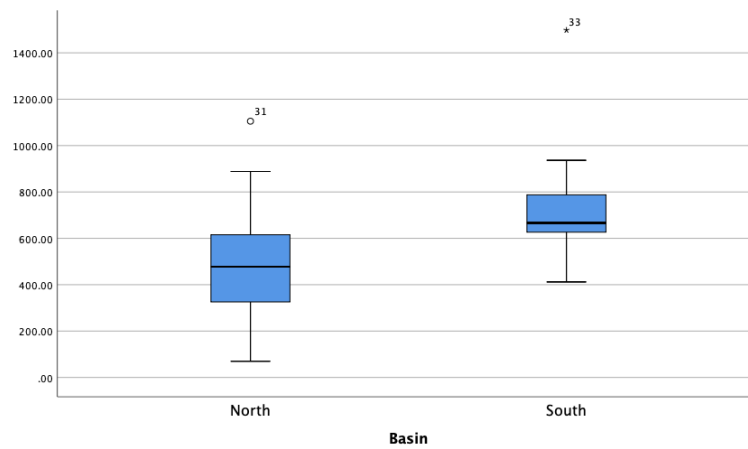


Figure 3. Means Difference between Groundwater Basins for Calcium

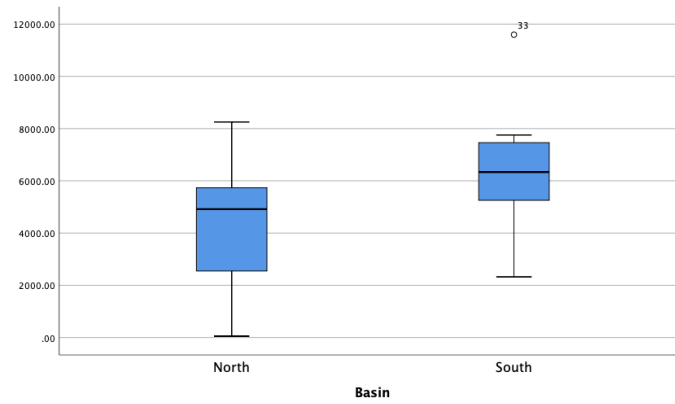


Figure 4. Means Difference between Groundwater Basins for Sulfate.

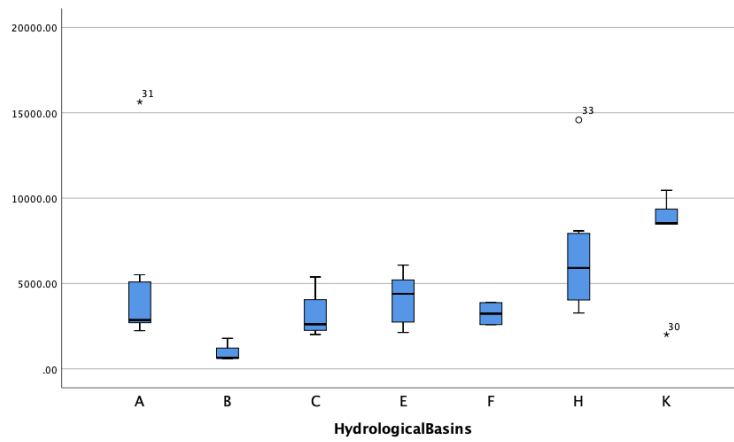


Figure 5. Means Difference between Hydrological Basins for TDS

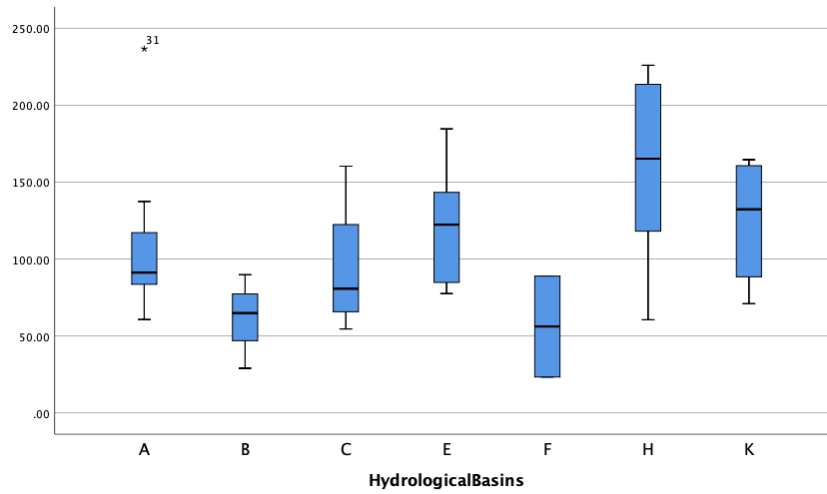


Figure 6. Means Difference between Hydrological Basins for Lithium.

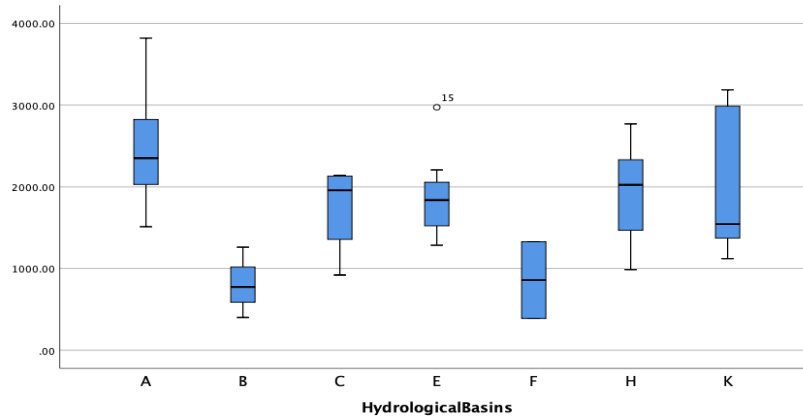


Figure 7. Means Difference between Hydrological Basins for Boron.

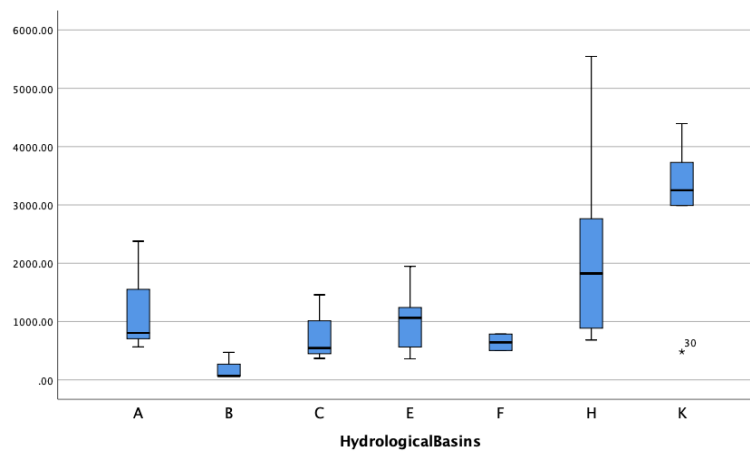


Figure 8. Means Difference between Hydrological Basins for Sodium.

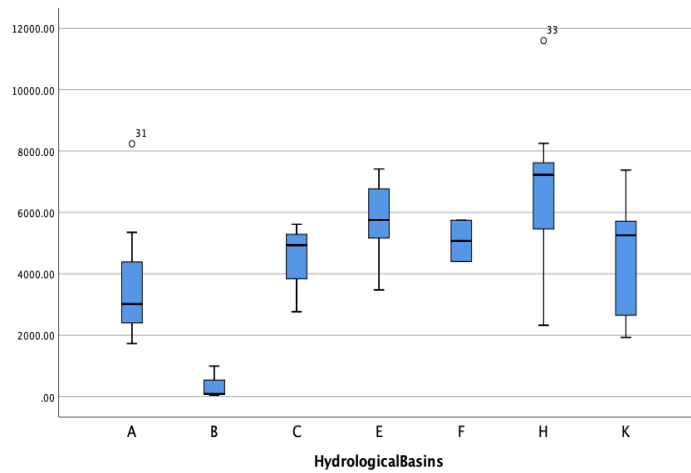


Figure 9. Means Difference between Hydrological Basins for Sulfate.

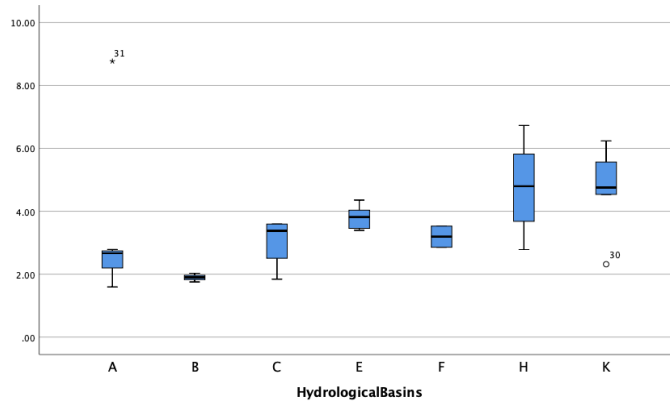


Figure 10. Means Difference between Hydrological Basins for Fluoride.

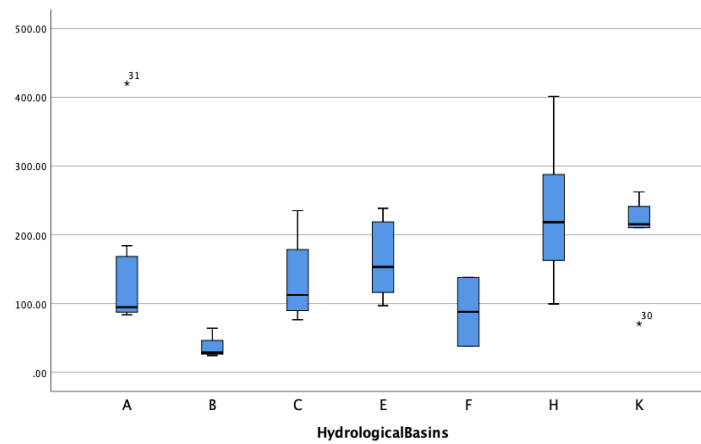


Figure 11. Means Difference between Hydrological Basins for Magnesium.

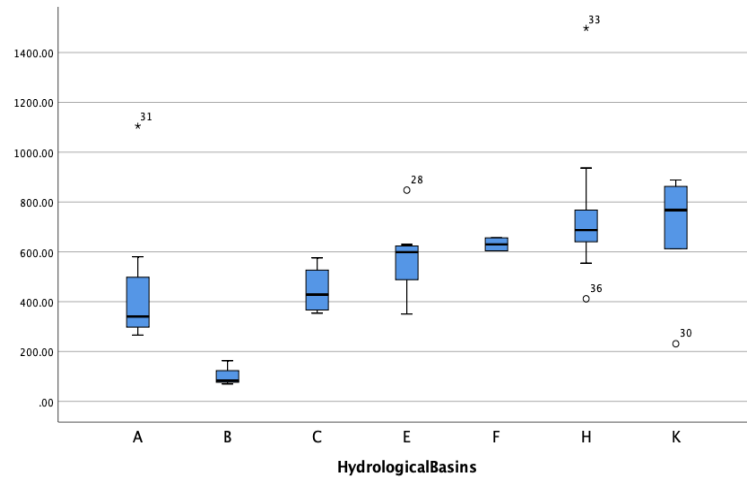


Figure 12. Means Difference between Hydrological Basins for Calcium.

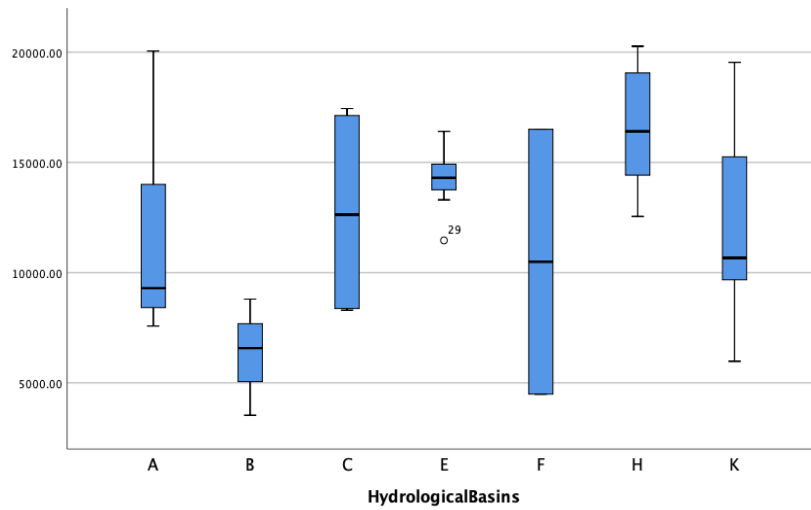


Figure 13. Means Difference between Hydrological Basins for Strontium.

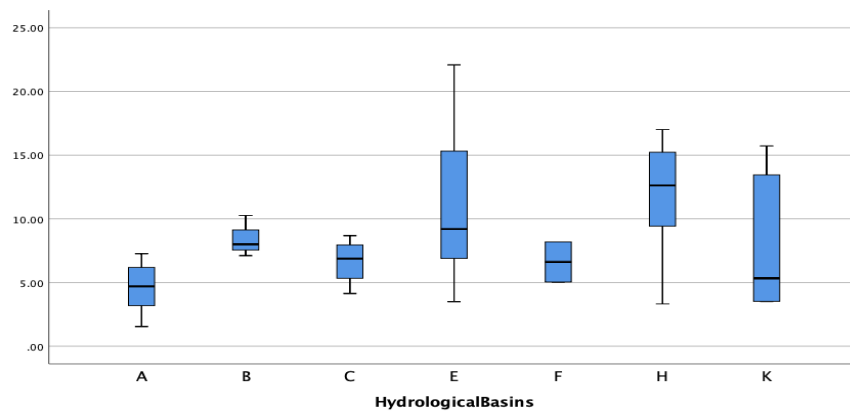


Figure 14. Means Difference between Hydrological Basins for Selenium.



Table 2. T-test for filed and lab pH

Paired Samples Statistics					
		Mean	N	Std. Deviation	Std. Error Mean
Pair 1	pHField	7.3151	114	.27345	.02561
	pHLab	7.3041	114	.26507	.02483

Paired Samples Correlations				
		N	Correlation	Sig.
Pair 1	pHField & pHLab	114	.949	.000

Paired Samples Test									
		Paired Differences							
		Mean	Std. Deviation	Std. Error Mean	95% Confidence Interval of the Difference		t	df	Sig. (2-tailed)
					Lower	Upper			
Pair 1	pHField - pHLab	.01096	.08673	.00812	-.00513	.02706	1.350	113	.180

Table 3. T-test for filed and lab conductivity

Paired Samples Statistics					
		Mean	N	Std. Deviation	Std. Error Mean
Pair 1	Lab	7.3059	114	4.84275	.45357
	Field	7.3352	114	4.88819	.45782

Paired Samples Correlations				
		N	Correlation	Sig.
Pair 1	Lab & Field	114	.999	.000

Paired Samples Test									
		Paired Differences							
		Mean	Std. Deviation	Std. Error Mean	95% Confidence Interval of the Difference		t	df	Sig. (2-tailed)
					Lower	Upper			
Pair 1	Lab - Field	-.02754	.16022	.01501	-.05727	.00219	-1.835	113	.069

Table 4  
statistical correlations analysis

Response (y)	Predictor (x)	P-value	a	b	R	Interpreting correlations
pH	Zinc	.016	7.24	0.014	0.53	Significant positive
pH	Strontium	.041	7.52	-1.66E-5	0.32	Significant negative weak
TDS	TOC	0.003	6045.94	-278.11	0.453	Highly significant negative
TDS	Lithium	0.000	-448.23	45.505	0.753	Highly significant positive strong
TDS	Boron	0.001	787.72	2.255	0.506	Highly significant positive
TDS	Sodium	0.000	1453.91	2.4	0.903	Highly significant positive strong
TDS	Potassium	0.000	121.87	54.51	0.921	Highly significant positive strong
TDS	Zinc	0.014	4630.83	191.08	0.542	Significant positive
TDS	Arsenic	0.044	2864.69	1081.68	0.317	significant positive weak
TDS	Strontium	0.000	-635.86	0.429	0.588	Highly significant positive
TDS	Barium	0.004	1516.04	345.02	0.441	Highly significant positive weak
TDS	Calcium	0.000	-1028.47	594.39	0.876	Highly significant positive strong
TDS	Magnesium	0.000	-537.71	32.96	0.931	Highly significant positive strong
TDS	Fluoride	0.000	-2244.25	1908.51	0.893	Highly significant positive strong
TDS	Chloride	0.000	1963.48	0.489	0.979	Highly significant positive strong
TDS	Bromide	0.000	2304.08	297.35	0.910	Highly significant positive strong
TDS	Sulfate	0.000	170.68	829.77	0.723	Highly significant positive strong
TOC	Vandium	0.000	5.535	0.033	0.533	Highly significant positive
TOC	Copper	0.004	9.924	3.427	0.439	Highly significant positive
TOC	Cadmium	0.014	11.836	38.37	0.437	Significant positive
Lithium	Boron	0.000	37.86	0.044	0.595	Highly significant positive
Lithium	Sodium	0.04	78.17	0.029	0.645	Significant positive strong
Lithium	Potassium	0.000	62.49	0.644	0.657	Highly significant positive
Lithium	Strontium	0.000	-0.273	0.009	0.756	Highly significant positive weak
Lithium	Selenium	0.030	86.62	3.822	0.34	Significant positive weak
Lithium	Zinc	0.018	113.17	2.511	0.524	significant positive
Lithium	Uranium	0.026	113.93	4.06	0.345	Dignificant positive weak
Boron	Sodium	0.002	1474.43	0.28	0.461	Highly significant positive
Boron	Potassium	0.000	1182.76	7.72	0.586	Highly significant positive
Boron	Copper	0.001	821.37	0.08	0.463	Highly significant positive
Sodium	Potassium	0.000	-61.7	16.94	0.775	Highly significant positive strong
Sodium	Arsenic	0.037	638.67	411.99	0.326	Significant positive weak
Sodium	Strontium	0.078	-179.75	0.124	0.462	Significant positive
Sodium	Barium	0.001	638.8	81.08	0.28	Highly significant positive
Sodium	Calcium	0.000	-567.875	3.56	0.79	Highly significant positive strong

Response (y)	Predictor (x)	P-value	a	b	R	Interpreting correlations
Sodium	Magnesium	0.000	-338.11	10.67	0.816	Highly significant positive strong
Sodium	Fluoride	0.000	-837.45	603.8	0.765	Highly significant positive strong
Sodium	Bromide	0.000	576.01	205.6	0.803	Highly significant positive strong
Sodium	Chloride	0.000	462.05	0.16	0.866	Highly significant positive strong
Sodium	Sulfate	0.000	-125.79	0.32	0.641	Highly significant positive strong
Aluminum	Cobalt	0.026	-0.730	58.12	0.612	Significant positive
Aluminum	Copper	0.044	0.027	2.253	0.567	significant positive
Potassium	Zinc	0.002	85.52	4.13	0.661	Highly significant positive
Potassium	Strontium	0.003	16.78	0.006	0.450	Highly significant positive
Potassium	Barium	0.001	23.52	6.5	0.494	Highly significant positive
Potassium	Calcium	0.000	3.609	0.152	0.740	Highly significant positive strong
Potassium	Magnesium	0.000	7.91	0.486	0.813	Highly significant positive strong
Potassium	Fluoride	0.000	-26	30.44	0.844	Highly significant positive strong
Potassium	Chloride	0.000	40.7	0.008	0.933	Highly significant positive strong
Potassium	Bromide	0.000	44.66	10.51	0.897	Highly significant positive strong
Potassium	Sulfate	0.000	18.79	0.014	0.628	Highly significant positive strong
Vandium	Chromium	0.038	11.93	0.619	0.326	Significant positive weak
Vandium	Arsenic	0.005	8.6	2.8	0.434	Highly significant positive weak
Vandium	Cadmium	0.007	12.51	33.86	0.471	Highly significant positive
Iron	Chromium	0.019	3.6	0.07	0.379	Significant positive weak
Iron	Nickel	0.04	-1.38	3.12	0.334	Significant positive weak
Iron	Zinc	0.018	1.16	0.078	0.564	Significant positive
Iron	Barium	0.035	-10.25	1.45	0.344	Significant positive weak
Manganese	Nickel	0.000	0.294	0.369	0.521	Highly significant positive
Manganese	Cobalt	0.003	0.502	7.12	0.448	Highly significant positive
Manganese	Molybdenum	0.014	0.375	0.012	0.383	Significant positive
Nickel	Cobalt	0.000	0.878	14.919	0.665	Highly significant positive
Molybdenum	Nickel	0.045	1.2	0.014	0.315	significant positive weak
Molybdenum	Uranium	0.000	40.56	8.15	0.864	Highly significant positive strong
Cobalt	Copper	0.013	0.025	0.034	0.383	Significant positive weak
Zinc	Barium	0.003	-11.74	1.6	0.625	Highly significant positive

Response (y)	Predictor (x)	P-value	a	b	R	Interpreting correlations
Arsenic	Molybdenum	0.014	1.56	0.008	0.382	significant positive weak
Arsenic	Uranium	0.002	1.85	0.095	0.461	Highly significant positive weak
Selenium	Molybdenum	0.017	6.69	0.016	0.369	Significant positive weak
Selenium	Barium	0.022	13.07	-0.411	0.357	Significant negative weak
Selenium	Uranium	0.034	8.32	0.344	0.332	Significant positive weak
Fluoride	Bromide	0.000	2.7	0.25	0.77	Highly significant positive strong
Chloride	Barium	0.000	-2148.78	826.62	0.527	Highly significant positive
Chloride	Magnesium	0.000	-4093.62	61.38	0.865	Highly significant positive strong
Chloride	Calcium	0.000	-4934.66	19.68	0.809	Highly significant positive strong
Chloride	Fluoride	0.000	-7586.68	3636.59	0.850	Highly significant positive strong
Sulfate	Selenium	0.036	3510.28	165.143	0.328	Significant positive weak
Sulfate	Strontium	0.000	145.6	0.365	0.677	Highly significant positive
Sulfate	Lithium	0.000	866.71	34.09	0.763	Highly significant positive strong
Sulfate	Boron	0.001	1995.19	1.58	0.480	Highly significant positive
Sulfate	Calcium	0.000	3222.64	8.16	0.908	Highly significant positive strong
Sulfate	Fluoride	0.000	117.89	1273.49	0.806	Highly significant positive strong
Sulfate	Chloride	0.000	3566.95	0.224	0.607	Highly significant positive
Sulfate	Magnesium	0.000	1295.47	21.76	0.831	Highly significant positive strong
Calcium	Bromide	0.000	384.16	42.9	0.752	Highly significant positive strong
Calcium	Magnesium	0.000	143.72	2.52	0.865	Highly significant positive strong
Calcium	Lithium	0.000	124.9	3.69	0.743	Highly significant positive strong
Calcium	Boron	0.017	314.6	0.136	0.37	Significant positive
Calcium	Strontium	0.000	46.43	0.04	0.659	Highly significant positive strong

Table 5. Pearson correlation analysis

		Correlations																		
		TDS	TOC	Na	K	Ca	Mg	F	Cl	Br	SO4	B	Li	Mo	Se	Sr	Mn	Cr	U	
TDS	Pearson Correlation	1	-.043	.903 <sup>*</sup>	.921 <sup>*</sup>	.876 <sup>*</sup>	.931 <sup>*</sup>	.893 <sup>*</sup>	.979 <sup>*</sup>	.910 <sup>*</sup>	.723 <sup>*</sup>	.506 <sup>*</sup>	.753 <sup>*</sup>	.033	.094	.588 <sup>*</sup>	-.068	-.039	.133	
	Sig. (2-tailed)		.789	.000	.000	.000	.000	.000	.000	.000	.000	.001	.000	.836	.557	.000	.673	.808	.406	
TOC	Pearson Correlation	-.043	1	-.004	-.013	-.177	-.063	-.141	-.033	-.084	-.164	.251	.049	-.078	.199	-.059	-.100	-.081	-.115	
	Sig. (2-tailed)	.789		.980	.935	.268	.696	.379	.838	.600	.306	.113	.760	.628	.212	.715	.533	.614	.476	
Na	Pearson Correlation	.903 <sup>*</sup>	-.004	1	.775 <sup>*</sup>	.795 <sup>*</sup>	.816 <sup>*</sup>	.765 <sup>*</sup>	.866 <sup>*</sup>	.803 <sup>*</sup>	.641 <sup>*</sup>	.461 <sup>*</sup>	.645 <sup>*</sup>	.036	.142	.462 <sup>*</sup>	-.073	.011	.165	
	Sig. (2-tailed)	.000	.980		.000	.000	.000	.000	.000	.000	.002	.000	.822	.375	.002	.648	.945	.303		
K	Pearson Correlation	.921 <sup>*</sup>	-.013	.775 <sup>*</sup>	1	.740 <sup>*</sup>	.813 <sup>*</sup>	.844 <sup>*</sup>	.933 <sup>*</sup>	.897 <sup>*</sup>	.628 <sup>*</sup>	.586 <sup>*</sup>	.657 <sup>*</sup>	-.008	-.014	.450 <sup>*</sup>	.006	-.160	.035	
	Sig. (2-tailed)	.000	.935	.000		.000	.000	.000	.000	.000	.000	.000	.958	.928	.003	.969	.317	.827		
Ca	Pearson Correlation	.876 <sup>*</sup>	-.177	.795 <sup>*</sup>	.740 <sup>*</sup>	1	.865 <sup>*</sup>	.856 <sup>*</sup>	.809 <sup>*</sup>	.752 <sup>*</sup>	.908 <sup>*</sup>	.370 <sup>*</sup>	.743 <sup>*</sup>	.084	.204	.659 <sup>*</sup>	-.086	-.110	.214	
	Sig. (2-tailed)	.000	.268	.000	.000		.000	.000	.000	.000	.017	.000	.602	.201	.000	.595	.493	.179		
Mg	Pearson Correlation	.931 <sup>*</sup>	-.063	.816 <sup>*</sup>	.813 <sup>*</sup>	.865 <sup>*</sup>	1	.889 <sup>*</sup>	.865 <sup>*</sup>	.778 <sup>*</sup>	.831 <sup>*</sup>	.538 <sup>*</sup>	.858 <sup>*</sup>	.059	.219	.687 <sup>*</sup>	-.057	.021	.160	
	Sig. (2-tailed)	.000	.696	.000	.000	.000		.000	.000	.000	.000	.000	.712	.170	.000	.723	.895	.317		
F	Pearson Correlation	.893 <sup>*</sup>	-.141	.765 <sup>*</sup>	.844 <sup>*</sup>	.856 <sup>*</sup>	.889 <sup>*</sup>	1	.850 <sup>*</sup>	.772 <sup>*</sup>	.806 <sup>*</sup>	.434 <sup>*</sup>	.796 <sup>*</sup>	.159	.266	.590 <sup>*</sup>	-.087	-.088	.232	
	Sig. (2-tailed)	.000	.379	.000	.000	.000	.000		.000	.000	.000	.005	.000	.320	.092	.000	.587	.585	.144	
Cl	Pearson Correlation	.979 <sup>*</sup>	-.033	.866 <sup>*</sup>	.933 <sup>*</sup>	.809 <sup>*</sup>	.865 <sup>*</sup>	.850 <sup>*</sup>	1	.954 <sup>*</sup>	.607 <sup>*</sup>	.431 <sup>*</sup>	.680 <sup>*</sup>	.036	.011	.490 <sup>*</sup>	-.083	-.058	.107	
	Sig. (2-tailed)	.000	.838	.000	.000	.000	.000	.000		.000	.000	.005	.000	.822	.947	.001	.607	.718	.504	
Br	Pearson Correlation	.910 <sup>*</sup>	-.084	.803 <sup>*</sup>	.897 <sup>*</sup>	.752 <sup>*</sup>	.778 <sup>*</sup>	.772 <sup>*</sup>	.954 <sup>*</sup>	1	.523 <sup>*</sup>	.318 <sup>*</sup>	.594 <sup>*</sup>	-.048	-.130	.414 <sup>*</sup>	-.098	-.143	.021	
	Sig. (2-tailed)	.000	.600	.000	.000	.000	.000	.000	.000		.000	.043	.000	.765	.418	.007	.542	.373	.896	
SO4	Pearson Correlation	.723 <sup>*</sup>	-.164	.641 <sup>*</sup>	.628 <sup>*</sup>	.908 <sup>*</sup>	.831 <sup>*</sup>	.806 <sup>*</sup>	.607 <sup>*</sup>	.523 <sup>*</sup>	1	.480 <sup>*</sup>	.763 <sup>*</sup>	.081	.328 <sup>*</sup>	.677 <sup>*</sup>	-.013	-.092	.191	
	Sig. (2-tailed)	.000	.306	.000	.000	.000	.000	.000	.000	.000		.001	.000	.613	.036	.000	.936	.567	.232	
B	Pearson Correlation	.506 <sup>*</sup>	.251	.461 <sup>*</sup>	.586 <sup>*</sup>	.370 <sup>*</sup>	.538 <sup>*</sup>	.434 <sup>*</sup>	.431 <sup>*</sup>	.318 <sup>*</sup>	.480 <sup>*</sup>	1	.595 <sup>*</sup>	.065	.126	.491 <sup>*</sup>	.140	-.081	.111	
	Sig. (2-tailed)	.001	.113	.002	.000	.017	.000	.005	.005	.043	.001		.000	.688	.432	.001	.383	.616	.488	
Li	Pearson Correlation	.753 <sup>*</sup>	.049	.645 <sup>*</sup>	.657 <sup>*</sup>	.743 <sup>*</sup>	.858 <sup>*</sup>	.796 <sup>*</sup>	.680 <sup>*</sup>	.594 <sup>*</sup>	.763 <sup>*</sup>	.595 <sup>*</sup>	1	.247	.340 <sup>*</sup>	.756 <sup>*</sup>	-.065	-.028	.348 <sup>*</sup>	
	Sig. (2-tailed)	.000	.780	.000	.000	.000	.000	.000	.000	.000	.000	.000		.119	.030	.000	.686	.864	.026	

		Correlations																		
		TDS	TOC	Na	K	Ca	Mg	F	Cl	Br	SO4	B	Li	Mo	Se	Sr	Mn	Cr	U	
Mo	Pearson Correlation	.033	-.078	.036	-.008	.084	.059	.159	.036	-.048	.081	.065	.247	1	.369*	.117	.383*	.014	.864*	
	Sig. (2-tailed)	.836	.628	.822	.958	.602	.712	.320	.822	.765	.613	.688	.119		.017	.467	.014	.930	.000	
Se	Pearson Correlation	.094	.199	.142	-.014	.204	.219	.266	.011	-.130	.328*	.126	.340*	.369*	1	.402*	.054	.132	.332*	
	Sig. (2-tailed)	.557	.212	.375	.928	.201	.170	.092	.947	.418	.036	.432	.030	.017		.009	.736	.410	.034	
Sr	Pearson Correlation	.588*	-.069	.462*	.450*	.659*	.687*	.590*	.490*	.414*	.677*	.491*	.756*	.117	.402*	1	-.030	-.065	.208	
	Sig. (2-tailed)	.000	.715	.002	.003	.000	.000	.000	.001	.007	.000	.001	.000	.467	.009		.850	.685	.193	
Mn	Pearson Correlation	-.068	-.100	-.073	.006	-.086	-.057	-.087	-.083	-.098	-.013	.140	-.065	.383*	.054	-.030	1	-.090	.250	
	Sig. (2-tailed)	.673	.533	.648	.969	.595	.723	.587	.607	.542	.936	.383	.686	.014	.736	.850		.577	.114	
Cr	Pearson Correlation	-.039	-.081	.011	-.160	-.110	.021	-.088	-.058	-.143	-.092	-.081	-.028	.014	.132	-.065	-.090	1	-.079	
	Sig. (2-tailed)	.808	.614	.945	.317	.493	.895	.585	.718	.373	.567	.616	.864	.930	.410	.685	.577		.626	
U	Pearson Correlation	.133	-.115	.165	.035	.214	.160	.232	.107	.021	.191	.111	.348*	.864*	.332*	.208	.250	-.079	1	
	Sig. (2-tailed)	.406	.476	.303	.827	.179	.317	.144	.504	.896	.232	.488	.026	.000	.034	.193	.114	.626		
**. Correlation is significant at the 0.01 level (2-tailed).																				
*. Correlation is significant at the 0.05 level (2-tailed).																				

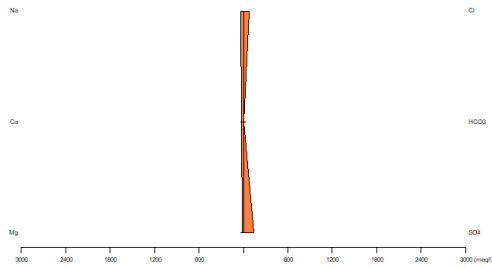
Table 6. Statistical Chemical Characteristics of Topsoil.

	N	Range	Minimum	Maximum	Mean	Std. Deviation	Variance
	Statistic	Statistic	Statistic	Statistic	Statistic	Statistic	Statistic
Potassium (mg/g)	41	11.85	7.18	19.03	13.1	2.8	7872.91
Sodium (mg/g)	41	40.66	11.15	51.81	25.56	9.62	92582.3
Lithium ( $\mu\text{g/g}$ )	41	22.03	9.06	31.09	16.27	5.79	33.58
Boron (mg/g)	41	14.88	1.13	16.02	4.90	2.85	8151.52
Selenium ( $\mu\text{g/g}$ )	41		0.03	5.97	2.62	1.68	2.83
Strontium ( $\mu\text{g/g}$ )	41	5.57	0.492	6.069	1.631	1.131	1279.73
Chromium ( $\mu\text{g/g}$ )	41	552.72	28.68	3588.92	193.88	3560.24	305507.31

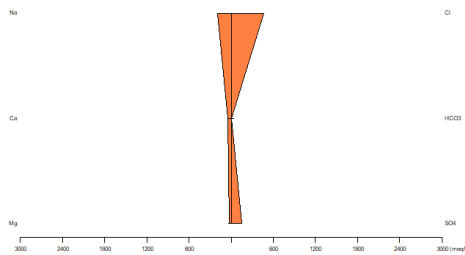
Manganese ( $\mu\text{g/g}$ )	41	750.08	168.71	918.8	408.24	151.24	22873.59
Iron (mg/g)	38	33.65	6.45	40.11	15.51	7.65	58643.51
Cobalt ( $\mu\text{g/g}$ )	41	19.47	3.19	22.66	7.42	4.61	21.32
Copper ( $\mu\text{g/g}$ )	41	38.84	12.15	51	25.68	9.72	94.59
Arsenic ( $\mu\text{g/g}$ )	41	13.22	0.23	13.45	5.50	3.08	9.53
Cadmium ( $\mu\text{g/g}$ )	41	0.437	0.02	0.457	0.167	0.108	0.012
Barium ( $\mu\text{g/g}$ )	41	294.52	213.02	507.55	355.43	60.07	3609.07

### Appendix D: Stiff Plots

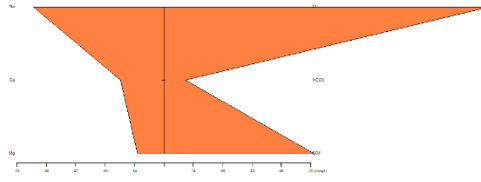
South



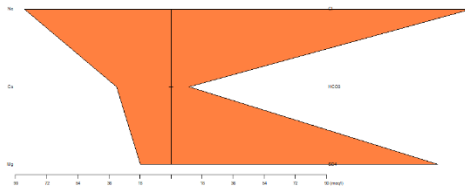
North



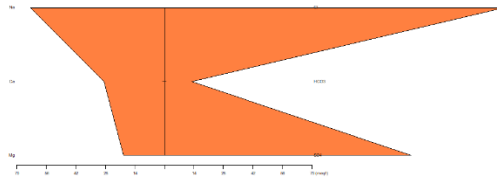
North



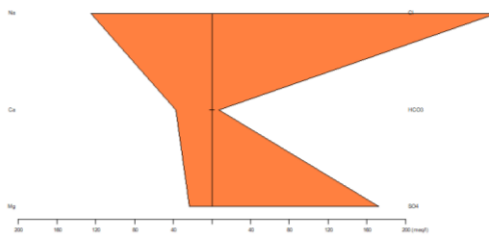
North



North

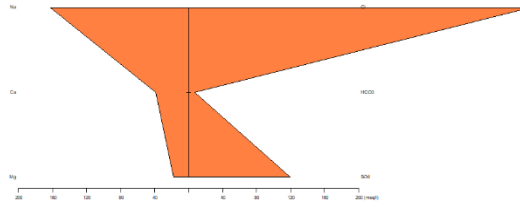


North

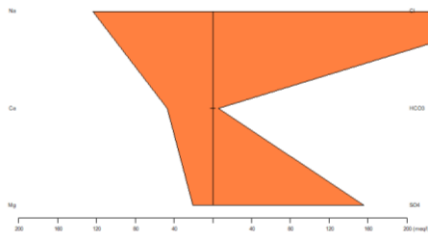




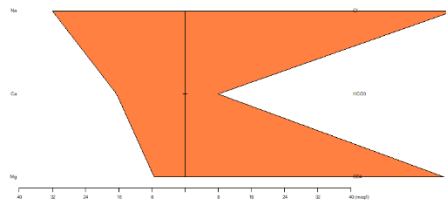
North



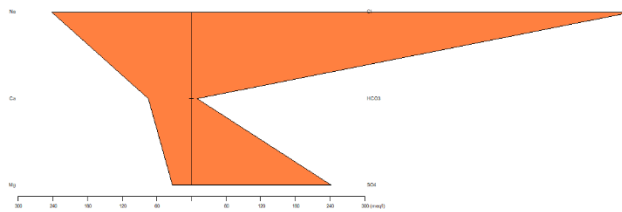
South



North

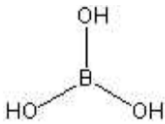
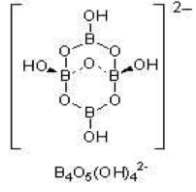



South



## Appendix E: Physical and Chemical Characteristic of Adsorbate

Table 1. The Physiochemical Properties of Boron and Boron Compounds (Cordia et al., 2003).

Typical substance	Boron (single boron)	Boric acid	Borax	Boron Oxide
Chemical formula	B	$B(OH)_3$	$Na_2B_4O_7$ (anhydride) $Na_2B_4O_7 \cdot 10H_2O$ (decahydride)	$B_2O_3$
Chemical Structure	Polymorphic element: Amorphous powder, four crystalline forms: $\alpha$ -rhombohedral, $\beta$ -rhombohedral, $\alpha$ -tetragonal, and $c$ $\beta$ -tetragonal			
Electronic configurations	[He] 2s <sup>2</sup> 2p <sup>1</sup> Electrons per shell: 2, 3			
Molecular Weight	10.81 g/mol	61.83 g/mol	201 g/mol (anhydride), 381 g/mol (decahydride)	69.62 g/mol
Appearance	Black or dark brown powder (amorphous form); clear red crystals ( $\alpha$ -rhombohedral form); black, opaque crystals with metallic luster ( $\alpha$ -tetragonal form); black ( $\beta$ -rhombohedral form)	White granules or colorless crystals	White crystals	Colorless crystals
Melting point	2180 °C	170.9 °C Changed to metaborate at 100°C with increased heating, it is transformed to boric oxide.	743°C (anhydride), 75°C (decahydride)	450 °C
Vapour Pressure	0.0119 mm Hg at 2,140 °C	Negligible at 20 °C about $9.9 \times 10^{-6}$ Pa at 25 °C	Negligible at 20 °C	Negligible at 20 °C
Boiling point	3650 °C	300 °C	1,575 °C (decomposition, anhydride), Decahydride is changed to anhydride at 100°C or above	1500 °C
Water solubility	Insoluble	58.0 g/L at 25°C	31.7 g/L at 25°C (anhydride), 47 g/L at 20°C (decahydride, dissociation)	rapidly hydrates to boric acid
Octanol-water Partition Coefficient		-1.09 at 22 °C	-1.53 at 22 °C	

Typical substance	Boron (single boron)	Boric acid	Borax	Boron Oxide
Oxidation States	-5, -1, +1, +2, +3 (a mildly acidic oxide)			
Electronegativity Pauling scale:	2.04			
Ionization Energy (kJ mol <sup>-1</sup> )	1st: 800.6 kJ/mol 2nd: 2427.1 kJ/mol 3rd: 3659.7 kJ/mol			
Atomic Radius	82 pm			
Ionic Radius (r <sub>ion</sub> )	41 pm			
Covalent Radius (r <sub>cov</sub> )	84±3 pm			
Van der Waals Radius (r <sub>w</sub> )	192 pm			

Table 2. The Physiochemical Properties of Molybdenum (Miessler, 2014).

Chemical formula	Mo
Atomic Number	42
Electronic configurations	[Kr] 4d <sup>5</sup> 5s <sup>1</sup> Electrons per shell: 2, 8, 18, 13, 1
Molecular Weight	95.94 g/mol
Density	10.22 g/cm <sup>3</sup>
Appearance	Dark-gray or black powder with metallic luster or coherent mass of silver white color; body centered cubic structure
Melting point	2610 °C
Vapour Pressure	1 Pa at 2469 °C (solid)
Boiling point	5560 °C
Water solubility	Insoluble in water
Oxidation States	-1, -2, -4, +1, +2, +3, +6, +4 (strongly acidic oxide)
Electronegativity Pauling scale:	2.16
Ionization Energy (kJ mol <sup>-1</sup> )	1st: 684.3 kJ/mol 2nd: 1560 kJ/mol 3rd: 2618 kJ/mol
Atomic Radius	139 pm
Ionic Radius (r <sub>ion</sub> )	79 pm, 73 pm,
Covalent Radius (r <sub>cov</sub> )	154±5 pm
Van der Waals Radius (r <sub>w</sub> )	210 pm

Table 3. The Physiochemical Properties of Lithium (Miessler, 2014).

Chemical formula	Li
Atomic Number	3
Electronic configurations	[He] 2s <sup>1</sup> Electrons per shell: 2, 1
Molecular Weight	6.94 g/mol
Density	0.5 g/cm <sup>3</sup>
Appearance	Silver white soft metal
Melting point	180.5 °C
Vapour Pressure	Pa at 723°C: 133
Boiling point	1342 °C
Water solubility	Violent reaction
Oxidation States	+1 (a strongly basic oxide)
Electronegativity Pauling scale:	0.98
Ionization Energy (kJ mol <sup>-1</sup> )	1st: 520.2 kJ/mol 2nd: 7298.1 kJ/mol 3rd: 11815.0 kJ/mol
Electron Affinity (kJ mol <sup>-1</sup> )	60
Atomic Radius	134 pm
Ionic Radius (r <sub>ion</sub> )	90 pm
Covalent Radius (r <sub>cov</sub> )	128±7 pm
Van der Waals Radius (r <sub>w</sub> )	182 pm

## Appendix F: Adsorption Models

### Monolayer Adsorption and the Langmuir Isotherm

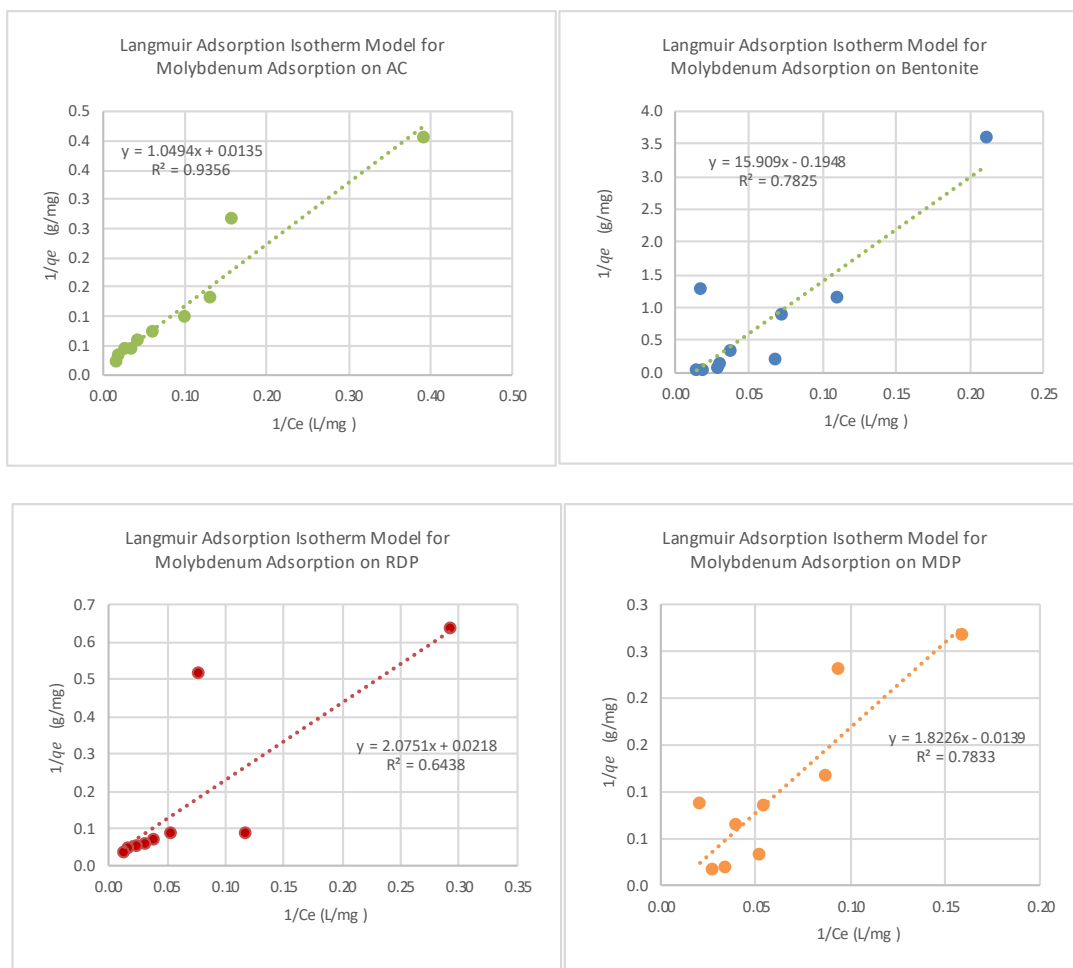


Figure 1. Langmuir model for molybdenum adsorption.

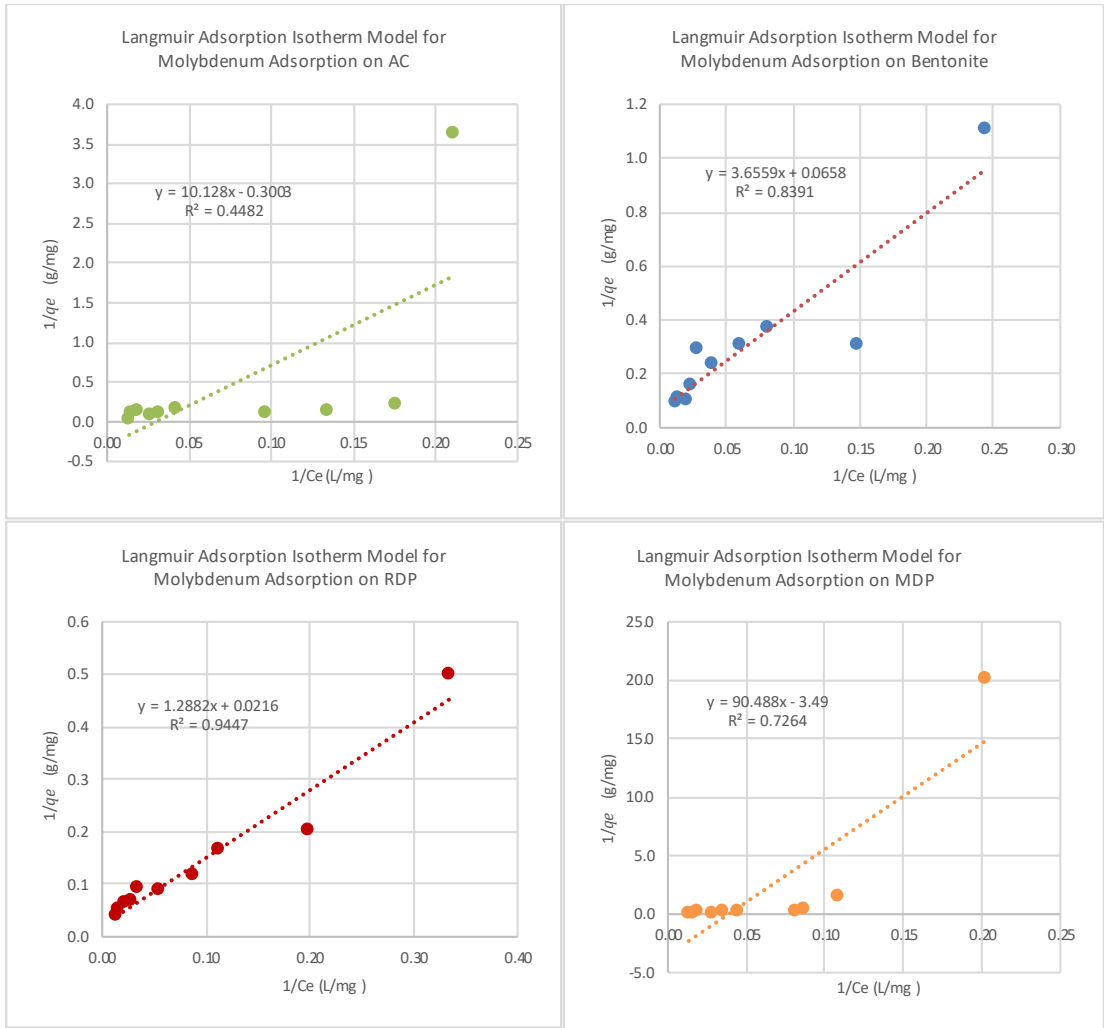


Figure 2. Langmuir model for molybdenum adsorption at 35 °C.

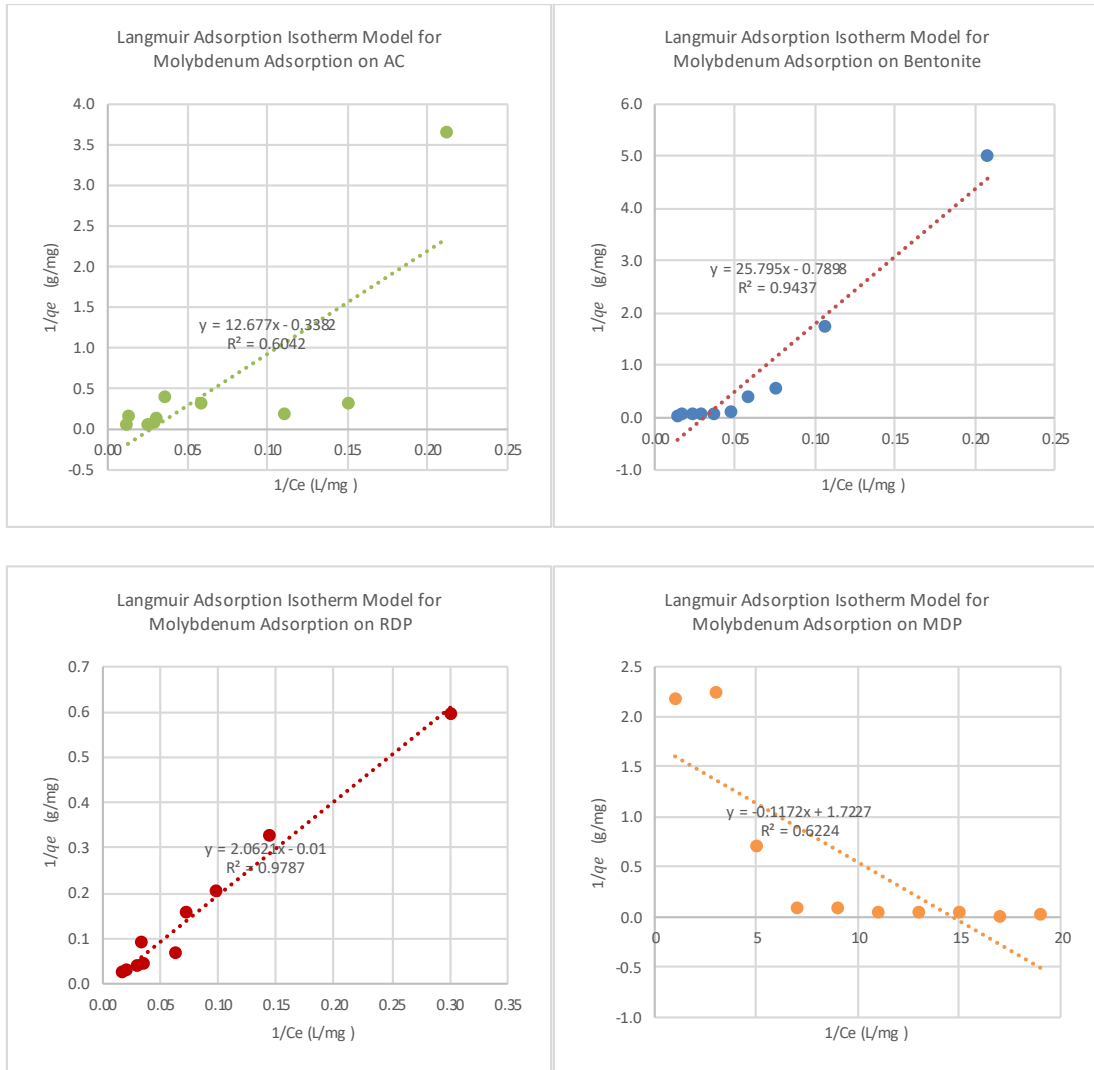


Figure 3. Langmuir model for molybdenum adsorption at 45 °C.



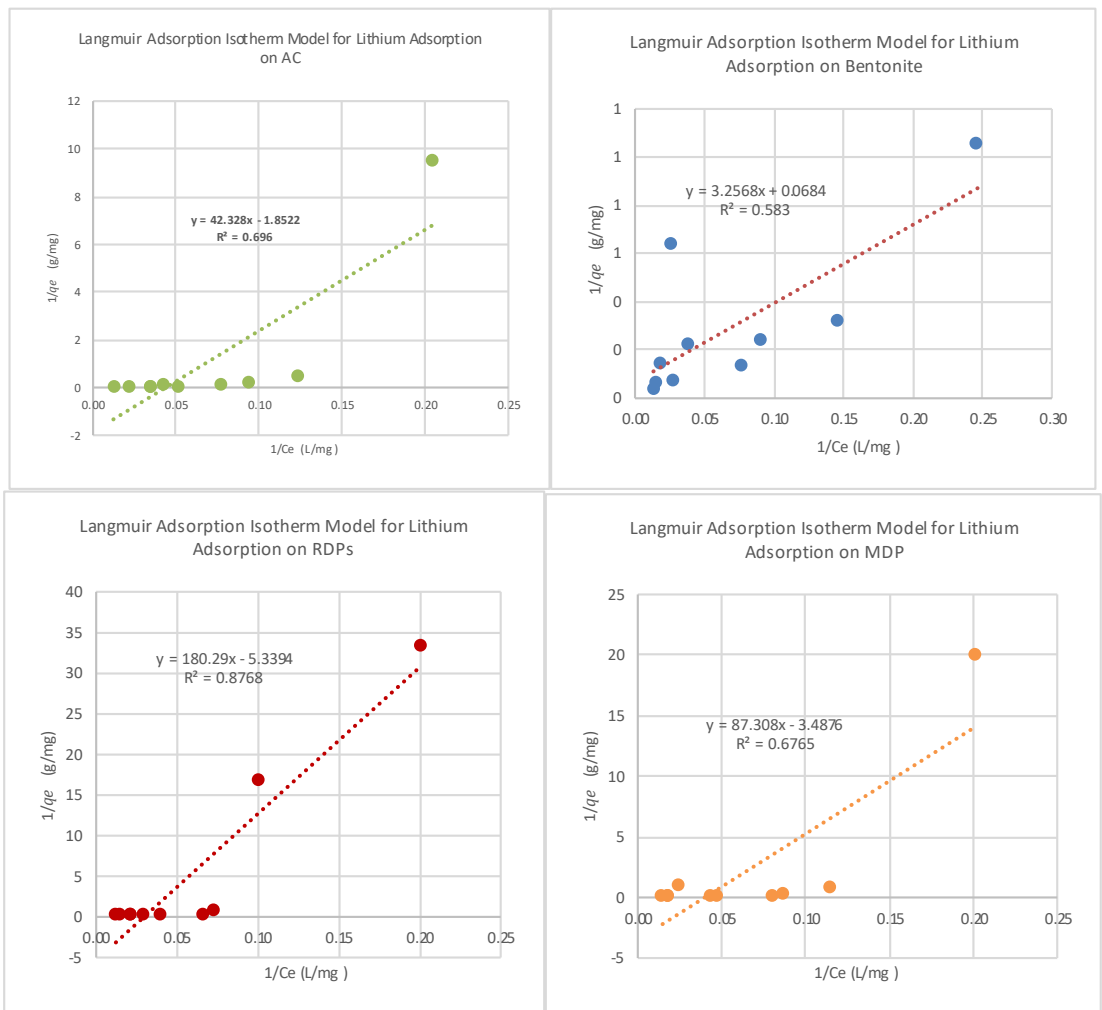


Figure 4. Langmuir model lithium adsorption.

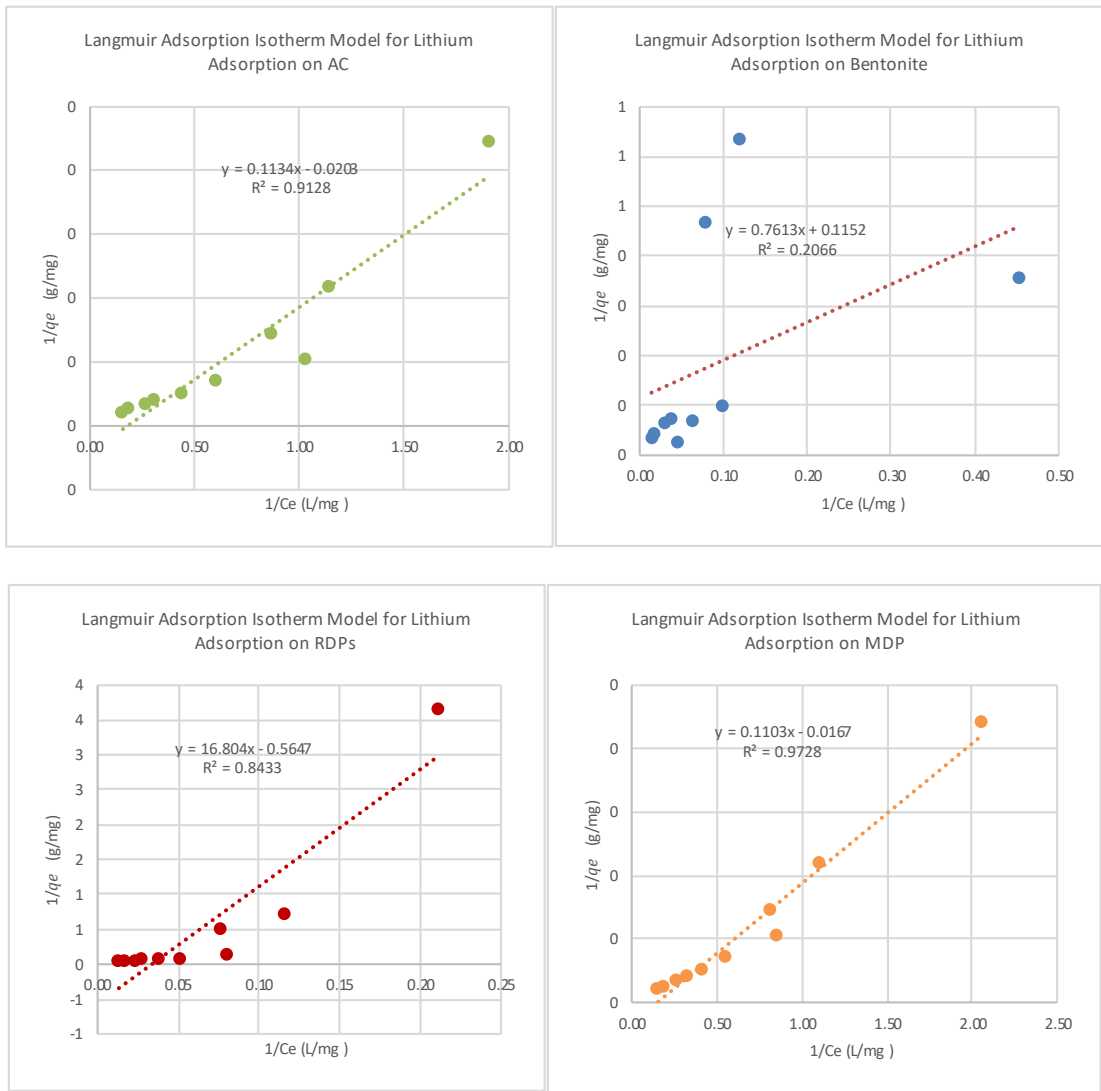


Figure 5. Langmuir model lithium adsorption at 35 °C.

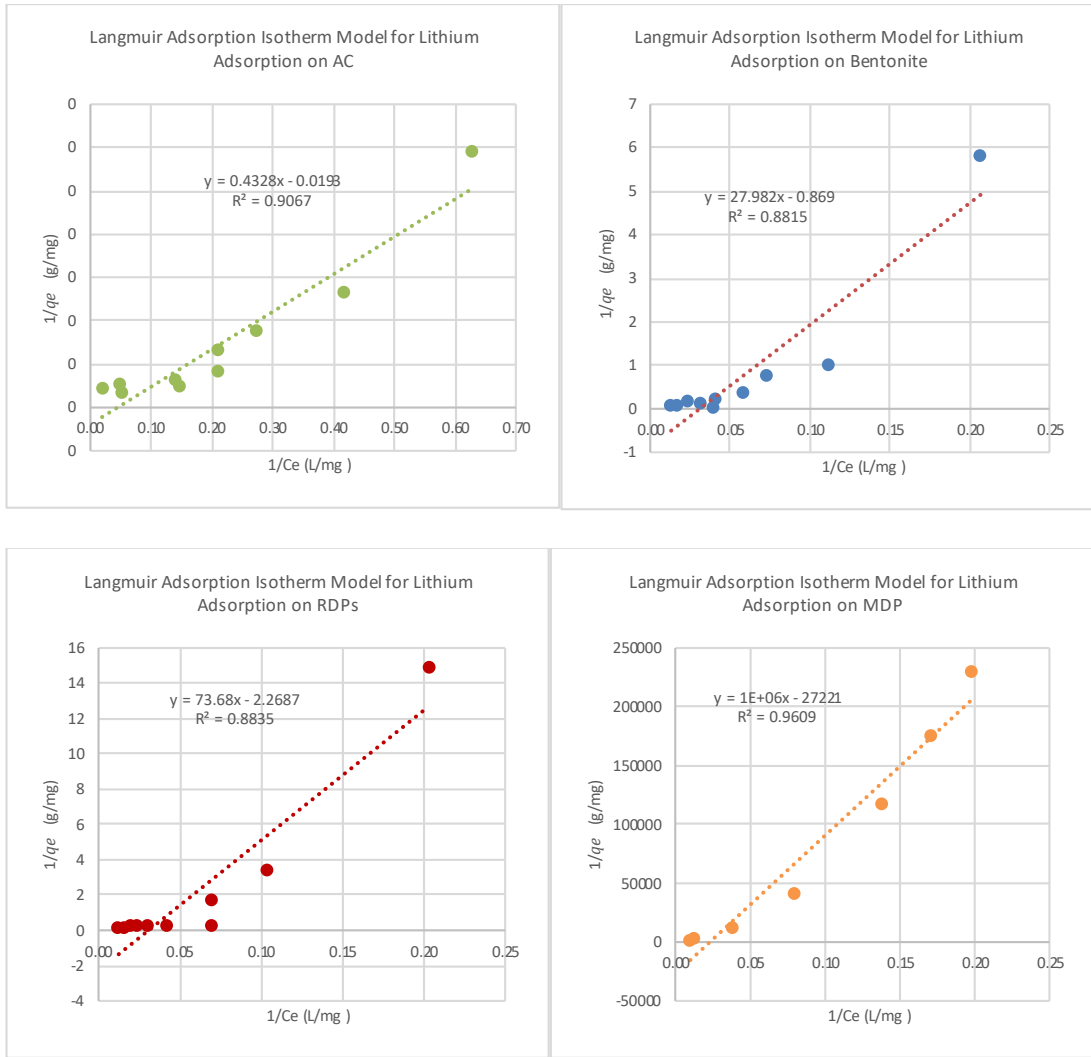


Figure 6. Langmuir model for lithium adsorption at 45 °C.

## Temkin Isotherm

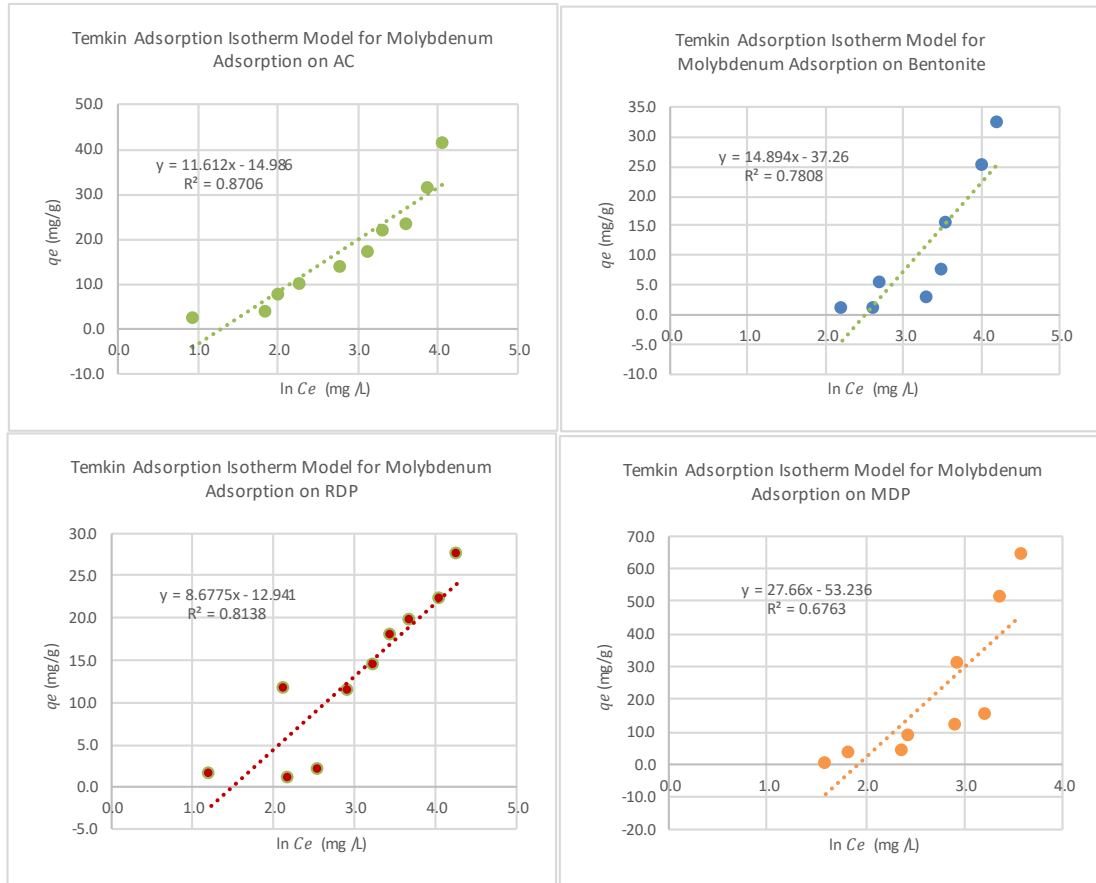


Figure 7. Temkin model for molybdenum adsorption.

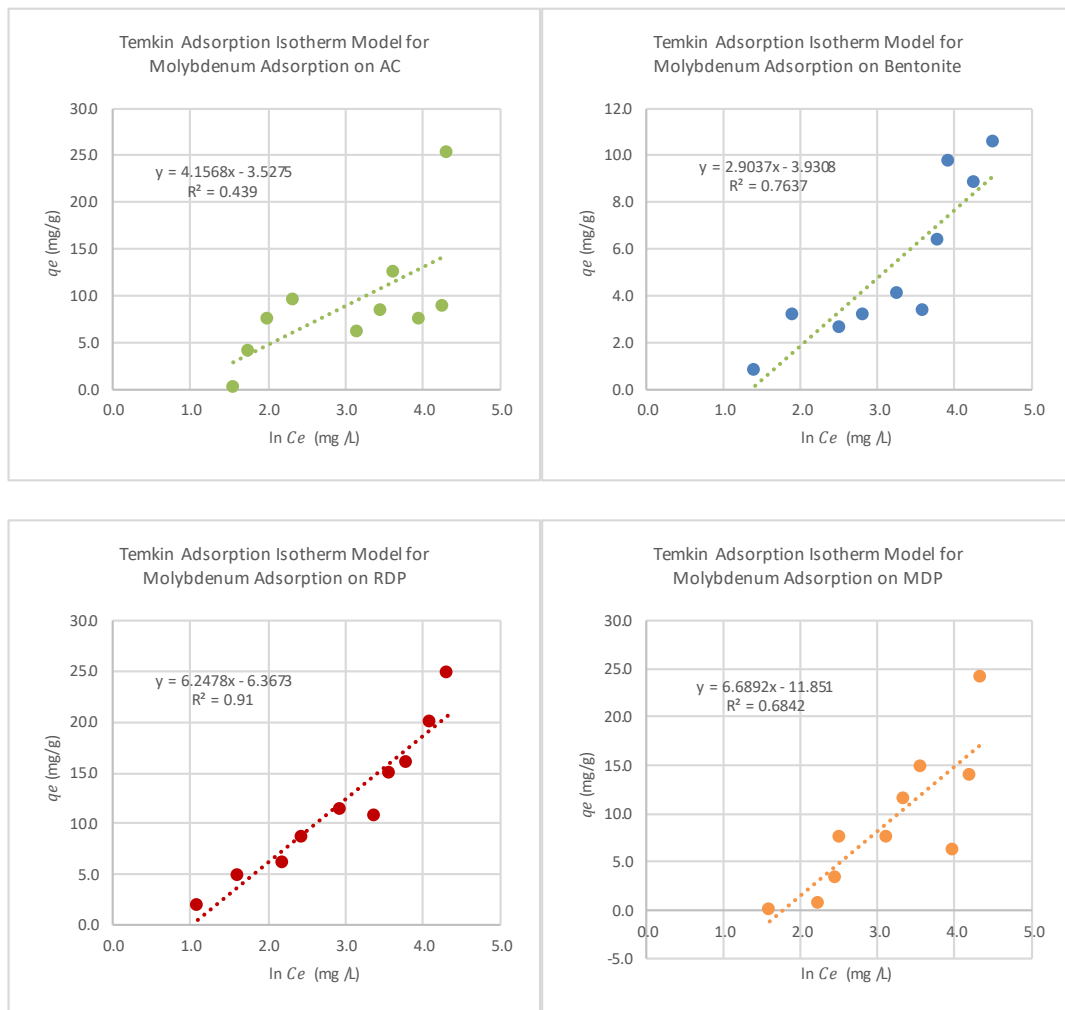


Figure 8. Temkin model for molybdenum adsorption at 35 °C.

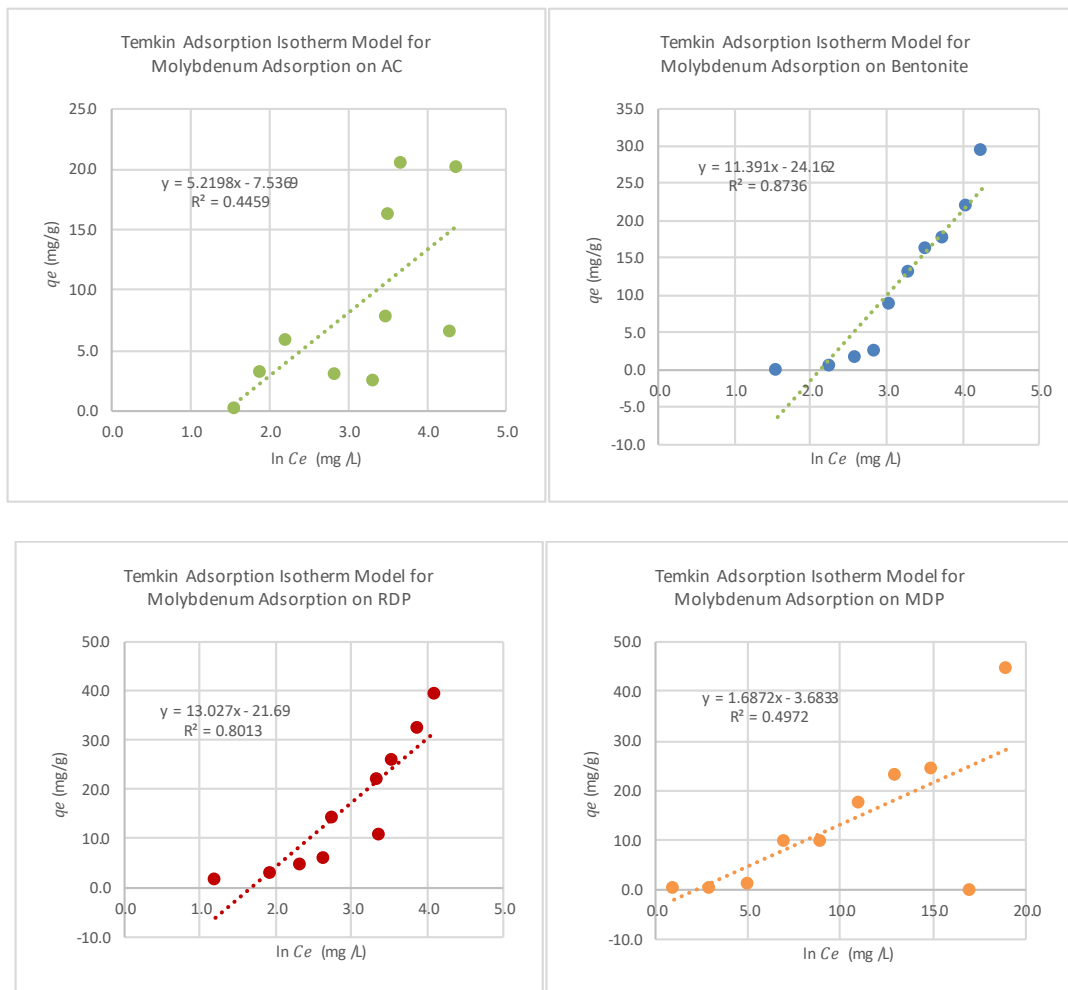


Figure 9. Temkin model for molybdenum adsorption at 45 °C.

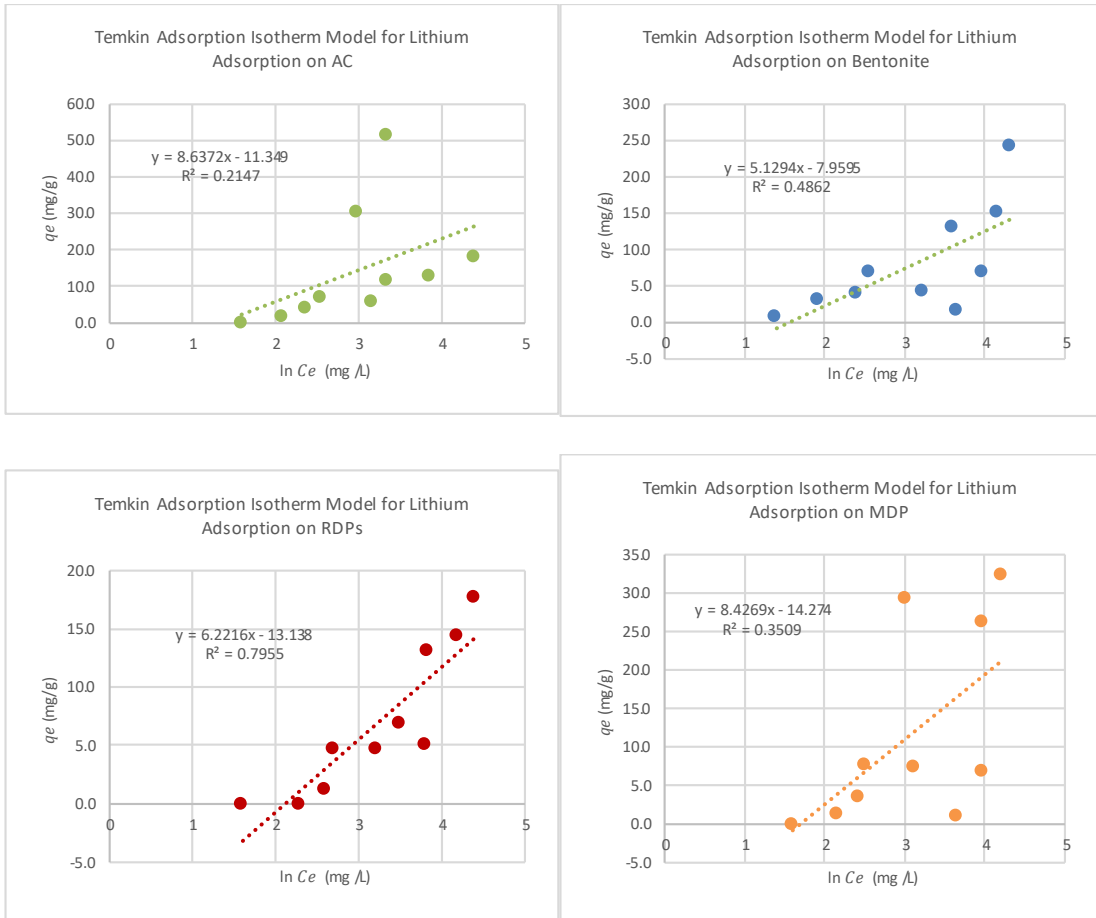


Figure 10. Temkin model for lithium adsorption.

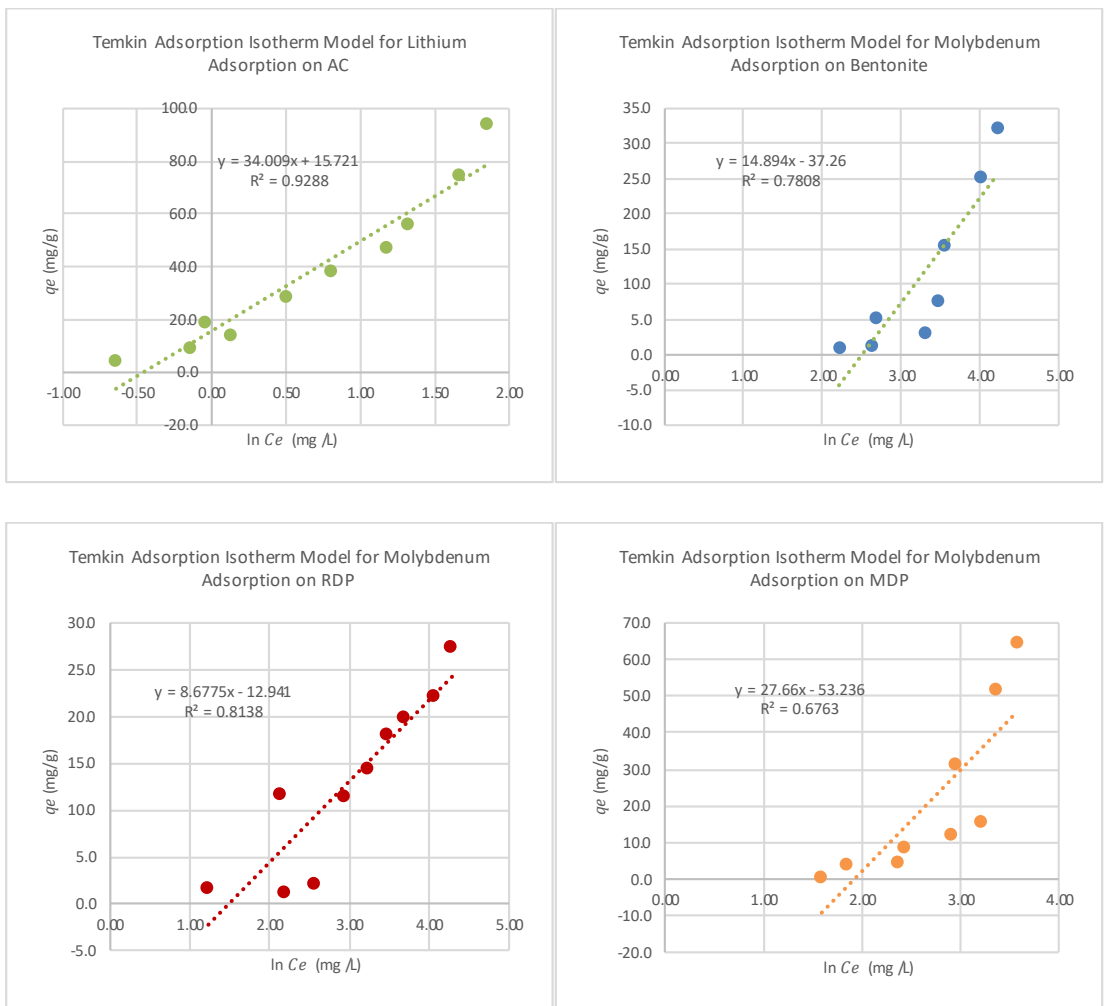


Figure 11. Temkin model for lithium adsorption at 35 °C.



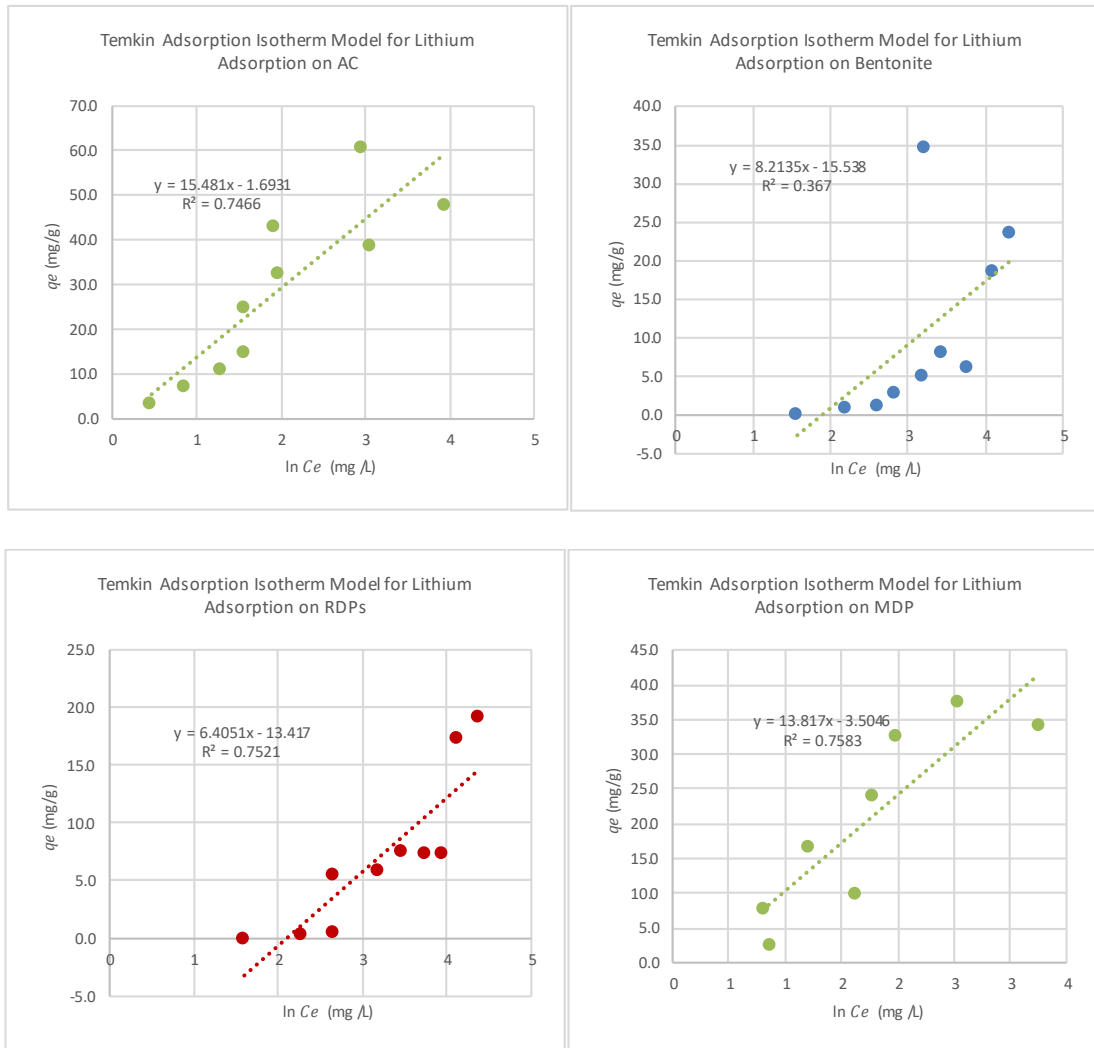


Figure 12. Temkin model for lithium adsorption at 45 °C.

## Freundlich Isotherm

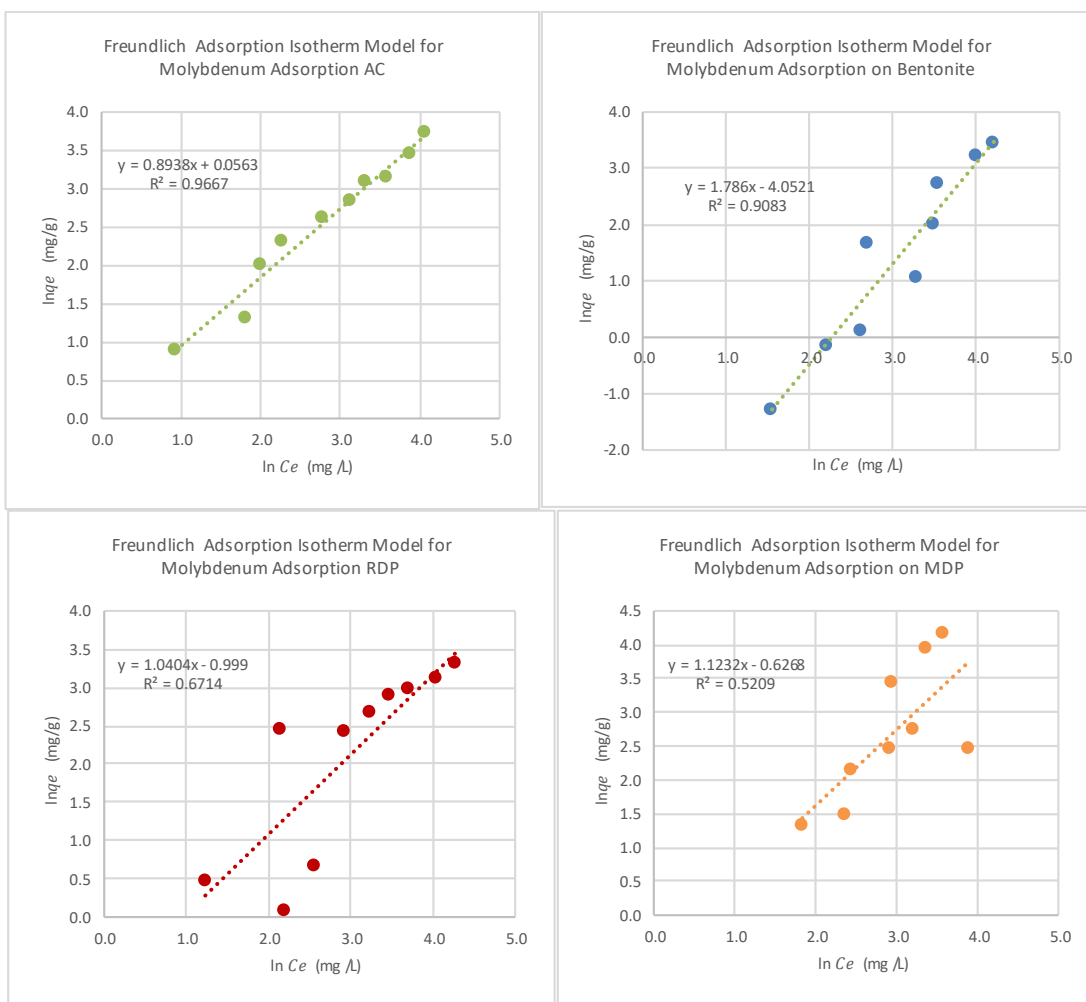


Figure 13. Freundlich model for molybdenum adsorption

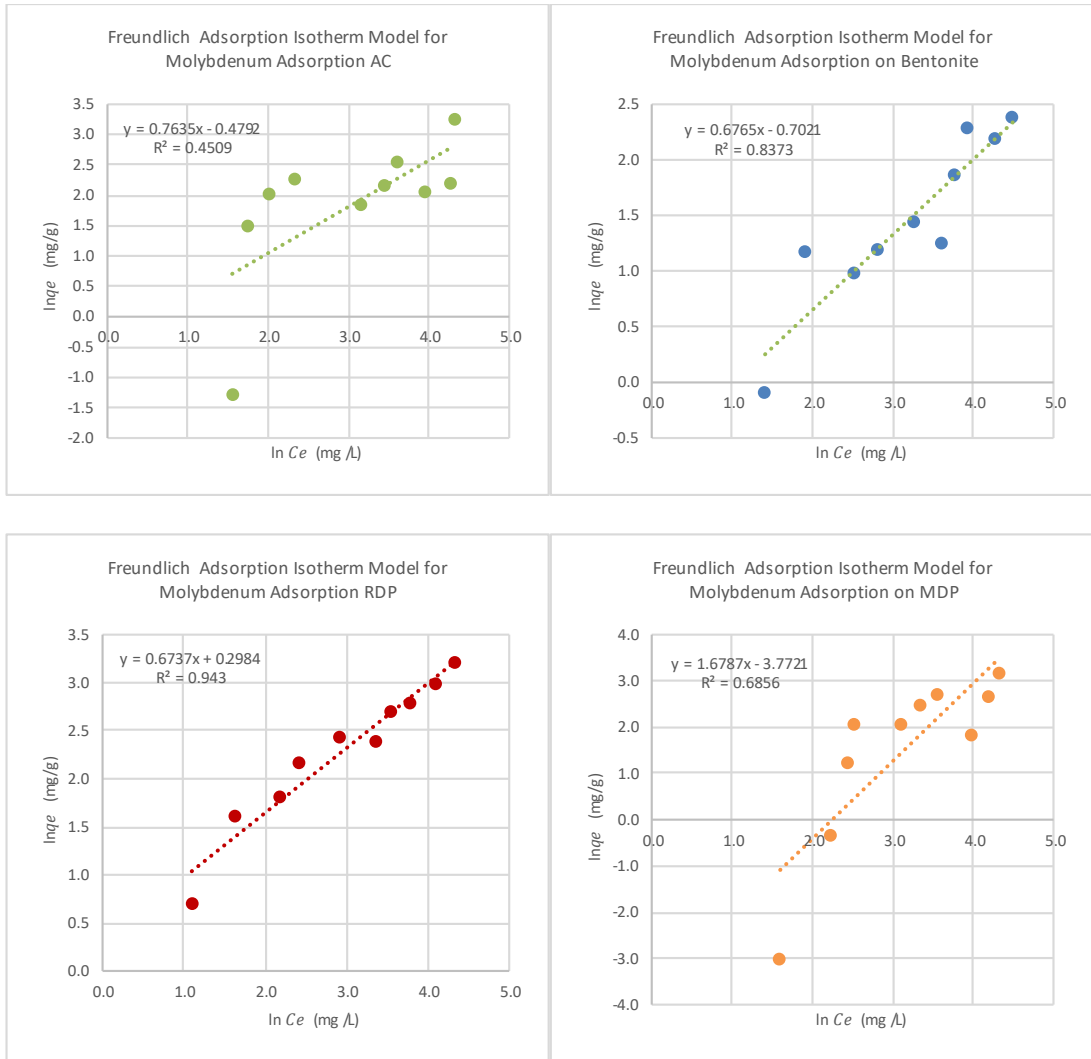


Figure 14. Freundlich model for molybdenum adsorption at 35 °C.

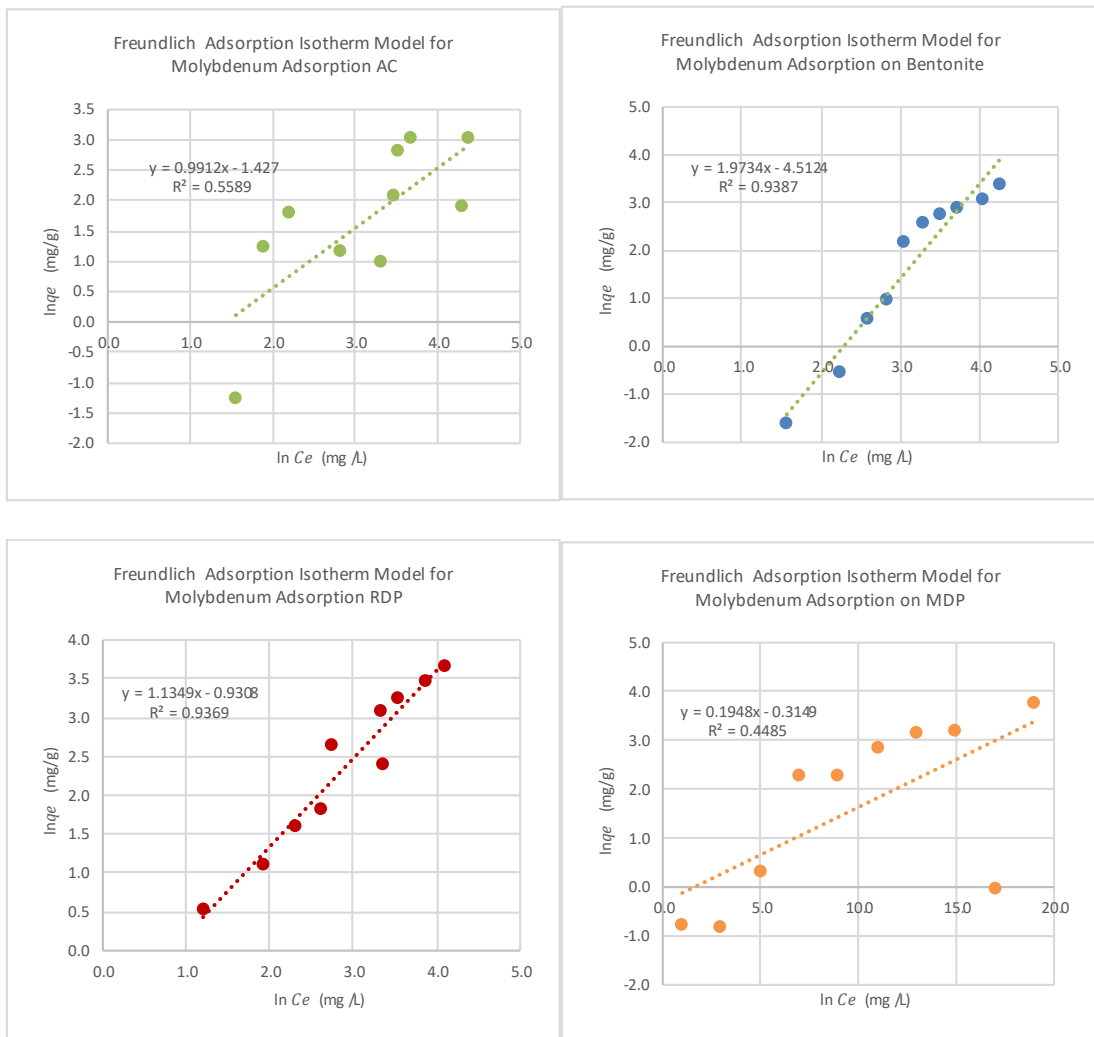


Figure 15. Freundlich model for molybdenum adsorption at 45 °C.

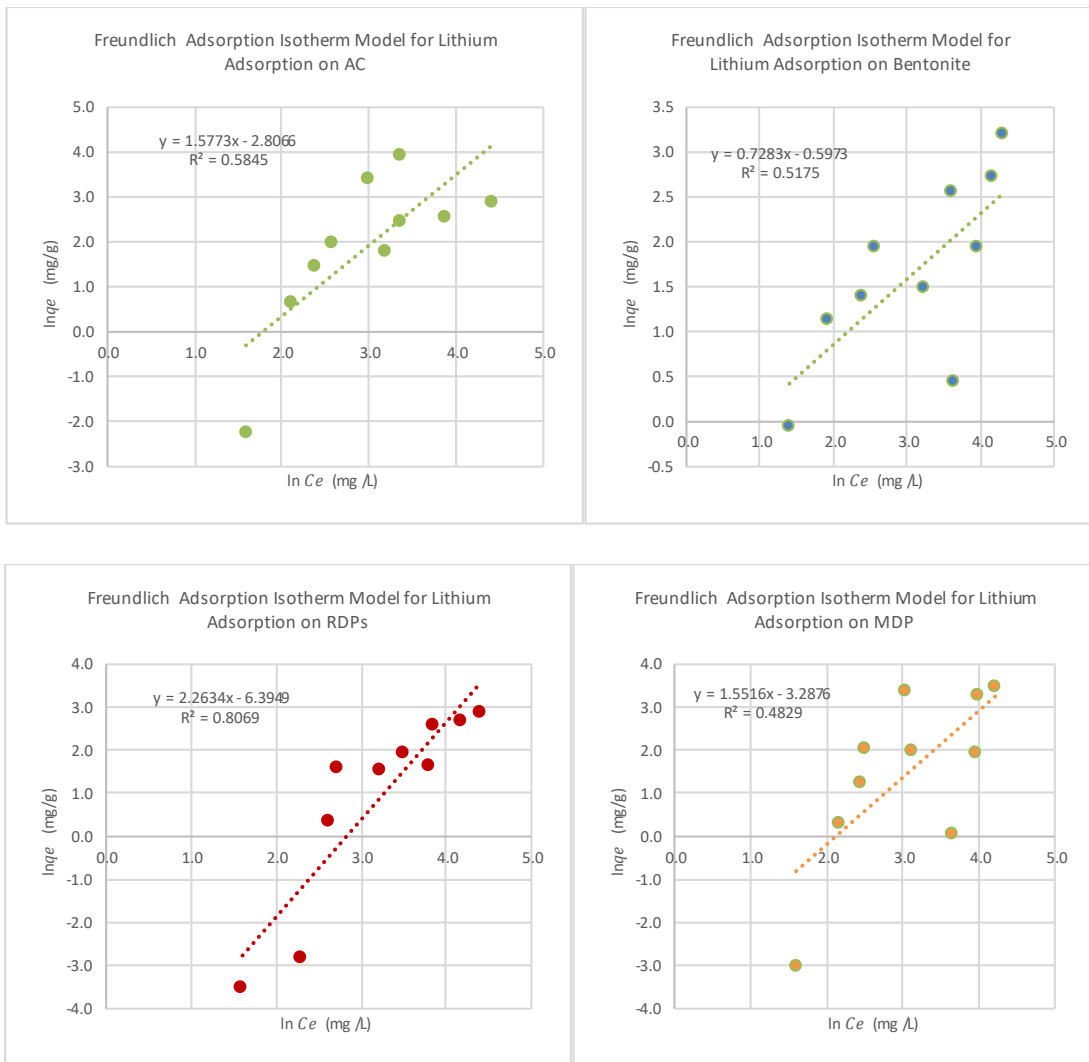


Figure 16. Freundlich model for lithium adsorption.

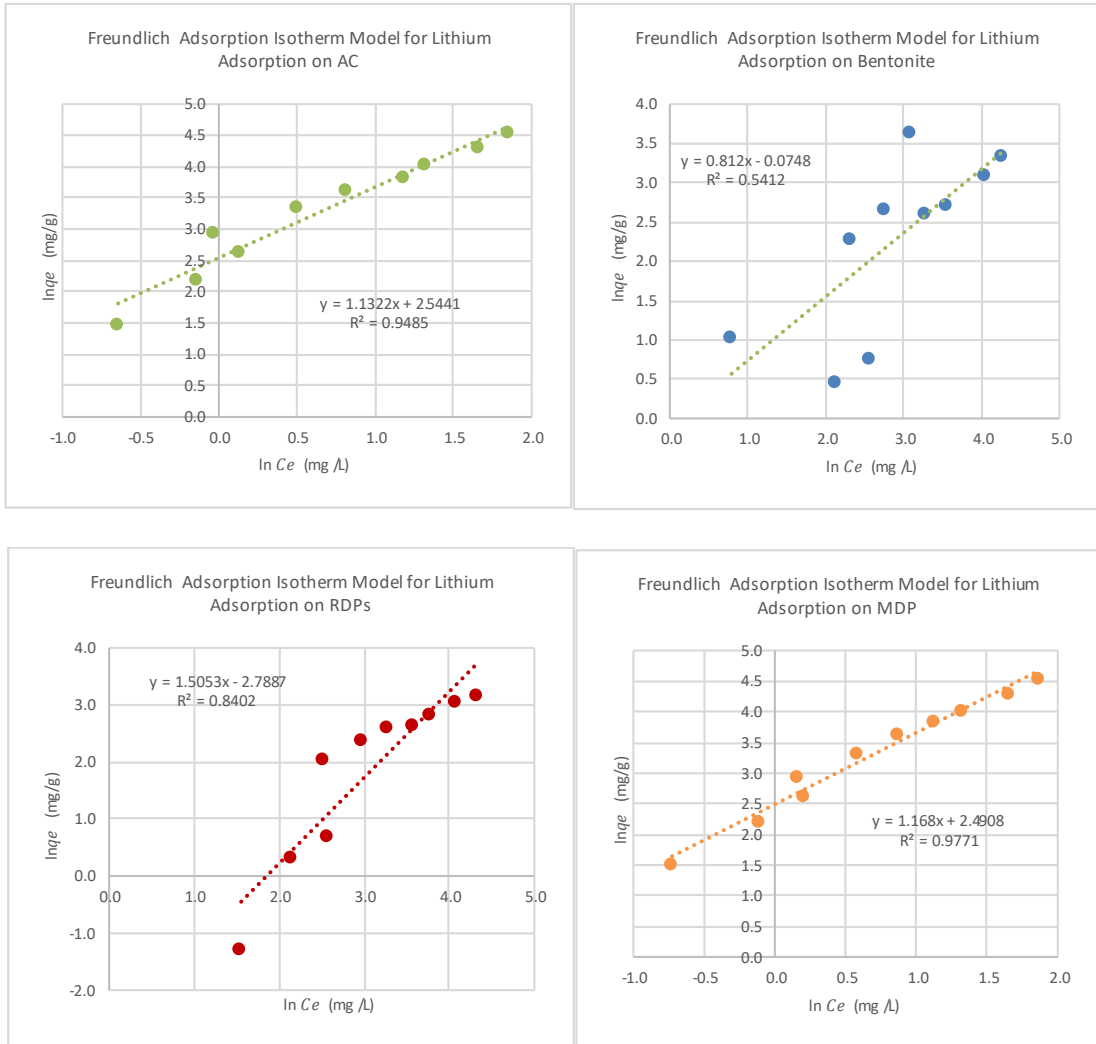


Figure 17. Freundlich model for lithium adsorption at 35 °C.

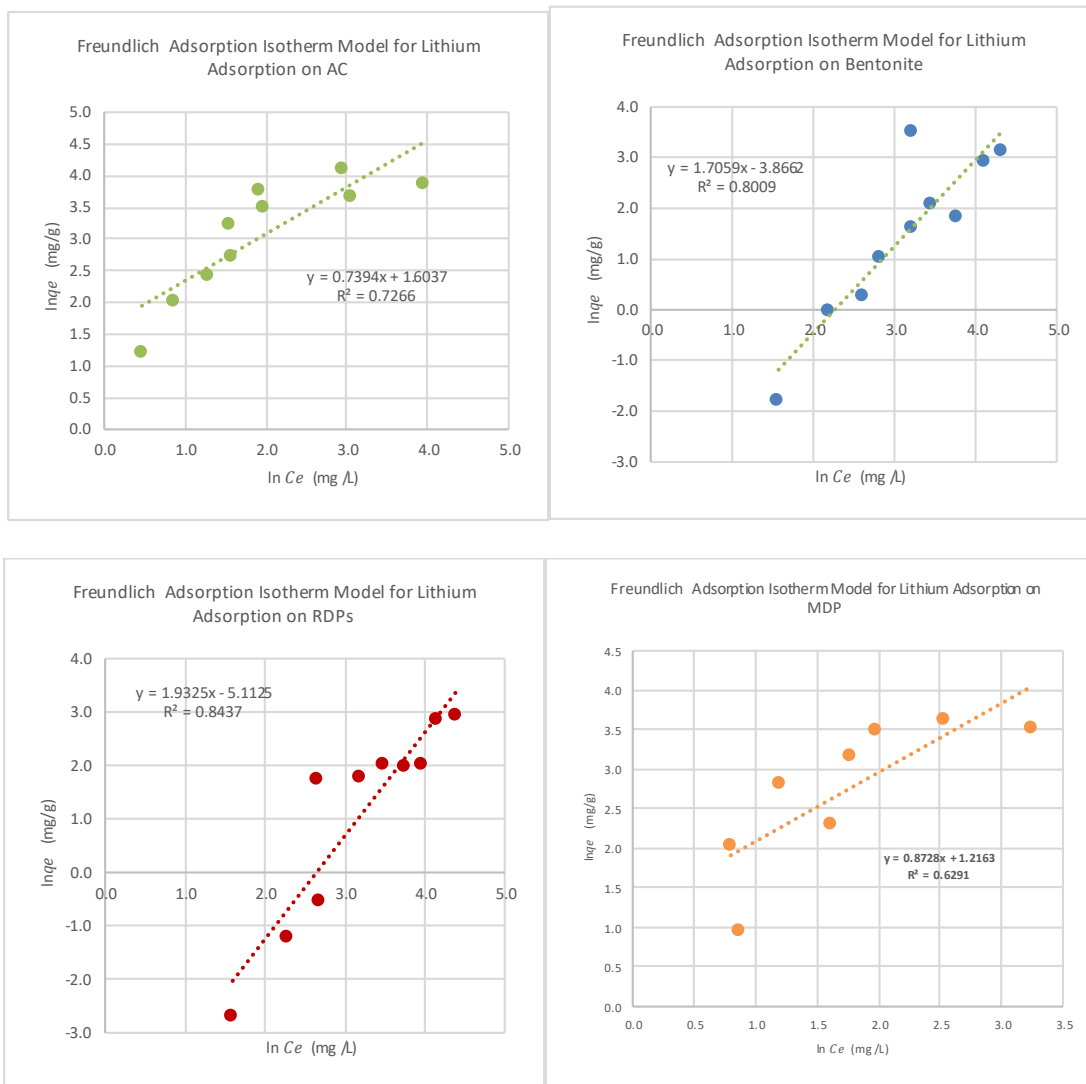


Figure 18. Freundlich model for lithium adsorption at 45 °C.

## Dubinin-Radushkevich (D-R) Isotherm

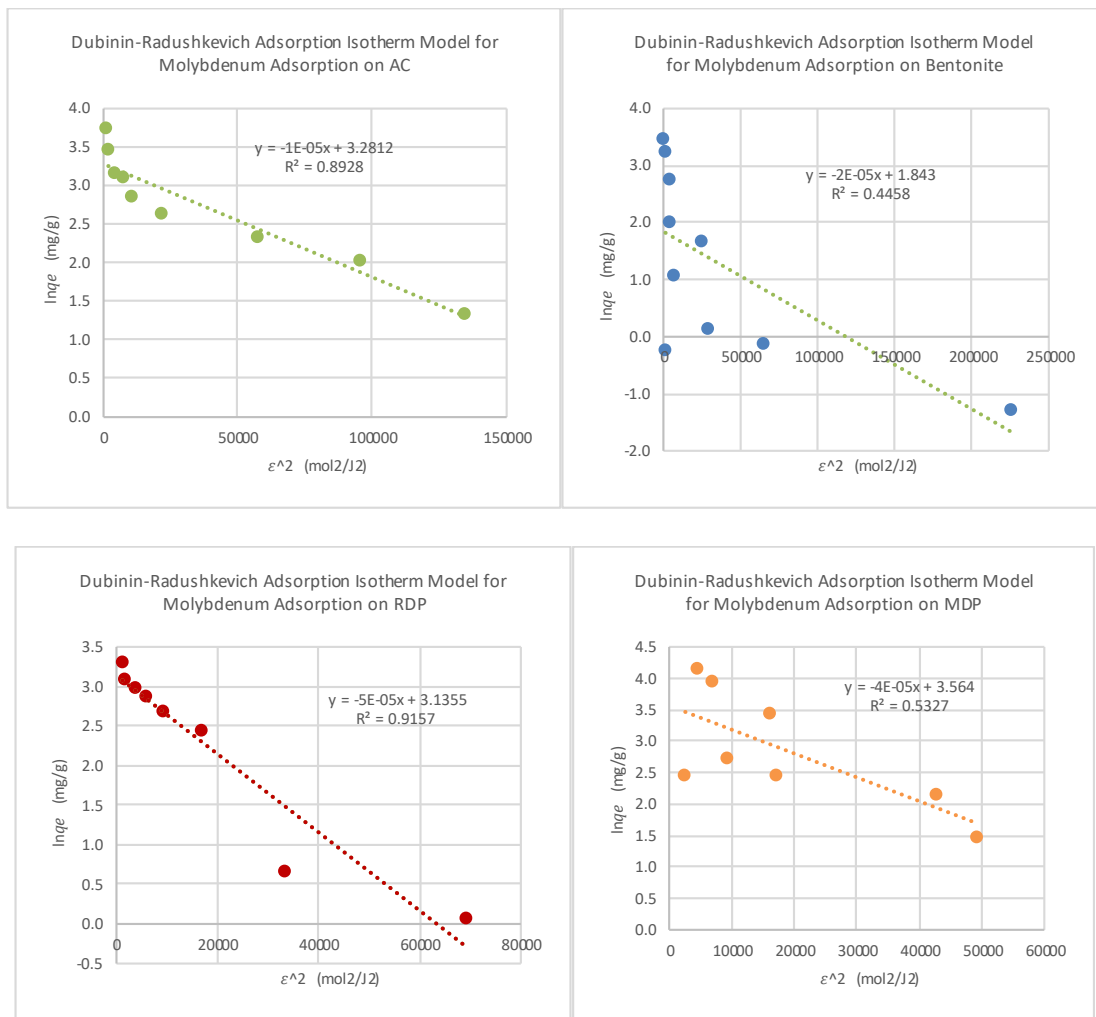


Figure 19. Dubinin-Radushkevich model for molybdenum adsorption



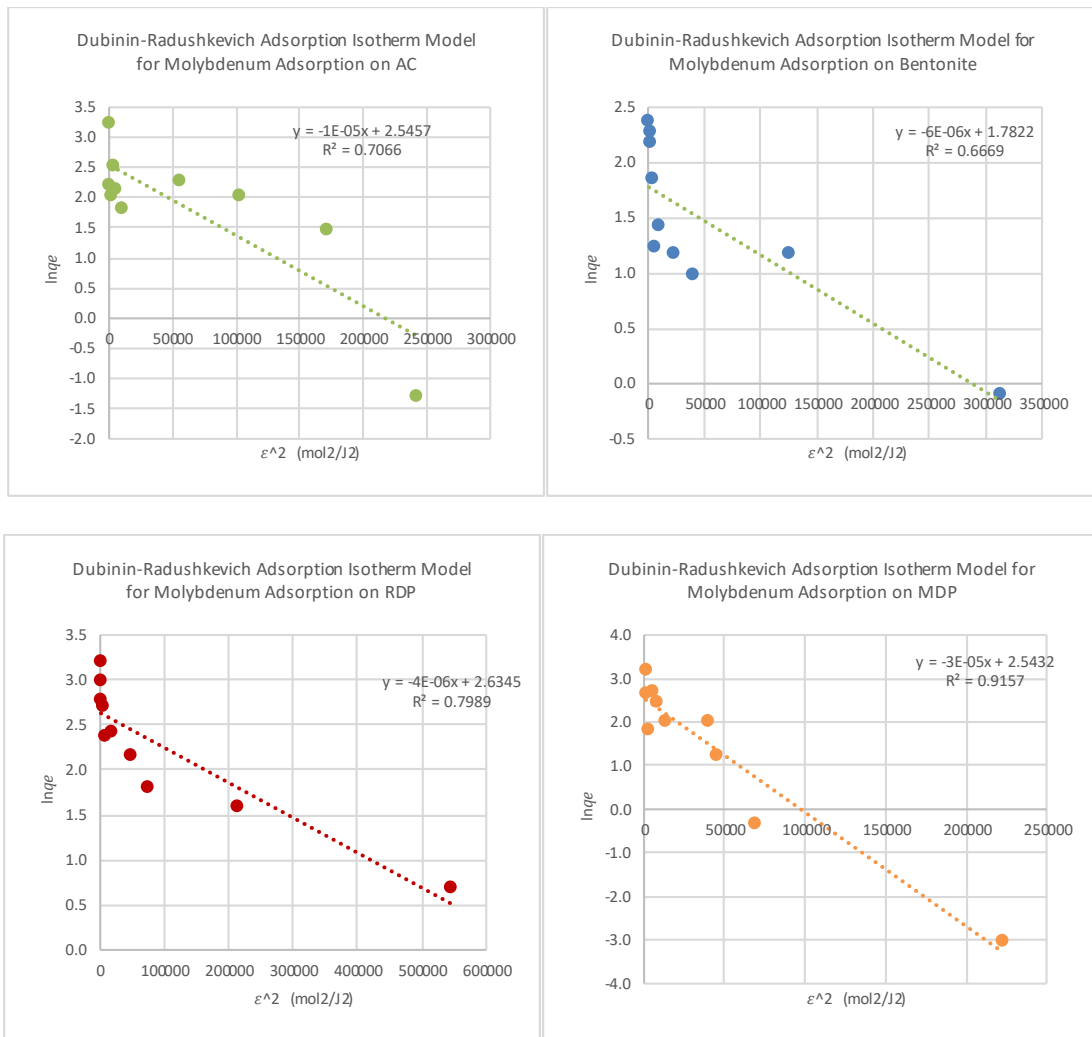


Figure 20. Dubinin-Radushkevich model for molybdenum adsorption at 35 °C.

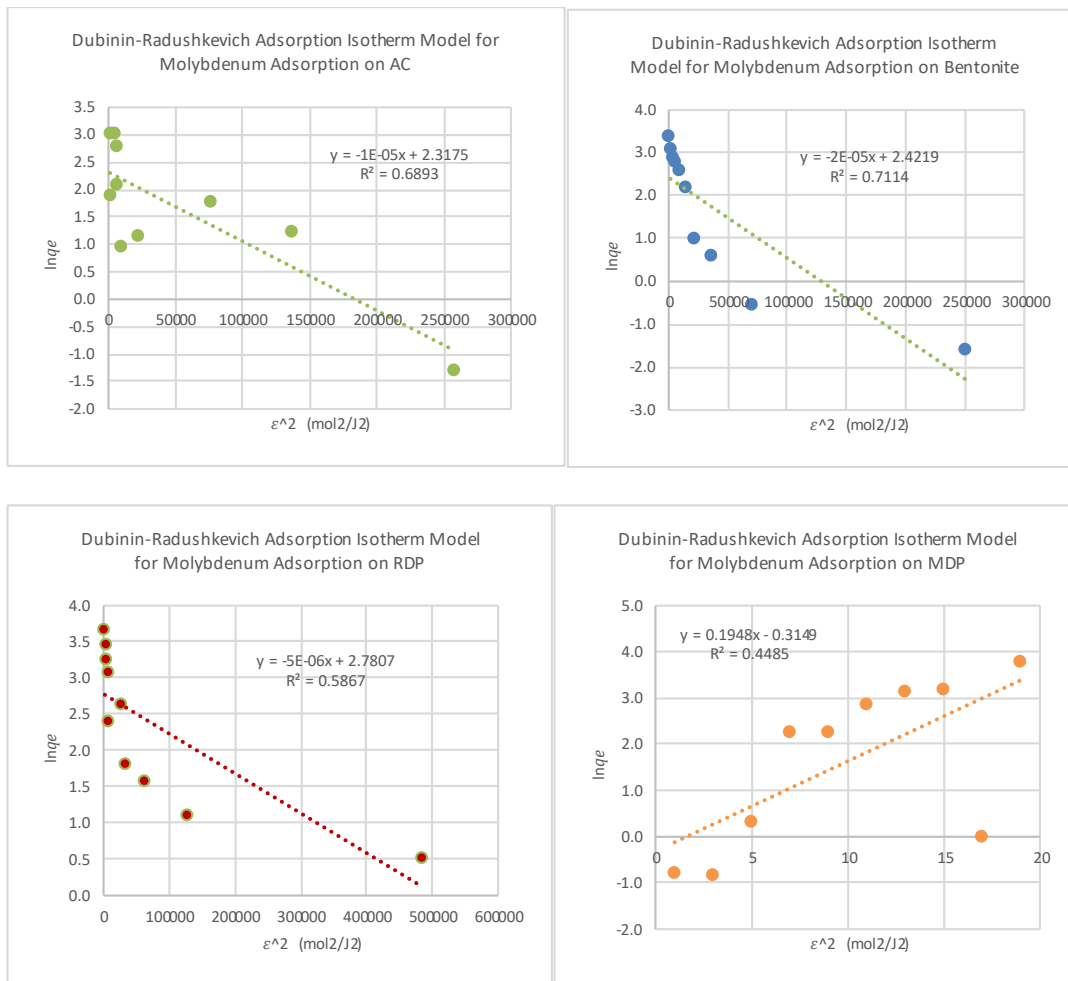


Figure 21. Dubinin-Radushkevich model for molybdenum adsorption at 45 °C.

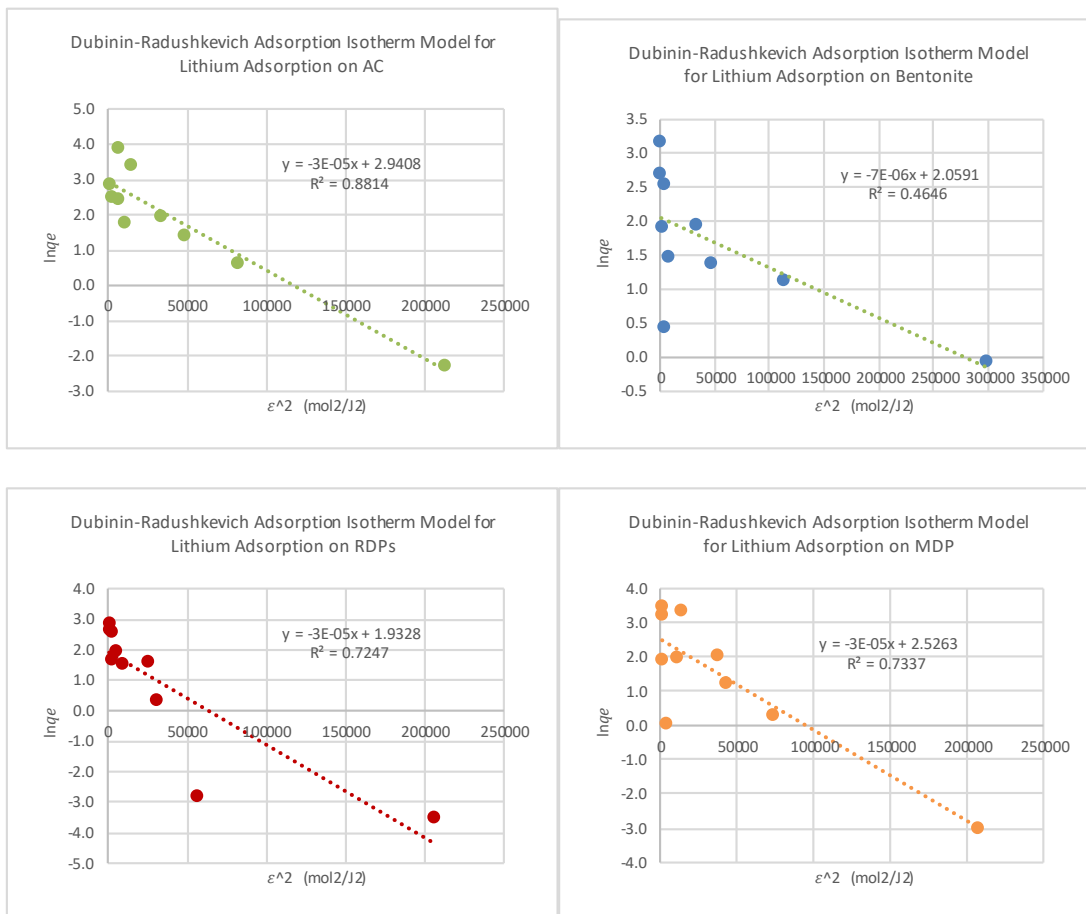


Figure 22. Dubinin-Radushkevich model for lithium adsorption.

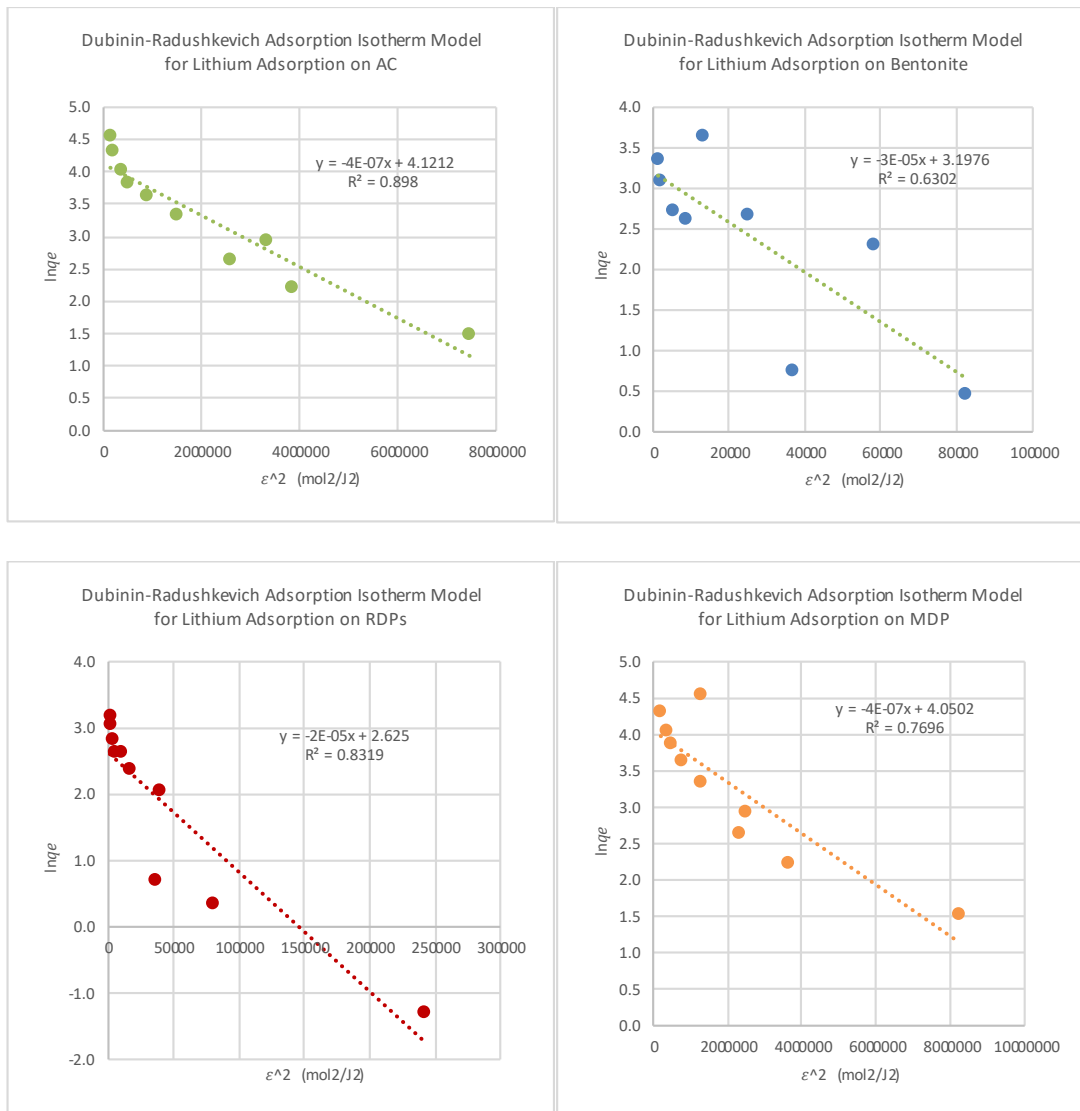


Figure 23. Dubinin-Radushkevich model for lithium adsorption at 35 °C.

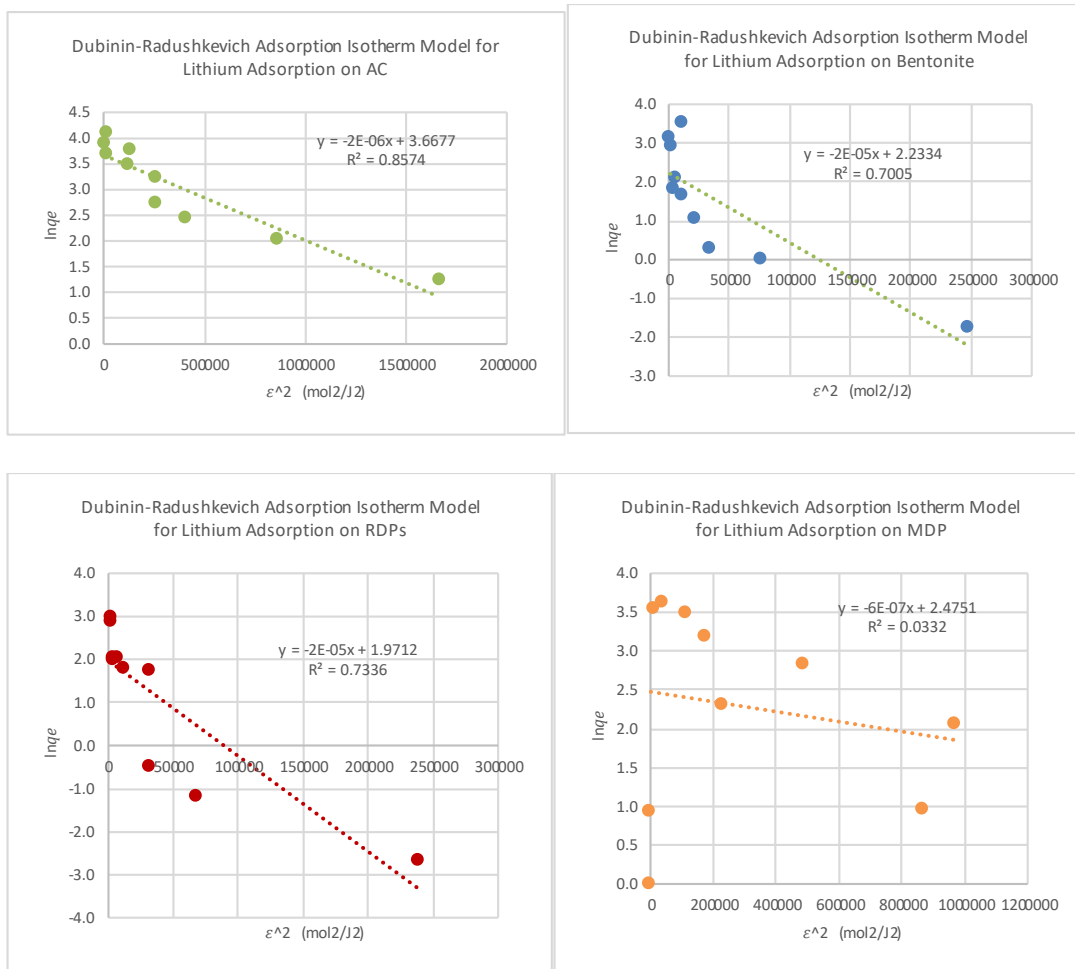


Figure 24. Dubinin-Radushkevich model for lithium adsorption at 45 °C.

## Appendix G: Statistical Analysis for Adsorption Experiments

Table 1. Study the effect of pH on Molybdenum adsorption

Anova: Single Factor						
SUMMARY						
<i>Groups</i>	<i>Count</i>	<i>Sum</i>	<i>Average</i>	<i>Variance</i>		
MRDP	5.000	187.790	37.558	228.057		
RDP	5.000	148.980	29.796	261.835		
Bentonite	5.000	147.000	29.400	690.148		
AC	5.000	152.490	30.498	123.174		
ANOVA						
<i>Source of Variation</i>	<i>SS</i>	<i>df</i>	<i>MS</i>	<i>F</i>	<i>P-value</i>	<i>F crit</i>
Between Groups	223.126	3.000	74.375	0.228	0.875	3.239
Within Groups	5212.856	16.000	325.804			
Total	5435.982	19.000				

Table 2. Study the effect of pH on Boron adsorption

Anova: Single Factor						
SUMMARY						
<i>Groups</i>	<i>Count</i>	<i>Sum</i>	<i>Average</i>	<i>Variance</i>		
MRDP	5	134.400	26.880	10.298		
RDP	5	147.500	29.500	0.924		
Bentonite	5	159.000	31.800	55.669		
AC	5	149.150	29.830	5.829		
ANOVA						
<i>Source of Variati</i>	<i>SS</i>	<i>df</i>	<i>MS</i>	<i>F</i>	<i>P-value</i>	<i>F crit</i>
Between Grou	61.316	3.000	20.439	1.124	0.369	3.239
Within Group	290.881	16.000	18.180			
Total	352.197	19.000				

Table 3. Study the effect of pH on Lithium adsorption

Anova: Single Factor						
SUMMARY						
<i>Groups</i>	<i>Count</i>	<i>Sum</i>	<i>Average</i>	<i>Variance</i>		
MRDP	5	38.250	7.650	15.973		
RDP	5	31.100	6.220	30.323		
Bentonite	5	48.750	9.750	7.090		
AC	5	36.560	7.312	36.812		
ANOVA						
<i>Source of Variation</i>	<i>SS</i>	<i>df</i>	<i>MS</i>	<i>F</i>	<i>P-value</i>	<i>F crit</i>
Between Groups	32.708	3.000	10.903	0.483	0.698	3.239
Within Groups	360.791	16.000	22.549			
Total	393.499	19.000				

Table 4. Study the effect of temperature on Molybdenum adsorption

Anova: Two-Factor With Replication						
SUMMARY	MDPs	Bentonite	AC	RDPs	Total	
<i>Tem 25</i>						
Count	10	10	10	10	40	
Sum	5.37	8.05	15.49	6.21	35.12	
Average	0.54	0.81	1.55	0.62	0.88	
Variance	0.04	0.02	0.05	0.02	0.20	
<i>Tem 35</i>						
Count	10	10	10	10	40	
Sum	319.19	356.53	318.85	290.14	1284.73	
Average	31.92	35.65	31.89	29.01	32.12	
Variance	633.42	804.78	706.39	603.50	639.87	
<i>Tem 45</i>						
Count	10	10	10	10	40	
Sum	233.12	296.76	322.93	248.91	1101.71	
Average	23.31	29.68	32.29	24.89	27.54	
Variance	239.24	461.85	690.16	345.81	414.21	
<i>Total</i>						
Count	30	30	30	30		
Sum	557.68	661.34	657.27	545.26		
Average	18.59	22.04	21.91	18.18		
Variance	452.17	632.60	647.87	456.95		
ANOVA						
<i>Source of Variat</i>	<i>SS</i>	<i>df</i>	<i>MS</i>	<i>F</i>	<i>P-value</i>	<i>F crit</i>
Sample	22771.885	2.000	11385.942	30.462	0.000	3.080
Columns	390.475	3.000	130.158	0.348	0.790	2.689
Interaction	358.632	6.000	59.772	0.160	0.987	2.184
Within	40367.663	108.000	373.775			
Total	63888.65	119.00				



Table 5. Study the effect of temperature on Boron adsorption

Anova: Two-Factor With Replication						
SUMMARY	MDPs	Bentonite	AC	RDPs	Total	
<i>Tem 25</i>						
Count	10	10	10	10	40	
Sum	293.95	306.66	378.32	333.95	1312.88	
Average	29.40	30.67	37.83	33.39	32.82	
Variance	503.39	546.88	902.52	970.75	685.39	
<i>Tem 35</i>						
Count	10	10	10	10	40	
Sum	268.22	232.00	357.95	357.65	1215.82	
Average	26.82	23.20	35.79	35.77	30.40	
Variance	530.37	269.26	1002.52	748.46	620.02	
<i>Tem 45</i>						
Count	10	10	10	10	40	
Sum	171.97	236.89	207.48	278.24	894.58	
Average	17.20	23.69	20.75	27.82	22.36	
Variance	230.64	336.69	368.47	546.33	357.64	
<i>Total</i>						
Count	30	30	30	30		
Sum	734.14	775.55	943.74	969.84		
Average	24.47	25.85	31.46	32.33		
Variance	420.91	369.81	765.62	714.56		
ANOVA						
<i>Source of Variat</i>	<i>SS</i>	<i>df</i>	<i>MS</i>	<i>F</i>	<i>P-value</i>	<i>F crit</i>
Sample	2396.635	2.000	1198.318	2.067	0.132	3.080
Columns	1399.387	3.000	466.462	0.805	0.494	2.689
Interaction	852.953	6.000	142.159	0.245	0.960	2.184
Within	62606.581	108.000	579.691			
Total	67255.557	119.000				

Table 6. Study the effect of temperature on Lithium adsorption

Anova: Two-Factor With Replication						
SUMMARY	MDPs	AC	Bentonite	RDPs	Total	
<i>Tem 25</i>						
Count	10	10	10	10	40	
Sum	294.17	266.68	329.30	341.12	1231.26	
Average	29.42	26.67	32.93	34.11	30.78	
Variance	498.46	534.62	638.09	651.88	544.94	
<i>Tem 35</i>						
Count	10	10	10	10	40	
Sum	26.35	26.13	261.52	298.50	612.50	
Average	2.64	2.61	26.15	29.85	15.31	
Variance	3.88	4.06	509.71	555.02	414.42	
<i>Tem 45</i>						
Count	10	10	10	10	40	
Sum	240.91	123.49	307.84	338.53	1010.77	
Average	24.09	12.35	30.78	33.85	25.27	
Variance	1217.07	240.23	541.78	636.00	677.95	
<i>Total</i>						
Count	30	30	30	30		
Sum	561.43	416.29	898.66	978.15		
Average	18.71	13.88	29.96	32.60		
Variance	672.23	342.70	532.63	575.87		
ANOVA						
<i>Source of Variati</i>	<i>SS</i>	<i>df</i>	<i>MS</i>	<i>F</i>	<i>P-value</i>	<i>F crit</i>
Sample	4917.411	2.000	2458.706	4.892	0.009	3.080
Columns	7192.803	3.000	2397.601	4.771	0.004	2.689
Interaction	2384.832	6.000	397.472	0.791	0.579	2.184
Within	54277.214	108.000	502.567			
Total	68772.260	119.000				

Table 7. Study the effect of a mixture concentration on Boron adsorption

Anova: Single Factor						
SUMMARY						
Groups	Count	Sum	Average	Variance		
AC	5	49.80	9.96	46.94		
Bentonite	5	48.24	9.65	43.30		
RDOs	5	50.40	10.08	51.54		
MRDPs	5	56.22	11.24	84.78		
ANOVA						
Source of Variati	SS	df	MS	F	P-value	F crit
Between Grou	7.311	3.000	2.437	0.043	0.988	3.239
Within Group	906.274	16.000	56.642			
Total	913.586	19.000				

Table 8. Study the effect of a mixture concentration on lithium adsorption

Anova: Single Factor						
SUMMARY						
Groups	Count	Sum	Average	Variance		
AC	5	48.08	9.62	29.19		
Bentonite	5	45.06	9.01	30.03		
RDOs	5	50.48	10.10	34.37		
MRDPs	5	49.44	9.89	32.46		
ANOVA						
Source of Variati	SS	df	MS	F	P-value	F crit
Between Grou	3.319	3.000	1.106	0.035	0.991	3.239
Within Group	504.221	16.000	31.514			
Total	507.539	19.000				

Table 9. Study the effect of a mixture concentration on molybdenum adsorption

Anova: Single Factor						
SUMMARY						
<i>Groups</i>	<i>Count</i>	<i>Sum</i>	<i>Average</i>	<i>Variance</i>		
AC	5	62.14	12.43	96.51		
Bentonite	5	60.22	12.04	102.54		
RDOs	5	62.50	12.50	114.83		
MRDPs	5	44.68	8.94	47.41		
ANOVA						
<i>Source of Variati</i>	<i>SS</i>	<i>df</i>	<i>MS</i>	<i>F</i>	<i>P-value</i>	<i>F crit</i>
Between Group	43.645	3.000	14.548	0.161	0.921	3.239
Within Group	1445.139	16.000	90.321			
Total	1488.784	19.000				

Table 10. Study the effect of a temperature on boron adsorption in GW samples

Anova: Two-Factor With Replication						
SUMMARY	AC	Bentonite	RDOs	MRDPs	Total	
Count	3.00	3.00	3.00	3.00	12.00	
Sum	7.76	7.92	7.70	7.93	31.30	
Average	2.59	2.64	2.57	2.64	2.61	
Variance	2.14	2.39	2.26	2.25	1.64	
<i>Tem 35</i>						
Count	3	3	3	3	12	
Sum	7.34	8.10	7.61	7.67	30.71	
Average	2.45	2.70	2.54	2.56	2.56	
Variance	1.75	2.34	2.00	1.95	1.47	
<i>Total</i>						
Count	6	6	6	6		
Sum	15.10	16.02	15.31	15.60		
Average	2.52	2.67	2.55	2.60		
Variance	1.56	1.89	1.71	1.68		
ANOVA						
<i>urce of Variati</i>	<i>SS</i>	<i>df</i>	<i>MS</i>	<i>F</i>	<i>P-value</i>	<i>F crit</i>
Sample	0.015	1.000	0.015	0.007	0.935	4.494
Columns	0.079	3.000	0.026	0.012	0.998	3.239
Interaction	0.032	3.000	0.011	0.005	0.999	3.239
Within	34.163	16.000	2.135			
Total	34.289	23.000				

Table 11. Study the effect of a temperature on lithium adsorption in GW samples

Anova: Two-Factor With Replication						
SUMMARY	AC	Bentonite	RDOs	MRDPs	Total	
<i>Tem 25</i>						
Count	3	3	3	3	12	
Sum	0.725	0.735	0.745	0.725	2.93	
Average	0.24166667	0.245	0.24833333	0.24166667	0.24416667	
Variance	0.03350833	0.034275	0.03635833	0.03350833	0.02503561	
<i>Tem 35</i>						
Count	3	3	3	3	12	
Sum	0.645	0.675	0.65	0.65	2.62	
Average	0.215	0.225	0.21666667	0.21666667	0.21833333	
Variance	0.025225	0.029575	0.02610833	0.02503333	0.01927879	
<i>Total</i>						
Count	6	6	6	6		
Sum	1.37	1.41	1.395	1.375		
Average	0.22833333	0.235	0.2325	0.22916667		
Variance	0.02370667	0.02566	0.0252875	0.02360417		
ANOVA						
Source of Variati	SS	df	MS	F	P-value	F crit
Sample	0.00400417	1	0.00400417	0.13150422	0.72162327	4.49399848
Columns	0.00017083	3	5.6944E-05	0.00187016	0.99988332	3.23887152
Interaction	0.00010417	3	3.4722E-05	0.00114034	0.9999444	3.23887152
Within	0.48718333	16	0.03044896			
Total	0.4914625	23				

Table 12. Study the effect of a temperature on molybdenum adsorption in GW samples

Anova: Two-Factor With Replication						
SUMMARY	AC	Bentonite	RDOs	MRDPs	Total	
<i>Tem 25</i>						
Count	3	3	3	3	12	
Sum	0.165	0.14	0.08	0.065	0.45	
Average	0.055	0.04666667	0.02666667	0.02166667	0.0375	
Variance	0.000175	5.8333E-05	5.8333E-05	5.8333E-05	0.00027045	
<i>Tem 35</i>						
Count	3	3	3	3	12	
Sum	0.095	0.115	0.1	0.045	0.355	
Average	0.03166667	0.03833333	0.03333333	0.015	0.02958333	
Variance	3.3333E-05	5.8333E-05	0.00013333	0.000025	0.00012936	
<i>Total</i>						
Count	6	6	6	6		
Sum	0.26	0.255	0.18	0.11		
Average	0.04333333	0.0425	0.03	0.01833333		
Variance	0.00024667	6.75E-05	9E-05	4.6667E-05		
ANOVA						
Source of Variati	SS	df	MS	F	P-value	Fcrit
Sample	0.00037604	1	0.00037604	5.01388889	0.03970376	4.49399848
Columns	0.00251979	3	0.00083993	11.1990741	0.00033064	3.23887152
Interaction	0.00067813	3	0.00022604	3.01388889	0.06079798	3.23887152
Within	0.0012	16	0.000075			
Total	0.00477396	23				